INVESTIGATION OF CONDENSERS APPLICABLE TO SPACE POWER SYSTEMS

PART II

JET CONDENSERS

EOS Report 1588-Final II

30 November 1962

Prepared by

Lance Hays
Project Supervisor, EOS

Under the Technical Direction of

Seymour Lieblein, Chief
Flow Processes Branch
Lewis Research Center
National Aeronautics and
Space Administration

Contract NAS 7-11

Approved by

B. M. Wilner, Manager
Chemical and Fluid
Systems Department, EOS

Approved by

J. Neustein, Manager
Advanced Power Systems
Division, EOS

ELECTRO-OPTICAL SYSTEMS, INC., - PASADENA, CALIFORNIA

ABSTRACT

An investigation of condensers suitable for operation as components of space power systems operating on the Rankine cycle has been continued. Several geometric variations of jet condensers and direct (radiator) condensers were tested and analyzed. The test fluid was mercury at temperatures ranging from 500°F to 800°F. Vapor velocities ranged from less than 20 fps to greater than 250 fps. Results of jet condenser analysis and testing are reported herein. Direct condenser analysis and testing are reported in Part I of this report.

The jet condenser investigation provided information on performance characteristics of several geometries. Vapor inlet diameters of 0.19 inch and 0.75 inch were tested. Stable closed-cycle operation, simple startup techniques, vapor-to-liquid outlet pressure rises, and high heat transfer rates were characteristics of the condensers tested. Conversion of thermal energy to pressure energy was demonstrated both by analysis and experimental results obtained with geometries (converging-diverging) designed to maximize pressure rise. Data are presented both to provide information on the internal flow and heat transfer processes and also to provide generalized relationships suitable for preliminary design.

All testing was performed with the condensers in a horizontal orientation. The majority of test units utilized quartz walls for the condensation region to enable visualization of the flow. High speed (4000-8000 frames per second) motion pictures were taken of jet condensers during steady-state and transient operation. Single frame sequences from these films are included in this report.

ACKNOWLEDGMENT

This work was conducted for the National Aeronautics and Space Administration during the period from November 1960 to May 1962. Overall administration was provided by Mr. W. Scott of the NASA Washington Office. NASA technical direction was provided by Mr. S. Lieblein of the Lewis Research Center.

CONTENTS

CONTENTS (Continued)

CONTENTS (Continued)

ILLUSTRATIONS

ILLUSTRATIONS (Continued)

ILLUSTRATIONS (Continued)

ILLUSTRATIONS (Continued)

NOMENCLATURE

Symbol	Parameter	Units (unless otherwise noted in text)
A	Area	ft^2
$\mathring{A}_1$	Area ratio of injector to tube inlet	
$\mathring{A}_2$	Area ratio of injector to throat	
$\mathring{A}_{th}$	Area ratio of throat to tube inlet	
C_d	Discharge coefficient	
C_p	Specific heat of liquid	BTU/lb^oF
d	Diameter	ft
g	Constant = 32.2	$(lbm/lbf)(ft/sec^2)$
h_{fg}	Heat of vaporization	BTU/lb
H_j	Jet condenser ideal power output	kw
H_j'	$(1 - 1/\Delta\mathring{P}_\ell)(\Delta\mathring{P}_v\mathring{m}_R)$	
K_d	Diffuser loss coefficient	
L	Length	ft, in
$\dot{m}$	Mass flow rate	lb/hr
$\mathring{m}_R$	Ratio of injected liquid mass flow to vapor mass flow (saturated vapor flow for quality less than unity)	
$\mathring{m}_R^*$	Mass flow ratio for $T_{\ell e} = T_{vo}$	
P	Pressure	psi(a)
ΔP_a	Pressure rise from jet condenser inlet to outlet	psi(d)
ΔP_i	Pressure drop across injector	psi(d)
$\Delta\mathring{P}_\ell$	Ratio of pressure rise, ΔP_a, to dynamic pressure of injected liquid	

NOMENCLATURE (Continued)

Symbol	Parameter	Units (unless otherwise noted in text)
ΔP_v°	Ratio of pressure rise, ΔP_a, to dynamic pressure of inlet vapor flow	
$\Delta P_{th\ell}^\circ$	Ratio of pressure rise from inlet to throat to dynamic pressure of injected liquid	
ΔP_{thv}°	Ratio of pressure rise from inlet to throat to dynamic pressure of inlet vapor flow	
Q_R	Heat rejected to liquid jet from condensing vapor	BTU/hr
r	radius	ft
Re	Reynolds number	
T	Temperature, time	°F, sec
ΔT_{sc}	Outlet subcooling = $T_{vo} - T_{\ell e}$	°F
ΔT_R	"Radiator" temperature drop = $T_{\ell e} - T_{\ell o}$	°F
V	Velocity	ft/sec
V°	Ratio of inlet vapor velocity to injected liquid velocity	
$\dot{W}$	Mass flow rate per unit area	lb/sec in^2
X	Distance	ft, in
X_{vo}	Inlet vapor quality	
α	Angle, thermal diffusivity	(°), ft^2/sec
α_t	Turbulent diffusivity for heat	ft^2/sec
β_μ	μ^{th} characteristic root of Bessel's Function, J_o	
η_a	Ratio of measured to calculated pressure rise	
η_i	Ratio of ideal to actual injector pressure	

NOMENCLATURE (Continued)

Symbol	Parameter	Units (unless otherwise noted in text)
ρ	Density	lb/ft^3
ρ_o	Ratio of liquid to vapor densities	
τ_w	Wall shear stress	lb/ft^3
ϕ	Stream potential	ft^2/sec
χ	Jet utilization factor = $(T_{\ell e} - T_{\ell o})/(T_{vo} - T_{\ell o})$	
Ψ	Heat transfer parameter = $\chi V_{\ell o}/V_R$	

Subscripts

o	Inlet of jet condenser, station number
1	Throat of jet condenser, station number
2	Outlet of jet condenser, station number
1,2,3	Multi-tube unit individual tube designations
b	Bulk, boundary
c	Condensation
(calc)	Calculated
d	Diffuser
e	Exit, outlet of jet condenser
i	Injector
j	Jet
ℓ	Liquid
m	Mixed
R	Rankine

NOMENCLATURE (Continued)

Symbol	Parameter	Units (unless otherwise noted in text)
Subscripts		
s	Saturated conditions	
t	Tube	
T	Total (for multi-tube unit)	
v	Vapor	
w	Wall	

1. INTRODUCTION

1.1 Background

The majority of dynamic space power systems currently under development utilize direct condenser-radiators as the heat rejection component. However, problems of startup, system ground testing, two-phase flow in a zero-gravity environment, and multi-tube instability, have resulted in serious interest in the application of indirect condensers (Ref. 1,2). Moreover, the role of indirect condensers in space will become much more prominent as power systems in the megawatt class are developed. For these large power levels, the problems associated with startup and stability of direct condenser-radiators may become more severe. Also, preliminary analyses indicate weight savings may result from the use of an indirect condensing system (Ref. 3 and 4).

In the indirect type of condenser, vapor is first condensed in a jet condenser or compact heat exchanger-condenser, and the heat released by condensation is subsequently rejected in an all-liquid radiator. Schematics of indirect condensing systems employing the jet condenser are shown in Fig. 1.

In the jet condenser, subcooled liquid working fluid is injected into the vapor stream. Physical mixing of vapor and liquid, and subsequent condensation of the vapor occur within a relatively short distance downstream of the region of injection. The resulting condensate-liquid flow circulates through a liquid radiator where the heat absorbed by condensation is rejected. Part of the resulting subcooled liquid is bypassed and injected into the jet condenser. The remainder is returned to the boiler to complete the flow cycle.

The jet condenser component is very compact relative to a direct condenser-radiator or a heat exchanger condenser. Moreover,

1a. Jet circulation pump

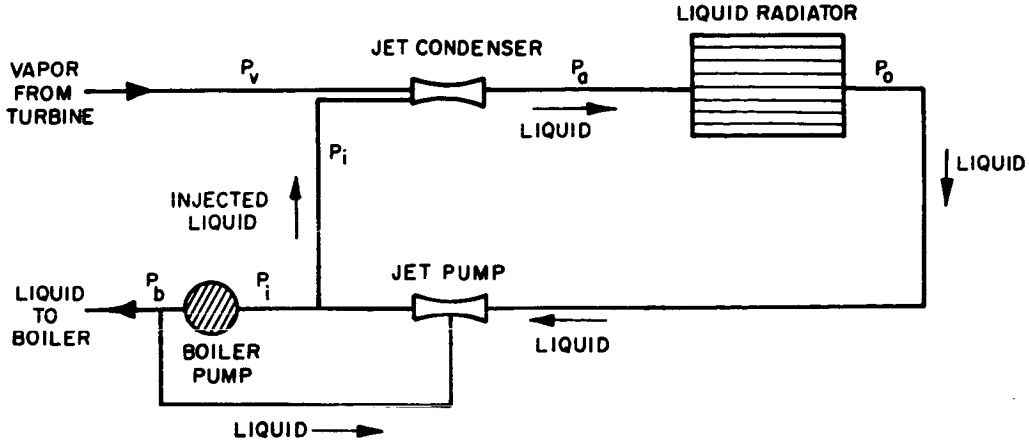

1b. No circulation pump

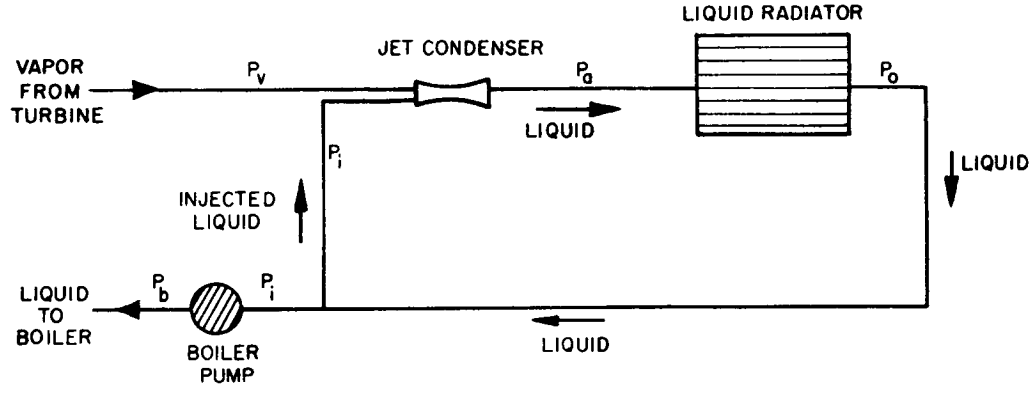

1c. Circulation pump

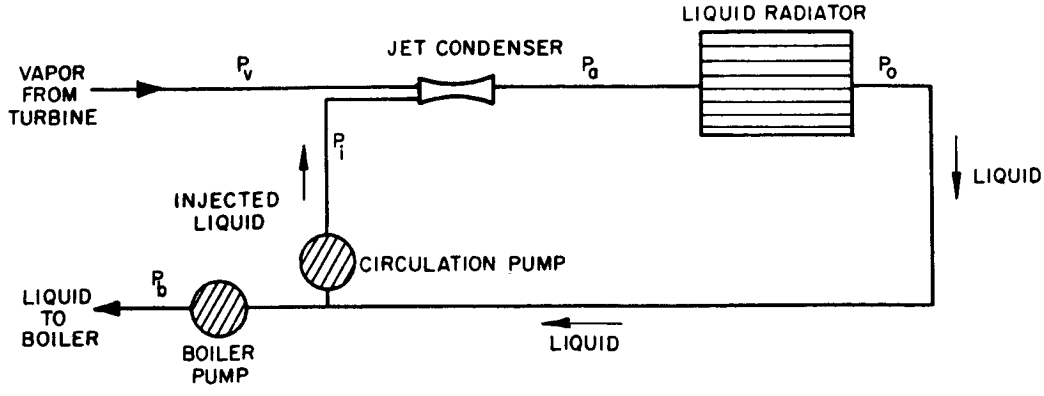

FIG. 1 SCHEMATIC OF INDIRECT CONDENSER SYSTEM USING A JET CONDENSER

this unit may provide significant pressure augmentation to circulate the liquid in the liquid-radiator loop. The amount of pumping power required for the bypass flow would depend on the net pressure drop experienced in the liquid radiator loop ($P_i - P_a$). In particular, for steady-state operation, if the pressure rise in the jet condenser ($\Delta P_a = P_a - P_v$) is equal to the sum of the injection pressure drop ($\Delta P_i = P_i - P_v$), the liquid radiator pressure drop ($\Delta P_{LR} = P_a - P_o$) and the total line-pressure drop ($\Delta P_\ell = P_o - P_i$), no external pressure boost would be required during steady-state operation to circulate the injected liquid flow.

Figure 1 depicts three possible arrangements for a jet condenser system. In the first (1a), a greater flow rate than that required for the boiler is pressurized by the boiler inlet pump. The excess is bypassed and is used in a jet pump to boost the pressure of the liquid by the amount required to effect injection of the required liquid flow rate into the condenser.

In the second system shown (1b), the jet pump is eliminated. This configuration would be feasible if the jet condenser pressure rise were sufficient to maintain circulation in the liquid loop and if stable operation could be achieved in the system.

The third configuration (1c), uses two circulation pumps. This arrangement might be required for applications where valving and controls were not adequate to maintain accurate flow division. Also, startup would probably be simplified over the arrangement in 1a.

The jet condenser appears to have many characteristics which favor its application to space power systems operating on a Rankine cycle. Use of the jet condenser can result in very high condensation rates and therefore a very compact unit. Augmentation of the primary pumping power, stable operation and simple startup techniques are also possible. The jet condenser appears to be insensitive to gravity forces as is the liquid radiator component of this system.

Jet condensers have previously been used in small steam power plants, for boiler feed water circulation (in place of a rotating pump)

and for several process applications (Refs. 5, 6, 7). In addition, use has been made of the basic momentum exchange process for steam ejectors (Ref. 7) to provide thrust and control turbine back pressure in torpedo powerplants (Refs. 8 and 9). However, none of the above applications have resulted in published information which is suitable to determine the required performance characteristics of jet condensers when used with liquid metals. As a consequence, the second phase of the current investigation was initiated to determine jet condenser performance characteristics with a liquid metal, mercury, as a test fluid. The primary objective of the program was to obtain experimental data suitable for preliminary design of a jet condenser in a mercury Rankine cycle power system.

1.2 Principal Results of Previous Work

1.2.1 Results with Water as a Working Fluid

Although jet condensers have been used with steam for 70 to 80 years, analyses or experimental data for the internal flow processes and/or performance characteristics are not widely available. Some of the more significant investigations of steam jet condensers have resulted from their more recent use in torpedoes. High thrust, efficiency, and powerplant control requirements have necessitated more detailed knowledge of operation of these condensers than was required for steam powerplant applications.

Reference 9 reports on one of a series of experimental investigations conducted upon jet condensers to determine their thrust augmentation characteristics for torpedoes. Internal measurements were made of temperature, static pressure, dynamic pressure and momentum in both the vapor and subcooled liquid. Some results of the pressure measurements are presented in Section 2 to illustrate some of the internal flow characteristics. These tests provided very useful information which enables an interpretation of the physical mechanisms and flow processes in jet condensers. However, in general, variables were not extended over a wide enough range to provide design data for other fluids or geometries.

A theoretical analysis of the pressure rise in a jet condenser used to condense turbine exhaust gases ("condensuctor") is reported in Ref. 8. Here the author treats the cases of a constant area mixing chamber and a constant pressure mixing chamber. The effect of noncondensable gases is included in this analysis. The results indicate constant pressure mixing to be superior to constant area mixing if high pressure rise or thrust augmentation is desired.

Earlier investigations at Electro-Optical Systems included an experimental and analytical evaluation of jet or spray condenser performance with steam and water during a six-month program sponsored by NASA (Ref. 4). The particular configuration tested consisted of inclined jets of subcooled water injected from an annulus into a central delivery tube through which steam flowed. The jets impinged at the axis of the tube to produce a stream of subcooled liquid which ranged in character from a highly dispersed spray to a turbulent jet. Test results were found to agree with calculated values of pressure rise to within 80 to 90 percent of theoretical for cases where moderate condensation lengths were involved. Condensing coefficients were obtained which were one to two orders magnitude higher than those reported for film or dropwise condensation. This result is in agreement with qualitative observations of Ref. 9. Another important result of this early work was the demonstration of jet condenser effectiveness in performing the final separation of vapor and liquid independent of gravity. That is, the units tested were operated with both horizontal and vertical upward flow such that gravity did not aid in the final separation of vapor and liquid.

1.2.2 Results with Mercury as a Working Fluid

The only known previous work performed on the use of jet condensers for mercury was conducted at Electro-Optical Systems and is reported in Ref. 4. Pressure rise and heat transfer characteristics of two test geometries were analyzed and results were used to correlate test data obtained for condensing mercury vapor. As with the water testing, the injector consisted of an annular header containing constant diameter

injector holes inclined to produce a conical array of impinging jets at the centerline of the condenser tube. Vapor flowed through a central delivery tube and was condensed in a constant area mixing chamber. A schematic and photograph of these early units are shown in Fig. 2. The internal diameter of the vapor tube was 0.19 inches. Mercury flow rate was varied from about 12 to 25 lb/hr; mass flow ratio of injected liquid to vapor was varied from 7 to 35 and vapor temperatures ranged from 700 to 860°F.

High heat transfer rates were obtained with mercury, as with water. In addition, the experimental pressure rise from vapor to condensate at the outlet agreed both in trend and magnitude with the analysis. The length required for complete condensation of the vapor was correlated using the parameters of the heat transfer analysis. However, the use of impinging jets and the resulting complex flow resulted in a correlation of test results which probably does not possess sufficient generality for design of other geometries. In addition, these units provided relatively poor pressure rise characteristics compared to other geometries.

To summarize, jet condenser principles have been understood and used for a relatively long period of time. However, although general performance characteristics are known, no previous work had supplied experimental data which was sufficient to provide a basis for design of such a component for a space power system using a liquid metal. This is particularly true for the case where such a component is to have a high pressure rise.

1.3 Scope and Objective of Present Program

In order to provide design data for mercury jet condensers, the theoretical and experimental investigations reported in Section 1.2 were extended. Improved injector (central injector) and mixing chamber (convergent) geometries designed to achieve higher pressure rise were tested over a wider range of test variables. Improved and more comprehensive measuring techniques were utilized. While emphasis in the earlier program had been placed upon the attainment of high heat

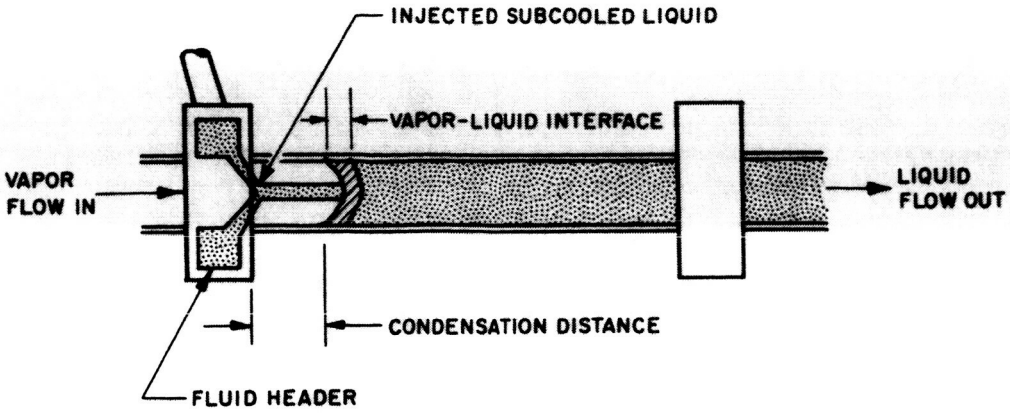

FIG. 2a SCHEMATIC OF EARLY JET CONDENSER GEOMETRIES

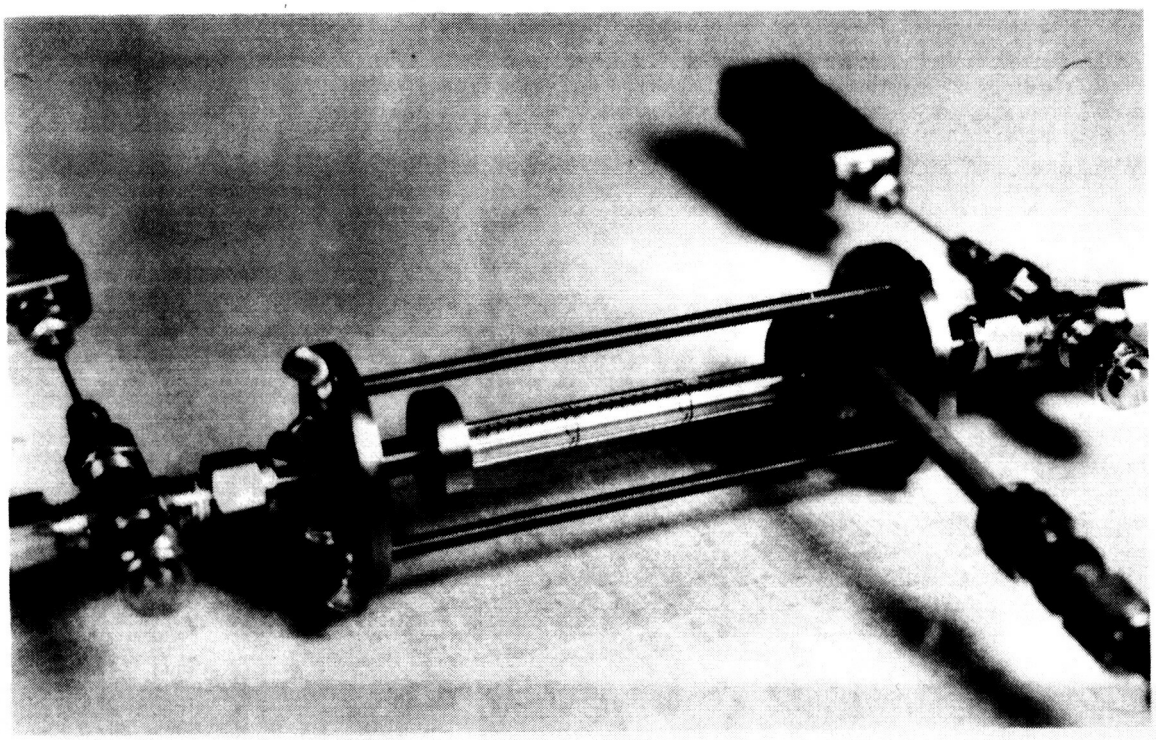

FIG. 2b EARLY JET CONDENSER GEOMETRIES

transfer rates, the present program also considered maximization of vapor to condensate pressure rise. In order to provide a guide in the design of test geometries and selection of the range of variables, additional analyses of pressure rise were performed for these geometries.

1.3.1 Theoretical Analyses

The most important analyses conducted on this program were related to the pressure rise performance of jet condensers. Geometries were conceived and analyzed to maximize the pressure increment from inlet vapor to condensate outlet. Several different special cases of the more general pressure rise equations were considered in order to identify important parameters in the condensation process, as well as to guide testing. Results of one of these cases (constant inlet pressure model) may be useful for extension of test results. Because of difficulties encountered in achieving independent experimental variations of the important operating parameters, use of non-dimensional parameters of the analysis were required to characterize performance.

Other analyses carried out where:

1. An improvement of the heat transfer analysis presented in Ref. 4.
2. An energy analysis which indicates the magnitude of the conversion of thermal energy to pressure energy in jet condensers.
3. Modification of the pressure rise analysis to express the pumping power output of jet condensers in terms of performance parameters.

1.3.2 Experimental Program

The experimental program was intended to provide performance data over a sufficiently wide range of variables and geometries for use in the preliminary design of jet condensers for space power systems. In order to accomplish the above objective, test sections were chosen which, while possessing many geometric features which may be used in a system, also had sufficient simplicity to enable test results to be correlated in terms of more basic flow

and geometric variables. Test performance characteristics then may be used together with results of the analysis to identify some of the more important features of operation of jet condensers. In order to make test results applicable to design, the range of test variables was determined largely by considering mercury space power systems presently being developed (Sunflower, SNAP-2, SNAP-8).

Among the more basic factors to be investigated during the experimental program were:

1. Feasibility and performance of a single central liquid injector.
3. Performance characteristics of jet condensers designed to achieve higher pressure rise.
4. Application of scaling relations to results obtained with smaller geometries.

In order to accomplish the above, several series of tests were conducted. These tests are summarized in Table I. The first series consisted of tests of a central injector-constant area jet condenser. These tests were conducted at flow rates and with other operating variables similar to those tested with impinging injector jet condensers to determine their heat transfer characteristics. In addition, a high speed photographic study was made of the process of interface formation in order to gain insight into physical behavior. The heat transfer results were used to provide information on the variation of condensation length with vapor and liquid flow parameters in order to estimate throat location for the desired operating conditions for variable area jet condensers.

Several (four) converging-diverging jet condenser geometries were fabricated and tested to assess their performance and determine the pressure rise characteristics of each geometry. These jet condensers used central injectors and the same inlet geometry as the constant area-central injector unit previously tested. Results of the constant area testing were, therefore, used to determine throat location

TABLE I

JET CONDENSER TESTS

Test Unit(s)	Purpose
1. Constant-Area Central Injector (0.19" vapor inlet diameter, Test Sections 1 and 2)	Determination of feasibility of a central injector. Data on changes of condensing distance and pressure rise as operating parameters are varied. Study of time-history of interface formation.
2. Converging-Diverging Central Injector (0.19" vapor inlet diameter, Test Sections 3, 4, 5, and 6)	Determination of feasibility of the use of the converging-diverging geometry to obtain higher pressure rise. Comparison of heat transfer and pressure rise data with constant area test unit. Data to enable an estimation of performance of converging-diverging units in larger systems.
3. Converging-Diverging Central Injector (0.75" vapor inlet diameter, Test Sections 7 & 8)	Provide design data over a range of variables for a larger geometric size where better dimensional control was available. Investigation of gravity effects(if any) on performance of a larger unit. Comparison of performance with smaller units. Investigation of the effect of a constant area throat on range of operation and/or performance. Preliminary investigation of scaling.
4. Multitube Jet Condenser (3 units, 0.43" vapor inlet diameter, Test Section 9)	Determination of feasibility of manifolding jet condensers. Evaluation of changes in performance and/or stability characteristics when manifolded.

for these geometries (where little freedom in the variation of condensation distance was possible). These units were tested over a wide range of variables to determine their pressure rise, heat transfer, and stability characteristics. In addition, one test section was operated to the maximum pressure rise which the test loop was capable of containing in order to ascertain if there were any inherent limit in pressure rise imposed by the jet condenser component itself.

The results of testing of these smaller diameter geometries (together with analysis) were used to design two larger test units. The large geometries utilized the full vapor and liquid flow capacities of the test loop. These units were tested over a wide range of variables in order to substantiate the validity of the scaling techniques used. Pressure rise, heat transfer, and stability of these units were examined. High speed motion pictures were taken to provide an insight into the internal flow processes.

In addition, since the larger geometric size of these units permitted more consistent jet alignment and better relative dimensional tolerances; tests were conducted in order to compare experimental results with analytical predictions. Variations in density ratio were made in order to maximize vapor velocity and provide results which may be applicable to other fluids. Results were correlated and analyzed and are presented in the form of design relationships, suitable for preliminary design of a jet condenser. In addition, transient behavior of the jet condenser for sudden changes in interface location during startup and shutdown were recorded.

A multitube jet condenser was fabricated and tested in order to determine the feasibility of manifolding several small units to condense a large vapor flow. Three identical units, which were based on the design of previous test sections, were operated in the 10 kw test loop. Results were obtained which indicate some changes in performance characteristics compared to single units.

The experimental portions of this program were not intended to supply information for the design of a jet condenser for

one specific requirement nor were they intended to provide basic information on the internal flow processes. Rather, the results are intended to provide a general background of jet condenser performance characteristics, so that a rational basis will be available for preliminary design of these devices for space power systems.

2. GENERAL DISCUSSION

The main purpose of the following discussion on internal flow processes is to suggest a model for the physical behavior of jet condensers which can be used as a basis to interpret and evaluate results of the analysis and experiments. In addition, some of the more important performance parameters and variables are summarized in Sections 2.2 and 2.3 to provide the designer with an understanding of these quantities and how they relate to jet condenser operation in a system.

2.1 Internal Flow Processes

Schematic illustrations of two types of jet condensers are presented in Fig. 3. Many possible variations of injector, mixing chamber, and throat geometry exist. However, this figure presents two simple geometries, converging-diverging and constant area, similar to those investigated on this program.

Vapor flows from left to right and enters the condenser at Station 0. At that location subcooled liquid is also injected in the form of a central jet. Vapor and liquid flow concurrently through a mixing chamber with simultaneous mass transfer, heat transfer and momentum exchange occurring. Finally, with sufficient heat exchange between vapor and subcooled liquid, at some location within a throat (or the mixing chamber) complete condensation of the vapor will occur.

In a closed cycle system the resulting liquid flow is subcooled in a liquid radiator. A portion is returned to the boiler to generate vapor, while the bulk of the flow (now subcooled) is injected into the condenser (cf. Section 1).

A complete description of the physical mechanisms of heat, mass, and momentum transfer across a vapor-liquid interface is currently not available, even for the case of a non-flowing system with moderate rate processes, such as dropwise or film condensation on a wall. For

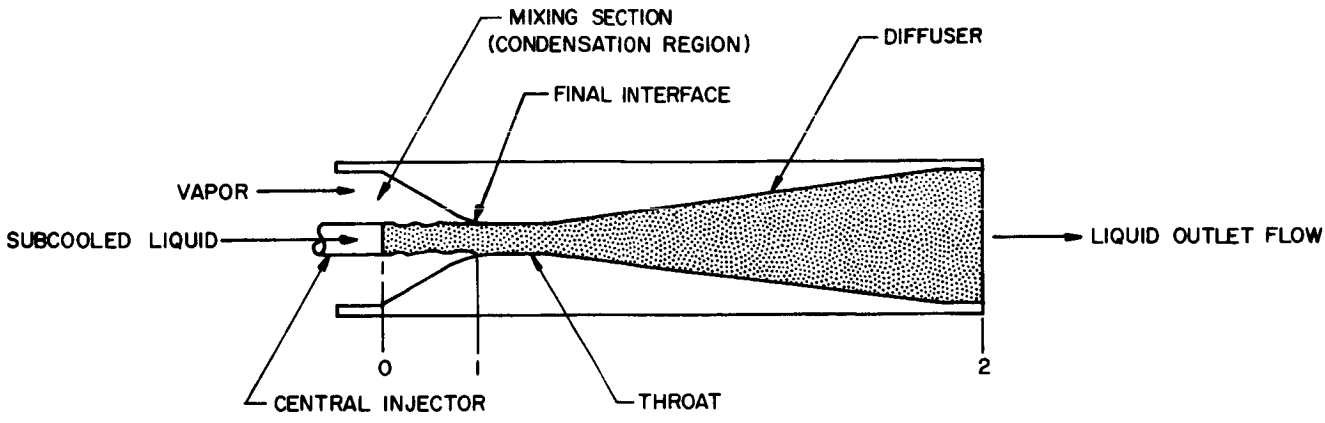

3a Variable area (converging-diverging) jet condenser

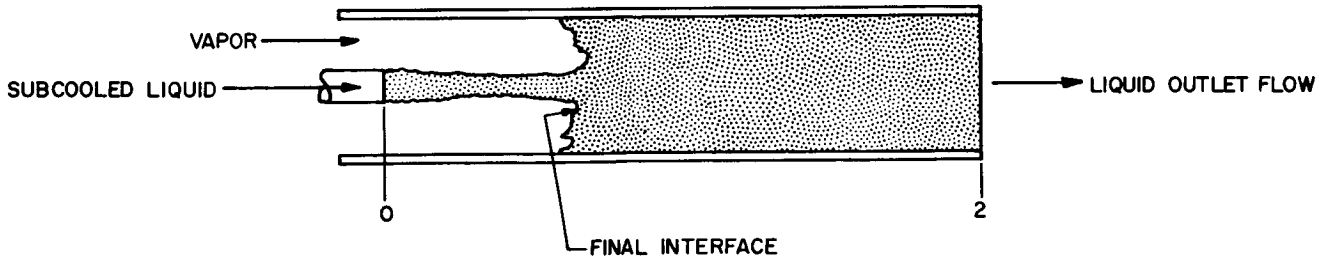

3b Constant area jet condenser

FIG. 3 SCHEMATIC OF JET CONDENSER GEOMETRIES

the jet condenser, further complications arise due to the presence of turbulent flow and very high transfer rates. In fact, the vapor-liquid "interface" is probably not a distinct boundary, but instead is a narrow region containing both phases. However, some insight into these phenomena can be obtained by considering some features of the flow within each phase.

2.1.1 Vapor Transport

The transport of vapor from the main flow stream to the subcooled liquid jet is primarily a result of the pressure difference from the main vapor stream to the subcooled liquid boundary. For a free boundary with no net mass transfer, the vapor pressure at the boundary must be in equilibrium with the saturation pressure of the liquid phase (neglecting surface tension effects). That is:

$$P_{vb} \approx P_{\ell b} \approx P_s\,(T_{\ell b}) \qquad (1)$$

Very strong pressure gradients within the vapor are likely to occur at the initial location of injected liquid. Here, the liquid is at the lowest temperature in the mixing chamber and the corresponding saturation pressure is lowest. Thus a rather strong interaction with the vapor flow and correspondingly, high initial condensation rates are possible. The maximum vapor flow rate which can be condensed on the jet at this point is determined by the jet area and the sonic velocity of the vapor (Ref. 10). However, as vapor is condensed on the jet, the heat released by condensation results in raising the jet temperature and liquid saturation pressure. Hence the pressure difference between the main vapor stream and the liquid jet is reduced, and the flux of vapor to the jet decreases.

The decrease of the pressure gradient of the vapor would modify both the vapor flux and the shape of the vapor streamlines. For example, Figure 4 is a schematic representation of a typical axial distribution of vapor condensation (Ref. 11) and a construction of the corresponding vapor streamlines, resulting if the jet is treated as an idealized mass sink. The entering streamlines which are close to the

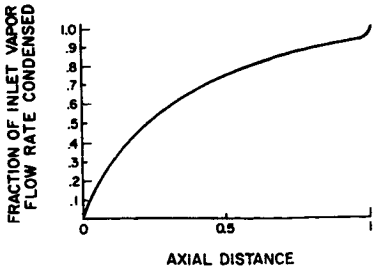

FIG. 4

TYPICAL DISTRIBUTION OF VAPOR CONDENSATION AND IDEALIZED REPRESENTATION OF VAPOR STREAMLINES

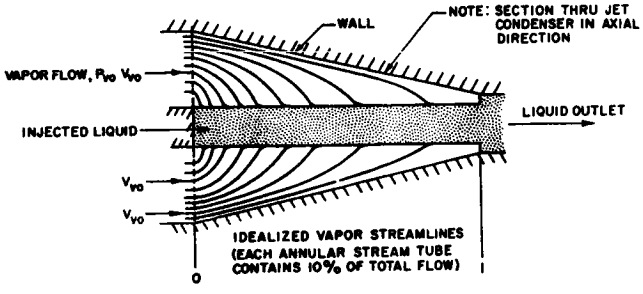

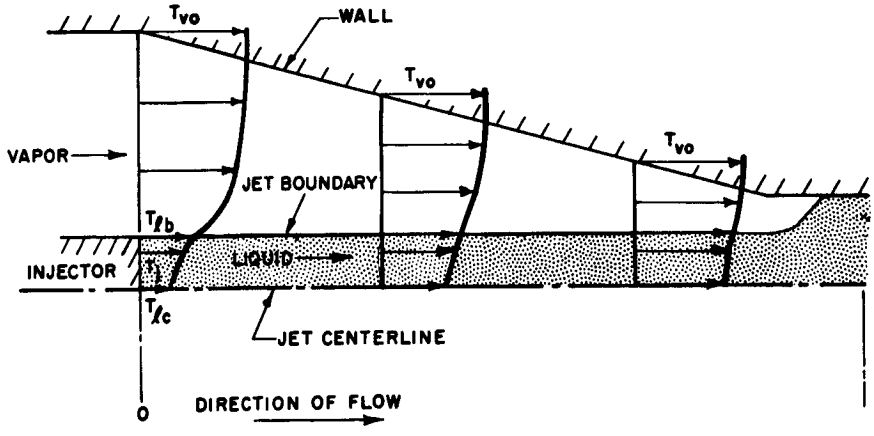

FIG. 5 IDEALIZED TEMPERATURE PROFILES IN JET CONDENSER (Constant vapor temperature at wall)

jet are strongly affected and would probably merge into the liquid phase at steep angles, within a relatively short axial distance. Those further from the jet are less influenced by the local liquid surface pressures and gradually merge with the liquid phase. In this figure, the streamlines appear to terminate, since the jet was represented as a mass sink. However, in the actual case the vapor particles become liquid particles and the streamlines continue within the liquid phase.

An increase in the temperature of the liquid jet at the surface (which tends to reduce the condensing vapor flux) will result as the bulk or mixed cup temperature of the jet increases due to heat addition from the condensing vapor. A temperature gradient within the jet is required to remove the heat of condensation released at the surface; thus the surface temperature will be greater than the bulk temperature for heat transfer into the jet.

These effects are illustrated in Fig. 5, an idealized representation of the vapor and liquid temperature gradients at different axial locations in the mixing chamber. The initial temperature field (at 0) consists of a large local temperature (and pressure) gradient in both the vapor and liquid near the interface. However, as heat is transferred, due to condensing vapor, the bulk temperature, T_j, is raised and the temperature gradient within the liquid phase decreases. The temperature at the jet surface, $T_{\ell b}$, is probably increased, as the vapor temperature gradient decreases. Finally as complete condensation of the vapor is approached, the bulk temperature of the fluid approaches its final value. The difference in free stream vapor pressure, P_{vo}, and the saturation pressure for the bulk temperature, $P_s(T_j)$, may still be a significant quantity. However, the surface temperature of the jet, $T_{\ell b}$, must be greater than the bulk temperature, T_j, to transfer heat to the interior. Therefore, the local vapor pressure difference, $P_{vo}-P_s(T_{\ell b})$, may be very small, with resulting low values of local condensation rate.

2.1.2 Heat Transfer in Liquid Jet

The heat transfer from the liquid surface to the interior is a combination of both conduction and turbulent exchange within the liquid. For fluids having lower values of thermal diffusivity, such as water, turbulent transfer of heat is probably the dominant mechanism. However, both modes of heat transfer may be important in liquid metals, where the higher values of thermal diffusivity are experienced.

The capacity of any given portion of the injected liquid to absorb heat is related to the time it spends in contact with the vapor. That is, a particle of liquid spending an infinite period of time in the vapor will eventually absorb the amount of heat which raises its temperature to the temperature of the vapor. If the velocity of the injected liquid is specified, the residence time of liquid in vapor is proportional to the length from the point of injection to the final vapor-liquid interface. Therefore, an analysis of the transient heat transfer process occurring within the jet can be performed (with the proper simplifying assumptions) which expresses the heat absorbed in the jet (or condensation rate) as a function of axial distance traversed in the condenser (cf. Section 3).

2.1.3 Pressure Distribution and Interface Formation

The condensation of vapor upon the liquid jet produces a sizable conversion of thermal energy to mechanical energy (pressure or velocity head). This conversion process has been demonstrated both by analysis and experiments (cf. Sections 3 and 5). The question may then be raised as to what effect the addition of this mechanical energy has upon the shape and character of the injected liquid. Moreover, what force mechanisms are present to produce all-liquid flow at the outlet when stratified vapor-liquid flow occurs upstream?

Qualitative answers to both questions may be postulated by considering the momentum exchange process, previous work on the stability of jets, and previous internal measurements made across vapor-liquid interfaces.

For the case where large condensation rates occur, Equation (1) must be modified to account for momentum exchange from the vapor to liquid. For a liquid surface which is not accelerating in the direction of vapor flow, it can be shown that:

$$P_{\ell b} - P_{vb} \sim \frac{\dot{W}_c V_c}{g} \qquad (2)$$

Hence, if the net local condensation flux(per unit area), $\dot{W}_c$, and vapor condensation velocity, V_c, are very high, such as may occur at the inlet

regions, the liquid pressure at the jet boundary may be maintained at significantly higher values than the vapor pressure at that location. However, at downstream locations, $\dot{W}_c$ and V_c may decrease to the extent that the pressure of the liquid at the surface is nearly equal to the vapor pressure at the surface. At these locations the jet pressure at the surface will probably never be greater than the free stream vapor pressure (which is nearly the pressure of the liquid jet as it enters the mixing region). Thus the following set of circumstances exist: significant amounts of vapor thermal energy have been converted to mechanical energy and added to the jet by the time it reaches downstream portions of the mixing chamber; however, the surface pressure of the liquid jet is no greater than, and probably less than the initial jet pressure.

These two apparently contradictory statements are compatible if one of several flow phenomena occur:

1. At downstream stations, liquid within the jet interior may be at higher pressures than the liquid at the jet surface (a positive radial liquid pressure gradient).
2. The entire jet may be accelerated to a velocity greater than the initial velocity.
3. Local portions of the jet at the surface could be accelerated to higher axial velocities and lower pressures than the main body of the jet.

In the actual internal flow of jet condensers of the types described, all three of these flow situations will probably occur simultaneously. However, it may be profitable to examine the physical significance of each, individually.

An internal pressure distribution within a free liquid jet with condensation has been determined experimentally. Reference 9 reports static pressure and temperature probes within a jet condenser which consisted of an annular water jet (in air) surrounding a steam cavity. Figure 6 gives the approximate vapor cavity contour (as

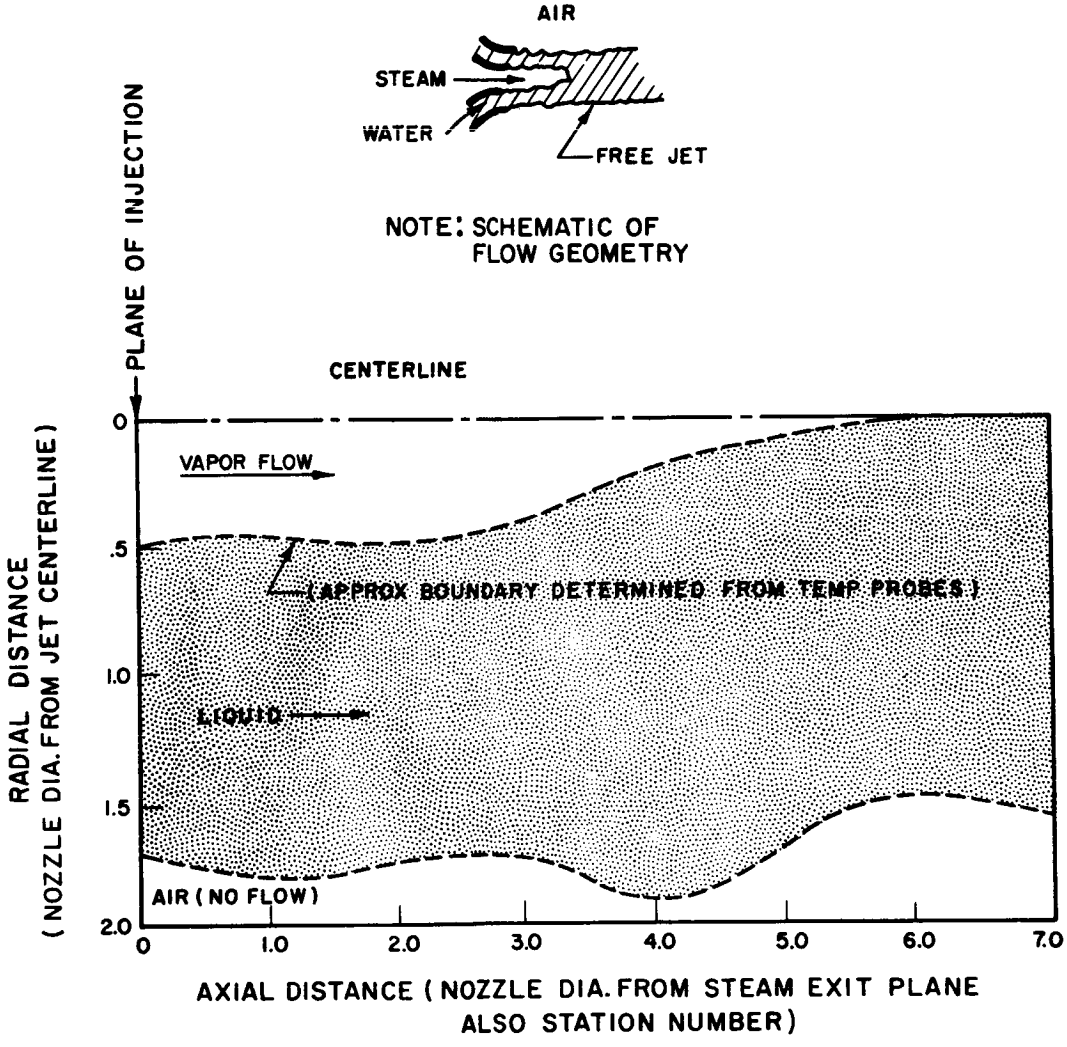

FIG. 6 VAPOR CAVITY CONTOUR IN STREAM JET CONDENSER (Water injected in an annulus) (From Ref. 9)

established by temperature probes) and Figure 7 reproduces the radial pressure distributions at several axial locations from the injector. The approximate locations of the vapor and liquid phases are indicated by the dashed lines.

It is of interest to note the static pressure distributions for axial Stations 2-5. An approximately constant radial pressure profile exists within the vapor phase. However, the pressure increases steeply from the liquid-vapor interface to the colder portions within the liquid phase.

The pressure distribution at the first station has particularly interesting features. At this location (where high condensation rates prevail) a sizable radial pressure gradient occurs within the vapor, in the direction to induce a component of vapor flow towards the subcooled liquid. However, at the liquid surface a very steep gradient in the opposite direction occurs, which results in the liquid pressure at the surface, $P_{\ell b}$, being higher than the pressure in the colder parts of the jet, $P_{\ell i}$. That is, if Equation (2) is applicable, $\dot{W}_c$ and V_c are very high at the entrance and, $P_{\ell b} \gg P_{vb}$ and $P_{\ell b} > P_{\ell i}$.

The most significant implication of the occurrence of a radial pressure gradient within the liquid, is that it provides a force mechanism for forming the final vapor-liquid interface. As a result of the radial liquid pressure gradient, the liquid flow acquires a radial component. This can be seen from the figures shown. At station 1 a strong radial liquid pressure gradient occurred in the outward direction (away from the vapor cavity). Examination of Fig. 6, the observed contour of the vapor cavity, reveals that the cavity opened somewhat after station 1. On the other hand, the downstream stations exhibit radial liquid pressure gradients toward the vapor. Inspection of the contour shows the cavity to be closing at these stations.

For the case of a jet condenser with a central liquid jet the following steps in the formation of the final interface are postulated and are illustrated by Fig. 8:

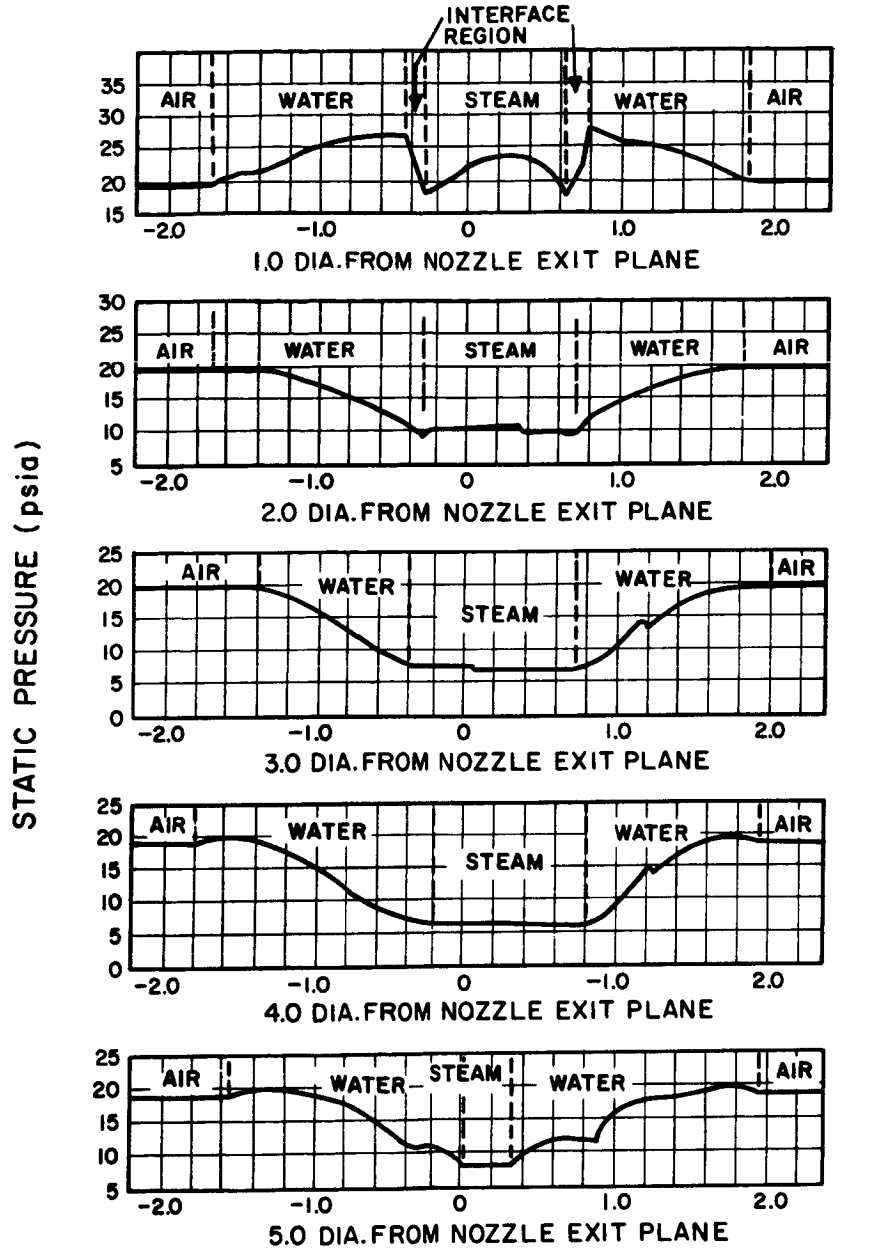

FIG. 7 STATIC PRESSURE DISTRIBUTION IN JET CONDENSER OF FIG. 6 (From Ref. 9)

1. At the point of injection , rapid condensation upon the liquid jet occurs. This results in a negative radial liquid pressure gradient, which in turn results in a reduction in the jet radius and produces surface waves which may or may not be amplified by the interaction of the vapor stream with the surface (station 1).
2. As condensation on the jet occurs, the jet temperature increases in the axial direction, suppressing condensation in the downstream regions.
3. As lower condensation rates occur, the liquid surface pressure is reduced to be more nearly equal to the vapor pressure, due to the decrease in the flux of vapor momentum received by the jet. This results in the establishment of a positive radial pressure gradient in the liquid (station 2).
4. The positive radial pressure gradient in the liquid results in a radial flow component in the liquid which tends to reduce the vapor flow area and fill the condenser flow passage.
5. When the passage is filled, the walls result in the establishment of a uniform radial pressure profile within the liquid.

It should be noted that the jet profile sketched in Fig. 8 was taken from a single frame of Fastax motion pictures (8000 frames per second) taken of a jet condenser operating with mercury (cf. Section 5).

The latter two flow phenomena (accelerating jet and high surface velocities) occur when the mechanical energy of the jet is increased by increasing liquid kinetic energy. Increasing the liquid velocity provides a means whereby the average total pressure

$$\left[\frac{1}{r_b}\int_{b}^{r_b}\left(P_\ell + \frac{\rho_\ell V_\ell^2}{2g}\right)dr\right]$$

of the jet may be increased when the liquid pressure at the boundary is equal to vapor pressure. This behavior may predominate whent the liquid phase is injected at lower velocities and is initially very subcooled. The jet then is accelerated and reduced

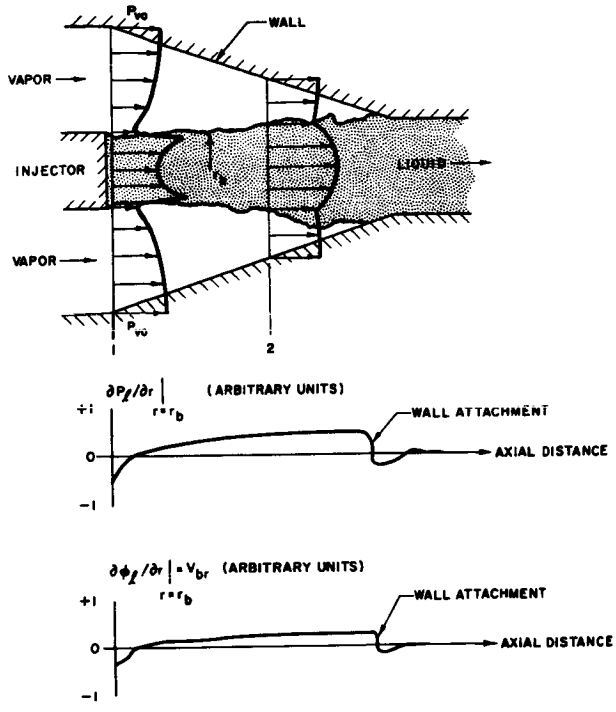

FIG. 8

SCHEMATIC ILLUSTRATION OF THE DEVELOPMENT OF RADIAL PRESSURE GRADIENT AND FLOW COMPONENTS IN A JET CONDENSER

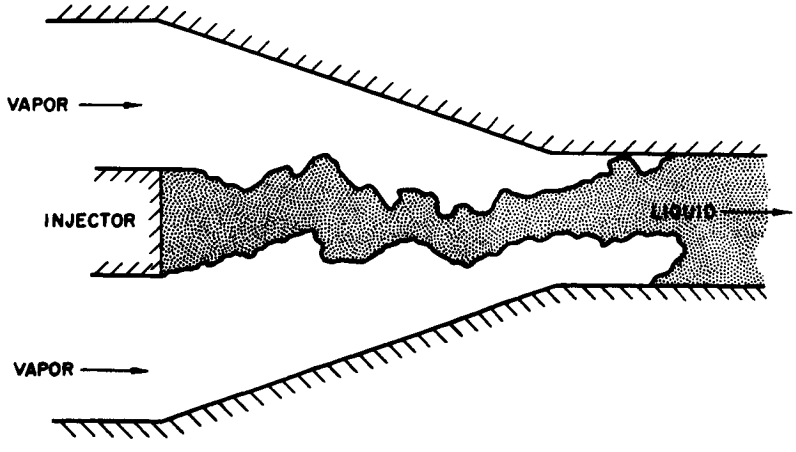

FIG. 9 JET CONDENSER OPERATION WITH LOW LIQUID FLOW VELOCITY AND HIGH INITIAL SUBCOOLING

in area and becomes varicose. Surface waves are formed and are rapidly accelerated to high velocities by the vapor shear and condensation forces. This general situation is illustrated in Fig. 9, (which is taken from a high speed motion picture of a jet condenser operating with lower liquid velocities than those of Fig. 8).

The high heat transfer rates and large pressure gradients (relative to condensation on a wall) occurring in jet condensers, result in a final separation of the vapor and liquid which is not strongly influenced by gravity body forces. This is particularly true if the final expansion of the jet required to fill the flow passage is small. The positive separation results in single phase flow out of the mixing section or throat. Therefore, effects of the increase in mechanical energy of the liquid can be treated in a conventional manner downstream of the interface.

2.2 Identification of Performance Parameters

The internal flow processes described in the preceding section are characterized by overall performance parameters which, in general, must be known for preliminary design of a jet condenser heat rejection system. The more important of these parameters (from the standpoint of system design) will be identified and discussed in this section. The influence of geometry and flow conditions upon these parameters will be indicated in the following section.

Condensation Length

The length required for complete condensation of the inlet vapor flow is an important operating parameter. Lower values of condensation length are a result of higher condensation rates and provide a smaller, lighter weight jet condenser. For a given geometry, information on the variation of condensation length with flow conditions is required to ensure that condensation occurs within a prescribed distance downstream of the injection plane. In addition, there are regimes of operation where condensation distance is very sensitive to flow perturbations. These regimes must be known and avoided for stable condenser operation.

Mass Flow Ratio

For a given set of operating conditions the mass flow ratio of injected liquid to condensing vapor must be known to enable accurate flow division for closed cycle operation. In addition, the value of mass flow ratio strongly influences the pumping power, liquid radiator temperature drop, start-up characteristics, and fluid inventory.

Liquid Radiator Temperature Drop

The temperature rise from injected liquid to the liquid at the outlet of the jet condenser is nearly equal to the temperature drop across the liquid radiator in a jet condenser heat rejection system. Operation with larger values of this temperature difference means a large temperature drop would have to occur through the radiator, which would result in an average radiating temperature lower than vapor temperature. Since heat rejection from that component to space is proportional to its temperature to the fourth power, higher values of temperature drop require larger areas for the liquid radiator and vice versa.

Outlet Subcooling

The jet condenser must always have some terminal temperature difference (as must any heat exchanger) from vapor to liquid to effect the transfer of the total heat released by the condensing vapor to the injected liquid, within a finite distance. The amount of subcooling required has an important effect on the average temperature level and on the area of the liquid radiator component. Smaller values of outlet subcooling result in the inlet temperature to the radiator being nearly equal to vapor temperature (the highest temperature possible) which results in the smallest liquid radiator. The outlet subcooling is also related to the excess mass flow ratio required above the mass flow ratio which would be required if the condenser could be operated with outlet temperature equal to vapor inlet-temperature. For a given value of radiator temperature drop, lower values of excess mass flow ratio also imply smaller liquid radiators.

Pressure Rise from Inlet Vapor to Liquid Outlet

One of the most significant features of jet condenser operation is the occurrence of a pressure rise through the condenser. Proper design of a jet condenser produces a pressure rise due to conversion of vapor thermal energy and recovery of the injected liquid dynamic pressure. This pressure rise characteristic obviates some of the problems associated with pressure drop in direct condensers. Under favorable circumstances, it may be possible to utilize this pressure rise to augment or even replace the liquid loop circulating pump in a Rankine cycle system. This pressure rise in itself is important to system design. However, several other performance parameters are required to fully evaluate the pressure augmentation performance of a jet condenser.

The ratio of pressure rise to vapor dynamic pressure provides a convenient non-dimensional reference for the pressure rise. For a fixed set of vapor inlet conditions, this parameter is directly proportional to the absolute magnitude of the pressure rise.

The theoretical pressure rise in a jet condenser can be readily calculated based on appropriate models for the wall pressure distribution in the geometries used (cf. Section 4.4). Comparison of the actual pressure rise to that calculated for this model provides a basis for extending results to other geometries and flow conditions.

Ratio of Pressure Rise to Injected Liquid Dynamic Pressure

For a perfect injector (discharge coefficient of unity and no losses) this parameter expresses the ratio of pressure rise to the pressure drop required to inject liquid into the jet condenser.

Values of this ratio which are equal to or greater than unity mean no net pumping power would be required to operate the jet condenser if no other pressure drop losses (such as line or liquid radiator losses) occurred through the rest of the system.

Jet Condenser Power

For all real applications, the net pumping power required to operate the jet condenser system must be determined. This will include

line losses, liquid radiator pressure drop, and the pressure drop (if any) required to operate the jet condenser. The net power output of the jet condenser which is available for liquid loop circulation is defined as the jet condenser power. For many applications this term may be positive; that is, the jet condenser contributes power to the circulation of the liquid which is in excess of that required to operate the condenser itself. The device then becomes a combination condenser and vapor driven pump.

Performance of the jet condenser with high values of power output has an influence on the weight optimization and reliability (if the circulating pump were eliminated) of a jet condenser system. Negative or low values of power output could result in a large pumping power weight penalty required to operate such a system. This penalty would indicate use of lower injected liquid flow rate and hence higher radiator temperature drop. Positive values of jet condenser power mean the liquid radiator could be operated with high circulation rates (low values of radiator temperature drop) without sizable pumping power penalties.

2.3 Principal Variables Controlling Performance

2.3.1 Geometric Variables

Several geometric variables must be considered in the design of a jet condenser. Among these are injector type, mixing chamber geometry, throat and diffuser geometry. A general treatment of the more important effects of these variables will be presented.

Injector

Perhaps the most fundamental consideration in design is the type of liquid injector to be used. Injectors may range from very simple geometries (central liquid delivery tube surrounded by vapor delivery tube) to more complex (multiple impinging jets or swirl nozzles). In any event, the fundamental characteristic behavior of any type must be related to the desired performance. For example, efficient pressure recovery in a jet condenser is favored by a coherent, axially directed,

liquid stream, such as that produced by a central injector. However, injected liquid in this form presents a relatively small surface for condensation. On the other hand, rapid condensation would be promoted by a finer dispersion of the liquid phase, such as might be produced by impinging jets. However, kinetic energy of the injected liquid must be expended in an irreversible manner in the liquid breakup processes. Consequently, the available pressure rise is decreased by using this type of injector. In a preliminary design, some type of compromise would probably be made, depending upon the weight to be given various operating characteristics.

Mixing Chamber Geometry

The two basic types of mixing chambers considered were the converging and the constant area geometries. Greater stability, higher pressure rise and higher condensation rates usually will result from the use of a converging geometry. However, a constant area geometry can provide for greater variation in condensation length without a severe change in operating characteristics. The effects of wall contour for the converging geometry are not understood at present. An estimate of the contour can be made if some criterion such as constant vapor pressure or constant vapor velocity is adopted. However, any results would probably not be meaningful in terms of the actual flow. In general, however, for a given condensation distance, the transition from initial vapor flow area to the area at the throat should probably be gradual and avoid sudden changes in flow area which might produce separation of the boundary layer.

Throat-Diffuser Geometry

For the case of a constant area jet condenser, the throat becomes identical to the mixing chamber and no significant requirements may exist for a diffuser. However, for a converging mixing chamber, the interface will probably be located in a constant area throat. The flow area of the throat should be nearly the same as that of the injected liquid for efficient pressure recovery and maximum stability. Losses and fluctuations which would result from the rapid expansion of

liquid flow area at the location where the final interface is formed would be eliminated.

Provision of a throat with a constant area length results in a geometry which may accommodate changes or fluctuations in condensation length without seriously affecting overall performance. Design of the diffuser is dependent upon the circulation velocity and pressure desired for the outlet liquid. Diffuser angles and contours can be chosen from standard single phase flow theory.

2.3.2 Flow Variables

Several flow variables were presented as performance parameters in Section 2.2. In this section, therefore, the discussion will be centered on the general effects of these and other flow variables upon condensation length, L_c, and pressure rise, ΔP_a. Among the more important of these variables are inlet liquid velocity, $V_{\ell o}$, inlet vapor velocity, V_{vo}, inlet vapor pressure, P_{vo}, outlet subcooling, ΔT_{sc}, and mass flow ratio, $\overset{o}{m}_R$.

Liquid Velocity

The velocity of the injected liquid is very important in determining both the condensation length and pressure rise. Lower liquid velocities produce a greater residence time of liquid in vapor for a given condensation length. For a given condensation length, lower liquid velocities may reduce the outlet subcooling and for the same amount of heat transfer, shorter condensation distances are possible. However, use of a lower liquid velocity (or mass flow ratio) results in a lower total pressure rise (although the jet condenser power output may increase).

Vapor Velocity

High values of inlet vapor velocity are very desirable in jet condensers. Higher velocities promote physical mixing of the vapor and liquid which effects higher condensation rates. In addition, both the total pressure rise and jet condenser power output increase with increasing vapor velocity.

Vapor Pressure

The vapor pressure at the condenser inlet will generally be fixed by the design vapor inlet temperature. However, it should be noted that higher vapor pressures (and densities) result in increased condensation rates (shorter condensation distances). For the same vapor velocity, higher values of vapor pressure also result in higher pressure rises.

Outlet Subcooling and Radiator Temperature Drop

The ratio of these two parameters has probably the most direct effect upon the condensation length. The more subcooled the liquid is, with respect to the overall temperature rise of the injected liquid, the greater is the driving potential for heat transfer. Thus, the smaller values of the ratio $\Delta T_{sc}/\Delta T_R$ produce longer condensation lengths and vice versa.

To summarize, the discussion of jet condenser operation and performance characteristics has necessarily been simplified due to lack of knowledge of the internal flow processes. Experimental information on performance will be presented later in Section 5. However, this section has attempted to present a general understanding of the more important operating principles and characteristic performance of jet condensers which will serve as guide in evaluating and interpreting test results.

3. THEORETICAL ANALYSIS

Analyses of the internal heat transfer and overall pressure rise characteristics of jet condensers were conducted during this program. The limited information available on the internal flow processes has the effect of limiting the accuracy of performance calculations. However, an indication of the important non-dimensional variables as well as approximate values of performance parameters have resulted from this effort.

3.1 Constant Area Pressure Rise Analysis

The first configuration considered for analysis was that of a constant area jet condenser. The pressure rise in a constant area geometry may be explained qualitatively by examining Fig. 3-b. Vapor and subcooled liquid are injected into the test section or condenser at station 0. If the heat exchange is adequate, at some location the vapor will be completely condensed and the flow will be all liquid. The resulting condensate-liquid mixture exits from the test section (station 2). Momentum exchange during condensation of the vapor and the subsequent recovery of the injected liquid velocity head, results in the conversion of vapor and liquid kinetic energy to pressure.

The vapor-liquid interface associated with condensation in a constant area tube is accompanied by a sudden expansion of the liquid flow as in Fig. 3-b. The flow is probably somewhat analagous to a sudden expansion in a pipe in single phase flow. Thus, relatively inefficient recovery of the jet kinetic energy occurs due to the large area ratio for expansion.

The geometry of Fig. 3-b was treated in an analysis which is summarized in Appendix A. The equation for conservation of momentum was applied to a control volume about the condenser. The analysis rests upon the following assumptions:

1. The radial pressure gradient at the inlet and outlet stations is zero.
2. Flow at the exit is homogeneous and in thermal equilibrium.
3. For an inlet vapor quality less than unity no vapor-liquid slip exists in the entering flow.
4. Wall friction within the mixing chamber is negligible compared to the magnitude of the pressure rise.
5. An injector discharge coefficient of unity is assumed.

The final expressions of the analysis were further simplified by considering complete condensation of the inlet vapor flow and by assuming an inlet vapor quality of unity. For these assumptions, the following equations were derived:

$$\Delta \overset{o}{P}_v = 2\left[\left(\frac{\overset{o}{m}_R}{\overset{o}{\rho}}\right)^2 \frac{(1-\overset{o}{A}_2)^2}{\overset{o}{A}_2} + (1 - \overset{o}{A}_2)\right] - \frac{2(1-\overset{o}{A}_2)^2}{\overset{o}{\rho}} (\overset{o}{m}_R + 1)^2 \quad (3)$$

$$\Delta \overset{o}{P}_\ell = 2\left[\overset{o}{A}_2 + \left(\frac{\overset{o}{\rho}}{\overset{o}{m}_R^2}\right) \frac{\overset{o}{A}_2^2}{(1-\overset{o}{A}_2)}\right] - 2\overset{o}{A}_2^2 (1 + \frac{1}{\overset{o}{m}_R})^2 \quad (4)$$

Equation (3) expresses the ratio of pressure rise to the vapor inlet dynamic pressure ($\Delta \overset{o}{P}_v$) in terms of the mass flow ratio of liquid to vapor ($\overset{o}{m}_R$), the density ratio of liquid to vapor ($\overset{o}{\rho}$) and the area ratio of the injector to tube ($\overset{o}{A}_2$). Expressing pressure rise as $\Delta \overset{o}{P}_v$ provides a means for the system designer to conveniently determine the absolute magnitude of the condenser pressure rise (since vapor inlet conditions will usually be prescribed).

Equation (4), which gives the ratio of pressure rise to the injected liquid dynamic pressure ($\Delta \overset{o}{P}_\ell$), provides a significant measure of jet condenser performance from the standpoint of pumping requirements. For an optimum design injector with a discharge coefficient of unity, the latter parameter expresses the ratio of pressure rise to the pressure drop required to inject subcooled liquid into the mixing chamber. If

$\Delta\overset{\circ}{P}_{\ell}$ were equal to unity, no net pumping power would be required to effect the injection of liquid into the jet condenser. The only power consumption would be that required to circulate the liquid through the lines and liquid radiator. Moreover, if values of $\Delta\overset{\circ}{P}_{\ell}$ higher than unity are obtained, the jet condenser can contribute to pumping the liquid through the radiator loop. These equations are plotted in Figs. 10 and 11 for a range of liquid-vapor mass flow ratios and injector to tube area ratios. Lines of constant vapor to liquid velocity ratio are presented for reference.

The curves were determined for a density ratio of liquid to vapor of 2620 which corresponds to that of mercury vapor at 700°F. From Fig. 10, the following conditions can be seen to favor a high absolute value of pressure rise (for constant vapor inlet conditions).

1. A low ratio of injector to tube area.
2. A high ratio of liquid to vapor flow rate.

For a given mass flow ratio, higher values of inlet vapor velocity result in a higher pressure rise. In addition, from Equation (3), high vapor densities (or a low ratio of liquid to vapor density) also result in high absolute values of pressure rise.

Examination of Fig. 11 reveals that opposite trends result in high values of $\Delta\overset{\circ}{P}_{\ell}$ in some instances. That is, conditions favoring a high absolute magnitude of pressure rise may result in smaller values of the ratio of pressure rise to injection pressure drop. From Fig. 11, the following favor a high ratio of pressure rise to injected liquid dynamic pressure:

1. A large ratio of injector to tube area.
2. Low ratios of liquid to vapor flow rate.

Also, from Equation (4), high values of liquid to vapor density ratio tend to increase $\Delta\overset{\circ}{P}_{\ell}$.

Relatively large numerical values of pressure rise coefficient can be obtained for some inlet conditions. For the values of mass flow ratio shown in Fig. 10, the pressure rise referred to vapor dynamic pressure

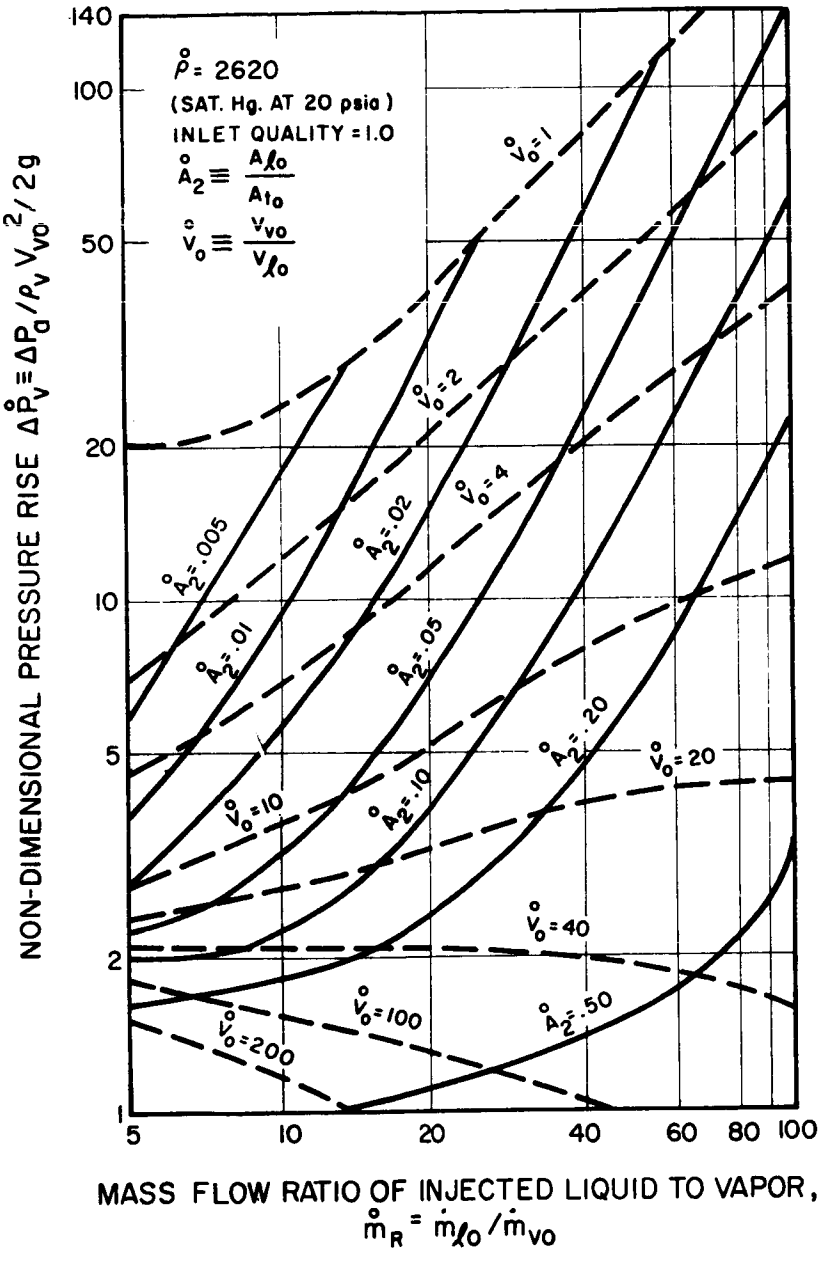

FIG. 10 CALCULATED PRESSURE RISE FOR CONSTANT AREA JET CONDENSER (Referred to vapor dynamic pressure)

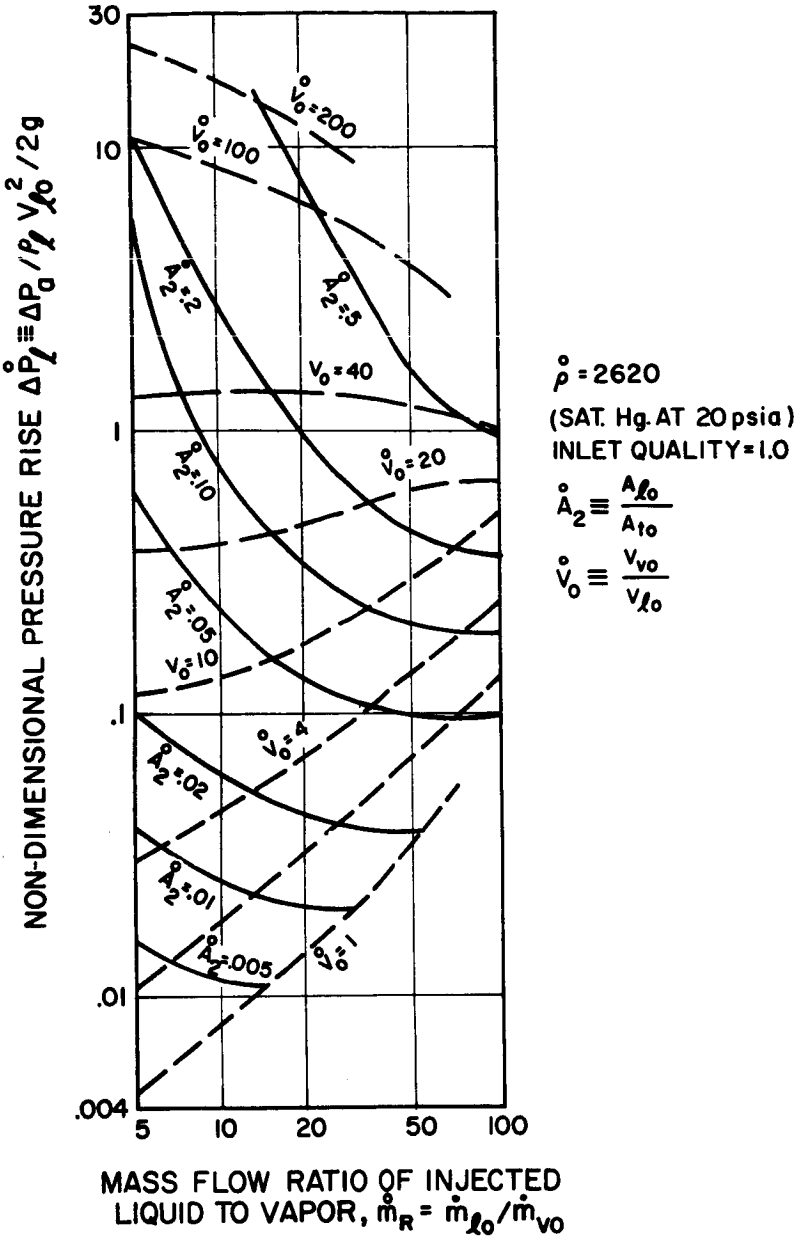

FIG. 11 CALCULATED PRESSURE RISE FOR CONSTANT AREA JET CONDENSER (Referred to liquid dynamic pressure)

attains values as high as 140; i.e., the pressure rise through the condenser would be 140 times that which would be obtained if the dynamic pressure of the vapor were recovered.

However, this magnitude of pressure rise would occur for low values of velocity ratio (approximately one). For realistic values of velocity ratio (approximately 20), a lower pressure rise results. As an example, for a vapor velocity of 300 fps and a liquid velocity of 15 fps with an area ratio of 0.20, Fig. 10 predicts a value for $\Delta \overset{o}{P}_v$ of

$$\Delta \overset{o}{P}_v \equiv \Delta P_a / \rho_v V_{vo}^2 / 2g \approx 3.6 \tag{5}$$

The absolute magnitude of ΔP_a would be

$$\Delta P_a \approx \frac{(0.29)(300)^2(3.6)}{(2)(32.2)(144)} \approx 10.1 \text{ psi}$$

Thus, based on the analysis, it would be possible for this example to add about 10 psi to the condenser inlet pressure of 20 psi.

In order to relate this pressure rise to the pressure drop required for injection, the value of $\Delta \overset{o}{P}_\ell$ must be determined. From Fig. 11 the value of $\Delta \overset{o}{P}_\ell$ for the above flow conditions is given as:

$$\Delta \overset{o}{P}_\ell \equiv \Delta P_a / \rho_\ell V_{\ell o}^2 / 2g \approx 0.56 \tag{6}$$

For a perfect injector,

$$\Delta P_i = \rho_\ell V_{\ell o}^2 / 2g \text{ or } \Delta P_i \approx \frac{10.1}{0.56} = 18 \text{ psi}$$

Since the value of $\Delta \overset{o}{P}_\ell$ is less than unity, some pumping power is required to inject the subcooled liquid to effect condensation and pressure rise.

The main results of the analysis from the standpoint of design trends can be summarized as follows:

1. The non-dimensional parameters in the expressions for pressure rise for constant area jet condensers are: density ratio, mass flow ratio and the ratio of injector area to tube area.

2. High vapor densities and high absolute magnitudes of either inlet vapor velocity or inlet liquid velocity tend to favor high absolute magnitudes of pressure rise.
3. Values of liquid to vapor mass flow ratio and of the area ratio of injector to tube which favor high absolute magnitudes of pressure rise may result in high pumping power requirements for a constant area jet condenser. If a large pressure rise relative to the pressure drop required for injection is desired, then higher ratios of injector to tube area and low values of liquid to vapor mass flow ratio should be used.

3.2 Variable Area Pressure Rise Analysis

Although the above analysis for constant area jet condensers is useful in evaluating experimental performance, the maximum pressure rise potential of jet condensers is not realized in this geometry. A geometry which should produce much higher values of vapor to liquid pressure rise is shown in Fig. 3-a. In this geometry the mixing chamber is contoured to effect condensation with little reduction in the jet velocity at the point of final condensation. Thus, the expansion losses of the constant area geometry are avoided. Moreover, if a diverging section is added for efficient diffusion, the pressure increment added to the vapor should be increased by a large amount over the constant area geometry.

Use of a converging-diverging geometry results in an additional complicating factor in the analysis of pressure rise. Since the mixing chamber geometry has an axial variation of flow area, the integral of the wall pressure must be evaluated in order to apply the conservation equation of momentum. Due to a lack of information for the internal pressure distribution in this region, the validity of the analysis must rest upon whatever assumptions are made as to pressure distribution.

In this section, the general equation for pressure rise is first derived. The case of inlet vapor pressure occurring at the mixing chamber wall is then treated. Deviations from this case are considered in

order to provide an indication of the magnitude of their influence.

In the derivation of the general equation the following assumptions were made:

1. Liquid pressure equals vapor pressure at Station 0.
2. No heat loss from the condenser wall.
3. Entering vapor quality equals unity
4. Homogeneous flow within each phase exists at entrance and exit stations (no mixing losses) with complete condensation.
5. The radial pressure and velocity gradients at the inlet and outlet are zero.
6. Injector discharge coefficient equals unity.
7. Uniform flow (constant velocity profile) occurs at the entrance and exit.

With these assumptions, application of the conservation equations for momentum, mass and energy from Stations 0 to 2 results in the following expression for pressure rise (cf. Appendix B):

$$P_2 - P_o = P_o(A_{to}/A_{t1} - 1) + \frac{\dot{m}_{vo}^2}{g\rho_v A_{t1}(A_{to}-A_{\ell o})} + \frac{\dot{m}_{\ell o}^2}{g\rho_\ell A_{t1} A_{\ell o}}$$

$$- \frac{\dot{m}_T^2}{g\rho_\ell A_{t1}^2} + \frac{\dot{m}_T^2}{2\, g\rho_\ell}\left[\frac{1 - K_d}{A_{t1}^2} - \frac{1}{A_{to}^2}\right]$$

$$\tau_w A_w(\cos\alpha)/A_{t1} - \frac{1}{A_{t1}} \int_o^{X_1} P_w \pi\, d_t \tan\alpha\, dx \qquad (7)$$

Equation (7) expresses the total pressure rise in terms of:

1. Geometry and inlet flow parameters
2. Two unknown terms which contain properties of the boundary flow, i.e., the shear stress of the vapor on the wall and the internal pressure distribution at the wall.

In order to obtain numerical results, assumptions must be made of the values of the quantities of Item 2. In all cases it is felt that

the friction term is small relative to the total pressure rise, (the extremely short condensation distance and high values of pressure rise measured during testing support this simplification). Another assumption which can be used to make Equation (7) tractable is to use the inlet vapor pressure as the pressure at the walls of the mixing chamber. This assumption appears to be reasonable in view of internal measurements made by other investigators (Ref. 9) and because of the saturated state of the vapor.

3.2.1 Wall Pressure Equal to Inlet Vapor Pressure

Results of the analysis carried out for the constant inlet pressure model are presented in terms of the parameters discussed in Section 4.4.1: the ratio of pressure rise to injected liquid dynamic pressure $\Delta\overset{o}{P}_{\ell}$ and the ratio of pressure rise to inlet vapor dynamic pressure $\Delta\overset{o}{P}_{v}$. Substitution of $P_w = P_{vo}$ into the pressure integral term of Equation (7) and neglecting vapor friction ($\tau_w = 0$) and diffuser losses ($K_d = 0$) results in the following expressions for pressure rise:

$$\Delta\overset{o}{P}_{th_v} \equiv (P_1-P_o)/\rho_v V_{vo}^2/2g = 2\frac{(1-\overset{o}{A}_2)}{\overset{o}{A}_{th}}\left[1 + \left(\frac{\overset{o}{m}_R^2}{\overset{o}{\rho}}\right)\frac{(1-\overset{o}{A}_2)}{\overset{o}{A}_2} - \frac{(\overset{o}{m}_R+1)^2}{\overset{o}{\rho}}\frac{(1-\overset{o}{A}_2)}{\overset{o}{A}_{th}}\right] \quad (8)$$

$$\Delta\overset{o}{P}_{th_\ell} \equiv (P_1-P_o)/\rho_\ell V_{\ell o}^2/2g = 2\overset{o}{A}_1\left[1 + \left(\frac{\overset{o}{\rho}}{\overset{o}{m}_R^2}\right)\frac{\overset{o}{A}_2}{1-\overset{o}{A}_2} - \left(1 + \frac{1}{\overset{o}{m}_R}\right)^2 \overset{o}{A}_1\right] \quad (9)$$

$$\Delta\overset{o}{P}_{v} \equiv (P_2-P_o)/\rho_v V_{vo}^2/2g = 2\frac{(1-\overset{o}{A}_2)}{\overset{o}{A}_{th}}\left[1 + \left(\frac{\overset{o}{m}_R^2}{\overset{o}{\rho}}\right)\frac{(1-\overset{o}{A}_2)}{\overset{o}{A}_2}\right] - \frac{(\overset{o}{m}_R+1)^2}{\overset{o}{\rho}}(1-\overset{o}{A}_2)\left[\frac{1}{\overset{o}{A}_{th}}^2 + 1\right] \quad (10)$$

$$\Delta\overset{o}{P}_{\ell} \equiv (P_2-P_o)/\rho_\ell V_{\ell o}^2/2g = 2\overset{o}{A}_1\left[1 + \left(\frac{\overset{o}{\rho}}{\overset{o}{m}_R^2}\right)\frac{\overset{o}{A}_2}{(1-\overset{o}{A}_2)}\right](1 + \frac{1}{\overset{o}{m}_R})^2(\overset{o}{A}_1^2 + \overset{o}{A}_2^2) \quad (11)$$

Equations (8) and (9) relate the pressure rise from the vapor to the liquid at the throat to the dynamic pressure terms. Equations (10) and (11) relate pressure rise from the vapor to liquid at the diffuser outlet to the dynamic pressure terms. The latter two equations are most suitable for design purposes and for evaluation of test data. However, the former expressions are also of interest in comparing the amount of pressure rise added by the diffuser to that resulting at the throat. Also, operation of a jet condenser with the diffuser exit area less than the vapor inlet area will result in a pressure rise in between the limits supplied by these equations.

Numerical examples of interest for the above equations were computed and are presented in Figs. 12 through 18 in order to illustrate predicted performance of variable area jet condensers. Figure 12 presents the calculated throat and diffuser pressure rises (referred to injected liquid dynamic pressure) vs. the mass flow ratio of liquid to vapor for a given liquid to vapor density ratio and injector to tube inlet area ratio. Curves are presented to show the influence of different values of the ratio of injector to throat area.

As in the case of constant area jet condensers, low values of mass flow ratio result in higher calculated values of pressure rise referred to liquid dynamic pressure. For example, the curve for $\overset{\circ}{A}_1$ = 0.895 predicts a value of $\Delta\overset{\circ}{P}_\ell$ = 4.7 at a mass flow ratio of 10, while at a mass flow ratio of 100, a value of $\Delta\overset{\circ}{P}_\ell$ = 1.0 results. Also, use of throat areas more nearly equal to injector area results in higher values of predicted pressure rise.

Comparison of the curves for the pressure rise at the throat to the pressure rise at the exit of the diffuser provides some interesting conclusions. At a mass flow ratio of 10, the pressure rise at the throat is within 80 percent of the pressure rise at the diffuser

exit ($\overset{o}{A}_1$ = unity). This implies that the contribution of the vapor to the total pressure rise is very high at lower values of liquid to vapor mass flow ratio; i.e., efficient recovery of the liquid dynamic pressure at the throat only increases the pressure rise by about 20 percent. However, as higher liquid flow rates are used the effect of the liquid head becomes more important than contributions from the vapor, and efficient recovery of the injected liquid velocity is required to achieve a high pressure rise. The above value of $\Delta\overset{o}{P}_{\ell}$ = 4.7 means that for an injector discharge coefficient of unity, 3.7 times the dynamic pressure of the injected liquid is available for circulation of the outlet liquid through the liquid radiator loop (cf.Fig. 1) back to the point of injection. For example, if a set of flow conditions were chosen such that the liquid dynamic pressure were 10 psi a total of 37 psi would then be available as a pressure difference for circulation of the outlet liquid flow. This result, if verified by experiments, has profound significance in the use of a jet condenser in a Rankine cycle system. It means that a jet condenser could be used with little, if any, pumping power weight penalty (if other performance requirements such as stable operation are met).

An interesting observation can be made as to the source of the energy producing the jet condenser pressure rise by referring to Fig. 12. For the mass flow ratio of 10 and the densities and area ratio of this figure, the inlet vapor dynamic pressure is approximately 0.2 times the inlet liquid dynamic pressure. Thus, if both were recovered with no losses a maximum value of $\Delta\overset{o}{P}_{\ell}$ of 1.2 could be obtained. The only other energy source which is available for the pressure rise through the condenser is the internal energy of the vapor which manifests itself as random thermal energy. Thus, the results predicted by the analysis could only result if conversion of vapor thermal energy to a directed mechanical energy in the liquid were to occur.

Figure 13 presents the calculated values of pressure rise referred to inlet vapor dynamic pressure for the same geometric and flow variables. Once again, as in the case of the constant area jet condenser, increasing mass flow ratio has an opposite effect upon

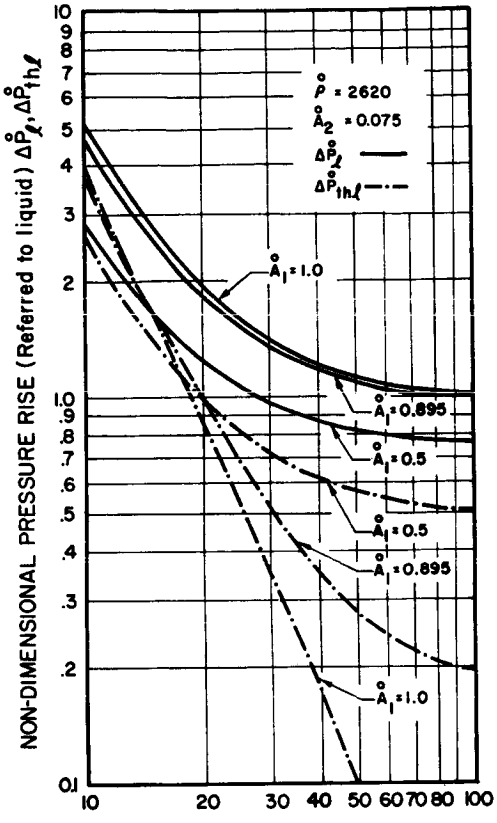

FIG. 12

CALCULATED PRESSURE RISE (Referred to liquid) FOR VARIABLE AREA JET CONDENSER, EFFECT OF INJECTOR-THROAT AREA RATIO

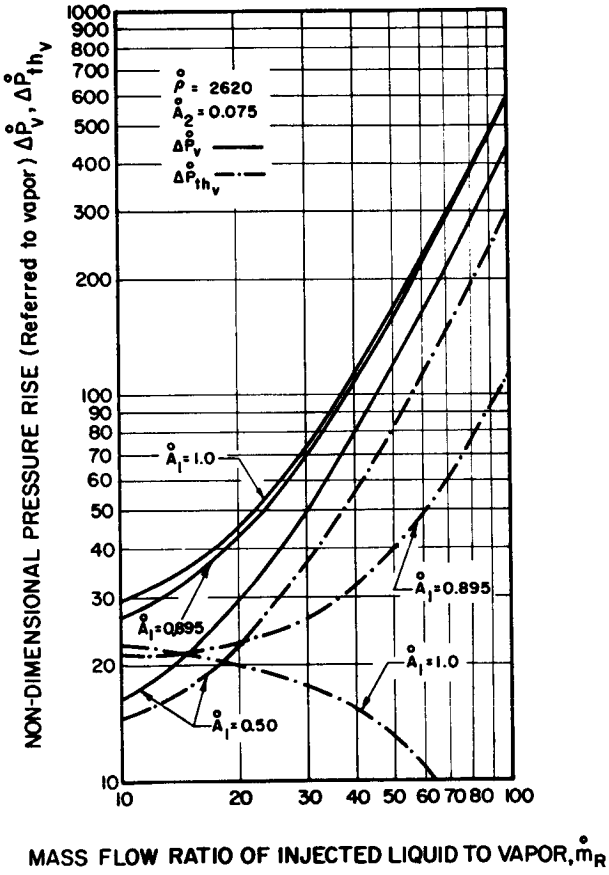

FIG. 13

CALCULATED PRESSURE RISE (Referred to vapor) FOR VARIABLE AREA JET CONDENSER, EFFECT OF INJECTOR-THROAT AREA RATIO

the magnitude of this pressure rise term from that of Fig. 12. That is, increasing mass flow ratio produces increasing values of $\Delta \overset{o}{P}_v$ and decreasing values of $\Delta \overset{o}{P}_\ell$. For example, increasing mass flow ratio from 10 to 100 produces an increase in $\Delta \overset{o}{P}_v$ from 30 to 600 for an area ratio of 1.0. This can be contrasted to the behavior of $\Delta \overset{o}{P}_\ell$ from Fig. 12 where a decrease from 5.1 to 1.0 is experienced. The same general trends are exhibited for the predicted pressure rise at the throat, with the exception that different area ratios have crossover points and the area ratio for $\overset{o}{A}_1 = 1.0$ falls off very sharply with increasing mass flow ratio.

In order to illustrate the effect of density ratio, Figs. 14 and 15 were computed for a given geometry ($\overset{o}{A}_1 = 0.90$ and $\overset{o}{A}_2 = 0.075$). As can be seen, higher values of liquid to vapor density ratio produce higher calculated values of $\Delta \overset{o}{P}_\ell$ and lower values of $\Delta \overset{o}{P}_v$. For example, increasing density ratio from 2620 (700^oF for mercury) to 14,500 (530^oF for mercury) produces an increase in $\Delta \overset{o}{P}_\ell$ from 1.85 to 6.0 (for a mass flow ratio of 20). A decrease in $\Delta \overset{o}{P}_v$ from 43 to 26 results from this change in density ratio. For constant mass flow ratio, this decrease in density can be interpreted as an increase in vapor velocity. Thus, it appears the jet condenser becomes a more effective pressure recovery device (for given geometry and mass flow rates) as lower vapor pressures are utilized.

The effect of the ratio of injector to tube area is illustrated in Figs. 16 and 17 (for a given density ratio and injector to throat area ratio). Results are similar in trend to those obtained for the constant area jet condenser; that is, increasing values of $\overset{o}{A}_2$ result in increases in the non-dimensional pressure rise referred to injected liquid dynamic pressure, or, an increase in the effectiveness of the jet condenser as a pumping device. On the other hand, from Fig. 17, it can be seen that the absolute magnitude of pressure rise (or pressure rise referred to inlet vapor dynamic pressure) is increased as lower injector to tube area ratios are used. Once again a trade-off is indicated. It is interesting to note the curve for $\overset{o}{A}_2 = 0.01$, an extremely low area ratio. The curve for $\Delta \overset{o}{P}_\ell$ approaches a lower limit of unity for

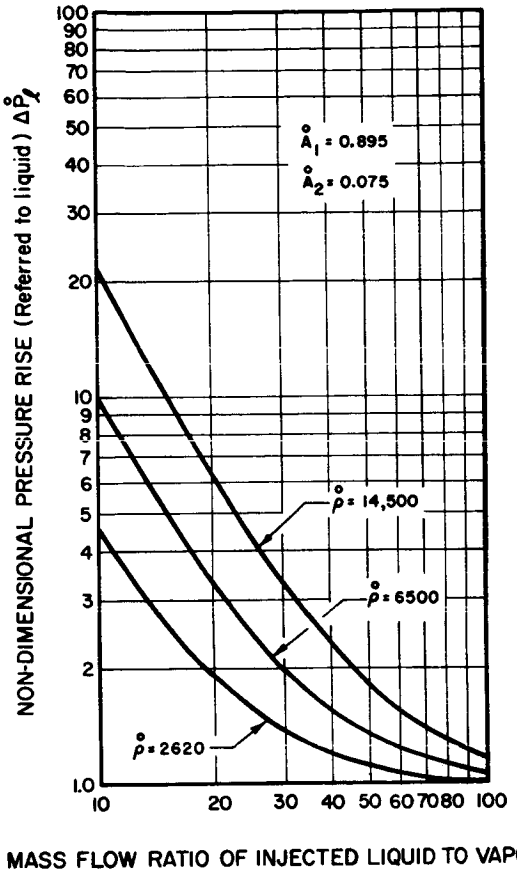

FIG. 14

CALCULATED PRESSURE RISE (Referred to liquid) FOR VARIABLE AREA JET CONDENSER, EFFECT OF LIQUID-VAPOR DENSITY RATIO

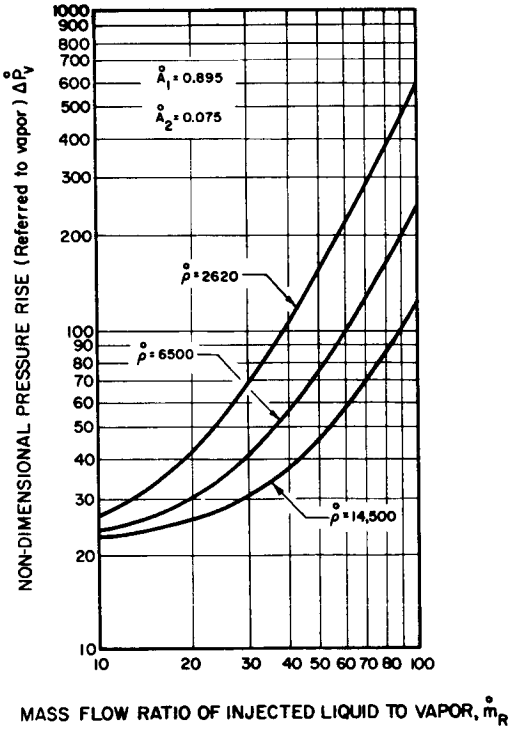

FIG. 15

CALCULATED PRESSURE RISE (Referred to vapor) FOR VARIABLE AREA JET CONDENSER, EFFECT OF LIQUID-VAPOR DENSITY RATIO

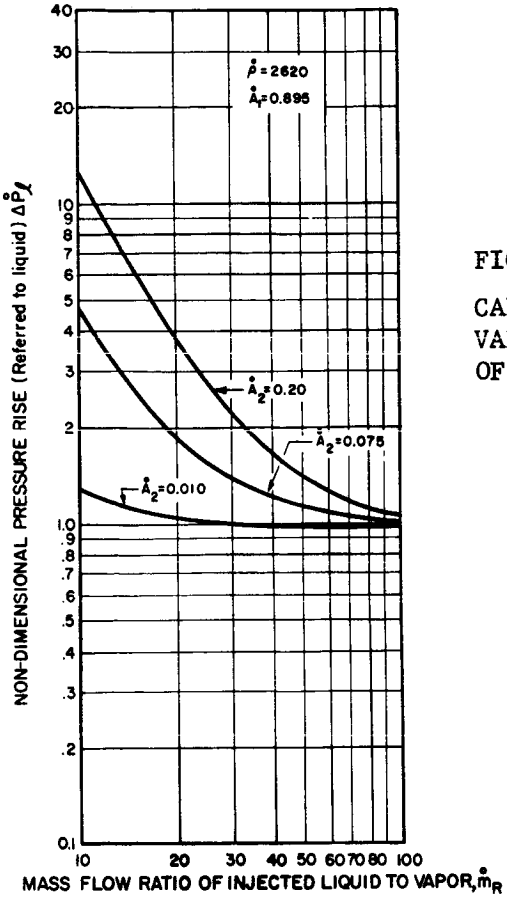

FIG. 16

CALCULATED PRESSURE RISE (Referred to liquid) FOR VARIABLE AREA JET CONDENSER, EFFECT OF THE RATIO OF THE INJECTOR AREA TO TOTAL INLET AREA

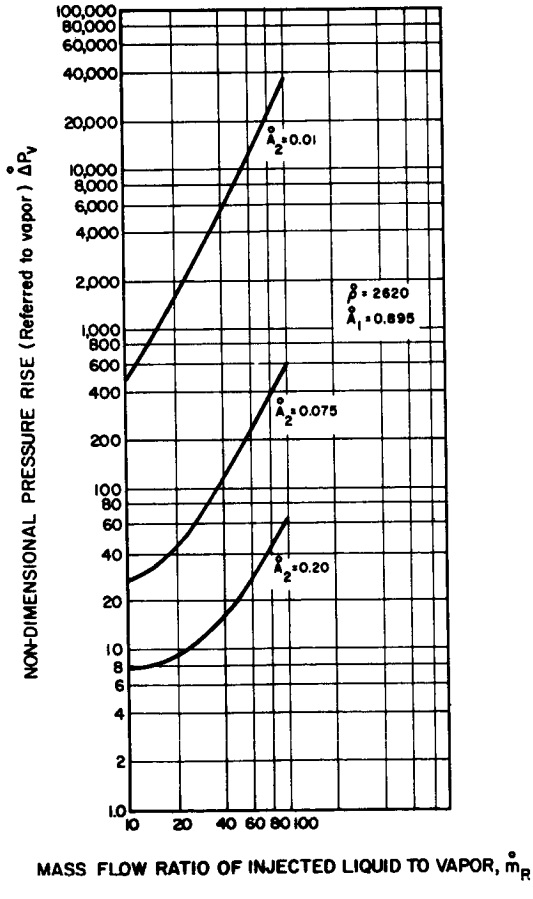

FIG. 17

CALCULATED PRESSURE RISE (Referred to vapor) FOR VARIABLE AREA JET CONDENSER, EFFECT OF THE RATIO OF THE INJECTOR AREA TO TOTAL INLET AREA

higher mass flow ratios. However, the curve for $\Delta \overset{o}{P}_v$ rises very rapidly and values on the order of 10^4 are obtained for mass flow ratios less than 100.

The above results are useful in expressing the values of pressure rise which may be possible using a jet condenser and to indicate major trends. However, it is also meaningful to examine the pumping characteristics of these devices.

The net power output (in kw) of a jet condenser which is available for circulation of the bypass liquid flow is given by:

$$H_j = \frac{(\Delta P_a - \Delta P_i)\dot{m}_{\ell o}}{738\rho}$$

or

$$H_j = \frac{\left(1 - \frac{\Delta P_i}{\Delta P_a}\right)(\Delta P_a \dot{m}_{\ell o})}{738\rho_\ell} \qquad (12)$$

for a perfect injector $(c_d = 1.0)$, $\frac{\Delta P_a}{\Delta P_i} = \Delta \overset{o}{P}_\ell$

Rearranging and substituting for ΔP_a and $\dot{m}_{\ell o}$ gives

$$H_j = \left(1 - \frac{1}{\Delta \overset{o}{P}_\ell}\right)\left(\Delta \overset{o}{P}_v \overset{o}{m}_R\right) \frac{\rho_v V_{vo}^2/2g}{738\rho_\ell} \dot{m}_{vo} \qquad (13)$$

Thus, Equation (13) expresses the power output in terms of jet condenser operating parameters. It should be noted that all values of $\Delta \overset{o}{P}_\ell$ less than unity produce a negative power output; i.e., pumping power is required by the condenser. For fixed inlet vapor conditions the effect of mass flow ratio on power output can be illustrated by plotting the expression:

$$H_j^t = \left(1 - \frac{1}{\Delta \overset{o}{P}_\ell}\right)\left(\Delta \overset{o}{P}_v \overset{o}{m}_R\right) \qquad (14)$$

This parameter, which is directly proportional to the useful power output, is plotted vs. mass flow ratio in Fig. 18 for three different area ratios (injector to total inlet). All three geometries exhibit maxima within the range of flow ratios considered. The smallest injector, while producing the highest calculated value of H_j', has the smallest range of operation; the useful power output going to zero at a mass flow ratio of 25. On the other hand an injector to tube area ratio of 0.075 theoretically provides useful power over the entire range of mass flow ratios of the curve (0-100). The peak value of H_j' for this geometry is 775 at a mass flow ratio of 60 vs. a peak of 1140 at a mass flow ratio of 13 for $\mathring{A}_2 = 0.010$. The calculated power output (in kw) for any set of vapor inlet conditions can be obtained from the following expression:

$$H_j = \frac{\rho_v}{\rho_\ell} \frac{V_{vo}^2 \dot{m}_{vo}}{1470g} H_j' \qquad (15)$$

where V_{vo} is in units of ft/sec

$\dot{m}_{vo}$ is in units of lbm/sec

$g = 32.2$ lbm/lbf ft/sec^2

3.2.2 Effect of Variations in Chamber Pressure

Deviations of vapor pressure at the wall of the mixing chamber from the inlet vapor pressure can occur. For example, if none of the vapor flow condensed upon the jet, the wall pressure would drop due to acceleration of the vapor in the converging geometry. On the other hand, if complete condensation of the inlet vapor flow rate were to occur upon the jet at some station upstream of the final interface location, separation from the wall could occur and a region might exist where the vapor pressure were equal to the saturation pressure of the liquid phase. There is no apparent mechanism existing, however, for the vapor pressure to increase in the mixing chamber since it must always follow the saturation curve.

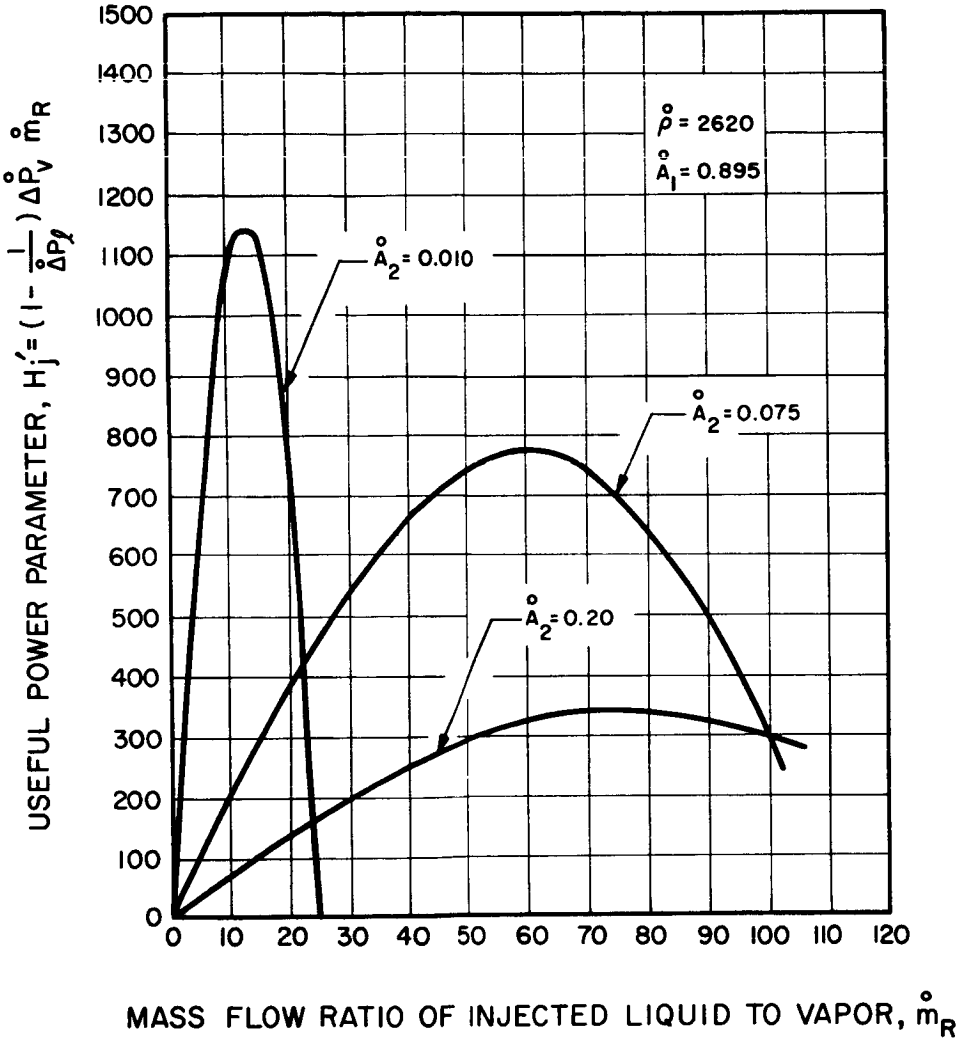

FIG. 18 USEFUL POWER PARAMETER (CALCULATED) FOR VARIABLE AREA JET CONDENSER VS MASS FLOW RATIO

In order to provide some insight into the effect of a lower wall pressure in the converging section upon the predicted pressure rise, analysis was conducted of two limiting cases. In the first case condensation of the entire inlet vapor flow rate was assumed to occur immediately after Station 0; i.e., the jet temperature was raised to $T_{\ell e}$, the outlet temperature, immediately after Station 0. The chamber pressure would then take the value of saturation vapor pressure $P_s(T_{\ell e})$ corresponding to the temperature $T_{\ell e}$. If the pressure were to drop any lower, liquid would evaporate from the jet to raise the vapor pressure to $P_s(T_{\ell e})$ (since the equilibrium vapor-liquid flow is assumed). Similarly any increases in vapor pressure would result in equilibrium condensation on the jet to reduce the vapor pressure to $P_s(T_{\ell e})$. The analysis for this case is essentially a modification of the analysis presented in Section 3.2.1 and is summarized in Appendix B. From this analysis, the pressure rise vs. outlet subcooling was calculated for a given set of geometric and flow conditions.

For the second case a linear (axially) variation of wall pressure from the inlet (P_{vo}) to the final interface was specified. The final pressure was taken to be $P_s(T_{\ell e})$, the saturation pressure corresponding to the outlet temperature. With these conditions the wall pressure integral of Equation (3) was evaluated and the pressure rise computed for the same set of geometric and flow conditions as the first case (cf. Appendix B). Figure 19 presents the results of the calculations. The solid curves are the calculated pressure rise for the cases given above and the broken curve is the pressure rise computed for the wall pressure equal to the vapor inlet pressure. As can be seen, very large increases in pressure rise are possible if the chamber pressure were decreased to be equal to the saturation pressure of the liquid phase or if a linear variation were to occur. For example, at an outlet sub-cooling of $100^{\circ}F$ the constant inlet pressure model predicts a pressure rise of 7.6 psi while Case I predicts a pressure rise of approximately 43 psi and Case II predicts a rise of 23 psi.

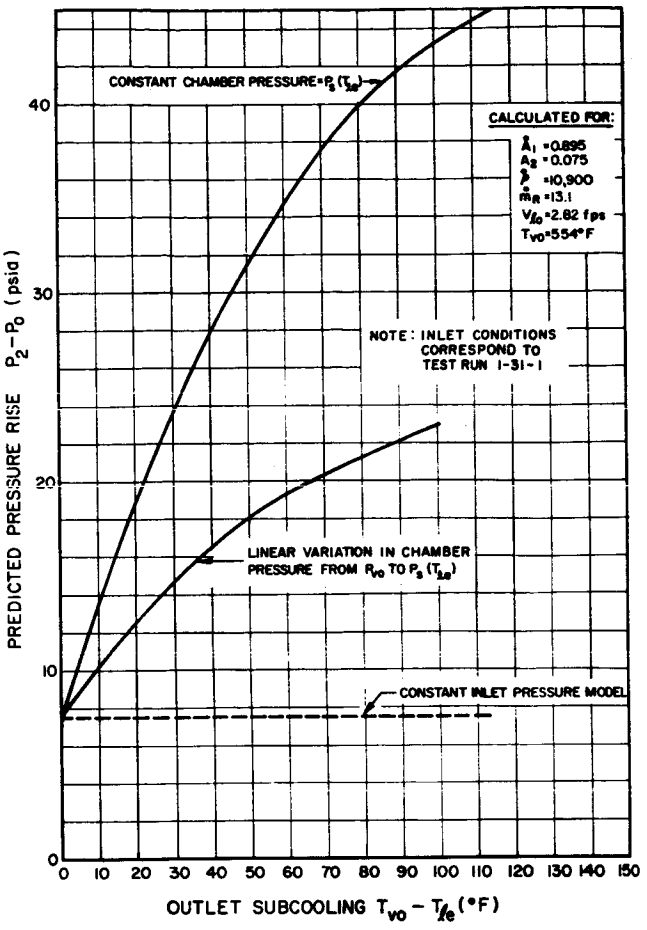

FIG. 19

COMPARISON OF PREDICTED PRESSURE RISE FOR DEVIATIONS IN JET CONDENSER CHAMBER PRESSURE FROM INLET VAPOR PRESSURE (Note: Inlet conditions correspond to test run 1-31-1)

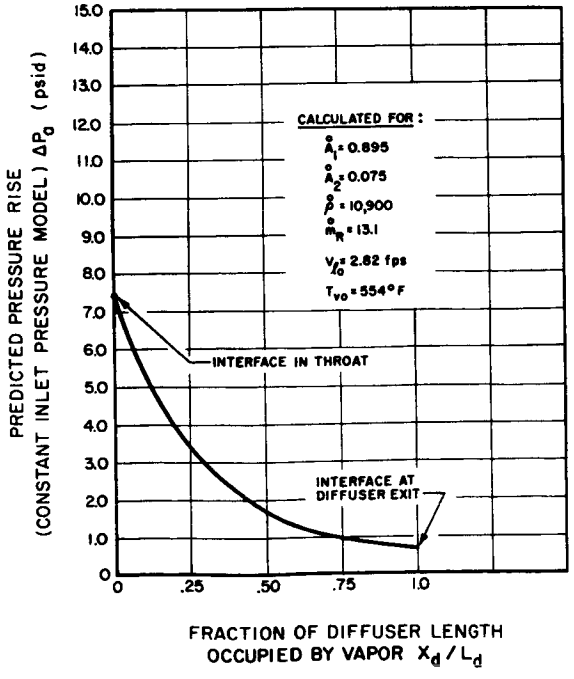

FIG. 20

VARIATION OF PREDICTED PRESSURE RISE WITH DOWNSTREAM LOCATION OF VAPOR-LIQUID INTERFACE IN DIFFUSER (Note: Inlet conditions correspond to test run 1-31-1)

Of course, it is very unlikely that the above flow could occur over the entire condensing chamber. However, local decreases in vapor pressure can occur due to this or other types of flow occuring in regions of the condensing chamber. The above treatment indicates that the pressure rise would be much greater for these cases than that which would be predicted assuming the inlet vapor pressure to exist at the wall of the mixing chamber. Thus, use of the constant inlet pressure model to predict outlet pressure should offer conservative values over treatments which seek to account for local variations in vapor pressure within the condenser. As such, it is felt that the constant inlet pressure model if substantiated by experimental results offers a reasonable prediction method for jet condenser pressure rise.

3.2.3 Interface in Diverging Section

If the vapor and liquid inlet conditions are not adjusted properly, condensation of the inlet vapor flow rate may not be complete at the throat location. The final vapor-liquid interface may occur in other regions of the condenser, such as in the diverging portion. The effect of this situation upon the condenser pressure rise can be illustrated in a simple example. Consider the inlet pressure to occur at all walls throughout the vapor region in the condenser. Moreover, the assumption is made that the central liquid jet is coherent up to the place of formation of the interface. The theoretical pressure rise can then be expressed as a function of the location of the interface in the diverging section of Fig. 3a (cf. Appendix B). With the results of the analysis presented in Appendix B, calculations were made to express the predicted pressure rise as a function of interface location in the diffuser. The geometric and flow conditions used in the previous example were also used in this case. Figure 20 presents the results. The predicted pressure rise decreases from a value of 7.6 psi, which occurs with the interface in the throat, to a value of approximately 0.7 psi if the interface is at the exit of the diffuser.

Once again, as in the example of Section 3.2.2, the calculations are based upon a simplification of the physical flow.

For example, dispersion of the liquid and vapor phases would probably result from the high vapor velocity in the throat. However, the results illustrate that significantly lower pressure rise may occur if the vapor-liquid interface is formed in the diverging section rather than the throat. Moreover, a very rapid decrease can be seen to occur. For example, the predicted pressure rise drops by about 50 percent for the interface occurring at a location of 25 percent of the diffuser length.

The results of Section 3.2.2 and 3.2.3 are mainly useful in providing an understanding of possible deviations of experimental pressure rise from that computed for the constant inlet pressure model. If the constant inlet pressure model is used to correlate test data or to predict pressure rise deviations may result due to either of the above flows.

3.3 Discussion of Principle Variables Effecting Pressure Rise

3.3.1 Factors Contained in the Ideal Pressure Rise Equation

Several non-dimensional flow and geometric parameters contained in Equations 8 - 11 appear to have a strong effect upon pressure rise of a jet condenser. These parameters provide the basis for the choice of test conditions as well as for the extension of test results to other variable ranges.

Density Ratio

The ratio of liquid to vapor density exhibits a strong influence in the pressure rise equation. In particular, for a constant mass flow ratio and given geometry, increasing values of $\overset{o}{\rho}$ produce increases in the non-dimensional pressure rise referred to liquid dynamic pressure. The most important reason is that increasing $\overset{o}{\rho}$ produces an increase in vapor dynamic pressure (relative to the liquid dynamic pressure). Since $\rho_v V_{vo}$ is equal to a constant for constant vapor mass flow rate, decreasing ρ_v produces an increase in the quantity $\rho_v V_{vo}^2/2g$. For a given system application the vapor temperature will generally be fixed. Therefore, the density ratio will not be an important design variable. However, if the jet condenser is to be used in a Rankine cycle system the effect of density

ratio upon pressure rise may be an important factor in influencing cycle operating conditions.

Mass Flow Ratio

The mass flow ratio of liquid to vapor is one of the most important design variables associated with a jet condenser heat rejection system. In addition to the influence upon pressure rise, this parameter is an important factor in determining the average operating temperature of the liquid radiator component. Higher values of mass flow ratio of liquid to vapor produce lower values of the pressure rise referred to liquid dynamic pressure. However, for a given set of vapor conditions the absolute magnitude of the predicted pressure rise will increase as the injected liquid flow increases. This result is illustrated in Fig. 13 in which the pressure rise is referred to vapor inlet conditions. Due to the temperature drop in the liquid radiator component the probable operating range of liquid to vapor mass flow ratio is from 20 to 50.

Geometry

Two important geometric ratios appear in Equations (8) to (11); the ratio of injector area to throat area ($\overset{o}{A}_1$) and the ratio of injector area to total inlet area ($\overset{o}{A}_2$). For the constant area jet condenser these two parameters are identical. Larger values of $\overset{o}{A}_1$ always result in higher predicted values of non-dimensional pressure rise. For higher mass flow ratios ($\overset{o}{m}_R$ greater than 30) a probable limit on $\overset{o}{A}_1$ will be unity. However, at lower mass flow ratios, acceleration and contraction of the liquid jet may enable use of a throat which is smaller than the injector. Smaller values of the ratio of injector area to tube area, produce higher absolute values of pressure rise, larger values result in higher values of the ratio of pressure rise to liquid dynamic pressure.

Pressure Integral

The pressure integral contained in Equation (3) was readily evaluated when the inlet vapor pressure was assumed to exist at the wall. However, the variation of vapor pressure in the mixing region is influenced by several parameters: the heat transfer rate of vapor to liquid, the rate of convergence of the mixing chamber, mixing chamber

contour, final vapor-liquid subcooling, and initial vapor pressure. The influence of heat transfer rate was indicated above; i.e., extremely rapid heat transfer rates may result in complete condensation of the inlet vapor flow within a short distance. This may result in separation of the boundary layer from the wall, with the occurrence of a region where the vapor pressure equals the saturation pressure of the liquid. Another limiting case; namely, that of zero heat transfer rate would result in a nearly isentropic expansion of the vapor which would also result in lowering the vapor pressure at the wall.

3.3.2 Real Flow Effects

While the above parameters appear to be the most important in determining the pressure rise characteristics of jet condensers during operation at a steady-state design point, several other factors must be considered in evaluating test results and off-design performance.

Off-Design

Perhaps the most serious of these effects would be operation of the jet condenser under a set of inlet conditions such that the location of the final vapor-liquid interface did not occur in the throat section of the condenser. Occurrence of the interface in the converging section (with stable flow) would result in a decrease in $\overset{o}{A}_1$, the ratio of injector area to the area at the final location of the vapor liquid interface. On the other hand, occurrence of the interface in the diverging portion would result in high frictional losses through the throat as well as a decrease in $\overset{o}{A}_1$.

Friction Losses

Frictional losses, while of utmost importance in most condenser designs, do not seriously influence the performance of a jet condenser. The values of pressure rise may be greater than two orders of magnitude higher than any frictional losses in the mixing chamber. This result is due to the extremely rapid rate processes occurring in the device and the short vapor flow distance required before complete condensation is effected.

Mixing Losses

Another source of loss in the jet condenser is incomplete mechanical mixing of the injected liquid and condensed vapor streams. Occurrence of non-uniform flow, pressure, and temperature distribution at the exit of the condenser can result in a degradation of pressure rise performance.

Misalignment of Injector

A practical source of loss is misalignment of the liquid injector with respect to the throat. If misalignment were severe enough to result in impingement of the liquid upon the mixing chamber wall, a high local wall pressure would result which would produce a decrease in the total pressure rise through the condenser. Alignment problems become critical where smaller geometric sizes are used.

3.4 Analysis of Heat Transfer into Jet

Several complex mechanisms occur during condensation of the vapor on a subcooled liquid jet. In order to provide a guide for testing and to obtain information on the important variables, an analysis was performed to identify the possible limiting resistance in the heat transfer process; i.e., the conduction and convection into the interior of the subcooled liquid phase of the heat released at the liquid-vapor interface.

3.4.1 Summary of Analysis

Fig. 21 gives a representation of the model considered for analysis. The liquid phase exists as a solid cylinder with a constant radius r_ℓ which is injected into the vapor at a constant velocity $V_{\ell o}$. The vapor temperature (T_{vo}) is assumed to remain constant throughout the mixing chamber. With these assumptions, it is then possible to write an expression for the rate of heat conduction and convection into the interior of the liquid. Details of this analysis are summarized in Ref. 4 . Equation 16 expresses the results:

$$\chi = \frac{T_{\ell e}-T_{\ell o}}{T_{vo}-T_{\ell o}} = \sum_{\mu=1}^{\mu=\infty} \frac{4}{\beta_\mu^2}\left\{1 - \frac{1}{\beta_\mu^2}\frac{V_{\ell o} r_\ell^2}{L_c(\alpha+\alpha_t)}\left[1 - \exp\left(-\frac{\beta_\mu^2 L_c(\alpha+\alpha_t)}{V_{\ell o} r_\ell^2}\right)\right]\right\} \qquad (16)$$

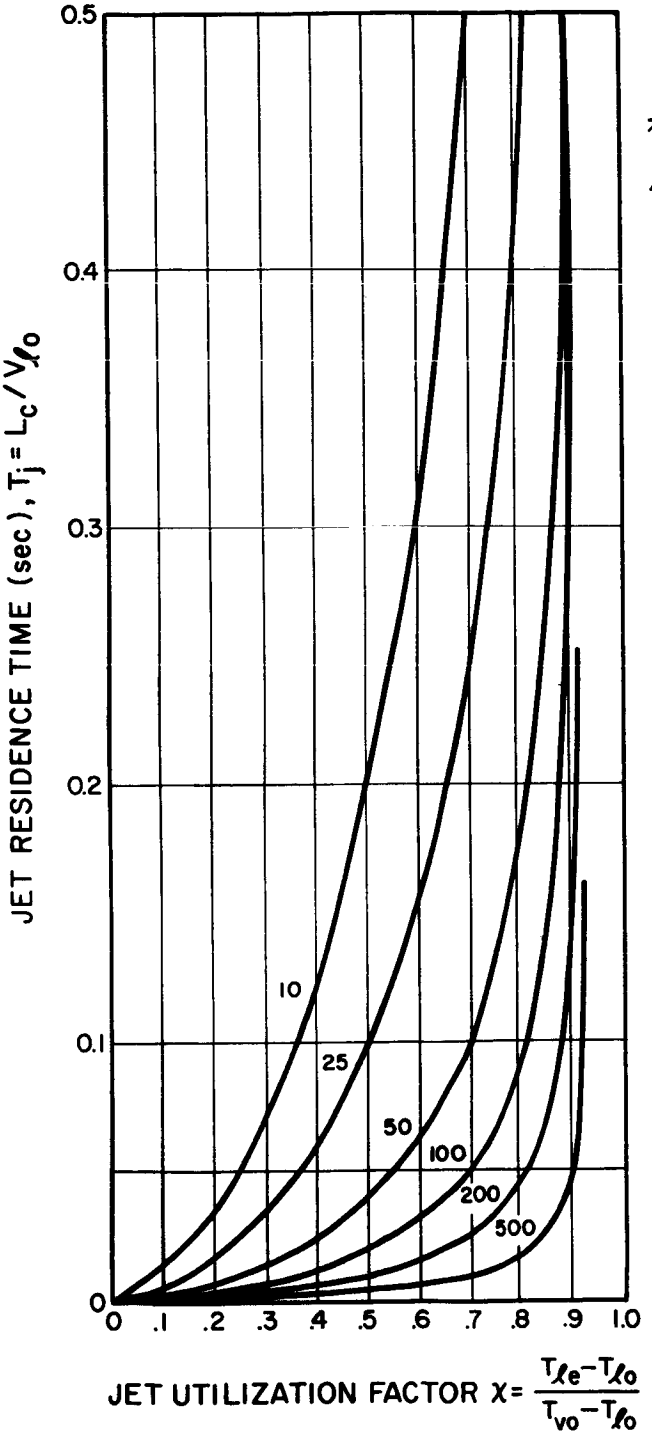

FIG. 21a

CALCULATED JET RESIDENCE TIME VERSUS JET UTILIZATION FACTOR (LINES OF CONSTANT $\frac{\alpha + \alpha_t}{r_\ell^2}$)

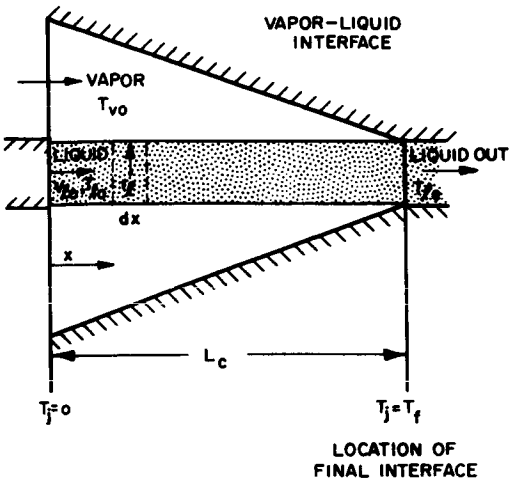

FIG. 21

SCHEMATIC OF MODEL USED FOR HEAT TRANSFER ANALYSIS

In this expression the temperature of the liquid at the exit, $T_{\ell e}$, is related to initial conditions of the jet and vapor, ($T_{\ell o}$, T_{vo}, $V_{\ell o}$, r_{ℓ},) to the properties of the fluid (α and α_t) and to the distance traversed by the jet (L_c).

Equation 16 is plotted in Fig. 21 as the residence time (of the liquid jet in vapor) required for heat transfer vs. the jet utilization factor (or non-dimensional temperature) of the liquid jet. Curves are presented for different values of the ratio of the total heat diffusivity to the square of the jet radius. Several interesting features may be determined by examining the curve.

1. Operation of the jet condenser with the final liquid temperature equal to vapor temperature would result in an infinite distance required for condensation of the vapor flow rate. (For a finite liquid velocity).
2. Increasing contributions of eddy heat transfer to the total heat transfer result in much shorter condensation distances (or jet residence time) for a given value of jet utilization factor .
3. For a given value of jet utilization factor and total heat diffusivity, lower jet velocities result in shorter condensation lengths. Attempts to operate with extremely high jet velocities would result in longer condensation lengths.
4. Decreasing values of jet radius, for a constant value of total heat diffusivity, result in shorter condensation lengths (for a given value of jet velocity and jet utilization).
5. Relatively short lengths of times are required to attain given jet utilization factors for reasonable values of diffusivity factors. For example, for a diffusivity factor of 50 a jet utilization factor of .8 is obtained after about 0.02 seconds. Thus, for a jet velocity of 10 ft/sec a condensation distance of .2 ft would be required.

Figure 21 cannot be used directly to predict condensation length due to a lack of information upon the local variation of eddy diffusvity for heat, α_t and because the jet radius and vapor temperature at the jet surface are somewhat different than parameters assumed for the calculation. However, the results indicate the major trends of condensation length with jet utilization factor and also provide information of the important variables of the problem.

3.4.2 Discussion of Important Parameters in Heat Transfer

A parameter of the analysis which is important both from the standpoint of heat transfer and system design is the jet utilization factor. This parameter is defined by the following equation:

$$\chi = \frac{T_{\ell e} - T_{\ell o}}{T_{vo} - T_{\ell o}} = \frac{Q_R}{\dot{m}_{\ell o} C_p (T_{vo} - T_{\ell o})} \tag{17}$$

The maximum possible value for χ is unity, which would occur if the final temperature of the injected liquid were equal to the inlet vapor temperature. However, as discussed above this occurrence would require an infinite length to transfer the heat. The physical significance of this parameter is that it represents the ratio of the enthalpy absorbed by the injected liquid to the maximum enthalpy which could be absorbed; i.e., the enthalpy which the liquid would absorb if raised to vapor temperature. This factor can be related to two other expressions which are useful for system considerations:

$$\chi = \frac{1}{\dot{m}_R - \dot{m}_R^*} + 1 \tag{18}$$

$$\chi = \frac{1}{\frac{T_{vo} - T_{\ell e}}{T_{\ell e} - T_{\ell o}} + 1} = \frac{1}{\frac{\Delta T_{sc}}{\Delta T_R} + 1} \tag{19}$$

Equation 18 relates the jet utilization factor to the excess mass flow required to effect condensation over the ideal mass flow ratio ($\dot{m}_R^*$) required from

the standpoint of a heat balance. Equation 19 relates the jet utilization factor to the ratio of the outlet subcooling of the jet condenser to the radiator temperature drop in a Rankine cycle system. From the system standpoint, the excess mass ratio of liquid to vapor should be zero and the outlet subcooling of the jet condenser should be zero. However, from these relations the jet utilization factor would then be unity and an infinite distance for condensation of the inlet vapor flow would be required.

The total heat diffusivity, α_T is a sum of the thermal and eddy or tubulent thermal diffusivity. Investigations to determine eddy diffusivity, based on the premise that the two diffusivities are additive, have been conducted. Included among these is a recent investigation where measurements of eddy diffusivities were made for mercury (Ref. 12). However, the results of these investigations have not been adequate to predict eddy diffusivity in pipe flow, let along flow of a free liquid jet in a vapor environment.

The effective jet radius, r_ℓ, used in the calculations was based on a model of constant liquid flow area. However, in the real case the jet has a varying radius and is characterized by surface waves and fluid particles which are not of a cylindrical nature. This parameter would not be constant for the entire mixing region. As noted in the discussion of Figure 21, decreasing values of jet radius produce better heat transfer characteristics.

The jet velocity enters the above analysis since the residence time of a liquid particle in vapor is inversely proportional to the velocity. Higher values of jet velocity reduce the time spent by any fluid particle in presence of the vapor. However, jet velocity also appears to influence the eddy diffusivity and local variation of jet radius. Therefore, in some instances increasing the velocity may result in an increase in heat transfer.

The density of the vapor, ρ_v, does not appear explicitly in Equation 16. However, this parameter has a very important influence upon the heat transfer. Larger values of vapor density result

in a higher flux of vapor molecules upon the liquid condensing surface. When internal heat transfer is the limiting resistance this factor may not be important. However, situations will exist in the overall heat exchange process where vapor properties (or the flux of vapor molecules to the liquid surface) may become limiting. Increasing vapor density would then result in increasing the heat transfer. The jet length required for condensation of the incoming vapor was simplified by assuming a constant area straight cylindrical jet. In some cases the jet will not be straight but will follow a irregular, tortuous path. Thus, the effective length in vapor which a given liquid particle traverses may be increased over the geometric distance from the point of injection to the point of final condensation. However, in general, the important trend is illustrated; increasing values of jet length result in increasing in the heat transfer capabilities of a given injected liquid flow.

3.4.3 Factors Influencing Jet Radius, Length, and Velocity

As discussed above the actual values of jet radius, length, and velocity are strongly influenced by flow parameters. One of the more important effects is produced by the vapor-liquid shear force upon the jet. Another is due to the disruptive forces occurring due to the rapid condensation of vapor upon liquid. High values of vapor velocity appear to promote breakup and disentegration of the liquid jet. (Refs. 13 and 14). In these references the relative vapor-liquid velocity is used directly as a parameter in predicting drop size for concurrent flow of vapor and liquid. High shear forces with the resulting liquid break-up result in smaller values of jet radius, longer jet lengths, and higher jet velocities than would be predicted using the model of Fig. 21.

The Reynolds Number of the injected liquid may have a very important influence upon the characteristics of the injected liquid. For a free jet injected into a still gas, break-up of the jet begins at a certain characteristic length which is dependent upon the

Reynolds Number of the injected liquid (Rayleigh instability). This breakup first takes the form of a varicose characteristic of the jet. Eventually physical breakup occurs and liquid droplets are formed. The length from the point of injection to the point where the varicose characteristic of the jet begins to become apparent is proportional to the liquid Reynolds Number. For a higher Reynolds Number the jet begins to assume a wavy character further downstream from the point of injection. The influence upon jet radius and length are clearly seen. Use of jet condensers with lower liquid Reynolds Number will result in decreased values of jet radius and increases in jet length due to appearance of a varicose characteristic. Injection of the liquid with high velocities results in a jet which is nearly constant in area and radius. This phenomena will be illustrated later in Fastax motion pictures taken of the injected liquid.

3.4.4 Influence of Heat Transfer Parameters on Pressure Integral in Pressure Rise Equations

Several of the parameters resulting from the analyses of jet heat transfer may also have an important influence upon the pressure rise integral which is found in the equation for predicted pressure rise of a jet condenser. The influence of these parameters may require their inclusion in correlations of experimental data.

The jet utilization factor, as discussed above, has a strong influence upon condensation rate of vapor on the liquid jet. From Section 3.3.1 , condensation rate may have an important influence upon the specific value of the pressure rise integral by affecting the vapor wall pressure. In addition, the jet utilization factor is a function of the outlet subcooling which also has an effect upon pressure rise integral.

The relative vapor-liquid velocity has an effect upon the heat transfer rate by the influence upon the character of the liquid jet as well as the eddy diffusivity of the jet. As discussed above, high values of vapor velocity or shear may increase the

eddy diffusivity within the jet. Through these effects upon heat transfer rate the relative vapor-liquid velocity will influence the value of the wall pressure integral as well as the specific location of the final vapor-liquid interface.

The primary influence of jet velocity is that for a given condensation length the jet residence time is inversely proportional to the jet velocity. High values of jet velocities result in smaller jet residence times which result in lower condensation lengths. On the other hand, lower values of jet velocities result in increased residence times of liquid in vapor, which tends to promote higher condensation rates (or lower values of outlet subcooling). In addition, as discussed above, higher values of jet velocity reduce heat transfer by producing a constant area jet instead of a liquid phase with a more irregular sinuous nature.

Finally, the density ratio of liquid to vapor, ρ, has an effect upon heat transfer and pressure integral. As discussed above, lower values of vapor density (or higher values of density ratio) result in lower condensation rates due to the decreased flux of vapor molecules impinging upon the liquid jet.

Due to the simultaneous interactions of these parameters, the jet condenser can be operated with the interface at the throat position with many different combinations of flow and thermodynamic variables. For example, a combination of high jet utilization factor, χ, and low injected liquid velocity, $V_{\ell o}$, or a low values of jet utilization factor and higher values of liquid velocity can be used to produce condensation at the desired location. In addition to influencing the final interface location these parameters also should influence the spatial distribution of condensation. High jet utilization factors and lower liquid velocities might produce the bulk of the condensation at the inlet region to the jet condenser while higher values of liquid velocity and lower values of jet utilization factor would probably tend to distribute the condensation over the length of the jet. Thus the specific combination of these variables can influence

the internal flow field in the mixing chamber and hence influence wall pressure integral and total pressure rise.

3.4.5 Conversion of Thermal Energy to Pressure Energy

One of the most important sources of pressure rise in the jet condenser is the thermal energy of the vapor. As discussed in Section 3.4.2 proper utilization of this source can result in pressure rises which are greater than 10 times the sum of dynamic pressures of the injected liquid and vapor. The physical mechanisms responsible for this phenomena are not well understood. However, it may be useful to think of the injected subcooled liquid as providing a pumping action upon the vapor; that is, as discussed in Section 2, the pressure at the boundary of the subcooled liquid and vapor is nearly equal to the saturation pressure of the liquid. This pressure is much lower than the free stream pressure for cases of interest. Thus, a sizable pressure difference or motive force is provided to accelerate the vapor to velocities which are even higher than the entrance velocity. In some cases the pressure ratio may be sufficient to produce sonic velocities at the interface. Condensation of the vapor at these high velocities then results in a greater momentum recovery than would be calculated based upon the inlet vapor velocity alone.

In order to assess the effect of conversion of thermal to pressure energy the energy conversation equation was applied at the inlet and outlet of a jet condenser. (Appendix C). A specific example for flow rates and pressure rise was chosen to illustrate the decrease in outlet thermal energy corresponding to a high pressure rise. For this example, the decrease in outlet temperature resulting from an increase in pressure of 62 psi was calculated to be on the order of $1/2^{o}F$. This amount is a small quantity, which by itself would not strongly effect cycle efficiency. However, it should be realized that as the pressure energy is expended throughout the rest of the system in overcoming friction, the temperature of the liquid is raised accordingly. Thus, for a jet condenser operating where the pressure rise is expended in circulation of fluid, no large effect upon cycle efficiency should result. The energy of the vapor is transferred to the fluid of

the liquid radiator loop, whether it be in the form of heat from condensation or as mechanical energy. This result means that a Rankine cycle power system with a jet condenser could probably be operated with high pressure drop through a liquid radiator loop with very small increases required in turbine output or heat addition to the boiler.

4. EXPERIMENTAL PROCEDURES

Experimental investigations of jet condensers were performed during this program using two closed cycle mercury test loops. The 1kw test loop and the 10kw test loop are described in detail in Part I of this report (Ref. 15). The 1kw loop was used for constant area jet condenser tests while the 10kw loop provided the means for testing variable area and multi-tube jet condenser geometries. Schematics of each test rig are shown in Figs. 22 and 23. In both loops, mercury vapor was generated in a pool boiler, circulated through baffles and superheaters to obtain a controlled quality, and then delivered to the test section. Liquid mercury at nearly ambient temperature was pressurized by a low speed gear pump, heated to the desired injection temperature, and subsequently was mixed with the vapor stream in the test section. The outlet flow of liquid from the test section was cooled to nearly ambient temperature and pressurized. Part of this flow was delivered to the test section (cf. above) and the remainder was returned to the boiler to complete the flow circuit.

4.1 Test Section Geometry

Design of the injector geometry for a jet condenser requires a compromise to be made between pressure rise and heat transfer characteristics. Vapor-liquid heat transfer is promoted by a high degree of dispersion of the liquid phase. However, this is usually accomplished through the dissipation of the kinetic energy of the injected liquid, which reduces the amount of energy available for pressure recovery. During the previous program (Ref. 4), test sections were designed to achieve rapid heat transfer rates. Subcooled liquid was, therefore, introduced in the form of several impinging jets. During this program, however, consideration of pressure rise capabilities, reliability, and simplicity led to

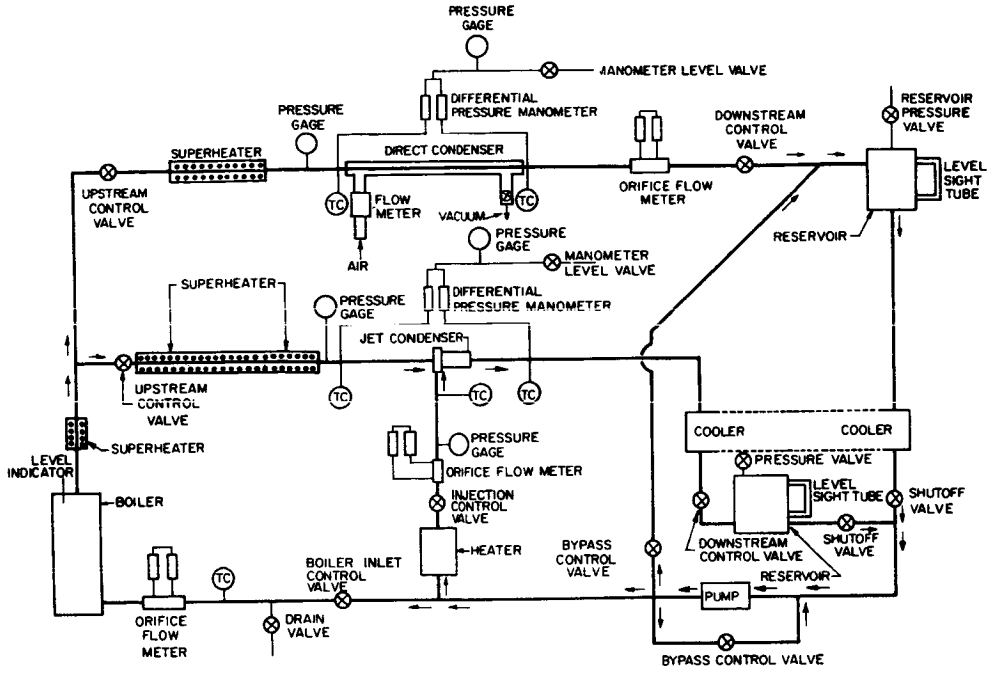

FIG. 22 1 kw MERCURY TEST LOOP SCHEMATIC

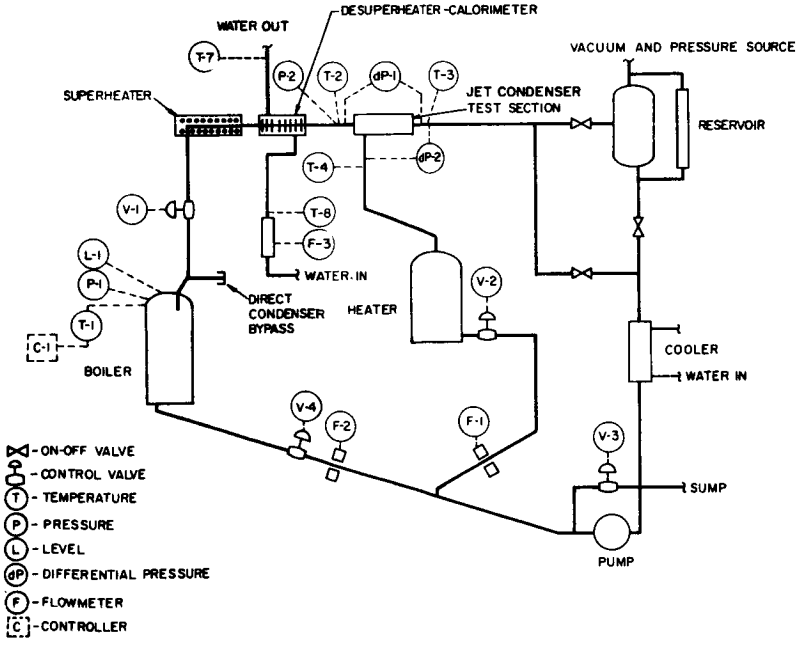

FIG. 23 10 kw TEST LOOP SCHEMATIC

the selection of a single central injector. Since improved pressure rise characteristics were obtained with relatively small decreases in heat transfer rate, this type of injector was used in subsequent test sections. Other schemes may be devised which result in lower pressure drop losses in the injector flow passages than for the geometries used. However, the test section configurations chosen provide a central stream of subcooled liquid with known initial properties, with simplicity and ease of construction.

The optimum mixing section geometry to insure both high pressure rise and high heat transfer rates consists of a properly designed converging section (cf. Section 3). However, initial tests were conducted on a constant area geometry to determine feasibility and heat transfer characteristics for central injectors. These data were used for sizing of variable area geometries.

The first test sections used had a vapor internal diameter of 0.19 inches. Results from these tests were used to scale condenser geometries to larger size units (vapor internal diameter of 0.75 inches). Finally, a multiple unit test section was built which had a capacity equal to the single units with 0.75 inch internal diameter. Table II furnishes a description of the various geometries tested during this program. In addition, for purposes of comparison two impinging jet geometries, which were previously tested, are included. Figure 24 is a schematic of a test section geometry which reflects the features of construction of most of the units. Figures 25-32 are photographs of one of the large diameter geometries and the multi-tube unit. Figure 28 furnishes a photograph of the jet condenser assembly and construction details for one of the large diameter units.

The majority of test sections were constructed with transparent mixing sections in order to record condensation length and obtain high speed photographs of the internal flow processes. However, some units featured all-metal construction for tests where very high pressure rises (greater than 50 psid) were to be obtained. The transparent sections were constructed of quartz in order to maximize high temperature strength

TABLE II - JET CONDENSER TEST SECTION GEOMETRY

Test Section No.	a	b	1	2	3	4	5	6	7	8	9*
Injector Type	IJ	IJ	CI	CI	CI	CI	CI	CI	CI	CI	CI
Number of Injectors	8	8	1	1	1	1	1	1	1	1	1
Angle of Injectors with Vertical to Tube Axis(^{o})	35	35	90	90	90	90	90	90	90	90	90
Injector I.D. (inches)	0.0156	0.0312	0.051	0.085	0.052	0.052	0.052	0.052	0.206	0.206	0.118
Vapor Inlet Diameter	0.190	0.190	0.190	0.190	0.190	0.190	0.190	0.190	0.750	0.750	0.430
Mixing Chamber Type	c.a	c.a	c.a	c.a	v.a	v.a	v.a	v.a	v.a	v.a	v.a
Mixing Chamber Material	quartz	quartz	quartz	quartz	quartz	quartz	SS	SS	quartz	quartz	quartz
Mixing Chamber Length (inches)	3	3	6	6	1/4	1/4	1/4	1/4	0.985	0.985	.565
Throat Diameter	0.190	0.190	0.190	0.190	0.099	0.060	0.057	0.055	0.218	0.218	0.125
Throat Length (inches)	-	-	-	-	3/8	3/8	3/8	3/8	1.48	$\sim$1/4	0.85
Diffuser Angle (included) (^{o})	-	-	-	-	13	13	11	10	10	10	10
Injector/Tube Inlet Area Ratio	0.054	0.216	0.072	0.20	0.075	0.075	0.075	0.075	0.075	0.075	0.075
Injector/Throat Area Ratio	0.054	0.216	0.072	0.20	0.28	0.723	0.83	0.90	0.90	0.90	0.90
Test Loop (kw)	1	1	1	1	10	10	10	10	10	10	10

NOTE: IJ - Impinging Jets

CI - Central Injectors

c.a - Constant Area

v.a - variable area (convergent-divergent)

* - Multi-tube unit; three of these geometries were manifolded during tests

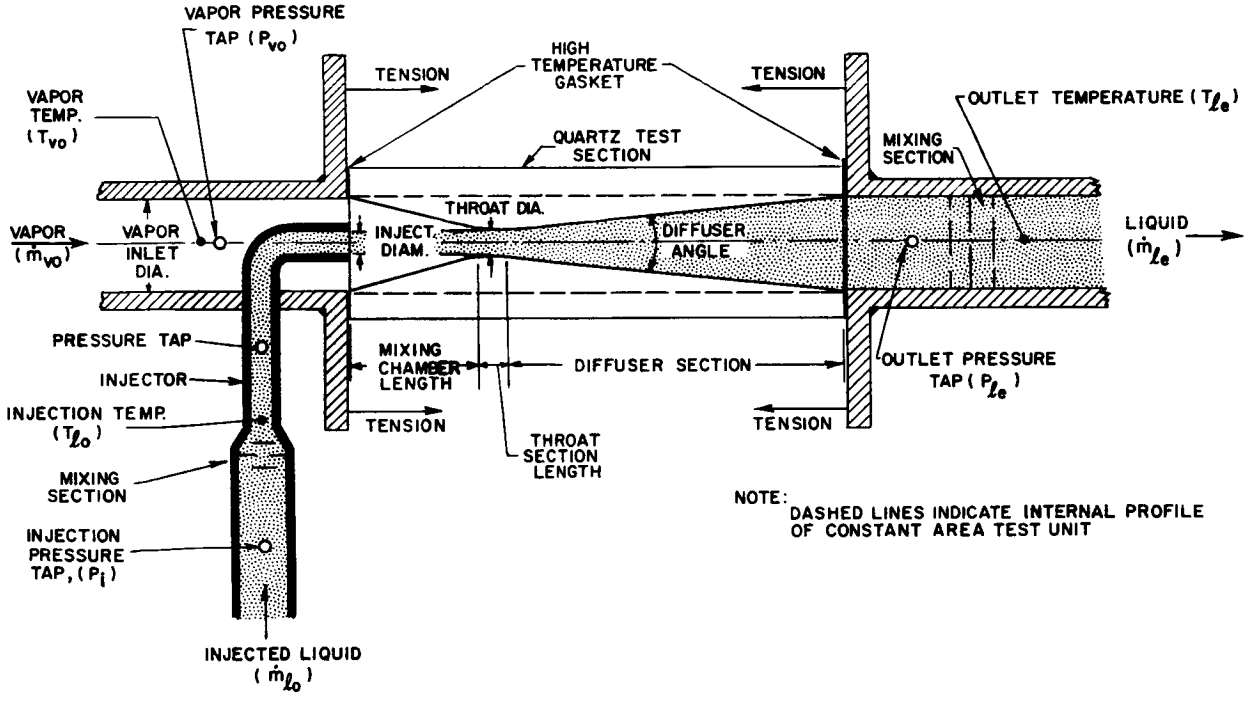

FIG. 24 SCHEMATIC OF TYPICAL JET CONDENSER TEST SECTION

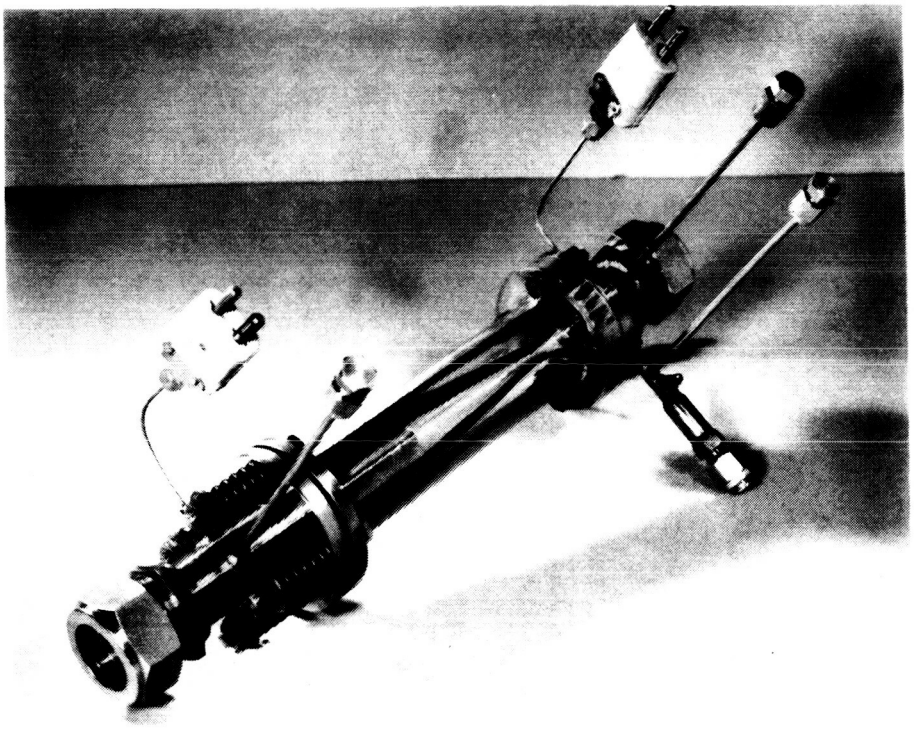

FIG. 25

LARGE DIAMETER
JET CONDENSER

FIG. 26

LARGE DIAMETER JET CONDENSER
ASSEMBLY

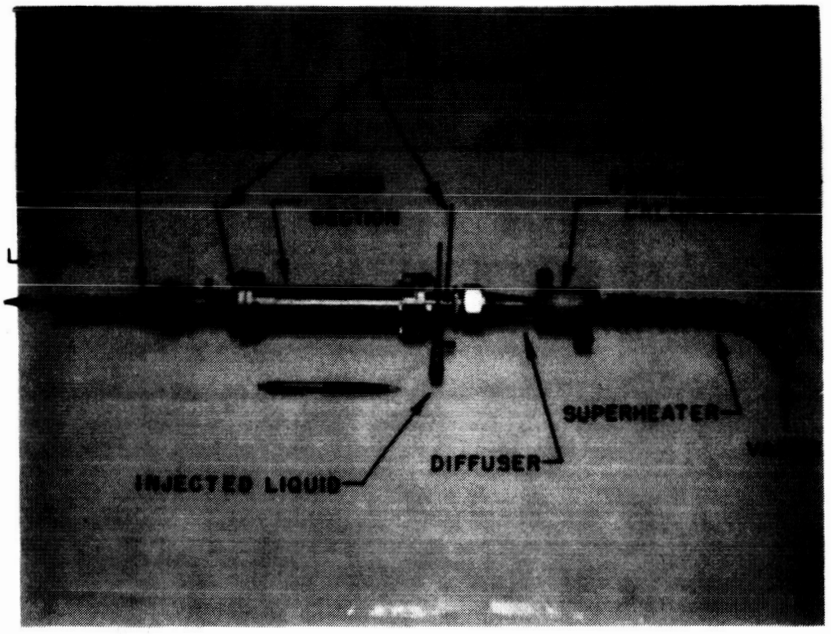

FIG. 27 LARGE DIAMETER JET CONDENSER ASSEMBLY

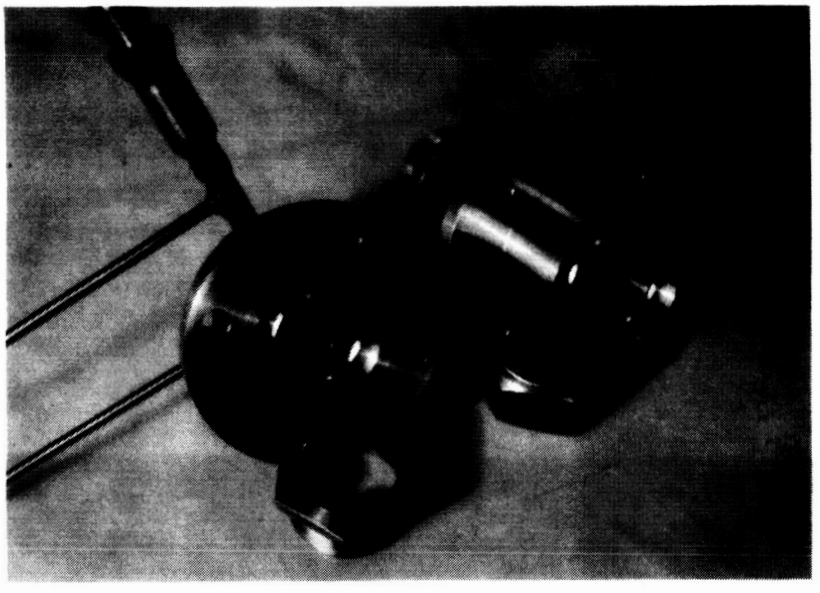

FIG. 28 LARGE DIAMETER JET CONDENSER INJECTOR AND DOWNSTREAM SECTION

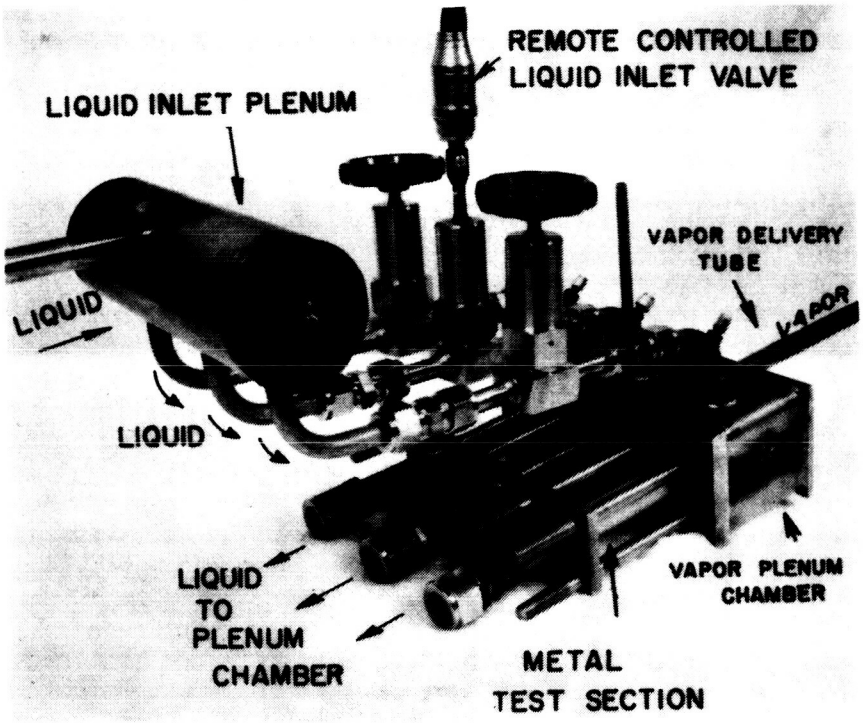

FIG. 29 MULTI-TUBE JET CONDENSER ASSEMBLY

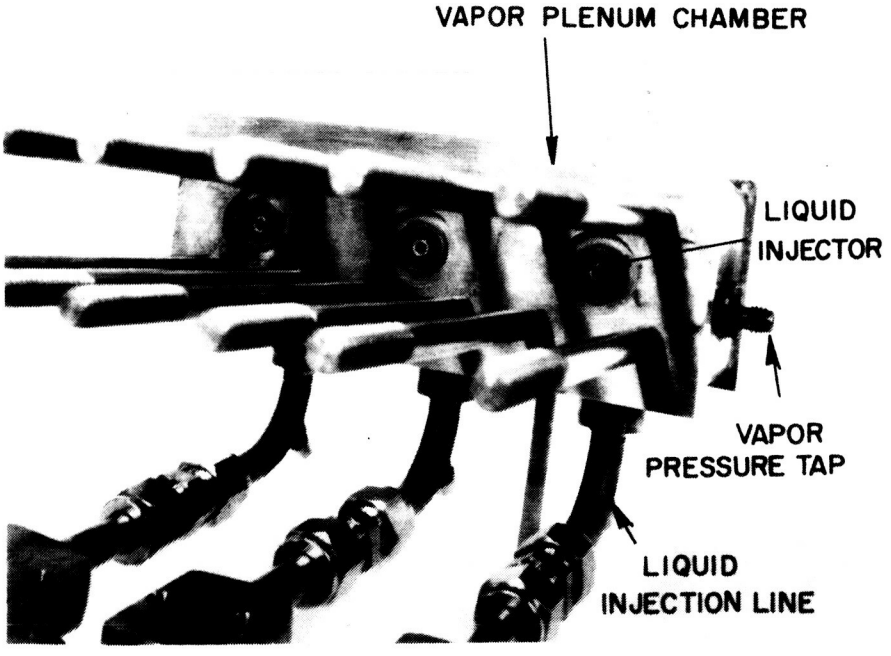

FIG. 30 MULTI-TUBE JET CONDENSER - LIQUID INJECTORS AND VAPOR INLET STRUCTURE

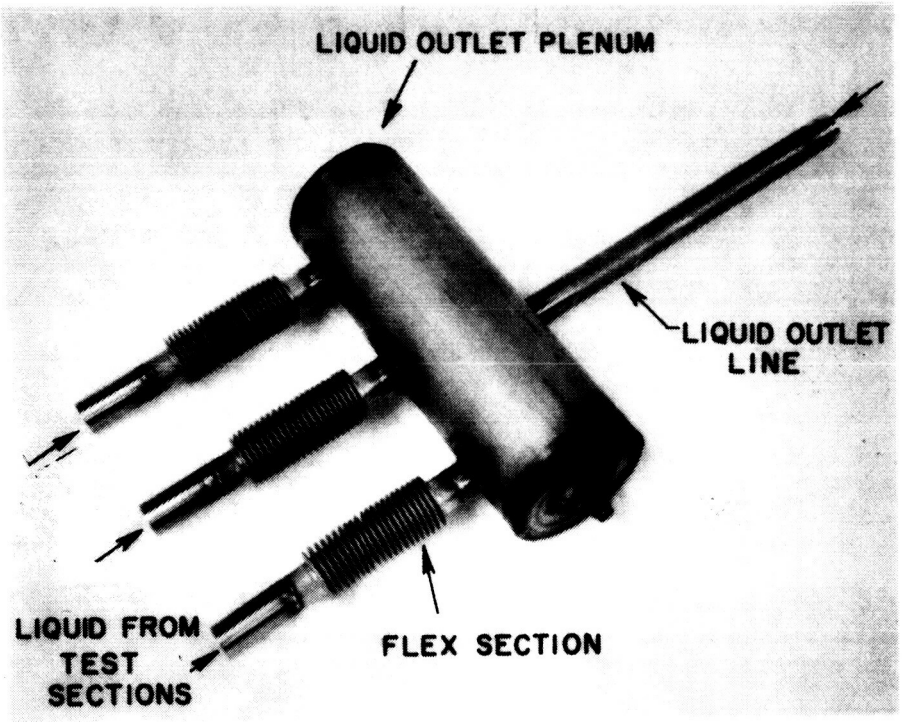

FIG. 31 MULTI-TUBE JET CONDENSER - LIQUID OUTLET PLENUM CHAMBER

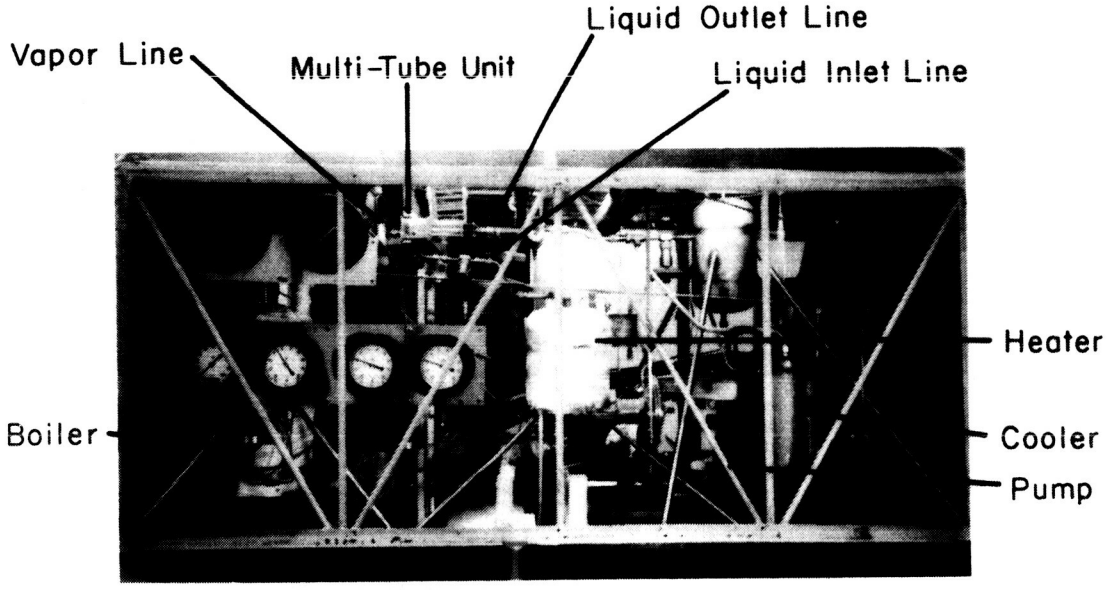

FIG. 32 10KW TEST LOOP MULTITUBE UNIT INSTALLED

and minimize problems of thermal shock (as opposed to Pyrex). Sealing between the stainless steel and quartz was accomplished by compression of a high-temperature gasket material at both ends. This construction technique resulted in some leakage problems at higher pressure rises (greater than 40 psid) but was satisfactory for the majority of test conditions.

During construction of the multi-tube test unit, careful control of the dimensions of each of the three jet condensers was maintained in order to eliminate the influence of any geometric non-uniformity. Dimensions on metal parts and metal mixing chambers were controlled to within 0.001 inch. The quartz mixing sections were constructed within a maximum tolerance of 0.002 inch. In order to verify the uniformity of these dimensions, flow tests using air were conducted with the multi-tube test unit. Air was supplied to the vapor plenum chamber from the vapor inlet tube. Water manometers and separate outlet orifices were used to provide an indication of the relative flow through each jet condenser tube. The pressure drops across these orifices were calibrated against a commercial flowmeter (2 percent accuracy) to determine the air mass flow rate. With this experimental arrangement the maximum deviation of the gas flow in any tube from the average was 2 percent, which is within the uncertainty of the measuring apparatus.

4.2 Range of Variables

The range of variables covered for the test units is furnished in Table III. Comparison of these variable ranges with design conditions for SNAP 8, SNAP 2, and Sunflower can be obtained by referring to this table and Table 3-2 of Part I of this report. All test units were operated in a horizontal attitude such that gravity did not aid in the final separation of vapor and liquid. Units had been tested with the flow vertically upward in the previous program, with no discernible differences in performance. Therefore, no similar tests were conducted during this program. The limiting values of pressure rise and mass flow ratios were established by test loop capabilities rather than by performance of jet condensers.

TABLE III - RANGE OF VARIABLES FOR MERCURY JET CONDENSER TESTS

Independent Variables	Previous Program *	Constant Area Small Diam.**	Variable Area Small Diam.**	Variable Area Large Diam.**	Multi-Tube Unit**
1. Test Section Numbers	a, b	1, 2	3,4,5,6	7,8	9
2. Inlet Vapor Temp-T_{vo} (^{o}F)	700-860	710-750	590-750	490-786	509-740
3. Inlet Vapor Pressure-P_{vo}(psia)	20-54	21-32	6.5-32	1.8-40	2.2-28.0
4. Inlet Vapor Flow Rate-$\dot{m}_{vo}$(lb/hr)	12-25	12-42	11-52	48.9-228	73.3-224
5. Inlet Vapor Velocity-V_{vo}(fps)	29-89	52-180	42-278	18-395	26.9-161
6. Inlet Vapor Reynolds No.-Re_{vo}	$6.4x10^3$-$1.4x10^4$	$6.4x10^3$-$2.2x10^4$	$6.1x10^3$-$3.0x10^4$	$7.8x10^3$-$3.64x10^4$	n.c.
7. Inlet Vapor Quality- x_{vo}	~ 0.8	1.0	1.0	1.0(1 run at 0.8)	1.0
8. Heat Rejection in Condensation of Vapor, Q_R (BTU/hr)	1490-3150	1500-5300	138-6740	6180-28,800	9300-28,900
9. Subcooling of Injected Liquid - (T_{vo} - $T_{\ell o}$) (^{o}F)	95-400	85-510	150-530	153-434	152-611
10. Injected Liquid Flow Rate $\dot{m}_{\ell o}$ (lb/hr)	214-740	370-985	520-1120	1270-8590	1520-7220
11. Density Ratio(liquid to vapor) $\overset{o}{\rho} = \rho_\ell/\rho_v$	950-2300	1575-2260	1620-8230	1250-25,700	1705-19,600
12. Injected Liquid Velocity- $V_{\ell o}$ (fps)	1.85-24.4	9.0-24	12.0-25.8	1.9-12.7	2.3-11.0
13. Mass Flow Ratio(liquid:vapor)$\overset{o}{m}_R$	7 to 35	13.5 to 72	14.6-67.5	13.1-66.1	7.9-75.9
14. Jet Utilization Factor - χ	0-1.0	0-1.0	0-1.0	0-1.0	0-1.0
Dependent Variables					
15. Outlet Subcooling with Interface in Test Section(T_{vo} - $T_{\ell o}$)(^{o}F)	5-150	21-250	50-372	11-211	53-344
16. Condensation Length-L_c (inches)	<0.05-3.0	<0.05-6.0	<0.05-3.0	<0.05 - ~ 5.0	<0.05 - ~ 3.0
17. Injection Pressure Drop-ΔP_i(psid)	4-98	12-83	14-107	3 - >41	n.c.
18. Pressure Rise from Vapor to Outlet Liquid- ΔP_a (psid)	<0-2.5	<0-6.4	<0-62	<0-33.5	<0-9.0
19. Nondimensional Pressure Rise (Referred to liquid) $\overset{o}{\Delta P}_\ell = \Delta P_a/\rho_\ell V_{\ell o}^2/2g$	<0-0.55	<0-0.17	<0-0.17	<0-12.1	<0-1.92

* Impinging jet injectors

** Central jet injectors

n.c. Not computed (or measured)

4.3 Operating Procedures

Two different procedures were used for jet condenser startup: injection of liquid into flowing vapor or introduction of vapor into the circulating liquid. Of the two, the latter was found preferable from the standpoint of control and minimizing thermal shock, and hence, was used for the majority of test runs. The former procedure was useful, however, in visualizing the processes of interface formation (Section 5). Both techniques were used in both the 1kw loop and the 10kw loop. The operation procedure used most frequently in the 10kw loop (cf. Section 2 of Part I) was as follows:

1. The entire system was pumped down to a vacuum of 29 to 30 inches Hg and filled from the sump (this step eliminated any trapped air pockets or voids).
2. After the boiler level was established, the boiler heaters were turned on and the boiler was shut off from the rest of the system. As the boiler temperature was raised to the operating point the boiler was periodically vented to vacuum (29 to 30 inch Hg) in order to remove dissolved or trapped non-condensible gases liberated by the boiling.
3. Liquid was circulated through the test section and reservoir while heated. The agitation and heating, coupled with the use of vacuum pressures, reduced the concentration of dissolved air in the liquid mercury.
4. When operating values of temperature and liquid flow rate were obtained, the pressure was adjusted to the proper value in the reservoir, and vapor was introduced to the test section. Flow conditions were then adjusted until the interface was in the desired location. Upstream superheaters were activated and adjusted until a vapor quality of unity was obtained at the test section inlet.
5. The inlet valve to the boiler was opened and adjusted until the flow into the boiler matched the vapor flow rate. When this

balance was obtained the reservoir was isolated from the rest of the test loop. Closed cycle operation was then maintained by adjusting the boiler inlet valve.

6. Adjustments of heaters, valves, and cooler were then made to finalize or change test conditions.

A certain amount of latitude was found to exist when adjusting the boiler inlet flow rate during closed cycle operation with variable area test sections; i.e., changing the boiler inlet flow rate from the vapor flow rate within a range (approximately $\pm$ 10 percent) resulted in a change in the operating conditions of the jet condenser to accommodate the initial mismatch. For example, if the inlet liquid flow to the boiler was greater than the vapor flow leaving the test section, the vapor pressure dropped, resulting in a higher vapor flow rate. Of course, this condition only occurred due to the thermal lag associated with the boiler heaters and materials. If a sufficient time were allowed (approximately 10 to 15 minutes), the mismatch would again be obtained in the condenser and the interface would eventually change location and/or collapse. However, these response characteristics simplified control and in addition, indicate variable area jet condensers may be self-regulating, under some circumstances, for small flow perturbations.

4.4 Instrumentation and Experimental Error

Pressure, temperature, and flow instrumentation were calibrated over the range of operation for jet condenser tests. Calibrations varied somewhat but the differences were small ($\sim \pm$ 1/2 percent) on all instrumentation with the exception of the electromagnetic flowmeters. These calibrations changed by approximately seven percent in six months due to decreases in the permanent magnet strength. Table IV presents a summary of the maximum probable error in measured parameters. This error estimate is based on the scatter encountered in calibrations, and on the least readings possible with the visual and electronic readout techniques used.

Differential pressure gage maximum error changed from test section to test section as different range gages were used due to the changes

TABLE IV

Summary of Experimental Error

Measured Parameters	1kw Test Loop	10kw Test Loop
Pressure (absolute)	± 1.0 psia	± 1.0 psia
Pressure (differential)	± 0.1 psid	± 0.2 psid-test Sec. No. 3 ± 0.5 psid- Test Sec. No. 4,7,8,9 ± 2.0 psid- Test Sec. No. 5,6
Flow Rates	± 2 percent	± 5 percent
Temperatures	± 2° F	± 2° F
Condensation Distance	± 1/16 inch	± 1/16 inch

in the magnitude of pressure rise. Testing of test Section No. 3 was conducted using a gage with a range of 10-0-10 psid. Test Section Nos. 5 and 6 were tested using the differences in readings from two absolute gages (0-200 psig) to determine pressure rise. The latter technique was used because some of the values of pressure rise were out of the range of the existing differential gages.

Calibrations were conducted periodically on the gages (every 3 or 4 test days). The maximum deviation among calibrations was always less than the maximum error given in the table. Figure 33 is an example of a calibration curve for the 0-50 psid gage. The zero reading on the gages shifted slightly from "cold" to test conditions due to the change in ambient temperature inside the test enclosure. However, the zero values were recorded with no flow both before and after each test sequence and the average applied to the gage reading to determine the actual pressure rise.

Thermocouples and the associated readout equipment were calibrated using the melting points of tin, lead, and zinc (450, 621, and 785^{o}F respectively). Freezing curves were plotted on the recorder for all thermocouples and the melting point determined by the constant temperature portion of the curve. As indicated in Table IV, the maximum deviation obtained of the readings from the above values was 2^{o}F.

4.5 Sample Calculations

In order to illustrate the methods of data reduction, the appropriate equations and sample calculations for Test Run #3-13-1 are presented in this section. The location of the measurements can be obtained from Figs. 22 and 24.

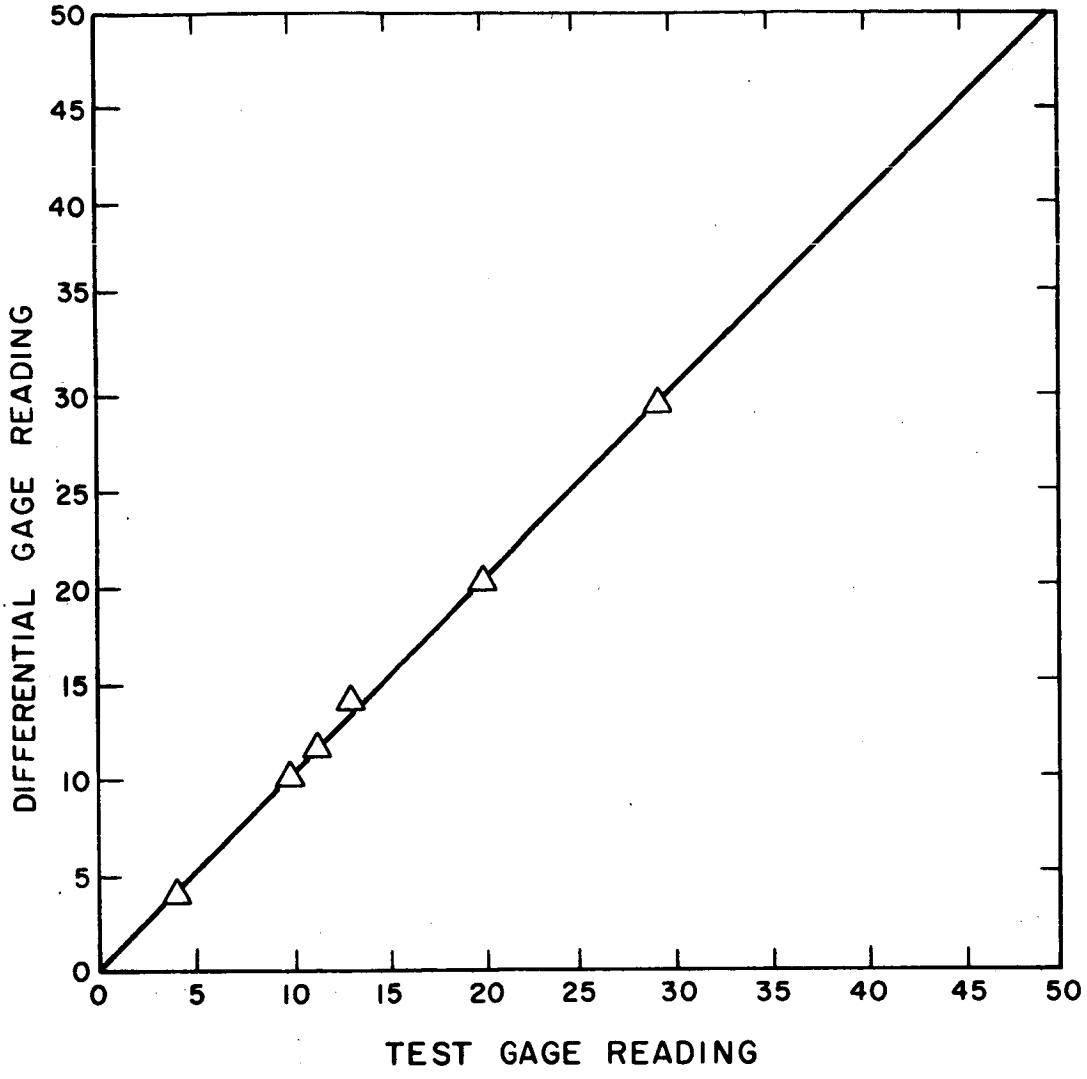

FIG. 33

SAMPLE CALIBRATION CURVE FOR 0-50
PSID BARTON DIFFERENTIAL GAGE
10-18-61

Measured Parameters

$T_{vo} = 536^{o}F$

$T_{\ell o} = 240^{o}F$

$T_{\ell e} = 408^{o}F$

$P_{vo} = 3.4$ psia

$P_{i} = 14.5$ psia

$\Delta P_{a} = 14.9$ psid

$\dot{m}_{\ell o} = 4200$ lb/hr

$A_{\ell o} = 2.32 \times 10^{-4}$ ft^2

$A_{to} = 3.07 \times 10^{-3}$ ft^2

$x_{vo} = 1.0$

$L_{c} = 1.0$ in

$\mathring{A}_{1} = 0.895$

$\mathring{A}_{2} = 0.075$

$d_{to} = 0.750$ in

$d_{i} = 0.206$ in

$A_{vo} = 2.84 \times 10^{-3}$ ft^2

Calculated Parameters

$$\chi = \frac{T_{\ell e} - T_{\ell o}}{T_{vo} - T_{\ell o}} = \frac{408 - 240}{536 - 240} = 0.572 \qquad (20)$$

$$Q_R = \dot{m}_{\ell o} C_p (T_{\ell e} - T_{\ell o}) = (4200)(.032)(408 - 240) = 22{,}600 \text{ BTU/hr} \qquad (21)$$

$$\dot{m}_{vo} = \frac{Q_R}{h_{fg} + C_p (T_{vo} - T_{\ell e})} = \frac{(22{,}600)}{126.4 + .032(536 - 408)} = 173 \text{ lb/hr} \qquad (22)$$

$$V_{vo} = \frac{\dot{m}_{vo}}{\rho_v A_{vo}} = \frac{(173)}{(.062)(2.84 \times 10^{-3})(3600)} = 273 \text{ fps} \qquad (23)$$

$$V_{\ell o} = \frac{\dot{m}_{\ell o}}{\rho_\ell A_{\ell o}} = \frac{(4200)}{(828)(2.32 \times 10^{-4})(3600)} = 6.09 \text{ fps} \qquad (24)$$

$$\overset{o}{\Delta P}_v = \Delta P_a / \rho_v V_{vo}^2 / 2g = \frac{(14.9)(64.4)(144)}{(0.062)\ 273)^2} = 29.9 \qquad (25)$$

$$\overset{o}{\Delta P}_\ell = \Delta P_a / \rho_\ell V_{\ell o}^2 / 2g = \frac{(14.9)(64.4)(144)}{(828)(6.09)^2} = 4.51 \qquad (26)$$

$$\Delta P_i = P_i - P_{vo} = 14.5 - 3.4 = 11.1 \text{ psid} \qquad (27)$$

$$\overset{o}{m}_R = \dot{m}_{\ell o} / \dot{m}_{vo} = 4200/173 = 24.2 \qquad (28)$$

$$\overset{o}{\Delta P}_{\ell(calc)} = 2\overset{o}{A}_1 \left(1 + \frac{\overset{o}{\rho}}{\overset{o}{m}_R{}^2} \frac{\overset{o}{A}_2}{1 - \overset{o}{A}_2}\right) - \left(\frac{1}{\overset{o}{m}_R} + 1\right)^2 (\overset{o}{A}_1{}^2 + \overset{o}{A}_2{}^2) \qquad (29)$$

$$= (2)(.895) \left[1 + \frac{(14300)(.075)}{(24.2)^2(.925)}\right] - \left(\frac{1}{24.2} + 1\right)^2 \left[(.895)^2 + (.075)^2\right]$$

$$= 4.50$$

$$\Delta P_{a(calc)} = (\overset{o}{\Delta P}_{\ell(calc)})(\rho_\ell V_{\ell o}^2 / 2g) = (4.50)(828)(6.09)^2/(64.4)(144) \qquad (30)$$

$$= 14.9 \text{ psid}$$

$$\eta_a = \Delta P^g_\ell / \Delta P^g_{\ell(calc)} = 4.52/4.50 = 1.002 \quad (31)$$

$$\eta_i = (\rho_\ell V_{\ell o}{}^2/2g)/\Delta P_i = (828)(6.09)^2/(64.4)(144)(11.1) = 0.298 \quad (32)$$

$$Re_{vo} = \frac{\rho_v V_{vo} d_{to}}{\mu_v} = \frac{(.062)(273)(.75)(3600)}{(.130)(12)} = 29,300 \quad (33)$$

$$Re_{\ell o} = \frac{\rho_\ell V_{\ell o} d_i}{\mu_\ell} = \frac{(828)(6.09)(.206)(3600)}{(2.90)(12)} = 107,500 \quad (34)$$

$$V_R = V_{vo} - V_{\ell o} = 273 - 6.1 \cong 267 \text{ fps} \quad (35)$$

$$\Psi = \frac{\chi V_{\ell o}}{V_R} = \frac{(.572)(6.09)}{(267)} = 0.0131 \quad (36)$$

NOMENCLATURE FOR SECTION 4

T	-	temperature
P	-	pressure
ΔP_a	-	pressure rise from vapor to condensate
$\dot{m}$	-	mass flow rate
A	-	area
X	-	quality
L_c	-	condensation length
$\overset{o}{A}_1$	-	area ratio of injector to throat
$\overset{o}{A}_2$	-	area ratio of injector to tube inlet
d	-	diameter
χ	-	jet utilization factor
Q_R	-	heat rejected in condensation of vapor
C_p	-	specific heat of liquid
h_{fg}	-	heat of vaporization
ρ_o	-	density
$\Delta\overset{o}{P}_v$	-	pressure rise divided by inlet vapor dynamic pressure
v	-	velocity
$\Delta\overset{o}{P}_\ell$	-	pressure rise divided by inlet liquid dynamic pressure
$\overset{o}{m}_R$	-	mass flow ratio of liquid to vapor
η_a	-	ratio of measured to calculated pressure rise
η_i	-	ratio of ideal to measured injector pressure drop
Re	-	Reynolds number
μ	-	viscosity

SUBSCRIPTS FOR SECTION 4

v - vapor

ℓ - liquid

o - inlet

i - injector

e - exit

t - tube

(calc) - calculated

5. EXPERIMENTAL RESULTS

5.1 Presentation of Data

5.1.1 Description of Tabulated Data

Experimental data obtained for the jet condenser test geometries (Table II) are summarized in Appendices D, E, F, and G. Original data and performance parameters derived from the measured data are included in tabular form.

For the data sets where condensation lengths are given, quartz test sections were used and visual estimates were made. No quantitative information for condensation length was available for runs where metal test sections were used (for high pressure rise). Liquid temperature measurements were made using turbulating devices (baffles, screens, etc.) upstream of a sheathed thermocouple. However, tests of jet condenser No. 8 were conducted with all obstructions removed in order to obtain the maximum liquid circulation rates. However, this test unit was well insulated such that the measured temperatures (centerline) should be within 5° to 10°F of the bulk temperature. No turbulation was provided for vapor temperature measurements since saturated vapor test conditions were used at all times. Vapor quality of unity was ensured on all test runs (except 3-16-9) by superheating the vapor and then reducing the superheat until saturated conditions were reached. For the majority of test runs, this point was reached with very little or zero power to the superheater (due to throttling of the vapor through the baffle, integral superheater, and vapor valve).

Pressure rise was measured from a point in the vapor delivery tube upstream of the injector to a point at the outlet of the test section (cf. Fig. 24). No attempt was made to correct for pressure losses due to injector drag and friction, or wall friction. For the injector tube area ratio tested (0.075) these losses were small ($< 5\%$)

compared to the total pressure rise. Testing of one geometry with a larger area ratio (0.20) resulted in losses which were too large to record meaningful data. It should be noted that these losses were characteristic of the particular injector configuration which was chosen for testing.

Injector pressure drop was measured by determining the difference between the absolute pressure in the liquid line upstream of the injector and the vapor pressure upstream of the injector. Liquid flow rate was determined upstream of the injection heater where the mercury temperature was approximately equal to ambient (70^{o} to 130^{o}F). Other parameters in the appendices are derived from the flow, temperature and pressure measurements using measured test section dimensions which are summarized in Table II.

5.1.2 Performance Parameters

A discussion of some parameters which characterize jet condenser operation was given in Section 2. However, it may prove useful to summarize the more important of these, which will be used as a basis for comparing performance for different geometries of varying flow conditions. These parameters or modifications will form the dependent variable for the majority of the curves to be presented in this section.

1. $\Delta P^{o}_{\ell} = \Delta P_a / \rho_\ell V_{\ell o}^{\ 2}/2g$ The non-dimensional pressure rise referred to injected liquid dynamic pressure relates the total pressure rise to the pressure drop required for injection with an ideal injector.

2. $\eta_i = \dfrac{\rho_\ell V_{\ell o}^{\ 2}/2g}{\Delta P_i}$ The injector efficiency relates the ideal injector pressure drop to measured values of pressure drop. These include bend and frictional losses.

3. $\Delta P^{o}_{v} = \Delta P_a / \rho_v V_{vo}^{\ 2}/2g$ The non-dimensional pressure rise referred to vapor dynamic pressure relates the pressure rise to inlet vapor conditions. A convenient parameter is therefore obtained whereby the absolute magnitude of pressure rise can be determined for a set of fixed vapor conditions.

4. $\eta_a = \Delta P_a / \Delta P_{a\ (calc)}$ The ratio of actual pressure rise to that calculated for a constant pressure model furnishes an indication of the effects not included in the theory of Section 3.2. In addition, a basis for extending test results to other geometries and flow conditions is provided.

5. L_c The condensation length provides an indication of the required condenser size and for a given vapor flow rate is inversely proportional to the average heat transfer flux.

Information on all parameters is presented for the constant area geometry tested. Pressure rise and condensation length were varied over a wide range. However, variable area geometries required a fixed location of the vapor-liquid interface for design operation. Consequently, information on heat transfer is mainly a correlation of the values of flow parameters required to maintain the interface at the throat location. Pressure rise characteristics were determined for all geometries. However, problems of injector-throat alignment and dimensional control resulted in inconsistencies for small diameter-variable area data. Consequently, the majority of variable area pressure rise plots were derived from test results for the large diameter (0.75 in. i.d.) units. Performance parameters for all test runs are summarized in the appendices.

5.1.3 Parameters Controlling Performance

The values of condensation length and pressure rise for jet condenser operation are primarily influenced by the liquid-vapor mass flow ratio, density ratio, and temperatures. Consequently, parameters derived from these quantities form the independent variables for most plots. The importance of mass flow ratio and density ratio have been previously discussed in Sections 2 and 3. However, there are several ways in which the operating temperatures of a jet condenser can be expressed and related to other quantities. These temperature relations will be discussed in this section:

1. $\chi = \dfrac{T_{\ell e} - T_{\ell o}}{T_{vo} - T_{\ell o}}$ The jet utilization factor expresses the ratio of the enthalpy change of the liquid to the amount it would experience if it were raised to vapor temperature. The derivation of this parameter from a heat transfer analysis and discussion of its significance in a jet condenser system is given in Section 3.4. In addition relationships with other parameters are developed, viz:

$$\chi = \frac{1}{\dfrac{T_{vo} - T_{\ell e}}{T_{\ell e} - T_{\ell o}} + 1} = \frac{1}{\dfrac{\Delta T_{sc}}{\Delta T_R} + 1}$$

$$\chi = \frac{1}{\dot{m}_R - \dot{m}_R^* + 1}$$

Thus, plots with χ as the independent variable can be rearranged such that the independent variable is the outlet subcooling, "radiator" temperature drop, or excess mass flow ratio. When vapor and liquid flow rates are held constant and the temperature varied, χ appears to be the controlling function which influences condensation length and/or pressure rise.

2. $\Psi = \dfrac{\chi V_{\ell o}^{a}}{V_R^{b}}$ The modified utilization factor is an empirical quantity which appears to provide the best correlation of the flow conditions required for a vapor-liquid interface to occur at the throat location in variable area condensers. For constant area jet condensers this same parameter (with different exponents) appears to have the most direct influence upon the condensation distance when liquid and vapor flow are varied, in addition to variations made in temperatures.

5.2 Constant Area Condenser

5.2.1 Condensing Length

Curves of condensation length vs. the jet utilization factor are shown in Fig. 34 for several average liquid-vapor mass flow ratios for test Section No. 1. A significant feature of each curve is the appearance of three general regions. In the first region at low values of χ, large changes in jet utilization factor can be accommodated with very little effect on condensation length. The second region represents a transition zone where changes in utilization factor produce moderate changes in condensation length. In the third region (which should be avoided in operation of a jet condenser in a power system), small changes in jet utilization factor can produce very large changes in condensation length. As an example, in Fig. 34, for the curve to the extreme right, the first region on the curve extends up to values of χ of about 0.7. The second region corresponds to a range of jet utilization factor from 0.7 to 0.87. The third region exists for a jet utilization factor greater than 0.87. The value of χ at which the condensation length exhibits a rapid increase appears to be dependent upon the mass flow ratio of liquid to vapor. For example the curve for $\overset{o}{m}_R = 66$ rises at a value of $\chi \cong 0.6$ while the curve for $\overset{o}{m}_R = 16$ rises at $\chi \cong 0.85$.

Choice of a high jet utilization factor in a jet condensing system has the effect of reducing liquid radiator weight and reducing the excess mass flow ratio (cf. Sec. 6). However, high values of χ may result in excessive condensation lengths, unstable conditions, and (as will be seen later)poor pressure recovery characteristics. A correlation of the relation between condensation length and χ(or Ψ) for variations in other flow parameters is therefore important for preliminary design purposes.

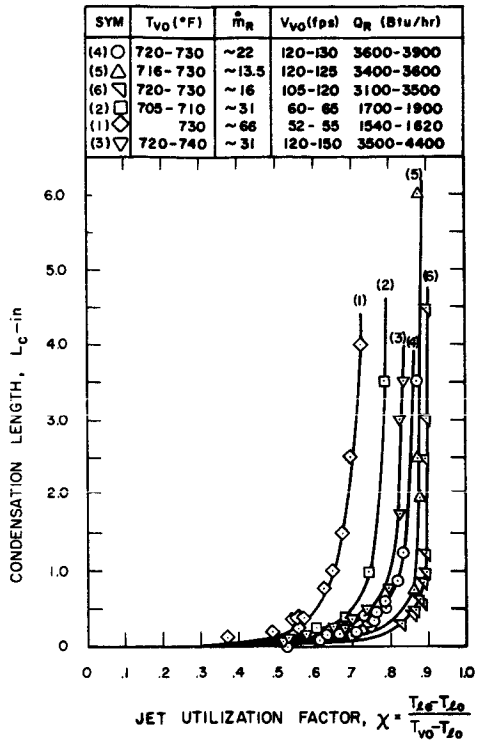

FIG. 34

CONDENSATION LENGTH VS JET UTILIZATION FACTOR FOR CONSTANT AREA JET CONDENSER

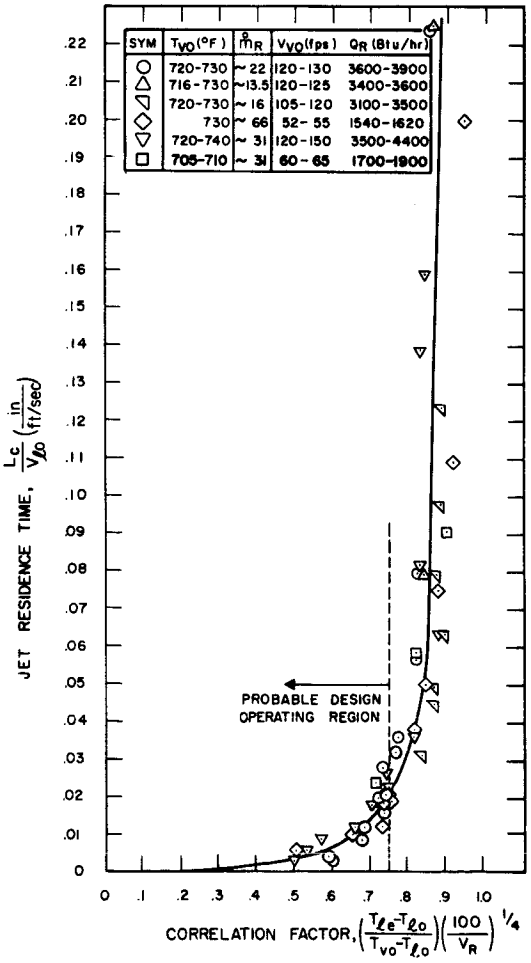

FIG. 35

JET RESIDENCE TIME VS CORRELATING FACTOR FOR CONSTANT AREA JET CONDENSER

Flow parameters have a strong influence on condensation length for a given jet utilization factor. As the vapor velocity is increased with liquid injection flow rate held constant, shorter condensation lengths are obtained for the same value of utilization factor. For example, curves (1) and (3) correspond to the same liquid injected flow rate with different vapor flow rates. Curve (1) which has a vapor velocity of about 55 fps shows a condensation length of 2-1/2 inches to occur at a value of $\chi = 0.7$. Curve (3), which is for a vapor velocity of about 130, gives a condensation length of only 3/8 inches for the same value of χ. A probable reason for this increase in heat transfer rate is the increase in heat transfer area caused by the greater breakup of the liquid jet due to higher values of vapor shear.

As the liquid injected flow rate is increased with vapor flow rate held constant longer condensation lengths occur for the same value of utilization factor. Curves (5) and (3) are for the same vapor velocity with mass flow ratios of 13.5 and 30 respectively. Curve (5) shows a condensation length of 3/8 inches at $\chi = 0.8$, while Curve (3) gives a condensation length of 1 inch for the same value of χ. This variation is probably due to two effects:

1. Decreasing liquid velocity results in a larger value of the relative vapor velocity ($V_{vo} - V_{\ell o}$) which increases vapor-liquid shear and heat transfer area.
2. Decreasing liquid velocity increases the time a given particle of liquid spends in the vicinity of the vapor. Thus, it is able to absorb a greater amount of heat and condense more vapor in traversing a given distance.

In order to incorporate these effects in the presentation of data, two additional plots were made. In the first plot, jet residence time, which is defined as the condensation length divided by the jet velocity, was plotted vs. jet utilization factor. This plot resulted in two curves, or two groups of data points, for two different vapor flow rates. For the next step jet residence time was plotted vs. the jet utilization

factor times the relative velocity ($V_{vo} - V_{\ell o}$) raised to an undetermined exponent. Previous work on sprays has indicated the relative velocity to be an important variable in determining drop size (Ref. 13). Plots were made for different values of the exponent until that value which gave the least spread of test data was found. The results are presented in Fig. 35.

The best fit of data was obtained when jet residence time, $\frac{L_c}{V_{\ell o}}$ was plotted versus $\Psi = \chi \left(\frac{100}{V_R} \right)^{1/4}$

A possible operating point for a preliminary design would be at a value of Ψ of about 0.75 as indicated by the dashed line in Fig. 35. If this value were taken as the operating point, then the following relations would hold for condensation length, jet velocity, jet utilization factor, and relative velocity between the vapor and liquid:

$$\frac{L_c}{V_{\ell o}} \cong 0.020 \tag{37}$$

and

$$\left(\frac{T_{\ell e} - T_{\ell o}}{T_{vo} - T_{\ell o}} \right) \left(\frac{100}{V_R} \right)^{1/4} = 0.75 \tag{38}$$

In general, it is desirable to use the highest possible values of critical Ψ in order to minimize the mass flow ratio for a given radiator temperature drop. However, a compromise may have to be made to obtain high values of pressure rise and injector efficiency.

If the operating point were chosen to be below the indicated value of $\Psi = 0.75$, then of course the above relationships do not hold. Choice of such an operating point might be made in order to obtain a particular pressure augmentation characteristic or minimize condensation length.

5.2.2 Pressure Rise

The values of pressure rise obtained during testing of the constant area jet condenser, while not exceedingly high, provide information of several important trends. The influence of mass flow ratio and jet utilization factor upon pressure rise are illustrated. A comparison of measured pressure rise with predicted is furnished and

the efficiency of the central injector test geometry is examined.

The net pressure rise divided by the dynamic pressure of the inlet vapor is plotted vs. mass flow ratio in Fig. 36. A trend of increasing pressure rise with increasing mass flow ratio (for fixed vapor conditions) is shown which is similar to the trend predicted by the constant area pressure rise analysis. The theoretical curve for $\overset{o}{\rho} = 2000$ is plotted for reference. The differences between test values and theoretical may possibly be attributed to frictional and mixing losses and to differences in vapor density for the test data compared to the calculated example.

The large amount of scatter of Fig. 36 is due to the variations of χ at each mass flow ratio. Increasing values of χ produce longer condensation lengths (Fig. 34) and hence larger friotional and mixing losses. This effect is illustrated in Figs. 37 and 38, which show the effect upon pressure rise of variation in the jet utilization factor at a constant mass flow ratio. Separate curves were determined for mass flow ratios of 13.6, 16.0, 22, 31, 64, and 69. In these plots the pressure rise is made non-dimensional by dividing by the dynamic pressure of the injected liquid. This parameter, $\overset{o}{\Delta P}_{\ell}$, illustrates the influence of χ better than $\overset{o}{\Delta P}_{v}$ due to better control and measurement of the liquid flow characteristics during testing than those of the vapor flow.

For the four lower mass flow ratios (13.6, 16.0, 22 and 31) a value of χ is reached at which the pressure rise falls off rather sharply. The value of χ for the decline appears to be a function of mass flow ratio. For example, for the above mass flow ratios the values of χ are about 0.89, 0.89, 0.85 and 0.79. The reason for this behavior is probably the influence of vapor and liquid conditions upon the relation between condensation length and jet utilization factor. For example, operation with a lower mass flow ratio means a lower liquid velocity (for fixed vapor conditions) and a longer residence time of liquid in vapor. Thus a higher value of χ is possible (for the same condensation length) than for higher mass flow ratios. On the above curves the value of ideal pressure rise is also plotted for each mass flow ratio. This

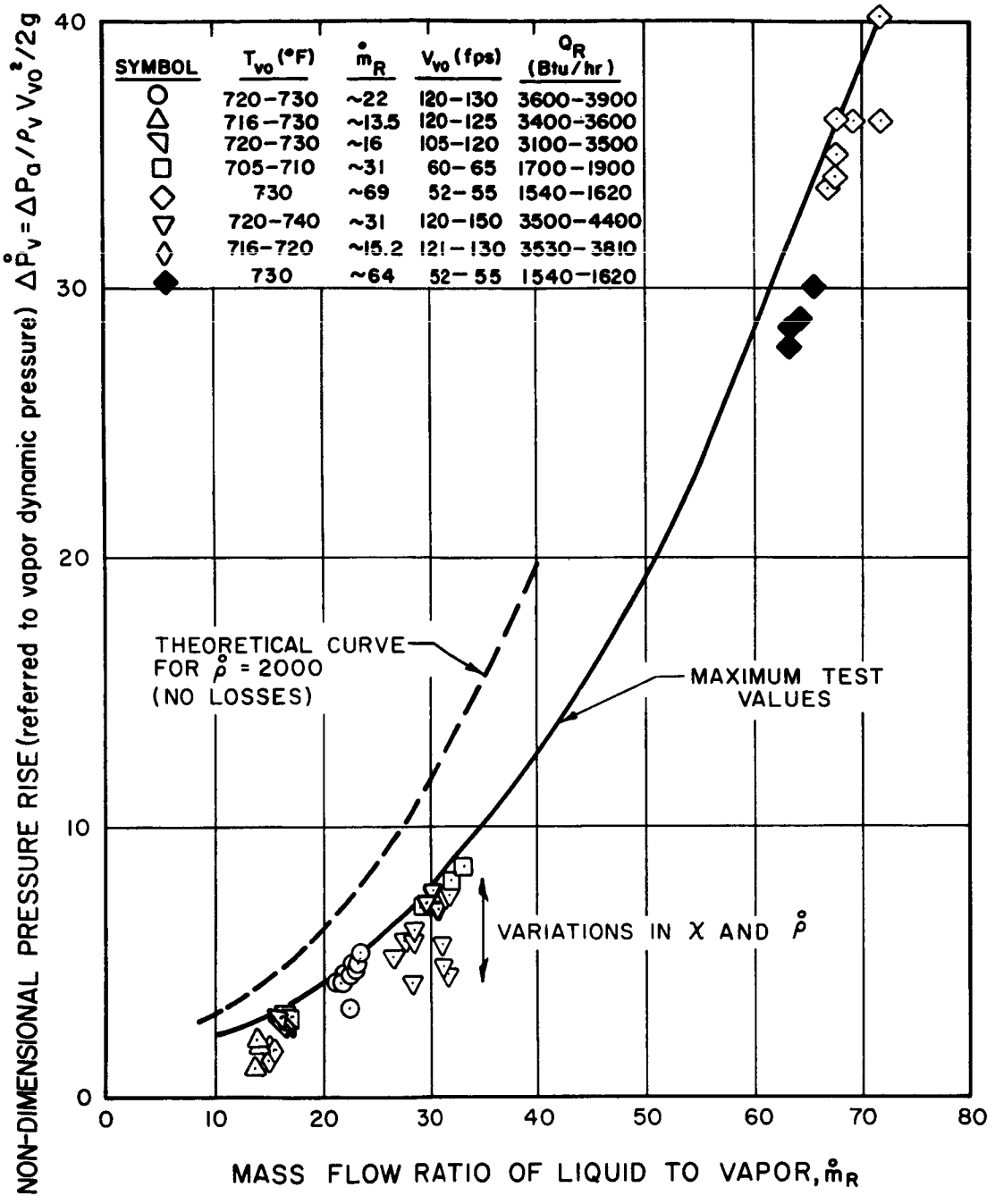

FIG. 36 NON-DIMENSIONAL PRESSURE RISE (referred to vapor) VS MASS FLOW RATIO FOR CONSTANT AREA JET CONDENSER

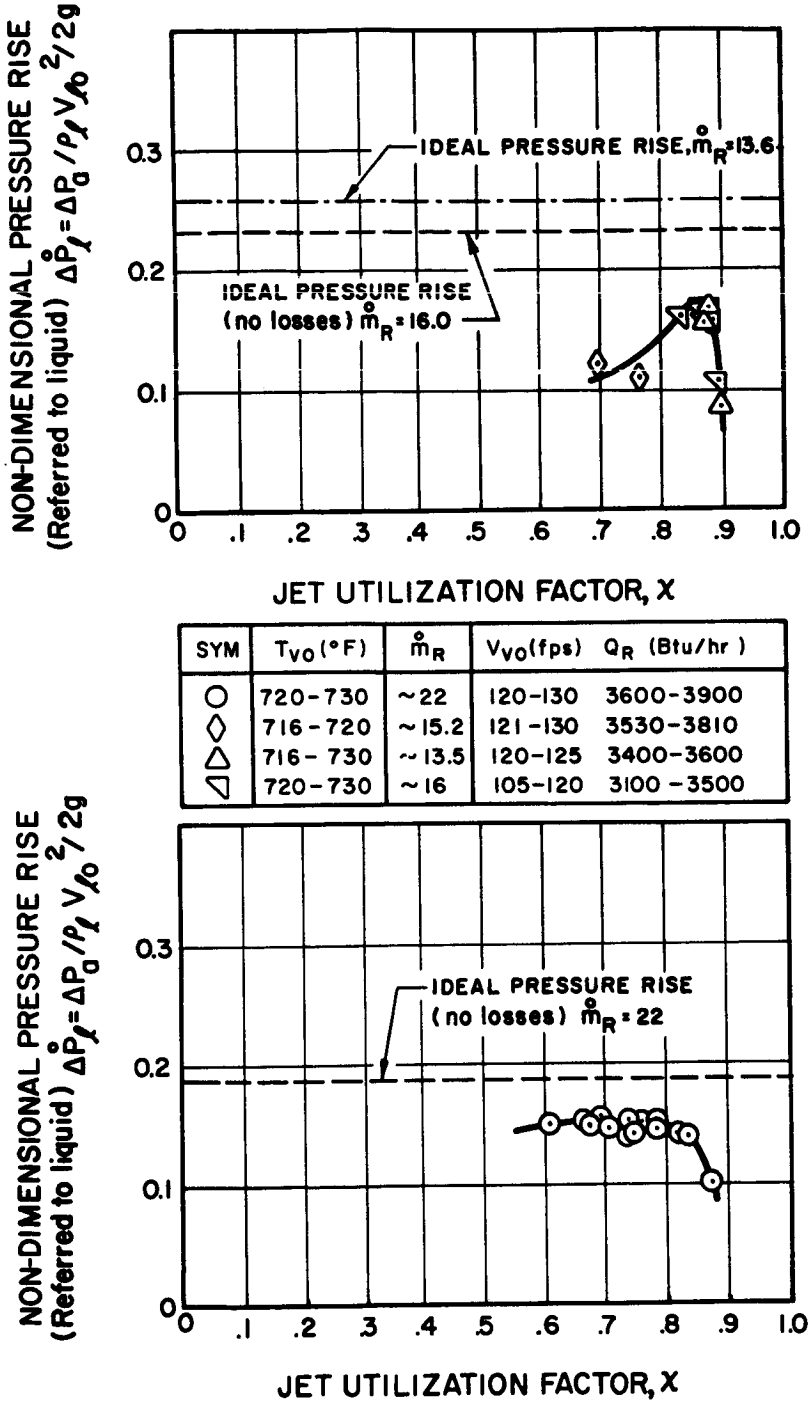

FIG. 37 NON-DIMENSIONAL PRESSURE RISE (referred to liquid) VS JET UTILIZATION FACTOR FOR CONSTANT AREA JET CONDENSER

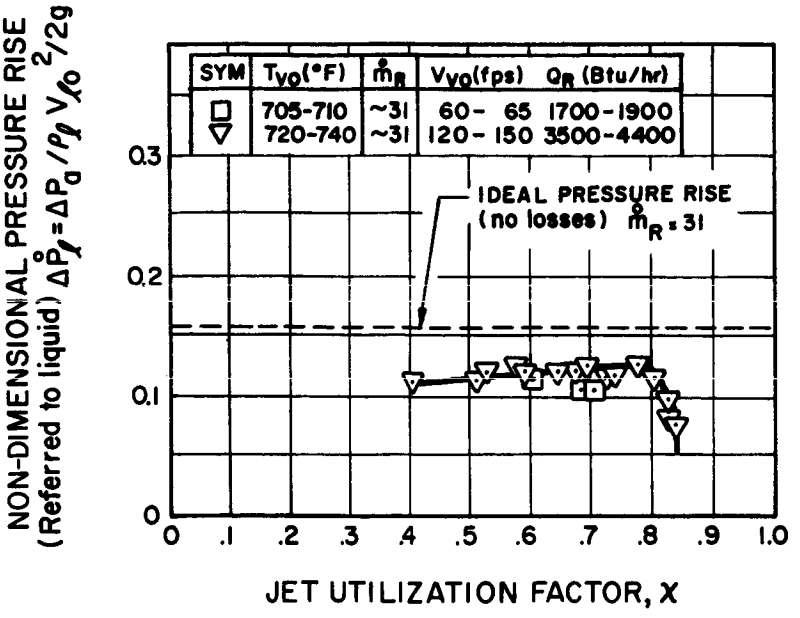

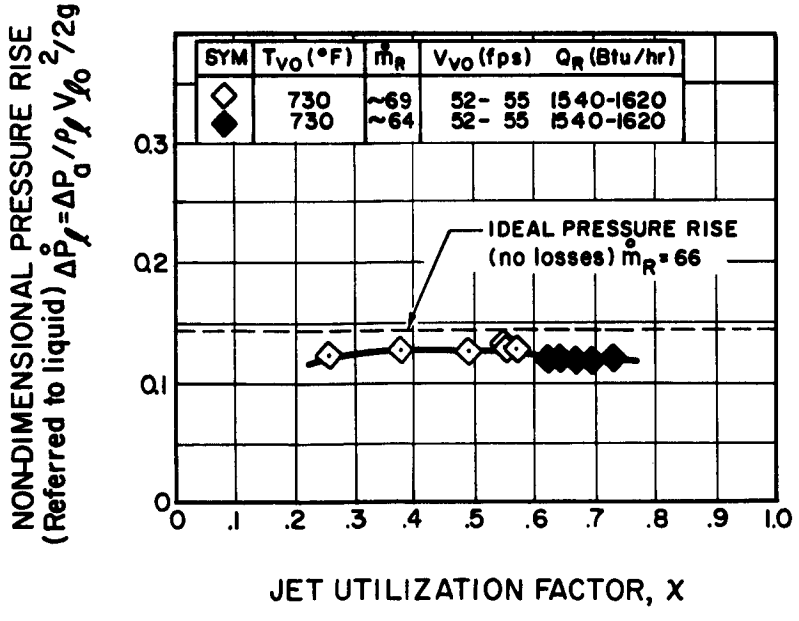

FIG. 38 NON-DIMENSIONAL PRESSURE RISE (referred to liquid) VS JET UTILIZATION FACTOR FOR CONSTANT AREA JET CONDENSER

quantity appears as a horizontal line since frictional or mixing losses were not included in the analysis.

The highest value of $\Delta\overset{o}{P}_{\ell}$ obtained during testing was approximately 0.17 for a mass flow ratio of 16.0. This point was obtained at the peak of that curve at a value of χ of 0.87. In general the values of $\Delta\overset{o}{P}_{\ell}$ decrease with increasing mass flow ratio. For example, the maximum value obtained for $\overset{o}{m}_R = 69$ is about 0.13. Of course the absolute magnitude of pressure rise can be higher for larger mass flow ratios. The maximum pressure rise obtained at $\overset{o}{m}_R = 69$ was about 5.0 psi which can be compared to a maximum of about 1.5 psi for $\overset{o}{m}_R = 16.0$

The measured pressure rise appears to be closest to the calculated pressure rise for the test runs which had the highest ratio of liquid mass flow to vapor. This trend is shown in Fig. 39 which contains a plot of η_a the ratio of actual to theoretical pressure rise, vs. the jet utilization factor, χ. Lines of constant mass flow ratio, $\overset{o}{m}_R$, are shown. The curve for $\overset{o}{m}_R = 69$ exhibits peak values of η_a which are greater than 90 percent. However, the curve for the lowest mass flow ratios (13.5 - 16.0) has a maximum value of η_a of only about 75 percent. The increase in losses resulting from operation of this geometry at lower mass flow ratios may be due to increased frictional and mixing losses. For the constant area geometry the main source of pressure rise appears to be the kinetic energy of the injected liquid. Operation at a lower mass flow ratio means the vapor flow is greater relative to a fixed injected liquid kinetic energy. Thus, frictional losses due to the vapor flow will be greater relative to the pressure rise resulting from the liquid, and η_a will be less than for a higher mass flow ratio.

This figure also illustrates the narrow range of operation for lower mass flow ratios. For example changing χ from 0.75 to 0.89 results in an increase in η_a from about 0.5 to 0.75. Further increases in χ from 0.89 to 0.90 result in a very steep drop in η_a from 0.75 to about 0.40. Comparison of this curve with the corresponding curve (No. 6) of Figure 34 provides the possible explanation for this behavior. The region of χ for peak pressure rise appears to be the same region of

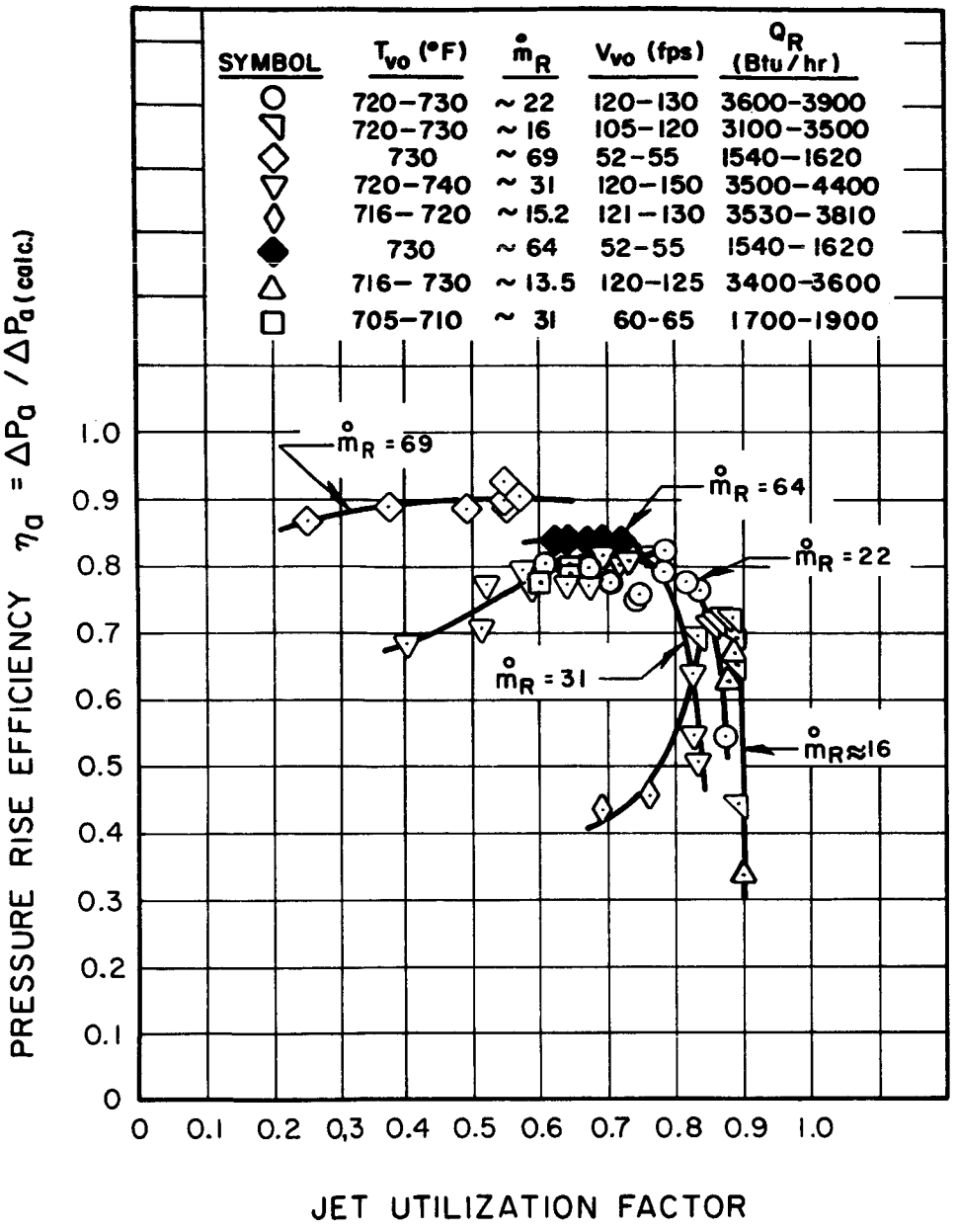

FIG. 39 RATIO OF ACTUAL TO CALCULATED PRESSURE RISE VS JET UTILIZATION FACTOR FOR CONSTANT AREA JET CONDENSER

χ in which condensation distance is very sensitive to small changes in χ. Very small changes (e.g., from 0.89 to 0.90) result in very large changes in condensation distance (from about 1.0 to 4.5 inches) with corresponding greater increases in frictional losses. As indicated previously, operation of a jet condenser system at higher values of χ is desirable in order to achieve a higher average liquid radiator temperature. However, considerations of stability, range of operation, and pressure rise must also be weighed in the selection of operating conditions.

The remaining aspect of performance of the test geometry as a pressure augmenting device is the efficiency of the injector. The pressure drop which would be required in a perfect injector (C_d = unity and no bends or restrictions) would be $\rho_\ell V_{\ell o}^2/2g$. However, for the geometry tested, the fluid is brought in perpendicular to the tube axis (cf. Fig. 24) and then undergoes a 90° bend, which produces losses. The injection pressure drop included this loss as well as line losses. The injector geometry was chosen to achieve simplicity of construction. In a design intended to reduce losses, the liquid would probably be accelerated from a low velocity to the injection velocity in a straight run with no flow obstructions or direction changes. Thus the only losses should be those encountered at the injector outlet.

Figure 40 furnishes the ratio of ideal injector pressure drop to the pressure drop measured for the constant area test geometry. Values appear to range between about 0.5 and 0.8. Some dependence upon vapor dynamic pressure and liquid dynamic pressure may be indicated but the data are not conclusive.

5.2.3 Stability and Startup

Several aspects of jet condenser operation and its interaction with the other portions of the flow loop were studied during this program. Included among these were:

1. Outlet fluid state
2. Fluctuations in condensation distance
3. Startup and interface formation processes

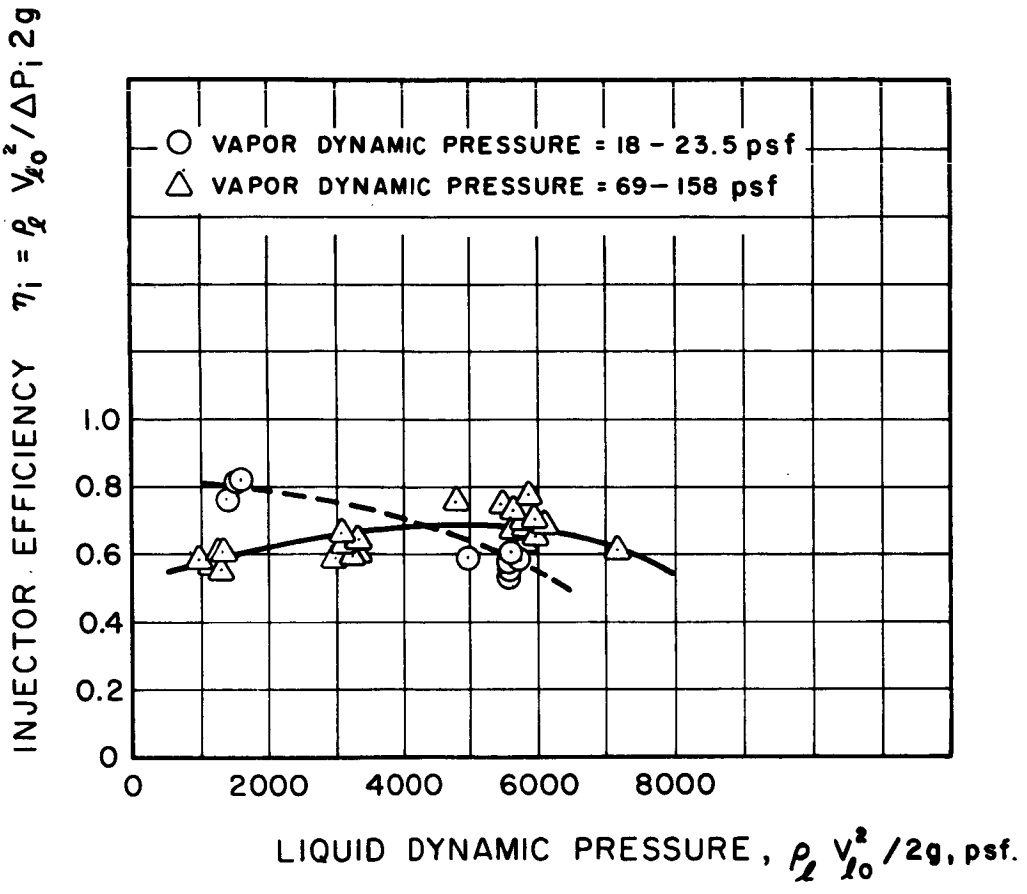

FIG. 40 INJECTOR EFFICIENCY VS LIQUID DYNAMIC PRESSURE FOR CONSTANT AREA JET CONDENSER

At no time during operation of the constant area jet condenser did slugging or vapor pockets at the outlet occur. This was observed over the range of operation conditions of Table III. Vapor occurred at the outlet only when χ values were such as to produce condensation lengths greater than the test section lengths.

The most noticeable flow disturbance observed was the oscillation of the condensation distance. The maximum oscillations occurred in the constant area condenser at high values of jet utilization factor (or in the region of operation where condensation length is very sensitive to small changes in jet utilization factor). Oscillations of as much as 2 inches were observed for condensation lengths of 5 to 6 inches. The oscillations were observed to decrease as condensation distance and jet utilization factor decreased, and below condensation lengths of about 1/2 inch, oscillations were always less than about 1/16 inch.

These oscillations were probably due to three effects:

1. Since these movements occurred during operation of the jet condenser in the "third region" discussed in Section 5.2.1, the oscillations could be due to local perturbations in temperature or mass flow rate.
2. Pressure fluctuations resulting from the sudden expansion of the liquid jet were probably a factor.
3. The presence of a constant pressure reservoir downstream of the test section during most test runs resulted in a source of fluid to feed any upstream pressure oscillations.

The magnitude of the oscillations decreased when the reservoir was isolated from the rest of the test loop. Although oscillations in condensation distance existed, fluctuations in flow rates and outlet pressure of less than 2-3 percent were normally encountered.

Other aspects of condenser operation which were examined were the problems of startup and interface formation. A series of tests were run in which subcooled liquid was injected into the test section initially filled with vapor. The resulting sequence of interface formation was recorded with a Fastax camera operating at 2000-4000 fps.

Figure 41 is a series of frames taken from the films approximately 0.01 sec apart. In the first frame vapor is seen flowing from left to right through the test section. In the second frame subcooled liquid is injected from the left concurrent to the vapor flowrate. In the ensuing frames the vapor-liquid interface, which was formed downstream, is moved to the operation point under the action of forces produced in the condensation process. The gradual establishment of the final interface location suggests the process of interface formation may be due mainly to the pressure forces resulting as the vapor is condensed rather than a shock type process.

It should be noted that the above procedure is not the same used during normal startup. The sequence used most often consisted of circulating liquid and then introducing the vapor (cf. Section 4.3).

5.3 Variable Area Jet Condenser

The performance of several converging-diverging jet condenser geometries was measured during this investigation. A total of six test units were operated, condensing mercury vapor over a range of flow variables (Tables II and III). As discussed previously, the main purpose for use of a converging-diverging geometry was to increase the pressure rise in the jet condenser. This result was demonstrated experimentally. In addition, improved heat transfer characteristics and flow stability were also realized compared to the constant area units. Four of the test units, which are denoted small diameter geometries, had a vapor internal diameter of 0.19 inches at the inlet. The other two (large diameter geometries) were constructed with a vapor internal diameter of 0.75 inches.

The results of testing small diameter geometries are limited due to problems of aligning the injector and the dimensional control

possible in the smaller sizes. Consequently, the data obtained with these smaller diameters are primarily useful for providing heat transfer characteristics and for indicating trends in pressure rise, operating range and control. Data obtained for the large diameter geometries are useful in establishing both heat transfer and pressure rise characteristics for these units. Sufficient control and measurement of geometric and flow variables was obtained to enable useful comparisons of experimental pressure rise with theoretical. The small diameter data are therefore used mainly for heat transfer comparisons and illustration of pressure rise trends which are not available from large diameter data due to the limited geometric variation.

5.3.1 Jet Profiles

High speed motion pictures were used to record jet profiles over a range of operating conditions for the variable area units tested. Items of interest which are apparent in the films are surface wave phenomena, the physical appearance of vapor-liquid boundaries, and the state of the outlet liquid.

Figure 42 shows the injected liquid jet profiles resulting from operation with four different mass flow ratios of liquid to vapor. Vapor and liquid are injected at the left and flow to the right. Vapor temperature, flow rate, and Reynolds number based on inlet diameter are nearly constant for all test runs in this figure. The variation in mass flow ratio was obtained by varying the injected liquid mass flow rate. The changes in liquid flow produced a variation in mass flow ratio from 15.3 to 50.8 which corresponds to a range of liquid Reynolds number (with the initial jet diameter as the characteristic length) of 66,900 to 214,000. The average vapor Reynolds number is about 26,800 for the four test runs.

A striking contrast exists between the jet profile at the lowest mass flow ratio and that at the highest ratio. In frame "a" (the lowest flow ratio) the jet structure is extremely varicose with the irregular protrusion of large fingers of liquid and a meandering characteristic of the jet. The liquid is rapidly accelerated by the vapor and

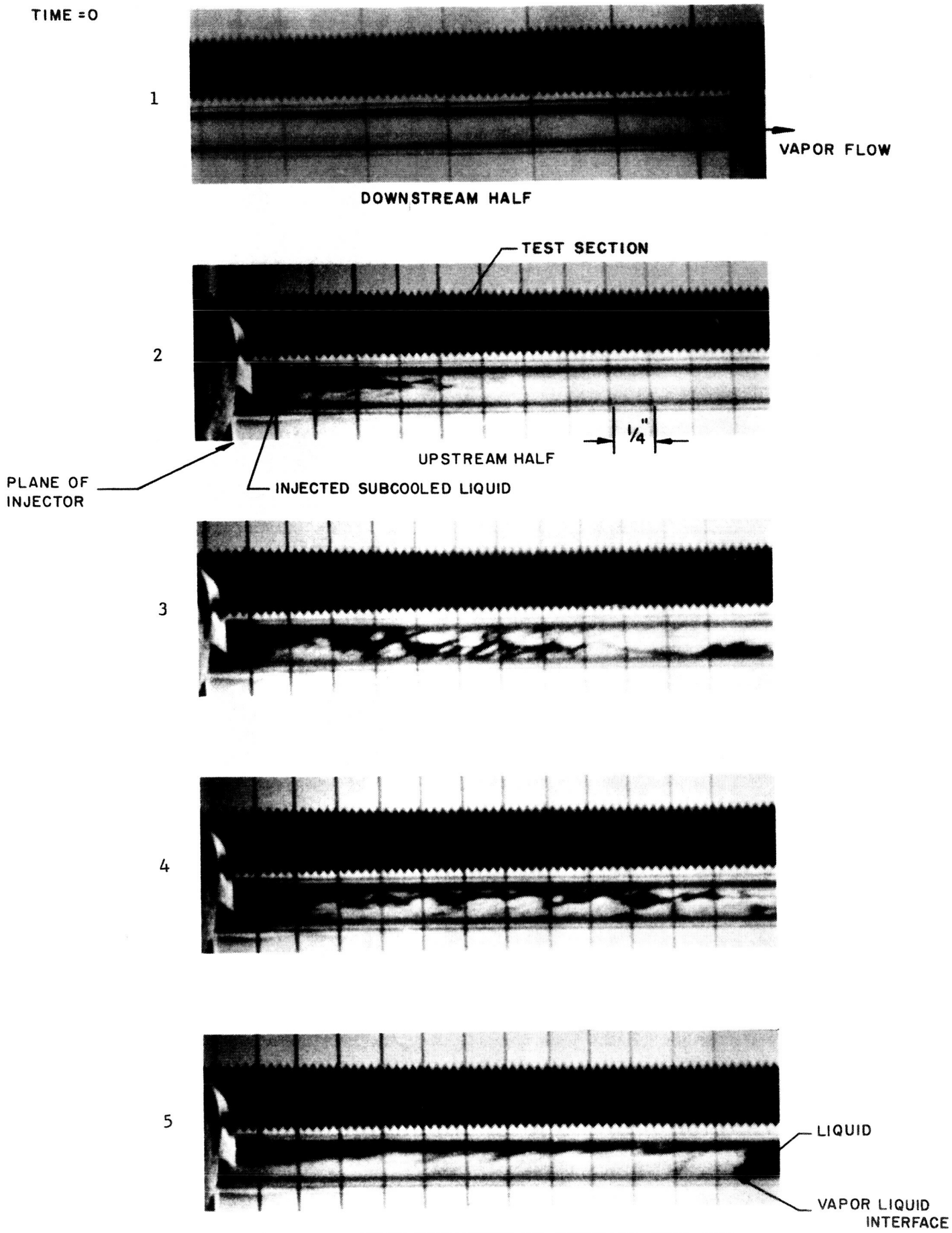

FIG. 41 INTERFACE FORMATION IN CONSTANT AREA JET CONDENSER. Liquid injected into all-vapor flow

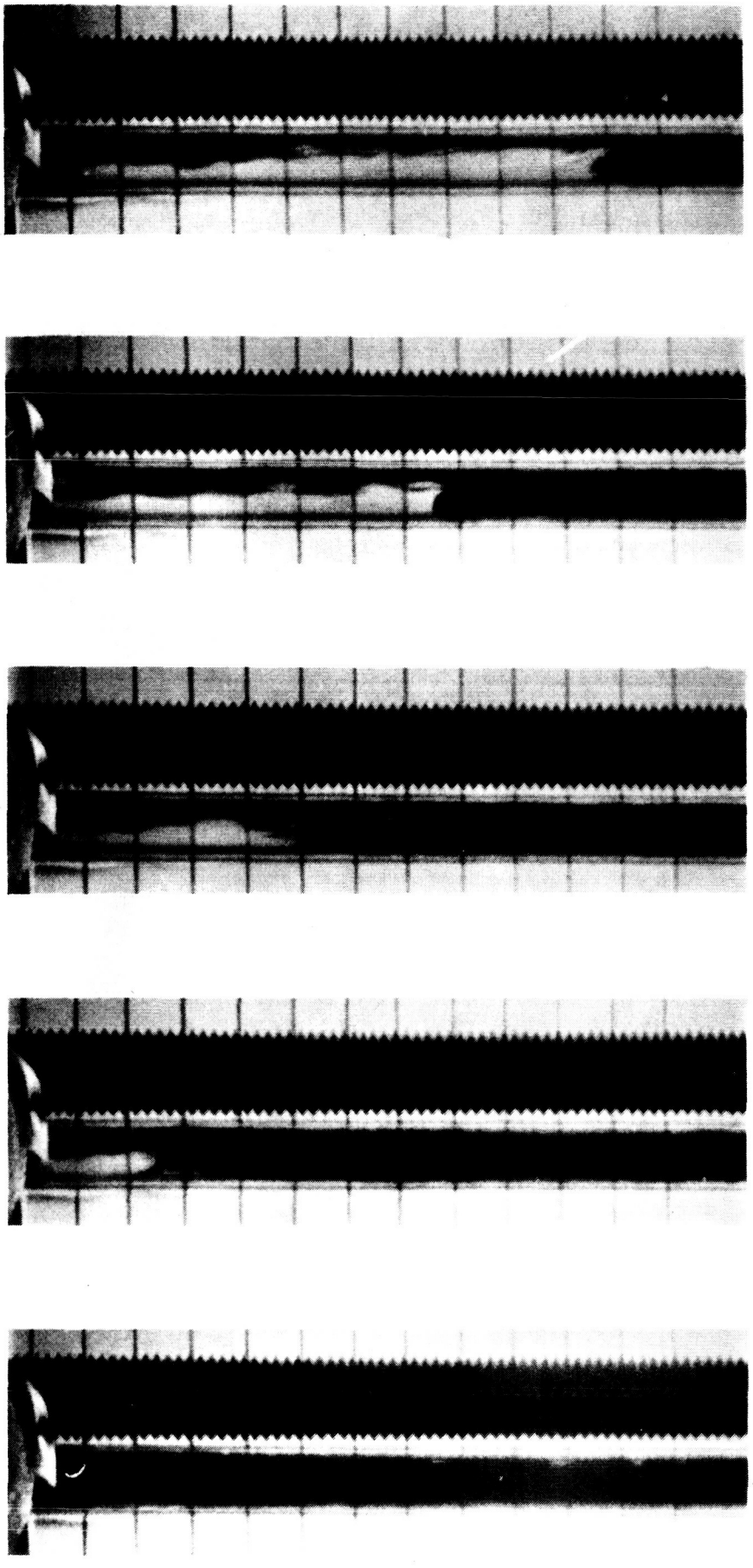

FIG. 41 (cont.) INTERFACE FORMATION IN CONSTANT AREA JET CONDENSER. Liquid injected into all-vapor flow

1588-Final II

in one region occupies a flow area which is less than 15 percent of the initial jet flow area. The velocity of the liquid at this location appears to be about 25 feet per second, compared with an initial velocity of 3.8 feet per second.

The acceleration of the liquid phase is probably mainly due to energy transferred from the vapor by two mechanisms:

1. Momentum is recovered from vapor condensing on the liquid phase.
2. Shear forces occur at the vapor-liquid boundary because of the high velocity of the vapor relative to the liquid.

At lower mass flow ratios the initial momentum transfer to the jet is probably greater than for higher mass ratios because the injected liquid has a lower initial temperature, which provides a greater driving force for condensation (cf. Section 2). The liquid should therefore experience larger axial and radial forces at the point of injection. The axial force should contribute to the axial acceleration of the liquid. Since the inertia of the injected liquid is lower relative to the internal shear forces, deformation of the jet due to the shear mechanism is more pronounced for lower mass flow ratios than for higher values.

Examination of frames "c" and "d" shows that as higher liquid Reynolds numbers and higher initial liquid temperatures are encountered, the jet becomes straightened and loses the varicose characteristic. Surface waves are still present but are apparently not as significant relative to the structure of the jet interior. At higher mass flow ratios, such as "d", the liquid flow area appears to increase from the initial value. As discussed in Section 2, the increase in jet area at higher flow ratios may imply that the momentum transferred from the condensing vapor has effected an increase in the internal pressure in the liquid jet rather than increasing the velocity, which apparently occurs at lower mass flow ratios.

The above profiles have a practical significance in the choice of throat size for a jet condenser. Operation at lower mass flow ratios may enable the use of a throat which is smaller than the injector in order to achieve improved pressure rise. Operation at higher ratios

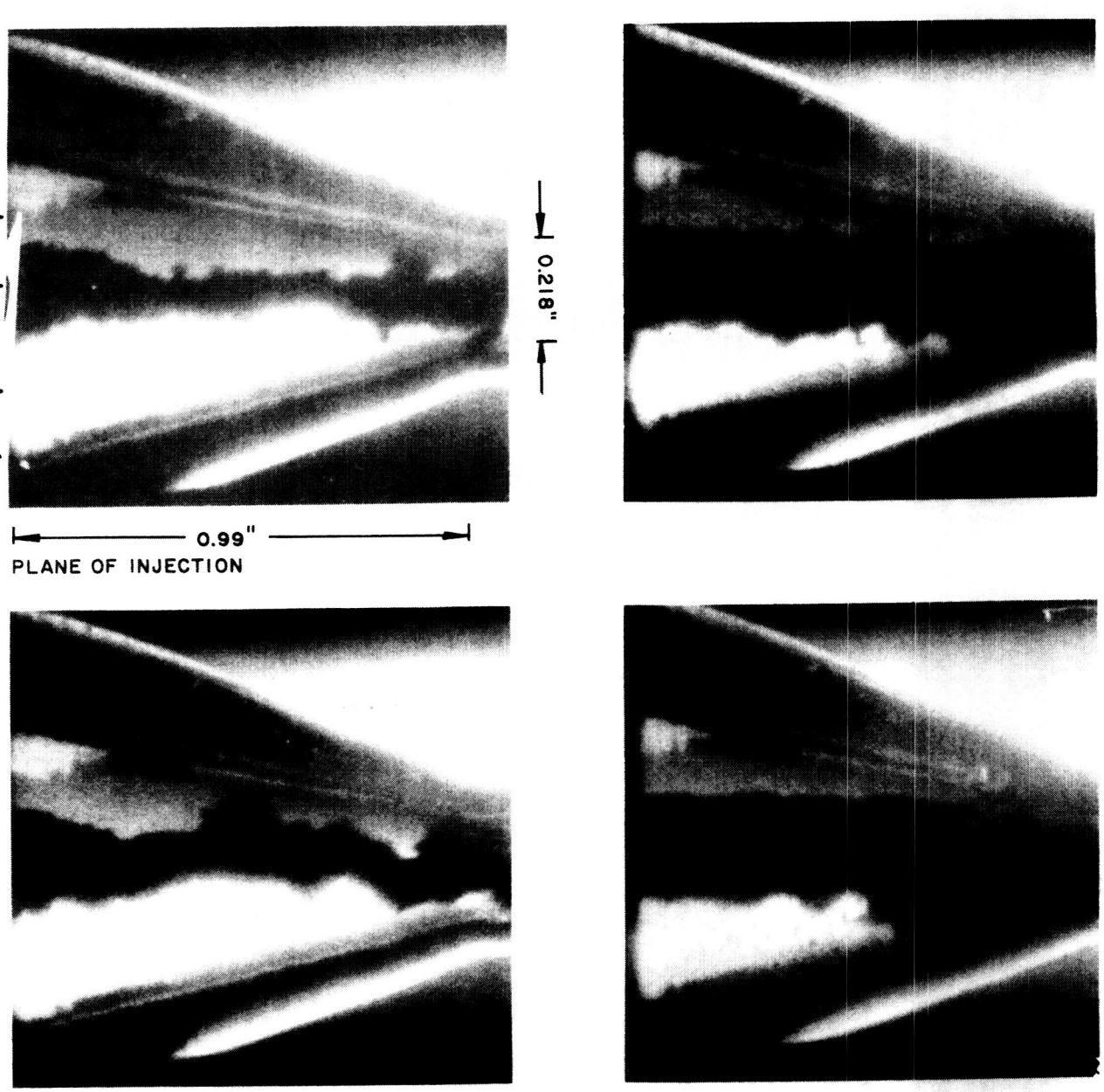

a. Mass flow ratio of liquid to vapor = 15.3

Test run no. 3-15-6
T_{vo} = 550°F
V_{vo} = 227fps
$V_{\ell o}$ = 3.8fps
Re_{vo} = 27,300
$Re_{\ell o}$ = 66,900
$T_{\ell o}$ = 116°F
$T_{\ell e}$ = 385°F

b. Mass flow ratio of liquid to vapor = 19.9

Test run no. 3-15-3
T_{vo} = 538°F
V_{vo} = 258fps
$V_{\ell o}$ = 4.81fps
Re_{vo} = 26,100
$Re_{\ell o}$ = 83,600
$T_{\ell o}$ = 141°F
$T_{\ell e}$ = 348°F

c. Mass flow ratio of liquid to vapor = 32.9

Test run no. 3-16-1
T_{vo} = 539°F
V_{vo} = 266fps
$V_{\ell o}$ = 8.4fps
Re_{vo} = 27,400
$Re_{\ell o}$ = 144,700
$T_{\ell o}$ = 274°F
$T_{\ell e}$ = 398°F

d. Mass flow ratio of liquid to vapor = 50.8

Test Run no. 3-16-7
T_{vo} = 562°F
V_{vo} = 187fps
$V_{\ell o}$ = 12.6fps
Re_{vo} = 26,400
$Re_{\ell o}$ = 214,000
$T_{\ell o}$ = 319°F
$T_{\ell e}$ = 400°F

FIG. 42 JET PROFILES IN LARGE DIAMETER VARIABLE AREA JET CONDENSER, TEST SECTION NO. 8 (Single frames of motion pictures taken at 8000 frames per second)

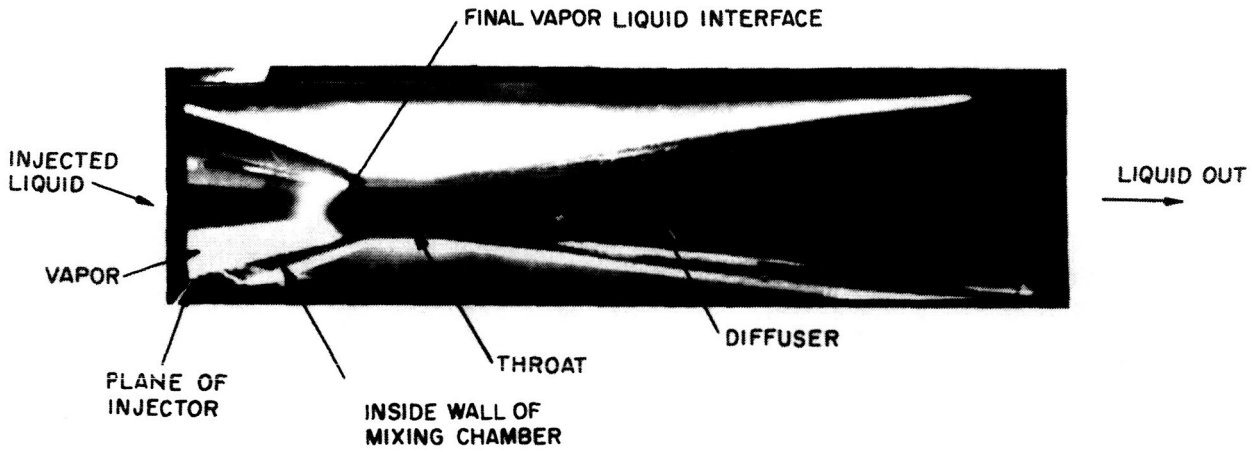

Jet Condenser

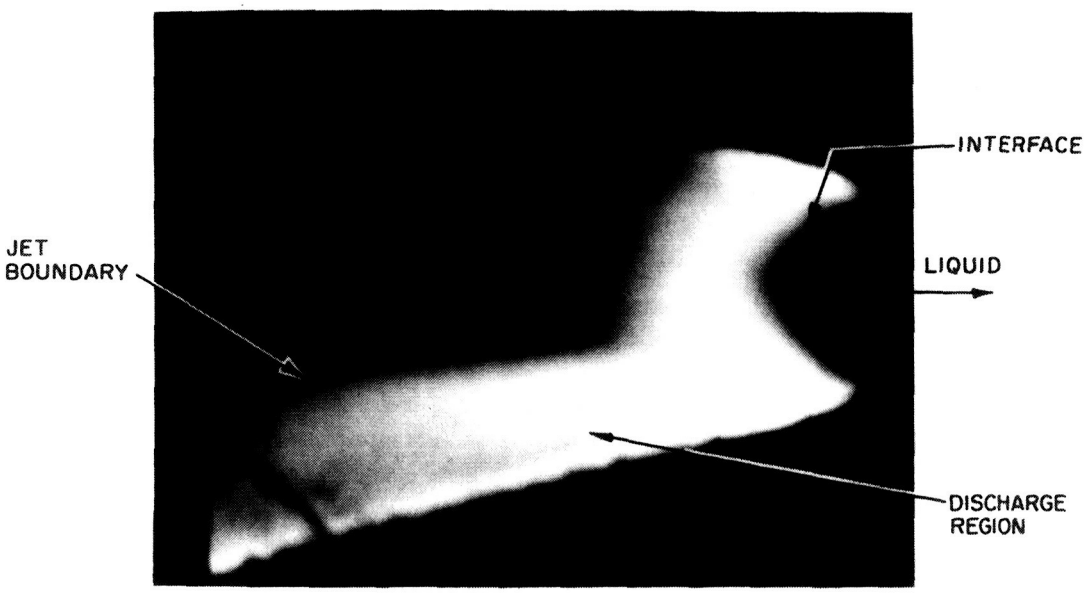

MERCURY DISCHARGE IN MIXING CHAMBER
(NO EXTERNAL LIGHTING)

FIG. 43 JET CONDENSER OPERATING WITH MERCURY VAPOR

These two photographs show the appearance of the large diameter jet condenser (Test Sec. No. 8) when operating at vapor temperatures less than about 650°F. In contrast to the high speed motion pictures, the jet appears to have a regular profile and the final interface is fixed at the throat location. A bluish discharge occurred in the condensation region and is shown in the photograph to the left. The discharge is similar to that occurring in a mercury vapor lamp and is probably a result of a static charge generated by the shearing action.

may require the use of a throat which is significantly larger than the injector if impingement of the jet on the converging wall is to be avoided.

The above profiles were obtained with effective film exposure times of about 10^{-4} seconds. Consequently, the irregularities of the jet and periodic phenomena are clearly revealed. However, the appearance is radically different than that observed visually. Figure 43, which contains photographs taken with an exposure time of about 0.1 second, shows operation of a jet condenser as it appears to the eye. No jet irregularities or fluctuations are apparent in either this photograph or from motion pictures taken at normal speed (24 frames per second). No measurable fluctuations in performance were found to occur during steady state operation of these units.

A consecutive sequence of several frames from a high speed motion picture is shown in Fig. 44. The condenser is the unit of Fig. 42 and the test run is number 3-15-3. The formation of surface waves and protrusions is illustrated in these pictures. The waves are formed and grow in size until colliding with the wall or final interface. The irregular nature of the flow and constantly changing surface area appear to have only a small influence on the location of the final vapor-liquid interface. The surface waves attain higher velocities than the initial jet velocity. For example, the wave indicated by the arrow can be seen to traverse about 0.4 inches in the total duration of 1.4×10^{-3} seconds for a velocity of about 24 feet per second. This value can be compared to the injection velocity of 4.8 feet per second. If this velocity head were entirely converted to pressure, a ratio of pressure rise to injected liquid kinetic energy of about 24 would result (compared to a measured value of 6.3). If the throat size were reduced to avoid further expansion losses resulting when the final interface is formed, much higher pressure rise might therefore be obtained for this mass flow ratio.

5.3.2 Heat Transfer

The most direct indications of the heat transfer characteristics of a jet condenser are the length required for condensation of

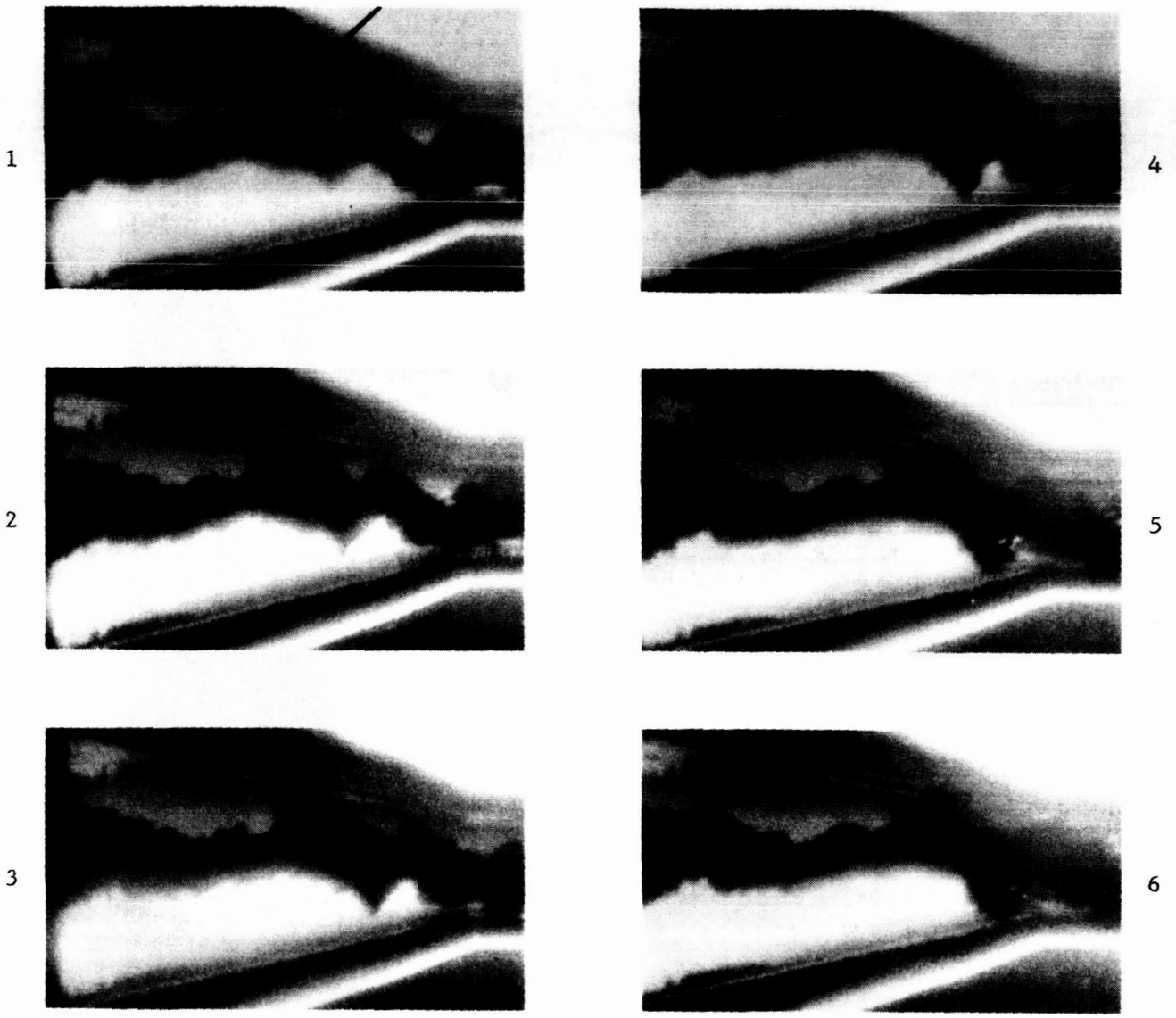

FIG. 44 JET CONDENSER OPERATION - CONSECUTIVE FRAMES FROM HIGH SPEED MOTION PICTURE. (See Fig. 42 for explanation) TEST SECTION NO. 8 TEST RUN NO. 3-15-3. Note: There is an interval of approximately 0.13 milliseconds between each frame. The total elapsed time for the sequence is about 1.4 milliseconds

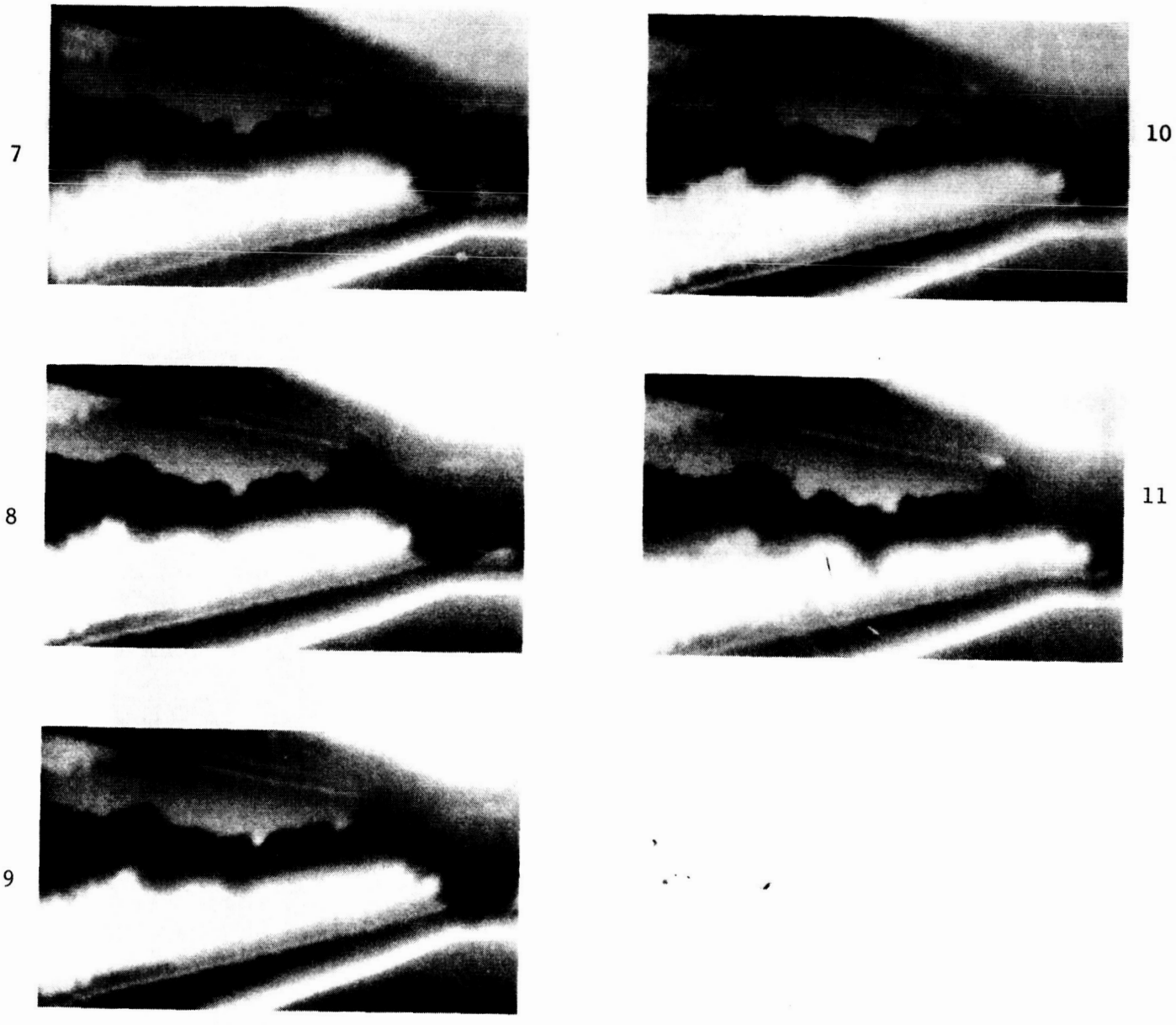

FIG. 44 (cont.) JET CONDENSER OPERATION - CONSECUTIVE FRAMES FROM HIGH SPEED MOTION PICTURE. (See Fig. 42 for explanation) TEST SECTION NO. 8 TEST RUN NO. 3-15-3. Note: There is an interval of approximately 0.13 milliseconds between each frame. The total elapsed time for the sequence is about 1.4 milliseconds

the inlet vapor flow and the enthalpy increase of the jet relative to the total possible enthalpy increase. Depending upon the values of these variables, heat transfer coefficients for condensing may range from zero to greater than two orders of magnitude higher than those resulting from film or drop wise condensation. The reasons for this behavior were discussed in Section 2.

Test results for constant area jet condensers showed the influence of jet utilization factor and other flow variables on condensation length. Wide variations in condensation length were possible during tests and in selection of the design operating point for a given constant area geometry. However, in the convergent-divergent condensers the interface must occur at the throat location, which is fixed by the geometry (cf Fig. 3), for maximum pressure rise and stable operation. Consequently, for a given test unit experimental results mainly provide information on the values of flow parameters required to maintain the interface (or condensation length) at the design point (throat). The most important flow variables examined for the variable area test units were jet utilization factor, injected liquid velocity, vapor velocity, and density ratio (vapor temperature).

Scaling Criterion

The distance from injector to throat (1/4 inch) for the small diameter variable area units was selected on the basis of the small diameter constant area test results (Section 5.2.1). The distance from injector to throat in the large diameter units was selected by choosing the ratio L_c/d_{to} to be a constant. Thus the condensation distance was scaled up directly as the diameter with the estimate that the value of flow parameters (χ, $V_{\ell o}$, $V_{vo} - V_{\ell o}$, and $\overset{o}{\rho}$) required to maintain the interface at the throat location would be the same for both sizes. The basis of this scaling criterion was as follows:

If χ, $V_{\ell o}$, $V_{vo}-V_{\ell o}$ and $\overset{o}{\rho}$ are constant and are the significant parameters in the internal heat transfer of the jet, then the remaining parameters which should influence the heat transfer are the amount of vapor to be condensed and the surface area of the jet available

for heat transfer. In particular if some average heat transfer coefficient $\bar{h}_c$ and temperature difference $\bar{T}_c$ are determined by the above four parameter then

$$\dot{m}_{vo} h_{fg} = \bar{h}_c A_j \Delta\bar{T}_c$$

or

$$\frac{\dot{m}_{vo}}{} \sim C_1$$

But $\dot{m}_{vo} \sim d_t^2$

and $A_j \sim L_c d_i \sim L_c d_t$ (since the area ratio $\overset{o}{A}_2$ is fixed)

Therefore

$$\frac{d_t^2}{L_c d_t} \approx C_2 \quad \text{or}$$

$$L_c \approx C_3 d_t$$

Performance Results

The results of testing the four small diameter units and two large diameter units are shown in Figures 45 and 46. In these curves the value of a correlating factor, $\Psi = \chi V_{\ell o}/V_R$ is plotted versus density ratio for all test runs where the interface was in the throat. For the smaller diameter units, where visual estimation of condensing length was difficult, test runs were selected where measured pressure rise was 50 percent or greater of the pressure rise calculated with the interface in the throat. The factor $\chi V_{\ell o}/V_R$ was determined by trial and error to provide the best correlation of test data. This correlating parameters is similar to that of the constant area geometry except that the relative vapor velocity enters with an exponent of unity instead of one quarter indicating a much stronger influence.

The value of χ obtainable for a particular set of the other parameters is provided by the curves. As noted above χ is the fraction of the heat absorbing capacities of the jet which can be utilized for a given condensation distance. A value of χ equal to unity

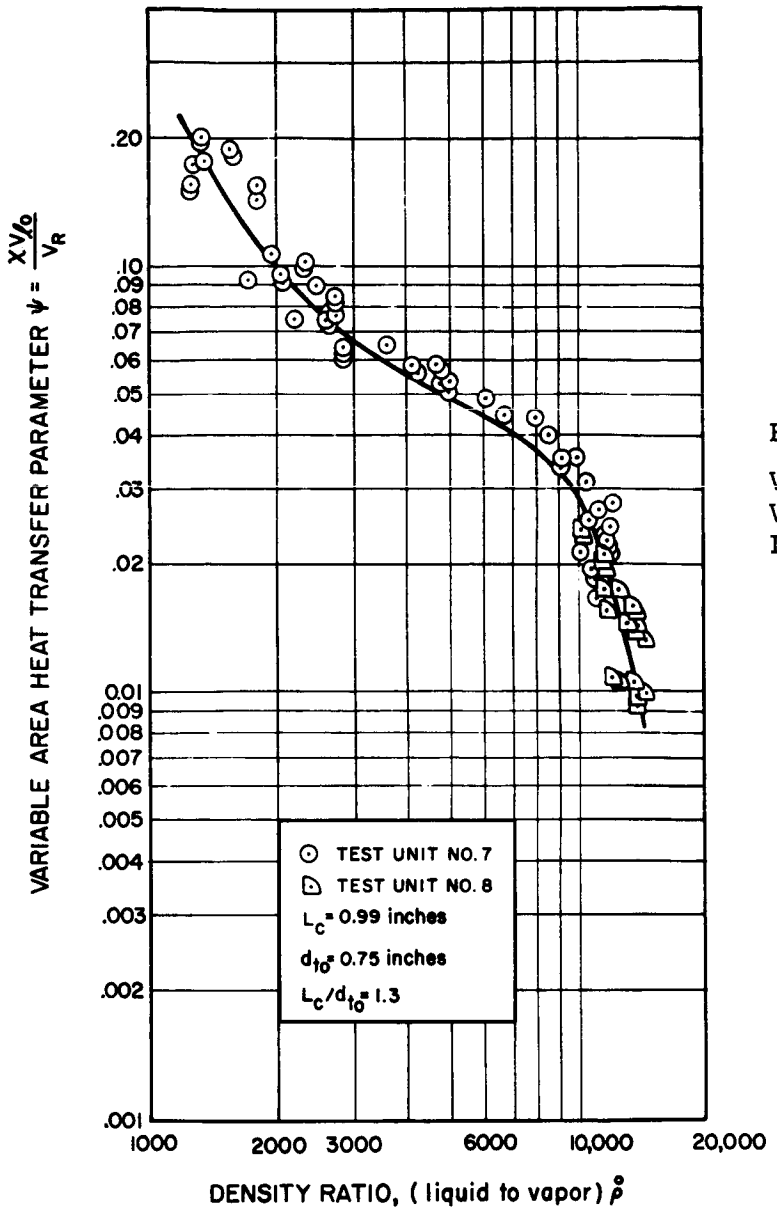

FIG. 45

VARIABLE AREA HEAT TRANSFER PARAMETER VS LIQUID TO VAPOR DENSITY RATIO FOR LARGE DIAMETER JET CONDENSERS

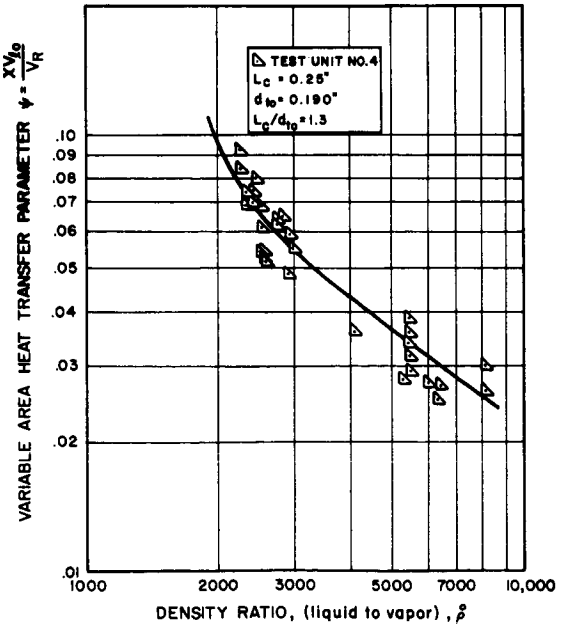

FIG. 46

VARIABLE AREA HEAT TRANSFER PARAMETER VS LIQUID TO VAPOR DENSITY RATIO FOR SMALL DIAMETER JET CONDENSERS

would result in the liquid radiator inlet temperature being equal to the vapor temperature. Thus, the radiator would operate at the highest possible temperature and would require the smallest size.

The effects of $V_{\ell o}$ and V_R on Ψ are as follows: Higher values of liquid velocity, $V_{\ell o}$, result in a shorter residence time of liquid in vapor. The fraction of the heat absorbing capacity of the liquid which is utilized (χ) is therefore reduced. On the other hand, high values of vapor velocity relative to the liquid ($V_R = V_{vo} - V_{\ell o}$) produce higher shear forces and tend to promote physical mixing, increasing the heat absorbed by the jet in a given distance. The vapor density has an important effect upon the jet. Increasing values of vapor density, (decreasing values of β) produce a higher flux of vapor molecules upon the jet. Thus for constant values of $V_{\ell o}$ and V_R, decreasing ρ^o results in increases in χ.

The figures shown illustrate these trends. For example from Fig. 45 the value of $\chi V_{\ell o}/V_R$ which produces an interface at one inch (large diameter test unit) decreases from about 0.10 at β = 2000 to about 0.045 at β = 6000. Further increases in β above about 10,000 appear to effect a very rapid decrease in the value of Ψ which can be achieved with the interface at the throat location. The reason for the strong change in trend around ρ^o = 10,000 is probably that as the vapor becomes more rarified the limiting resistance in the heat transfer process becomes the vapor flux attainable at the jet surface rather than the internal liquid heat transfer.

The curves of Figs. 45 and 46 indicate that for a given value of vapor density the value of χ for a given condensation distance can be increased by either increasing the vapor velocity or decreasing the liquid velocity. For example, the values of Ψ at $\rho^o \cong 2600$ (700°F) for Fig. 45 were obtained with a variation of χ from 0.71 to 0.95. Of course, variations in $V_{\ell o}$ and V_R to achieve better heat transfer characteristics will also influence the pressure rise through the jet condenser. Interaction between these performance parameters and limitations on the value of χ are discussed in Section 6.

The relatively close agreement between figures 45 and 46 is significant for scaling of heat transfer results to larger sizes. The performance curves of Ψ versus $\overset{o}{\rho}$ are identical at $\overset{o}{\rho}$ = 2000 with the curve for the smaller diameter (0.19") test units falling off to a maximum of about 30 percent lower than the curve for larger diameter geometries (0.75") at $\overset{o}{\rho}$ = 6000. Moreover, the discrepancies may well be due to measurement and alignment inaccuracies for the smaller units. If this result is valid, then even larger geometries scaled such that the ratio L_c/d_{to} is equal to 1.3 should exhibit nearly the same curve of $\chi V_{\ell o}/V_R$ versus $\overset{o}{\rho}$ as the two groups of smaller units. Minor adjustments in the values of $V_{\ell o}$ and V_R might be required to achieve the design value of χ. However, it would appear that such an extrapolation may even be conservative (larger values of χ attainable than predicted), since the curve for the larger test units is somewhat higher than that of the smaller geometries.

In order to illustrate the use of these curves, consider Fig. 45. If this geometry were to be operated at 700°F with a jet utilization factor of 0.90 then:

$$\overset{o}{\rho} \approx 2600$$

$$\Psi = 0.075 \text{ from curve}$$

$$V_{\ell o}/V_R = 0.075/0.90 = 0.083$$

Thus the ratio of liquid velocity to relative vapor velocity should be about 0.083 to maintain the interface at the throat location. If an inlet vapor velocity of 200 fps were specified, then a liquid velocity of:

$$V_{\ell o} = (0.083)(V_{vo} - V_{\ell o})$$

or

$$V_{\ell o} = \frac{(0.083)(200)}{1.083} = 15.3 \text{ fps}$$

would be required for operation with the interface at the throat location.

Range of Operation

Part of the scatter in Figs. 45 and 46 is due to the fact that for each geometry there is a limited range of values of Ψ which can be used if the interface is to remain in the throat. A series of tests was conducted on the large diameter test units to produce variations in

Ψ and to observe the changes in condensation distance. The results of these tests are summarized in Fig. 47. For each test run shown the vapor inlet flow rate and temperature and liquid inlet flow rate were held nearly constant. Temperature of the injected liquid was then varied to produce the change in Ψ. Changes in Ψ then are mainly due to changing values of χ. However, small variations in vapor and liquid flow rate occurred as the inlet liquid temperature was varied. Thus changes in the factor $\chi V_{\ell o}/V_R$ had to be considered rather than χ only. The results for tests at the higher vapor temperatures (725°F) indicate Ψ(or χ) may be varied by as much as $\pm$ 15 percent with the interface remaining in the throat. Tests conducted at a lower vapor flow rate (126 lb/hr vs 210 lb/hr) than this example showed a reduction in this range to about $\pm$ 5 percent. Combining the results of the two curves for lower vapor temperatures (553 - 560°F) and higher flow rate (170 - 182 lb/hr) indicates a range of Ψ(orχ) of about $\pm$ 24 percent is possible. These results are important for operation of a jet condenser in a power system. A relatively large range of operation of of χ, $V_{\ell o}$ or V_R can be tolerated with this geometry without losing the vapor liquid interface from the throat with the subsequent degradation of pressure rise and stability. Quantitative data as shown in Fig. 47 are not available for the large diameter geometry in which the throat length was reduced from about 1.5 inch to .25 inch (Test Section No. 8). However, observations made during test runs indicate the maximum range of operation of Ψ for this geometry with the interface in the throat was about $\pm$ 5 percent. Thus it would appear that use of a constant area throat can contribute significantly to increasing the range of operation possible for variable area jet condensers.

5.3.3 Pressure Rise

One of the most important advantages exhibited by variable area jet condensers over constant area units is higher pressure rise from vapor to condensate. Results of the analysis in Section 3 provided the first indication of this conclusion. Experimental verification of the high pressure rise performance of variable area jet condensers was

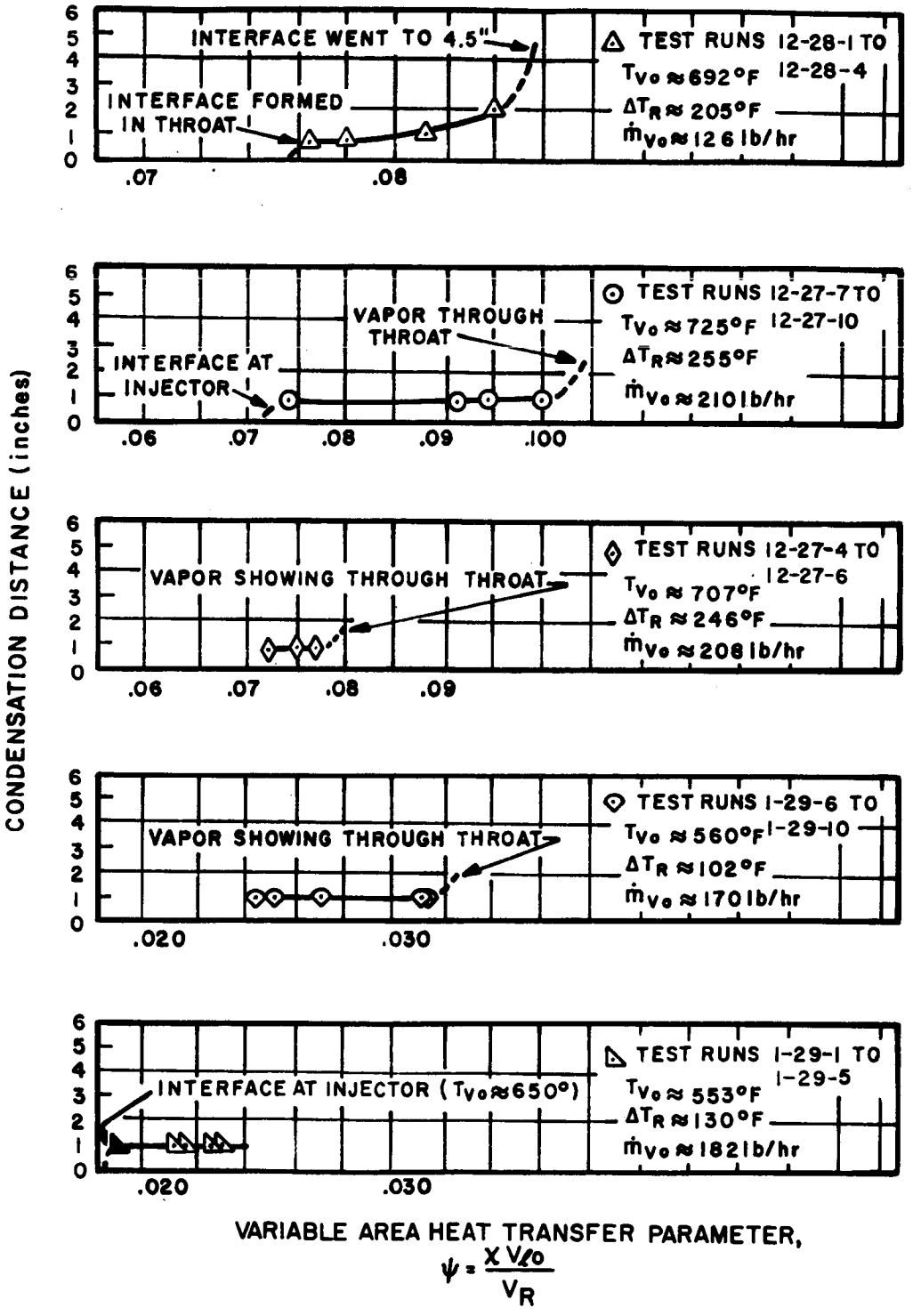

FIG. 47 RANGE OF OPERATION FOR LARGE DIAMETER VARIABLE AREA JET CONDENSER

also obtained and is reported in this section. For example, Fig. 48 summarizes some representative test runs for the constant area jet condenser and four small diameter variable area test units. The data points are the maximum pressure rise which could be obtained during tests conducted within the vapor temperature and mass flow ratio range indicated. Pressure rise and pressure rise divided by liquid dynamic pressure are plotted vs. the ratio of injector to throat area. The area ratio of 0.072 represents the constant area jet condenser and the data points at the other four area ratios are for the small diameter variable area test units. Pressure rise is increased from about 6 psi with the constant area condenser to a peak of 62 psi with the variable area unit with an area ratio of 0.83. Non-dimensional pressure rise increases from about 0.15 for the constant area geometry to a maximum of 1.4. Thus, for these tests, an increase in pressure rise performance by a factor of about ten was demonstrated. (The decrease encountered for still higher area ratios for these small geometries is probably due to impingement of the jet upon the chamber wall.)

Performance Characteristics

In order to obtain pressure rise performance of variable area jet condensers the test units described in Table II were operated over an extended range of variables. As discussed previously, problems of alignment and dimensional control produced a great deal of scatter in data for the small diameter units. Therefore, performance and trends for variable area jet condensers will be mainly derived from test results for the large diameter units. Performance is described by two parameters: the ratio of pressure rise to injected liquid dynamic pressure and the ratio of pressure rise to inlet vapor dynamic pressure. The former is a measure of the jet condenser's efficiency as a pumping device. For a value of $\Delta\bar{P}_{\ell}$ of unity and a perfect injector (discharge coefficient = 1.0) the pressure increase added to the vapor is equal to the pressure drop required to inject liquid, and no net pumping power is required to circulate liquid through the jet condenser component itself. Values of $\Delta\bar{P}_{\ell}$ greater than unity mean an excess pressure $(\Delta\bar{P}_{\ell} - 1)$ $(P_{\ell}V_{\ell o}{}^{2}/2g)$ is

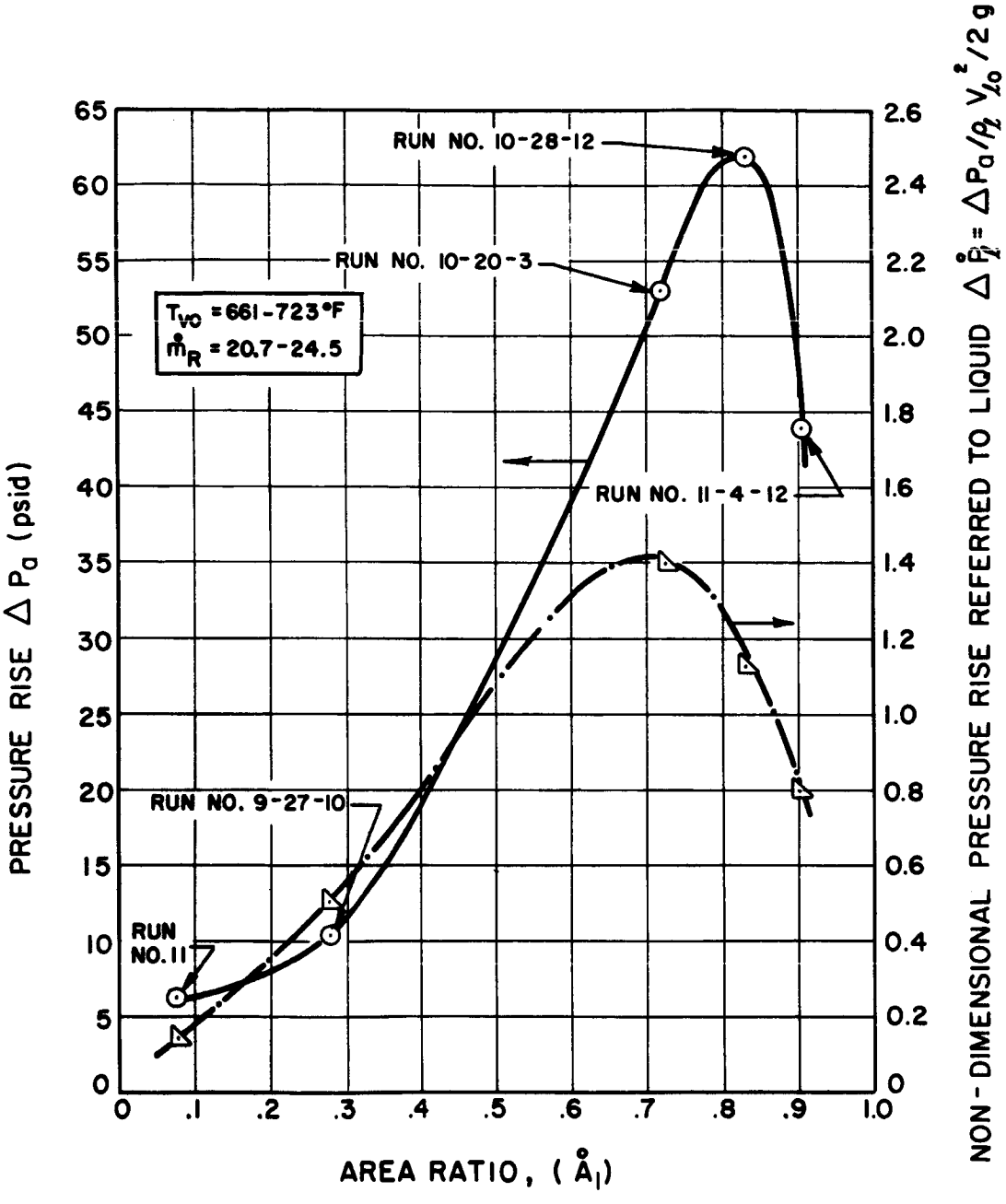

FIG. 48 PERFORMANCE FOR REPRESENTATIVE SMALL DIAMETER JET CONDENSER TESTS VS AREA RATIO OF INJECTOR TO THROAT

available for circulation of liquid external to the jet condenser (as in a liquid radiator loop). In this instance, the condenser also becomes a circulating pump which is driven by the thermal energy of the vapor.

The parameter, $\overset{\circ}{\Delta P}_v$, provides a convenient means for the designer to determine the pressure rise through the condenser (ΔP_a) when vapor inlet conditions are fixed ($\rho_v V_{vo}^2/2g$).

The pressure rise divided by liquid dynamic pressure is plotted versus mass flow ratio in Figs. 49, 50, 51 for the two large diameter jet condensers. All test runs with the interface in the throat and with a pressure rise greater than 2.0 psi are shown.

Values of $\overset{\circ}{\Delta P}_\ell$ were obtained which are as much as eight times the values which could be achieved if the vapor and liquid dynamic pressure were the only sources of pressure rise. For example, in Fig. 49 the maximum value of $\overset{\circ}{\Delta P}_\ell$ obtained is about 12. That is, the measured pressure rise through the jet condenser (ΔP_a) is 12 times the dynamic pressure of the injected liquid($\rho_\ell V_{\ell o}^2/2g$). For this particular test run the dynamic pressure of the inlet vapor ($\rho_v V_{vo}^2/2g$) was only about 0.4 times the liquid dynamic pressure. Thus the ratio of measured pressure rise to the sum of the dynamic pressure terms is 8.7. In order for this result to occur, conversion of vapor thermal energy to liquid mechanical energy must occur in the jet condenser. This experimental result supports the conclusions reached in Sections 2 and 3. As a consequence a very large source of energy is made available for liquid circulation in a Rankine cycle system.

All three curves of $\overset{\circ}{\Delta P}_\ell$ versus $\overset{\circ}{m}_R$ show the trends predicted by analysis; i.e.,

1. Decreasing mass flow ratio produces an increase in the ratio of pressure rise to injected liquid dynamic pressure.
2. Increasing density ratio (decreasing vapor density) usually effects an increase in $\overset{\circ}{\Delta P}_\ell$.

Figures 49 and 51 include calculated curves for the maximum density ratio of the test runs for reference. As can be seen

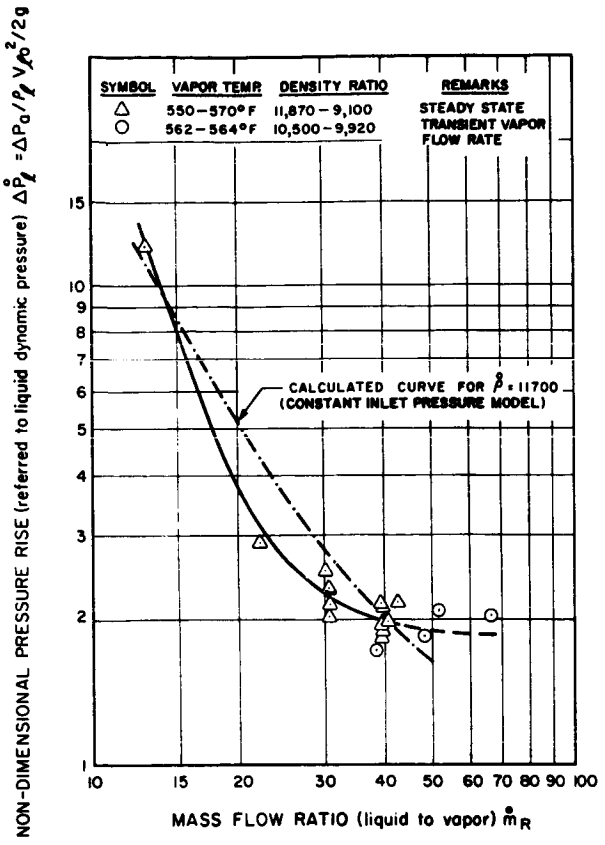

FIG. 49

NON-DIMENSIONAL PRESSURE RISE (referred to liquid dynamic pressure) for LARGE DIAMETER JET CONDENSER (Test Sec. No. 7) VS MASS FLOW RATIO OF LIQUID TO VAPOR

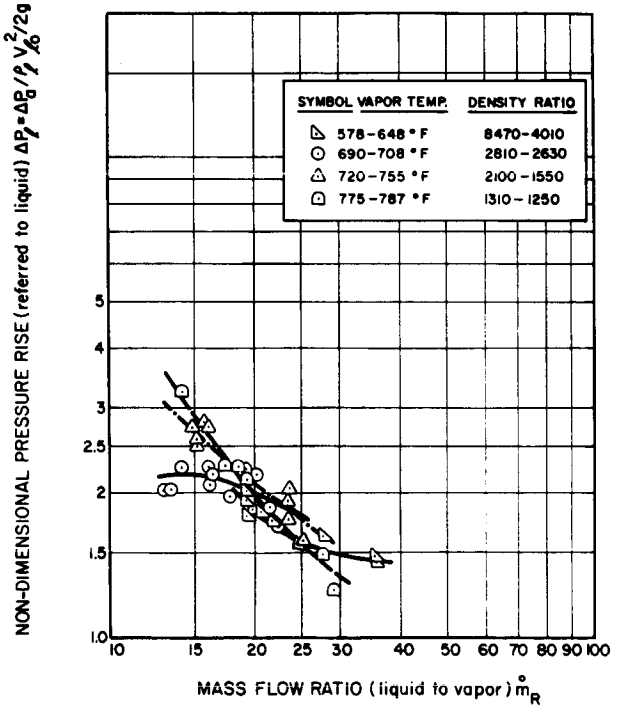

FIG. 50

NON-DIMENSIONAL PRESSURE RISE (referred to liquid dynamic pressure) FOR LARGE DIAMETER JET CONDENSER (Test Sec. No. 7) VS MASS FLOW RATIO OF LIQUID TO VAPOR

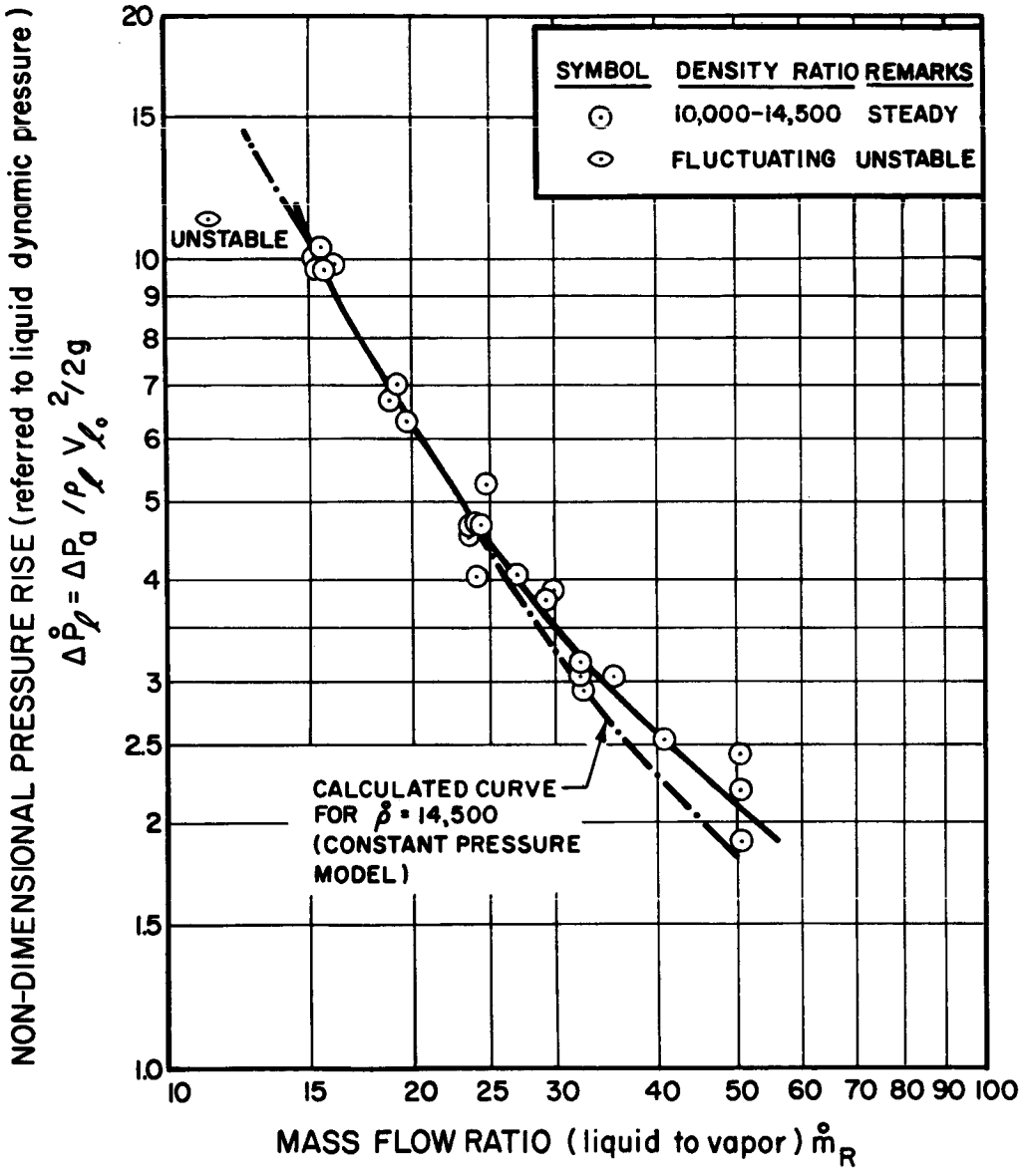

FIG. 51

NON-DIMENSIONAL PRESSURE RISE (referred to liquid dynamic pressure) FOR LARGE DIAMETER JET CONDENSER (Test Sec. No. 8) VS MASS FLOW RATIO OF LIQUID TO VAPOR

the trend of the analysis is followed relatively closely over the range of $\Delta \overset{o}{P}_{\ell}$ (1.7 - 12.0) and mass flow ratio (13-66) for these curves. The deviations which do occur for the two lower vapor pressure curves and for the curve of higher vapor pressures (Fig. 50) may be due to deviations in the wall pressure from inlet pressure (cf. Section 3) and frictional and momentum losses.

The lowest value of $\Delta \overset{o}{P}_{\ell}$ obtained for steady-state operation with the interface in the throat location was 1.25 with the majority of the test data falling above 1.5. Thus, for these operating variables and for a perfect injector (discharge coefficient of unity), the pressure increment added to the vapor would always be greater than that required to inject the liquid. For a mercury Rankine cycle system the operating parameters for a jet condenser would probably include a vapor temperature of 600-700°F and a mass flow ratio of 20-40. For these conditions the large diameter jet condensers tested had a range of $\Delta \overset{o}{P}_{\ell}$ of about 1.25 to 2.0. However, if the geometric trends of the analysis are followed (as were those for flow variables) higher values of $\Delta \overset{o}{P}_{\ell}$ should be obtainable for these conditions by use of a larger area ratio of the injector to tube inlet.

Figure 51 contains a point at $\overset{o}{m}_R = 11.5$ for which stable operation of the jet condenser was not possible. An attempt to operate at this lower value of mass flow ratio resulted in very large oscillations in the interface location and vapor and liquid flows. Non-dimensional pressure rise was decreased from the points at $\overset{o}{m}_R = 15.0$. The flow conditions for this point are given in Appendix F.

The pressure rise divided by inlet vapor dynamic pressure is plotted in Figs. 52, 53 and 54. While $\Delta \overset{o}{P}_{\ell}$ provides a measure of the efficiency of the jet condenser as a pumping device, $\Delta \overset{o}{P}_{v}$ provides a convenient means of determining the absolute magnitude of pressure rise when vapor conditions are specified. All curves shown exhibit the trends for $\Delta \overset{o}{P}_{v}$ predicted by analysis:

1. Increasing mass flow ratio produces increasing values of $\Delta \overset{o}{P}_{v}$. For fixed vapor conditions the value of

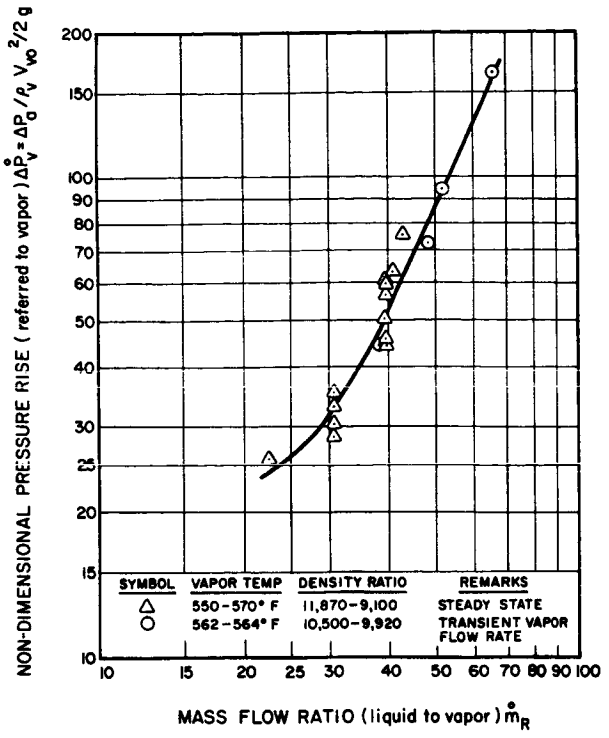

FIG. 52

NON-DIMENSIONAL PRESSURE RISE (referred to vapor dynamic pressure) VS MASS FLOW RATIO OF LIQUID TO VAPOR FOR LARGE DIAMETER JET CONDENSER. (Test Sec. No. 7)

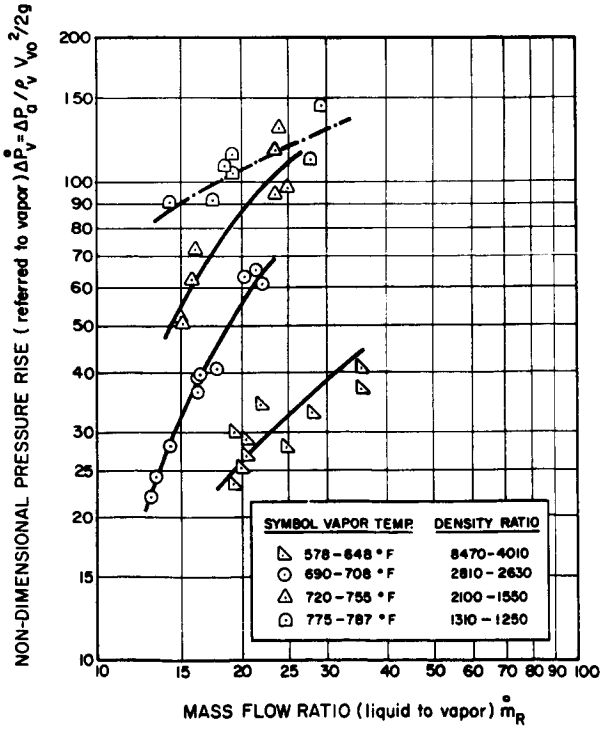

FIG. 53

NON-DIMENSIONAL PRESSURE RISE (referred to vapor dynamic pressure) VS MASS FLOW RATIO OF LIQUID TO VAPOR FOR LARGE DIAMETER JET CONDENSER (Test Sec. No. 7)

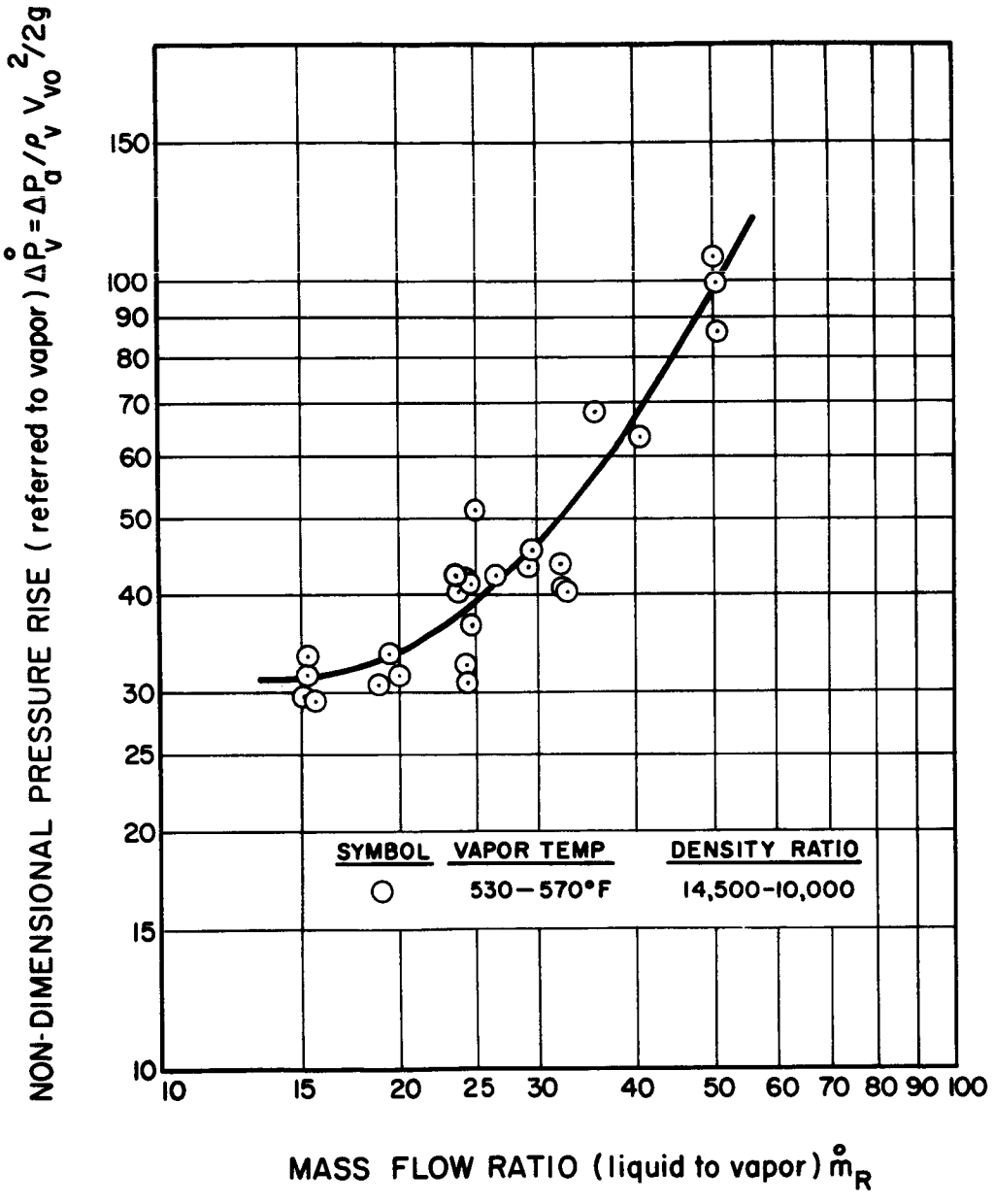

FIG. 54 NON-DIMENSIONAL PRESSURE RISE (referred to vapor dynamic pressure) vs MASS FLOW RATIO OF LIQUID TO VAPOR FOR LARGE DIAMETER JET CONDENSER (Test Sec. No. 8)

pressure rise increases with increasing mass flow ratio.

2. Decreasing density ratio (increasing vapor temperature) effects an increase in ΔP_v^o.

The curves of Fig. 53 which were obtained for higher vapor temperatures do not follow the analytical trend as closely as do the data obtained for lower vapor temperstures (Figs. 52 and 54). The probable explanation is that these runs had much lower vapor velocities (due to the increase in density) and lower pressure rise than test runs for lower vapor temperatures. Thus a relatively large amount of scatter is found in the values of ΔP_v^o.

Values of ΔP_v^o range from about 20 to 170 on these plots. Therefore, a total of 20 to 170 times the inlet dynamic pressure of the vapor was added to the inlet vapor pressure during these test runs. It is very interesting to note that for a fixed set of vapor conditions no limit on pressure rise is set by the inlet vapor pressure. That is, whether the inlet pressure is 1.0 psia or 100 psia, the pressure increment added, ΔP_a, is increased as the mass flow ratio increases. This result means the jet condenser could be very useful for condensing vapor at a very low turbine exhaust pressure. Problems of excessive pressure drop or choke flow, which may be common to a direct condenser-radiator, will be less severe with a jet condenser, since a pressure increase can be added to the inlet vapor pressure.

A description of variable area jet condenser performance by plotting non-dimensional pressure rise versus jet utilization factor was attempted. This approach was valid for the constant area geometry where a wide range of operating points existed, each corresponding to a definite value of χ. However, for a given density ratio and mass flow ratio Figs. 45-47 indicate a range of values of χ may exist for any design operating point. In the curves of Fig. 47 the range of χ was as much as $\pm$ 24 percent with the interface in the throat. The possible explanation for the range of values of χ which can be accommodated is that the large pressures and dynamic forces occurring at the interface in a variable

area geometry require much larger changes in heat transfer rate to effect movement of the interface than in a constant area unit.

Figure 55 is a plot of $\overset{\circ}{\Delta P}_{\ell}$ versus χ for the test data of Test Section No. 8. The lack of a definitive relation between $\overset{\circ}{\Delta P}_{\ell}$ and χ is apparent, although somewhat of a trend is indicated. Higher average values of χ are associated with higher values of $\overset{\circ}{\Delta P}_{\ell}$. The reason is that higher values of $\overset{\circ}{\Delta P}_{\ell}$ result from lower mass flow ratios of liquid to vapor (or lower values of the ratio $V_{\ell o}/V_R$). Thus for a fixed density ratio, the lower value of $V_{\ell o}/V_R$ requires higher values of χ in order for the parameter $\chi V_{\ell o}/V_R$ to remain constant due to the reasons discussed above. However, as discussed above, a range of χ is possible at any design point. The dashed curves of Fig. 55 denote probable design limits for χ as established by observing interface location during tests.

Comparison with Calculated Pressure Rise

In order to enable more general use of the test results, experimental performance can be compared to that predicted by analysis by using the model which incorporated the assumption that the mixing chamber wall pressure was equal to the inlet vapor pressure (Section 3). The results are shown in Fig. 56 which plots measured pressure rise versus calculated. The average deviation appears to be about + 30 percent and - 25 percent of measured from calculated. Considering the simplifying assumptions of the analysis, possible uncertainties in the values of density ratio used in the analysis, and the possibility of off-design operation, the agreement shown is considered to be reasonably good. Thus, the calculation method used for predicting pressure rise appears to be useful for preliminary design purposes. The results suggest that the calculated values would probably provide a low estimate of the pressure rise in jet condensers.

Examination of the test data for Test Section No. 7, where vapor temperature was varied over a wide range, reveals an influence of jet utilization factor upon the deviation of measured from calculated pressure rise. Figure 57 contains plots of η_a, the ratio of measured to calculated pressure rise, versus jet utilization factor for different groupings of vapor temperature and injection velocity. These curves appear to indicate that lower values of χ tend to result in values of

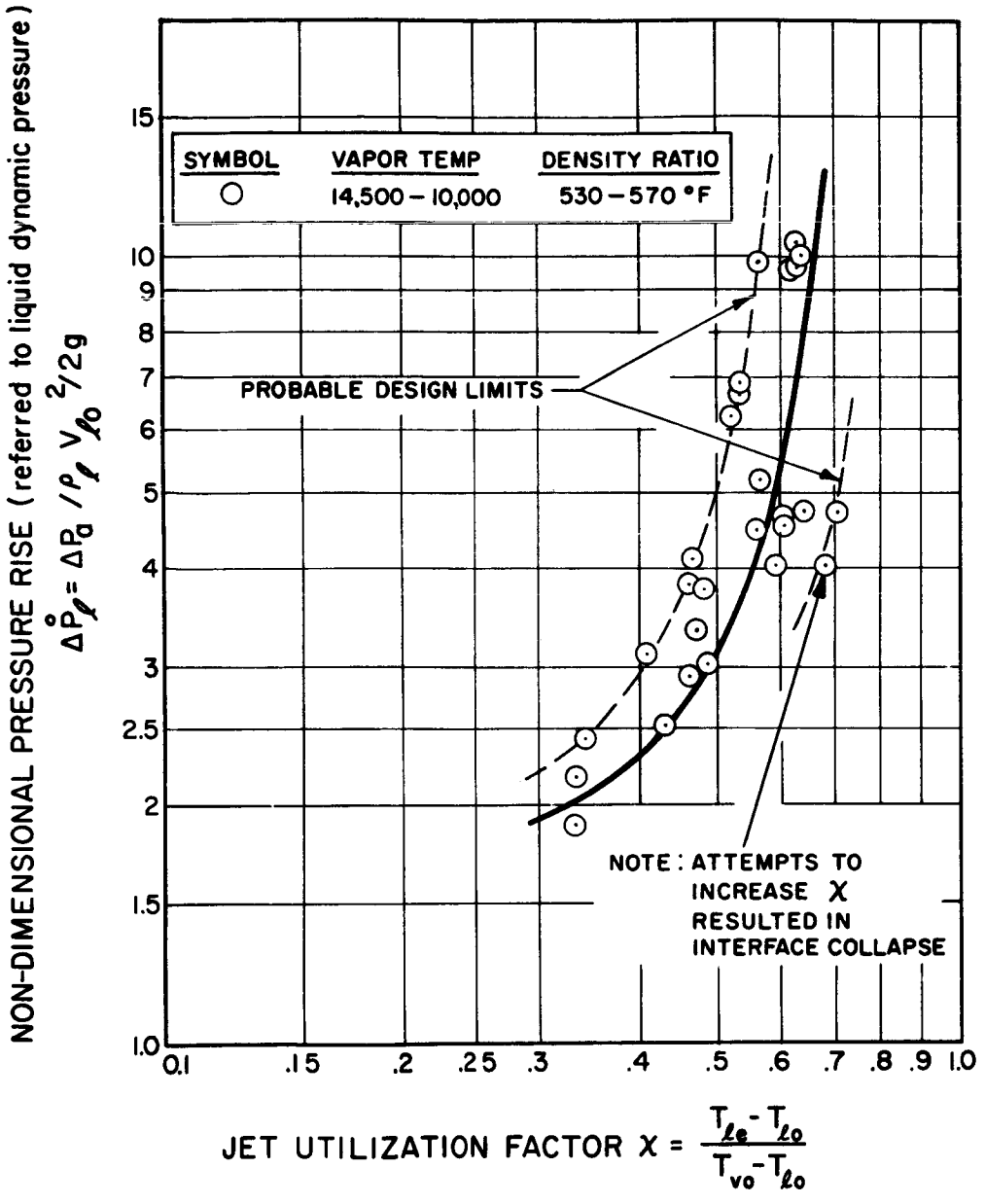

FIG. 55 NON-DIMENSIONAL PRESSURE RISE (referred to liquid dynamic pressure) VS JET UTILIZATION FACTOR FOR LARGE DIAMETER JET CONDENSER

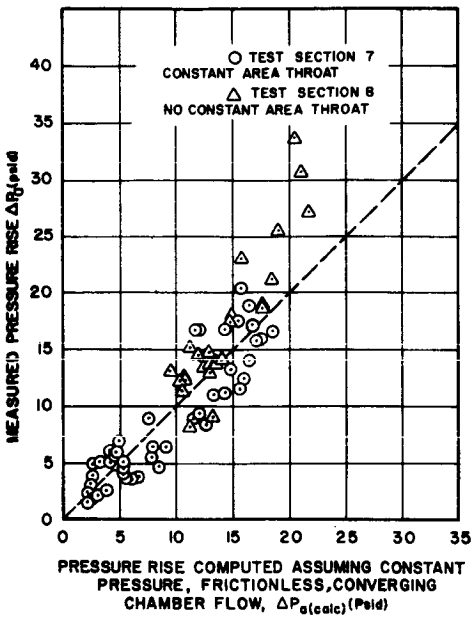

FIG. 56

COMPARISON OF MEASURED PRESSURE RISE IN LARGE DIAMETER JET CONDENSERS (for all test runs with interface in throat and steady state conditions) WITH CALCULATED VALUES

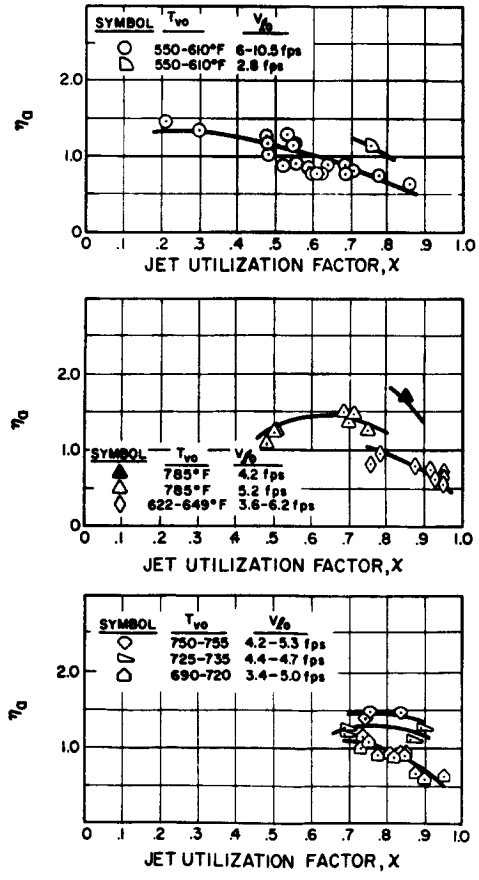

FIG. 57

RATIO OF MEASURED PRESSURE RISE TO CALCULATED (constant inlet vapor pressure) VS JET UTILIZATION FACTOR

η_a greater than unity (measured pressure rise higher than calculated) while at higher values of χ, η_a falls below unity. Operation of a jet condenser at higher values of χ may therefore result in some degradation of pressure rise performance, even though visual observation indicates the interface to be at the throat location. A possible reason for this behavior is that changing the value of χ influences the spatial distribution of condensation in the mixing region which in turn influences the flow and wall pressure distribution.

Range of Operation

As noted in Fig. 55, useful pressure rise may be obtained in a jet condenser over a considerable range of operating parameters. As might be expected, the same correlating parameters which determine the range of operation for which the vapor liquid interface remains in the throat appear to have the most important influence on pressure rise.

Figure 58 furnishes information on the variation of pressure rise as the heat transfer parameter Ψ is varied for five test sequences. These test runs are indentical to those of Fig. 47 where the influence of Ψ on condensation length was presented. The ordinate of the plots of Fig. 58 is η_a, the ratio of measured to calculated pressure rise. This parameter was used to eliminate the effect of variations in flow rates which produced values of absolute pressure rise which were different in trend than the actual performance of the jet condenser. The gross pressure rise characteristics of these plots follow the same trend as the condensation length. At higher values of Ψ the interface moves into the diffuser and pressure rise falls off sharply. At lower values of Ψ the interface advances upstream to the injector and a similar drop in pressure rise is experienced. However, within the range of Ψ for which the interface is in the throat, appreciable variations in pressure rise can occur. For example, in the fourth and fifth plots η_a varies from about 0.75 to 1.20 as Ψvaries from 0.019 to 0.031. The probable explanation for this behavior is that changing Ψproduces a change in the heat transfer and hence wall pressure distribution in the mixing chamber. In addition, while the average position of the interface

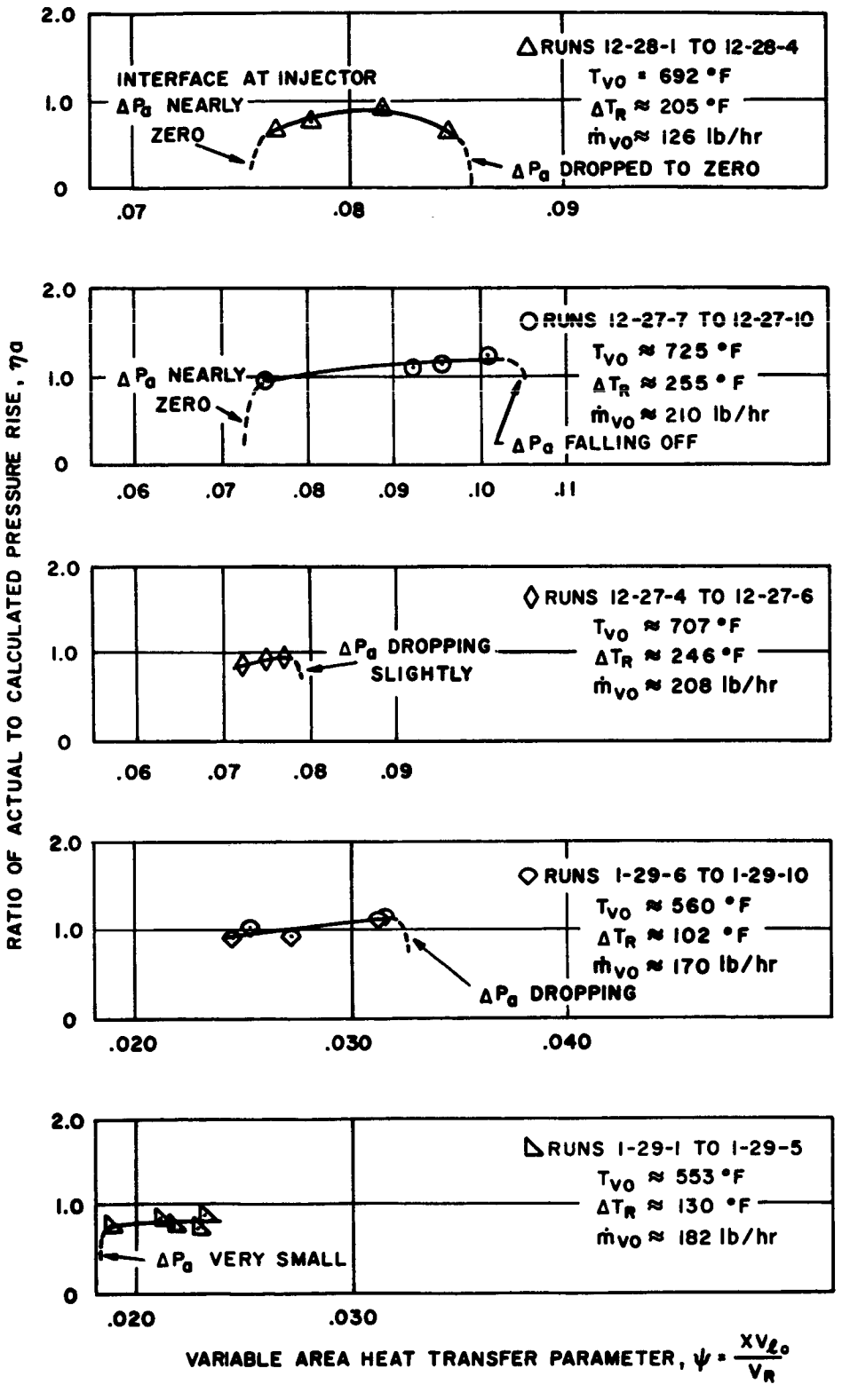

FIG. 58 RANGE OF OPERATION FOR PRESSURE RISE VS VARIABLE AREA HEAT TRANSFER PARAMETER FOR LARGE DIAMETER JET CONDENSER

is within the constant area throat (as determined visually), high speed motion pictures reveal the location to vary. At times, the interface exists just upstream of the throat in the converging section. Therefore, lower values of Ψ may increase the time spent in the converging section by the final interface, resulting in a deleterious effect upon pressure rise. Similarly, the higher values of Ψ may result in occurrence of the interface in the diffuser a fraction of the time with a resulting decrease in the measured (time average) pressure rise due to momentum and frictional losses. However, no fluctuations in measured pressures were noted.

Injector Performance

The performance of the liquid injector is indicated in Fig. 59, which plots η_i versus the dynamic pressure of the injected liquid. As can be seen, very low values of efficiency were measured. At higher values of dynamic pressure, values of η_i as low as 0.2 were obtained. However, these values are mainly characteristic of the experimental setup rather than the injector. The sketch on the bottom of Fig. 49 indicates the injector configuration which was used. The measured value of ΔP_i includes the losses from two right angle bends in addition to contraction and frictional losses. If the contraction losses $\left(\approx .3 \frac{\rho_\ell V_{\ell o}^2}{2g}\right)$ and the first bend loss $\left(\approx .9 \frac{\rho_\ell V_{\ell o}^2}{2g}\right)$ were subtracted from ΔP_i the range of η_i for the injector would be approximately 1.0 to 0.3. If line friction is included, then values of η_i would range from about 3.0 to 0.35. Values of η_i greater than unity are possible when the local pressure at the injector exit is lower then the values measured upstream due to the highly subcooled liquid and resulting pressure gradient in the vapor. Thus, injector performance cannot be defined precisely for the test section geometries used. However, design of a smoothly contoured injector for an actual application, should result in a discharge coefficient greater than about 0.90 for most cases.

5.3.4 Stability and Startup

Several aspects of jet condenser performance were examined which relate to stability and starup of this component. Here,

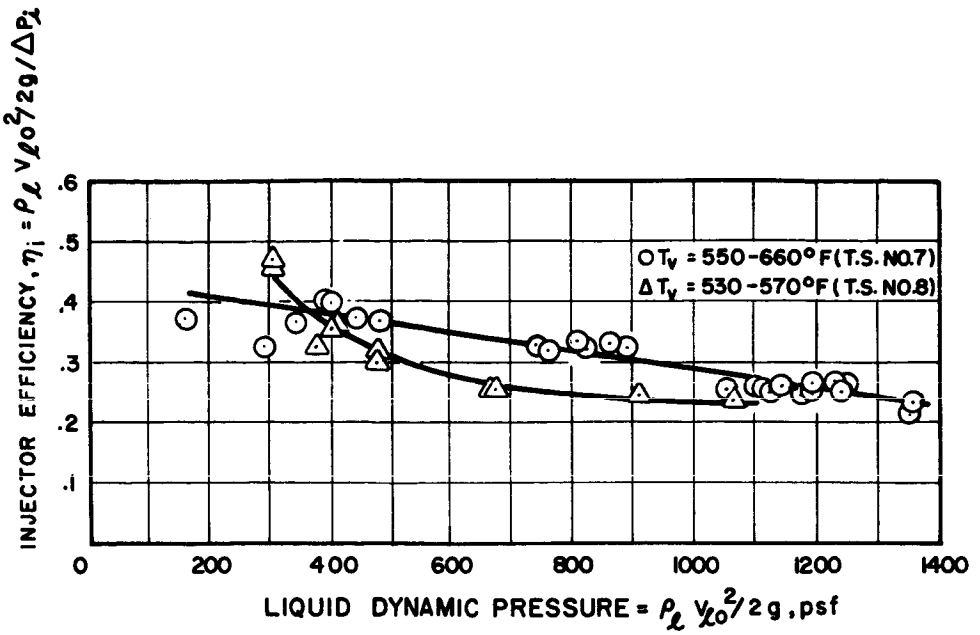

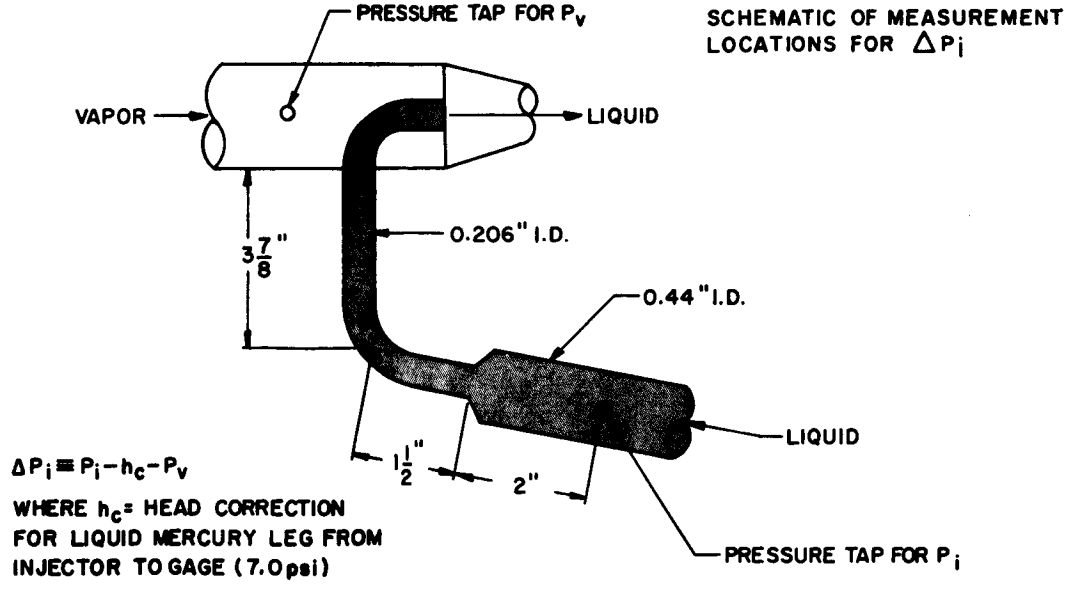

FIG. 59 INJECTOR EFFICIENCY FOR LARGE DIAMETER JET CONDENSERS

stability must be discussed in terms of operation of the jet condenser component itself and/or interactions with the other components of the 10 kw test loop. However, the performance observed can be used to indicate possible trends of stability and startup in a Rankine cycle system. For purposes of this discussion, stable operation of the jet condenser is defined as operation with the following characteristics:

1. Vapor free flow at the outlet.
2. All fluctuations of flow rates, temperatures and pressures are small ($<$ 1-2 percent) compared to the average (measured) values.
3. All flow rates, temperatures and pressures are controllable.
4. All other components of the test loop operate with the criteria of No.s 2 and 3.

Stable operation was achieved for the entire range of variables of Table III. The only flow conditions resulting in unstable operation are those of run numbers 1-31-2 and 3-15-3a where very low mass flow ratios, liquid velocities and vapor velocities were used. In this case the instability appeared as large oscillations ($\pm$ 50 percent) in flow rates and pressures and in oscillations in the location of the vapor-liquid interface (0 to 1 inch). For all other combinations of the variables listed jet condenser operation was controllable and measured fluctuations were within the limits indicated above.

As noted in Section 4, the jet condenser was self regulating for small mis-matches ($\approx$ 10 percent) of boiler inlet flow to vapor inlet flow. The initial mis-match resulted in a decrease or increase in condenser pressure level which then acted to correct the vapor flow to the proper value.

The regulating properties of these condensers are illustrated in Fig. 60 which is a record of performance during a drop in vapor load from 170 lb/hr to less than 50 lb/hr. The vapor temperature, liquid inlet temperature, liquid outlet temperature, heat transfer parameter, Ψ, jet utilization factor, χ, vapor flow rate, pressure rise,

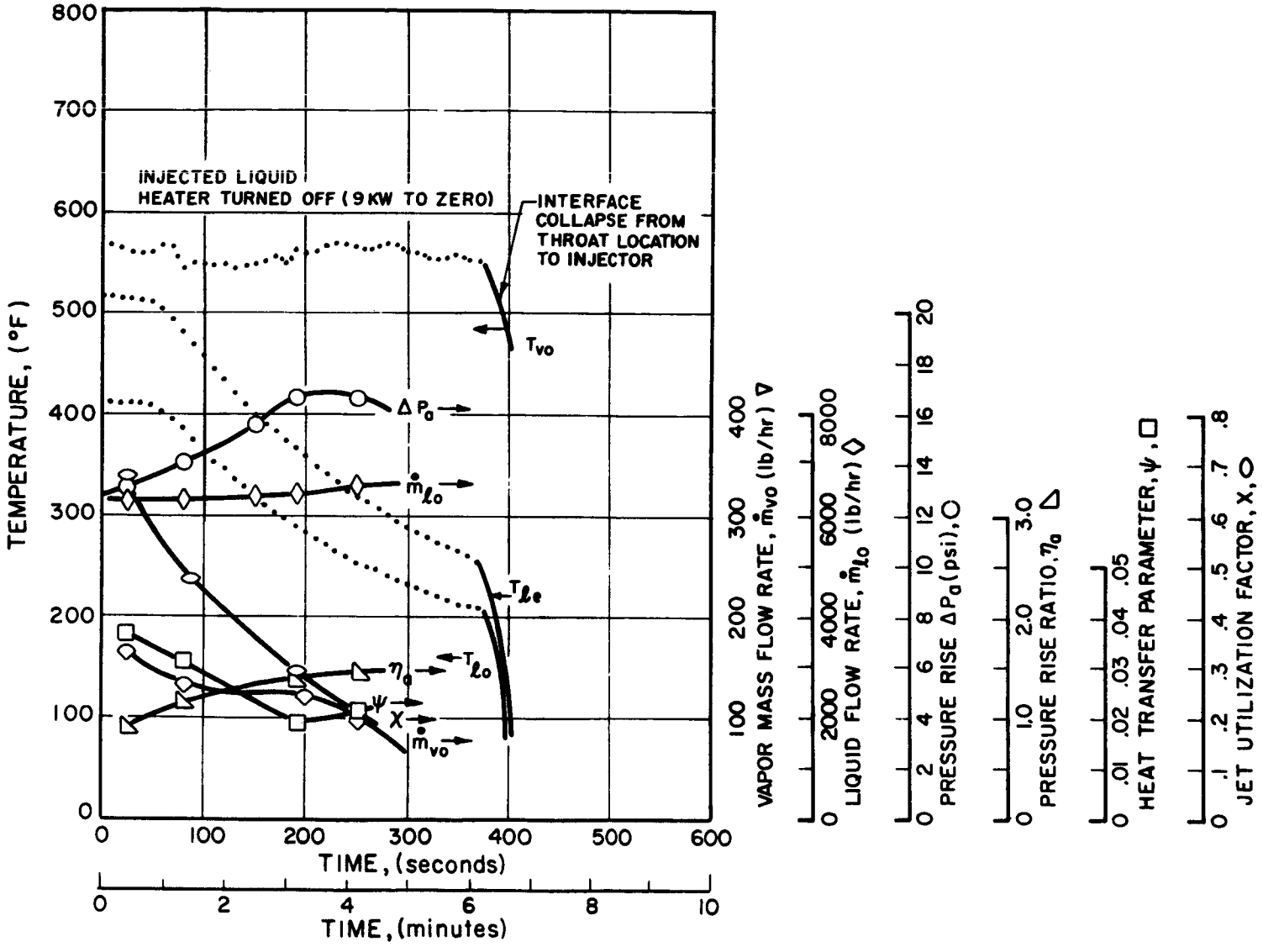

FIG. 60 OPERATION CHARACTERISTICS OF JET CONDENSER DURING LOSS OF VAPOR FLOW AND INJECT LIQUID HEATER

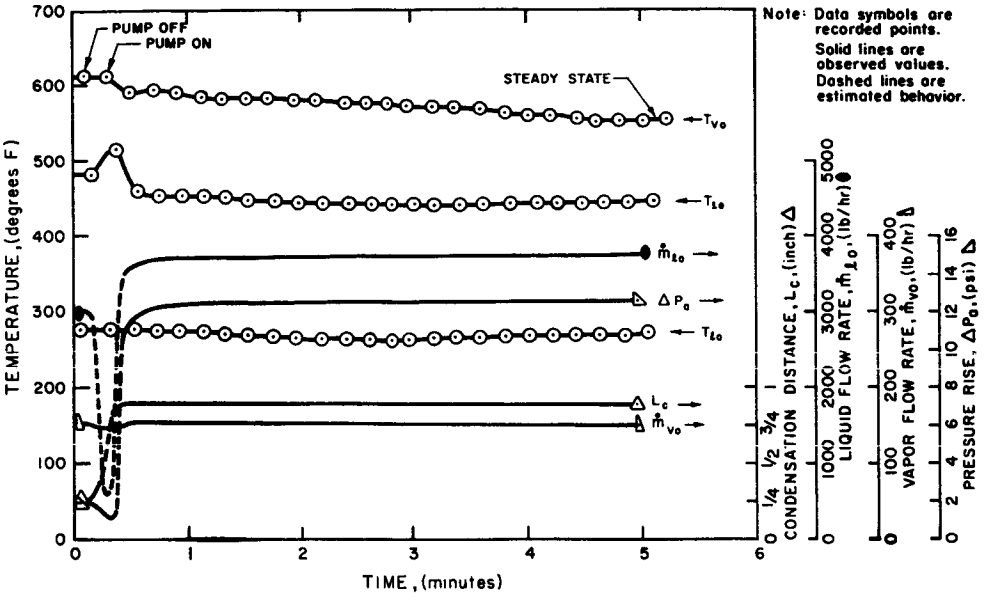

FIG. 61 OPERATION CHARACTERISTICS OF JET CONDENSER DURING TRANSITION FROM INTERFACE LOCATION AT INJECTOR TO INTERFACE LOCATION AT THROAT

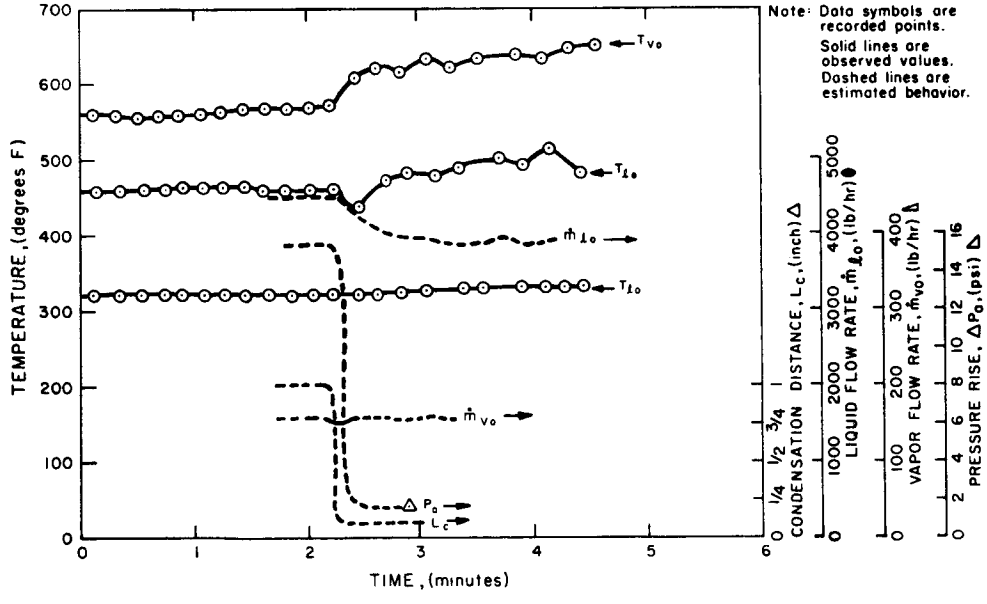

FIG. 62 OPERATION CHARACTERISTICS OF JET CONDENSER DURING COLLAPSE OF INTERFACE FROM THROAT LOCATION TO INJECTOR LOCATION DUE TO OFF-DESIGN CONDITIONS

ratio of measured to calculated pressure rise, and liquid flow rate are plotted versus time following the shut-off of the boiler heaters. The most significant aspect of these curves is the fact that by varying the liquid injection temperature (as the vapor flow dropped) the vapor inlet temperature was maintained in the range 540-570°F until final collapse of the interface. The fact that the liquid flow and/or temperature can be varied to maintain a constant vapor pressure (and temperature) at very low vapor flow rates is very important to the use of a jet condenser in a Rankine cycle system . Current startup methods for these power systems involve starting the boiler at about 10 percent or less of rated flow. If a direct condenser-radiator is used, the heat load is so small that the condenser cannot be maintained at vapor pressures near rated operating conditions without auxiliary heating or radiation shields. Operation at near rated pressure is required for satisfactory pump performance. Even with these auxiliary devices, stable interface formation for the low dynamic forces resulting from the lower vapor flow rates may be difficult. These problems may be avoided in a jet condenser system. Liquid mass flow rate and temperature may be varied nearly independently of boiler flow rate in order to maintain constant condenser and pump inlet pressures.

Startup of jet condensers in the laboratory loop was accomplished in several different modes. Probably the simplest was gradual introduction of vapor to flowing liquid in the test section. The liquid injection temperature was adjusted such that the interface was maintained at the injector. Vapor flow and liquid temperature were both increased until nearly equal to the desired operating values. At this point the liquid flow was momentarily perturbed by interrupting pump operation. This moved vapor into the throat. Reactivation of the pump after 10-12 seconds then produced the final vapor liquid interface at the throat. The time dependency of several operating variables during this startup sequence are shown in Fig. 61. Steady-state values of outlet pressure, temperature and flow were established to about 2 percent within one to two minutes. However, approximately five minutes were

required for the steady-state value of vapor temperature (555°F) to be attained (probably due to the thermal lag of the boiler). A large increase in pressure rise (1.8 to 12.6 psi) occurred as the interface made the transition from the converging section to the throat. As a result of the increase in pressure rise, the liquid circulation increased from about 2900 lb/hr to 3750 lb/hr.

The opposite circumstance, collapse of the interface to the injector location, is recorded in Fig. 62. This collapse resulted when the condenser was being operated with a value of heat transfer parameter, Ψ, which was too low for the interface to be supported in the throat location. For this sequence the pressure rise dropped from 15.4 psi to about 1.5 psi. Liquid flow dropped from 4500 lb/hr to about 3800 lb/hr and vapor temperature increased from 570°F to about 650°F. Clearly the above behavior is to be avoided for satisfactory operation of the jet condenser in a Rankine cycle power system. Gross changes in operating conditions would result from such a change in interface location. Therefore, the condenser must be operated under heat transfer conditions (Fig. 45) such that the interface is maintained at the throat location.

Oscillations in the location of the final vapor-liquid interface were not apparent from visual observation of the quartz mixing sections. However, high speed motion pictures revealed small oscillations ($\approx \pm$ 1/16 inch) to be present with very small periods ($\approx$ .005 seconds). Of course these oscillations had no apparent effect upon measured temperatures and pressures due to the longer response time of the thermocouples and pressure gages used. However, it is more significant that such oscillations had no effect upon the measured flow rates. Liquid flows were measured using electro-magnetic flow meters where response was only limited by the electronic circuitry of the microvoltmeter used for indication. Therefore, it is felt that the oscillations observed in the high speed motion pictures will have very small, if any, effects upon performance of the rest of a Rankine cycle system.

Another interesting aspect of jet condenser operation which was examined during this program was the process of interface formation. A high speed motion picture was taken of the injection of subcooled liquid into a jet condenser initially filled with flowing vapor. A similar test was conducted with the constant area jet condenser (Fig. 41) with highly subcooled liquid. For those flow conditions, the interface was formed at the injector. However, for the large diameter variable area jet condenser tests, liquid flow conditions were set so that the interface should be formed at the throat. The length of time required to establish the final interface at that location was sought. The resulting sequence is shown in Fig. 63. As noted, the time required from injection until a vapor liquid interface was established in the throat with all-liquid flow out of the jet condenser was approximately 0.02 seconds.

Further operation resulted in adjustments of the jet profile and interface shape, but the interface remained at the throat location. The short time required and the absence of any large oscillations are indicative of the large pressure forces which tend to maintain the interface at the throat location if the flow parameters are adjusted such that the required heat transfer rates are attained (Fig. 45).

To summarize, for the conditions described above, startup or stability problems were not apparent during jet condenser operation in the 10 kw test loop. Startup was accomplished from cold conditions with the loop evacuated and with no external devices (such as reservoirs). Operation while maintaining a nearly constant vapor inlet pressure during a variation from design conditions to very low vapor flow rates was demonstrated. Fluctuations in condensation distance (due probably to variations in jet heat transfer area) were observed in highspeed motion pictures but had no apparent effect upon performance. Control, stable operation, and flow division were achieved using only manually operated controls. Tests conducted under conditions with very low liquid and vapor dynamic forces

(smaller than would be used in design applications) resulted in unstable flow. However, stable operation was achieved for the entire range of test variables presented in Table III.

5.4 Multi-Tube Jet Condenser

In order to condense higher vapor flow rates, typical of Rankine cycle power systems, an increase in capacity of the test units discussed previously is required. Larger capacity can be obtained either by increasing the physical size of a single unit or by manifolding several smaller condensers. The former technique would be simplest but some uncertainty may exist in scaling test results to larger sizes. Manifolding several smaller condensers would enable use of the actual test geometries in system design, if performance and stability did not change. Therefore, the main purpose of the multi-tube tests was to determine if several (three) smaller jet condensers (0.43 inches i.d) could be manifolded to condense vapor flow rates typical of a larger geometry (0.75 inches i,d.) while retaining its performance characteristics.

As discussed in Section 4, the same area ratios, $\overset{o}{A}_1$ (0.895) and $\overset{o}{A}_2$ (0.075), were used in the multi-tube units as for the large diameter geometries.

The theoretical pressure rise characteristics were therefore identical for both the multi-tube and large diameter test units. Since the ratios of L_c/d_{to} were also identical (1.3), the values of Ψ producing an interface in the throat location should be the same if no manifolding effects were present. However, as will be indicated below pressure rise and heat transfer characteristics of the multi-tube test unit were different from those of the large diameter unit. In addition, problems of unstable operation were encountered for the experimental arrangement used.

Heat Transfer

The main sources of comparison of multi-tube heat transfer data with that of the large diameter jet condenser are test run No.'s 5-15-15 through 5-15-18 (Appendix G).

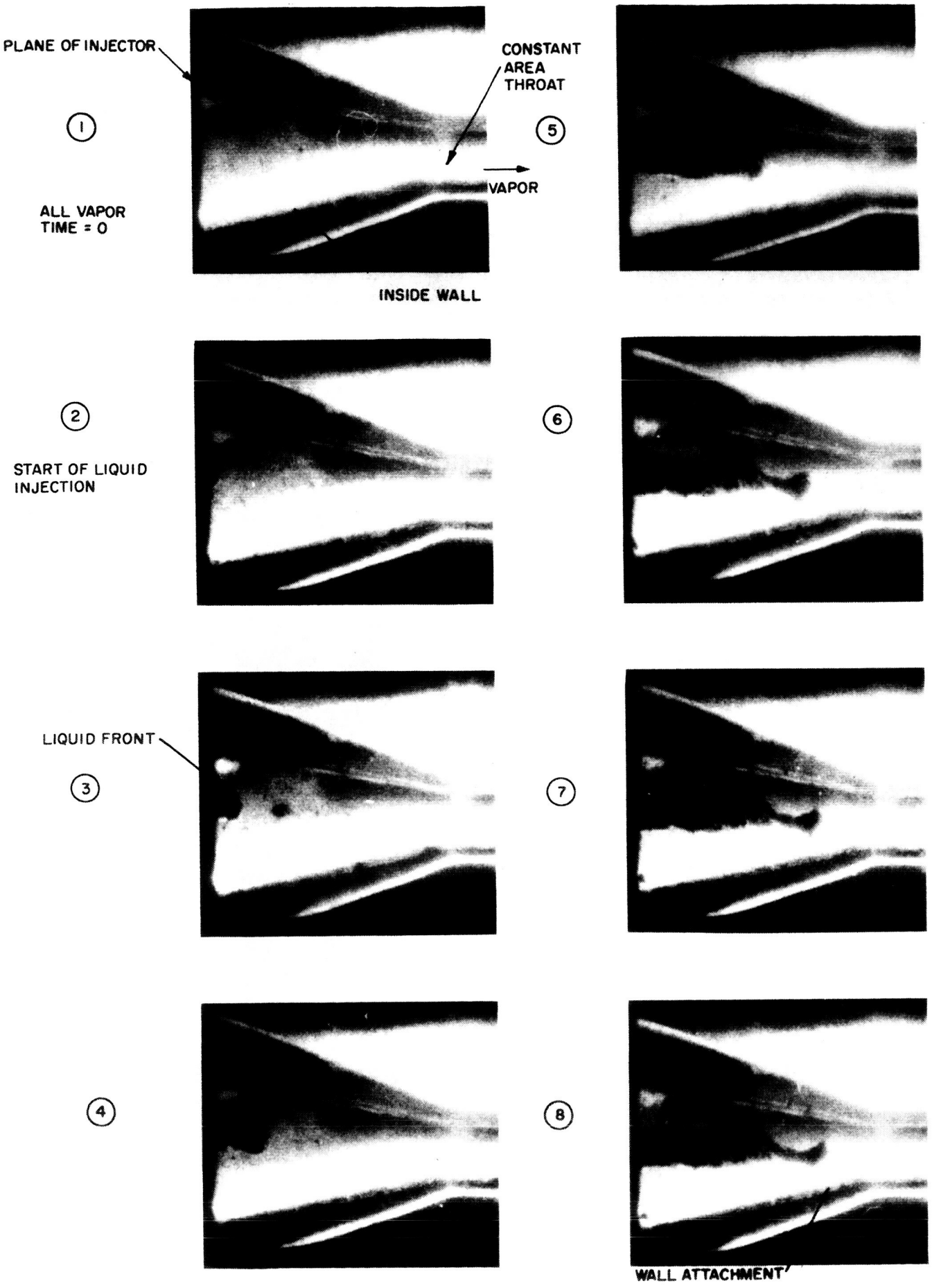

FIG. 63 INJECTION OF LIQUID INTO VAPOR FILLED VARIABLE AREA JET CONDENSER. SINGLE FRAMES FROM HIGH SPEED MOTION PICTURE. (8000 frames per second).

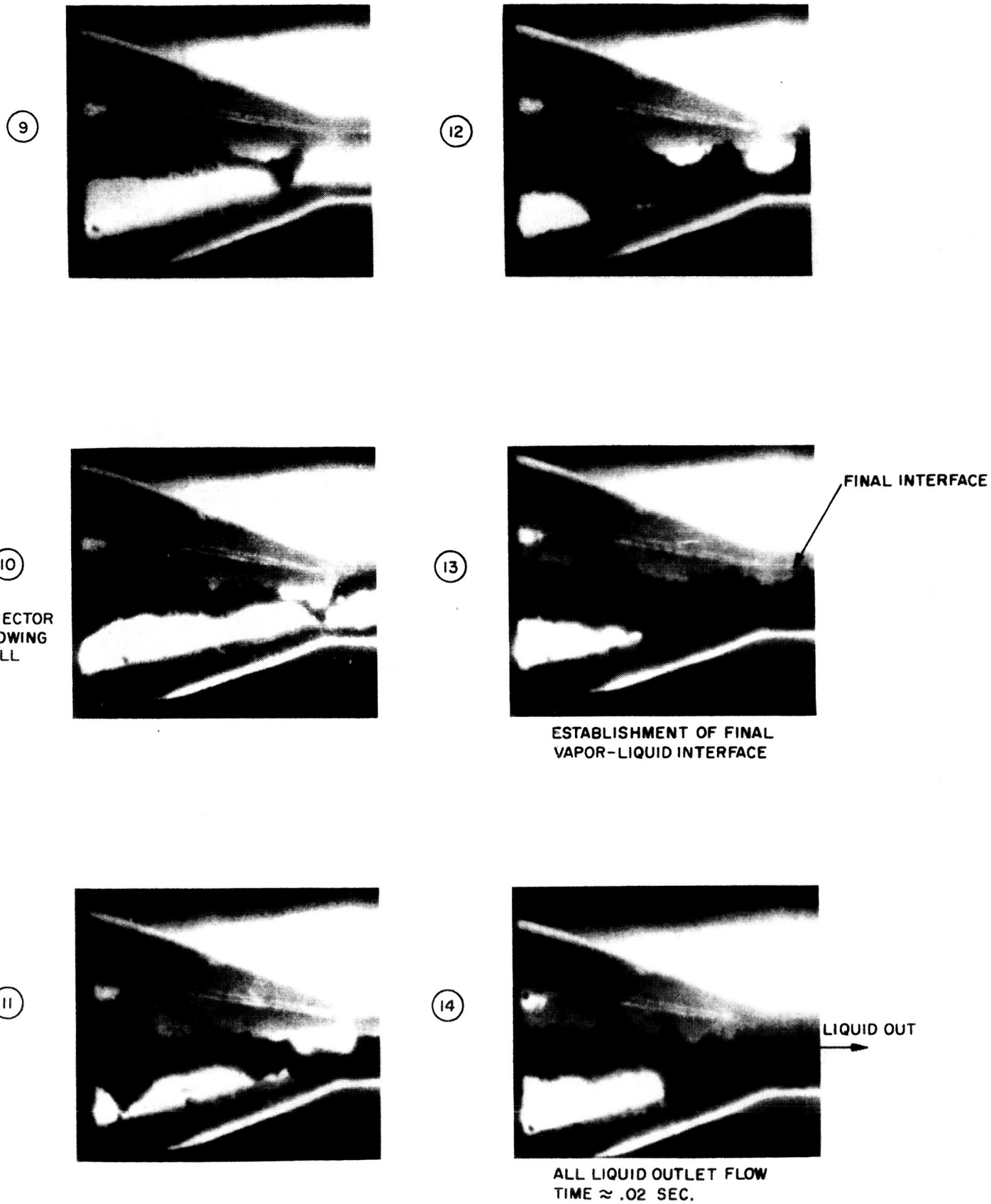

FIG. 63 (cont) INJECTION OF LIQUID INTO VAPOR FILLED VARIABLE AREA JET CONDENSER. SINGLE FRAMES FROM HIGH SPEED MOTION PICTURE. (8000 frames per second)

During these tests the vapor-liquid interfaces were located at the throat positions for all three test units except for periodic collapses (cf. below). The values of Ψ obtained ranged from 0.0800 ($\overset{o}{\rho}$ = 2960) to 0.138 ($\overset{o}{\rho}$ = 2100). These values can be compared to the average values (for corresponding density ratios) for the large diameter unit of 0.070 and 0.100 (cf. Fig. 45). The maximum values of Ψ obtained for the large diameter units were about 0.078 and 0.120 at these density ratios. Therefore, the heat transfer rates (or attainable values of χ for constant $V_{\ell o}$ and V_R) appear to be somewhat higher for the multi-tube unit than for the larger diameter condenser. However, the differences are small enough that no serious problems should be present in applying the results for single tube units for a preliminary estimate of heat transfer.

Pressure Rise and Stability

The pressure rise and stability characteristics of single jet condensers were seriously degraded when manifolding was attempted. The maximum values of pressure rise which could be obtained in conjunction with stable flow conditions were about equal to the dynamic pressure of the injected liquid. Attempts to operate with higher values of pressure rise (where significant contributions of the vapor energy would occur) resulted in severe oscillations of outlet pressure and flow and periodic collapse of one or more interfaces.

Figure 64 furnishes an illustration of this behavior. The ordinate is $\Delta\overset{o}{P}_\ell$, the ratio of pressure rise to injected liquid dynamic pressure. Operation at lower mass flow ratios produced very low values of $\Delta\overset{o}{P}_\ell$ due to the occurrence of the interface in the converging section or diffuser. Very steady outlet conditions were observed for these operating points. Attempts to place the interface at the throat location by adjusting flow rates and/or temperatures always resulted in very erratic flows and pressures. Usually two interfaces would back up to the injector and vapor would exit from the remaining condenser.

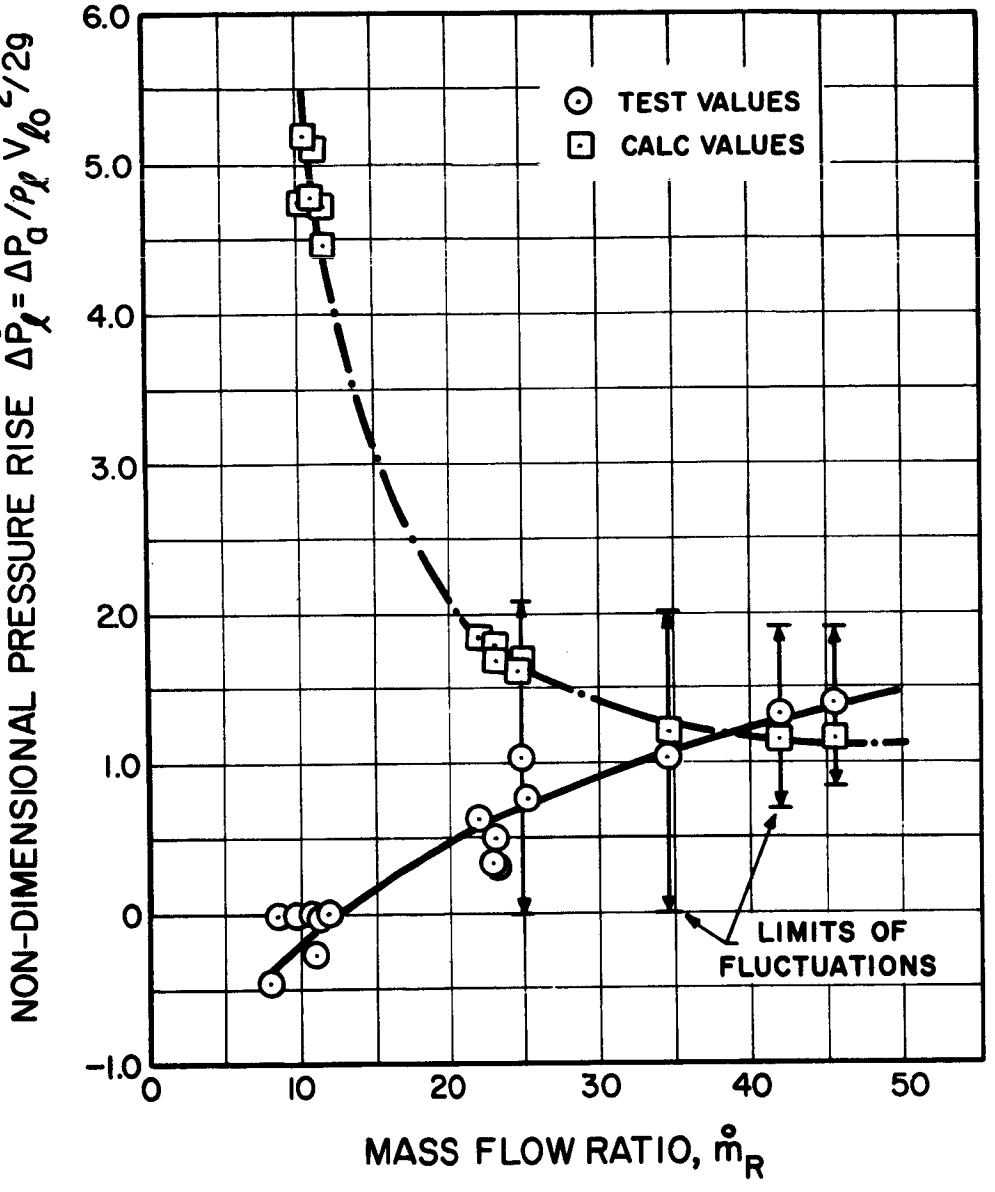

FIG. 64 NON-DIMENSIONAL PRESSURE RISE (referred to liquid) VS MASS FLOW RATIO FOR MULTI-TUBE JET CONDENSER (Density ratio = 2100-3800 test runs of 5-15-62)

As the mass flow ratio was increased, somewhat higher values of ΔP_{ℓ}^{o} were obtained. For example, a value of 0.75 occurred at $\dot{m}_{R}^{o}$ equal to 25. For this test run the interfaces were all at the diffuser exit. Further increases in mass flow ratio (> 25) resulted in flow conditions where the interfaces would remain the the throat location for longer periods (≈ 5-10 minutes). However, as shown in Fig. 64, very large fluctuations in pressure rise occurred. For these test conditions, ΔP_{ℓ}^{o} varied from 0 to 2.0 and ΔP_{a} from 0 to 7.0 psi. During these oscillations the interfaces would remain in the throat locations until the upper limit of pressure rises shown were reached. At that time one interface would collapse to the injector, the pressure rise would drop to zero, and the sequence was then repeated. The pressure rise limits, period of oscillations, and usually the interface which collapsed were repeatable.

Fluctuations in heat transfer rate and in the nature of the injected liquid probably provide the disturbances responsible for the instabilities exhibited. For example the fluctuations and loss of interface at higher mass flow ratios were induced to occur sooner when perturbations to the injected liquid flow in one tube were applied by changing the inlet valve position (cf. Fig. 29). However, when interfaces occurred in either the converging section or diffuser, perturbations and/or gross adjustments in the inlet flow in one tube had no apparent influence on overall performance. Apparently the liquid and vapor flows were redistributed among the tubes in order to accommodate the mismatch.

To summarize, the multi-tube geometry tested was operated with stable flow for pressure rises less than the injected liquid dynamic pressure. Heat transfer characteristics appeared to be similar to the large diameter jet condensers tested. However, pressure rise could not be increased above the liquid dynamic pressure without inducing serious flow oscillations and instabilities. The tests conducted represent only a cursory investigation of the problems involved in manifolding such units. Modifications such as a check valve arrangement to eliminate feedback of distrubances from one tube to another may improve performance. Operation with other area ratios or wall contours may result in different stability characteristics.

For the present, because of the limited performance characteristics obtained with the multi-tube set condenser and in view of the more favorable results obtained with the large diameter jet condensers, manifolding cannot be recommended for use in a system design. Instead, the scaling criteria developed (which was used to increase the flow area of single units by a factor of about 16) should probably be applied for preliminary design of single large jet condensers.

6. DESIGN APPLICATIONS

The results of the analysis and experimental investigations described in the preceding sections can be used for preliminary design of a jet condenser for a Rankine cycle power system. Since the heat transfer and pressure rise characteristics were established for a definite area ratio ($\mathring{A}_2 = 0.075$) and value of L_c/d_{to} (1.3), design curves and a design example will be presented for these values only. A summary of the possible effects of changes in geometry and fluid upon performance will also be given later.

6.1 Design Relations for $\mathring{A}_2 = 0.075$ and $L_c/d_{to} = 1.3$

Application of the results of Sections 3 and 5 to preliminary design is relatively straightforward if the area ratios of the test geometries are retained and the scaling criterion of Section 5 is used for larger size units. The curves presented in this section are derived from the following assumptions:

1. The heat transfer correlation of Fig. 45 ($\chi V_{\ell o}/V_R$ vs. $\mathring{\beta}$) is valid for larger geometries if the ratio of condensation length to inlet diameter is held constant, equal to 1.3.
2. The pressure rise is given by the expressions derived in Section 3 (which were confirmed by experimental data to within about $\pm$ 30 percent).
3. For vapor quality less than unity the velocity of the saturated liquid is taken to be negligible compared to the saturated vapor velocity (slip close to zero). Thus, heat transfer and pressure rise are mainly determined by the ratio of injected liquid flow rate to saturated vapor flow rate.

The above assumptions should provide conservatively low estimates of pressure rise and heat transfer characteristics of a jet condenser for larger vapor flow rates. The heat transfer scaling criterion, when applied to the 0.19 inch vapor internal diameter test units, resulted in somewhat improved heat transfer for the larger (0.75 inch vapor internal diameter) units. The trend of experimental pressure rise results appeared to be slightly higher than the predicted values.

The lower vapor quality ($\sim$ 0.81) test run produced values of pressure rise and heat transfer parameter, Ψ, which were higher than the predicted values based on only the saturated vapor flow.

With these assumptions, the results of Sections 3 and 5 were used to prepare Table V, a summary of design relations for jet condensers (with the geometric ratios of test units) operating with mercury vapor. The independent variables for these equations are the saturated vapor mass flow rate ($\dot{m}_{vo}$), inlet vapor velocity (V_{vo}), and the inlet vapor temperature, density and pressure (T_{vo}, ρ_v, P_{vo}). The geometric variables of Items 1 through 8 are determined from continuity and the geometric ratios of the large diameter test unit (Test Section No. 8). The relationship between χ, $V_{\ell o}$ and V_R (Item 9a) was determined by trial and error to provide the best correlation of test results. Item 9b is the heat balance for a jet condenser. These two equations can be solved to provide a relation between ΔT_{sc} and ΔT_R and the mass flow ratio, $\overset{o}{m}_R$. Since Items 12 and 13 show the dependency of pressure rise upon mass flow ratio, a tradeoff between pressure rise and temperature drop can therefore be obtained (cf.below). The nozzle pressure drop can be estimated by dividing the ideal pressure drop (for zero approach velocity) by the discharge coefficient squared. The value given in the table for discharge coefficient was obtained from Reference 16 as a typical value for a nozzle with rounded approach contours. This calculation assumes a nozzle contraction coefficient of unity.

The approximate relationship between radiator temperature drop, outlet subcooling and mass flow ratio can be obtained by combining the equations of Items 9a and 9b. Solving for ΔT_{sc} and ΔT_R gives:

TABLE V

SUMMARY OF DESIGN RELATIONS FOR MERCURY JET CONDENSERS USING GEOMETRIC RATIOS OF TEST UNITS

	Parameter	Design Relation	Source
1.	Tube Inlet Area	$A_{to} = \frac{\dot{m}_{vo}}{0.925\ \rho_v V_{vo}}$	Continuity
2.	Inlet Diameter	$d_{to} = (A_{to}/.785)^{1/2}$	Geometric Relation
3.	Injection Area	$A_{\ell o} = 0.075\ A_{to}$	Area Ratio for Test Geometry
4.	Injector Diameter	$d_{\ell o} = (A_{\ell o}/.785)^{1/2}$	Geometric Relation
5.	Condensation Length (Converging Chamber Length)	$L_c = 1.3\ d_{to}$	Scaling Criterion for Test Geometries
6.	Throat Diameter	$d_{tl} = d_{\ell o}/0.947$	Area Ratio for Test Geometry
7.	Throat Length	$L_{th} = 2\ d_{to}$	Scaling Criterion for Test Geometries
8.	Diffuser Angle	$\alpha_d = 10^o$	Value for Test Geometries
9.	Relation between Jet Utilization Factor, Liquid Velocity and Relative Vapor Velocity	(a) $\chi V_{\ell o}/V_R = K_1$ (b) $h_{fg}\dot{m}_{vo} + C_p \Delta T_{sc}\dot{m}_{vo} = C_p \Delta T_R \dot{m}_{\ell o}$ $K_1 = 0.075$ for $T_{vo} = 700^oF$ $K_1 = 0.043$ for $T_{vo} = 600^oF$	(a) Experimental Relation for Large Diameter Test Units, Fig. 45 (b) Heat Balance
10.	Maximum Values of Jet Utilization Factor Tested	$\chi \approx 0.95$ at $T_{vo} \approx 700^oF$ $\chi \approx 0.94$ at $T_{vo} \approx 620^oF$	Experimental Results for Large Diameter Test Unit, Appendix F

(Cont'd)

TABLE V (Cont'd)

	Parameter	Design Relation	Source
11.	Relation Between Outlet Subcooling, Radiator Temperature Drop, and Jet Utilization Factor	$\chi = \dfrac{1}{\dfrac{\Delta T_{sc}}{\Delta T_R} + 1}$	Modification of Definition of χ, Section 3
12.	Pressure Rise Coefficient Coefficients	$\Delta \overset{o}{P}_\ell = 2\overset{o}{A}_1\left[1 + \left(\dfrac{\overset{o}{\rho}}{\overset{o}{m}_R^{\,2}}\right)\dfrac{\overset{o}{A}_2}{1-\overset{o}{A}_2}\right] - \left[\overset{o}{A}_1^{\,2} + \overset{o}{A}_2^{\,2}\right]\left[\dfrac{1}{\overset{o}{m}_R} + 1\right]^2$	Results of Analysis, Section 3. Agreement with Test Results from Large Diameter Units to Within about ± 30 percent.
		$\Delta \overset{o}{P}_v = 2\dfrac{(1-\overset{o}{A}_2)}{\overset{o}{A}_{th}}\left[1 + \dfrac{\overset{o}{m}_R^{\,2}}{\overset{o}{\rho}}\dfrac{(1-\overset{o}{A}_2)}{\overset{o}{A}_2}\right] - \dfrac{(\overset{o}{m}_R + 1)^2}{\overset{o}{\rho}}(1-\overset{o}{A}_2)\left[\dfrac{1}{\overset{o}{A}_{th}^{\,2}} + 1\right]$	
13.	Jet Condenser Power	$H_j' = \dfrac{1}{\overset{o}{\rho}}\dfrac{V_{vc}^{\,2}\,\dot{m}_{vo}}{1470g} H_j'$	Modification of Analysis for Pressure Rise, Section 3
		$H_j' = \left(1 - \dfrac{1}{\overset{o}{\Delta P}_\ell}\right)(\Delta \overset{o}{P}_v \overset{o}{m}_R)$	
14.	Nozzle Pressure Drop	$\Delta P_i \approx \dfrac{\rho_\ell V_{\ell o}^{\,2}}{2gC_d^{\,2}}$	Ref. 16, Pgs. 122-125

where $C_d \approx 0.98$

Units and Comments

$\dot{m}_{vo}$ - lb/sec, This parameter is the saturated vapor flow which is equal to the inlet quality multiplied by the total inlet vapor flow

$\dot{m}_{\ell o}$ - lb/sec

(Cont'd)

TABLE V (Cont'd)

ρ_v, ρ_ℓ - lb/ft^3

V_{vo}, $V_{\ell o}$, V_R - ft/sec

A_{to}, $A_{\ell o}$ - ft^2

d_{to}, $d_{\ell o}$, L_c, d_{t1}, L_{th} - ft

ΔP_i - lb/ft^2

g - 32.2 (lbm/lbf)(ft/sec^2)

H_j - kw

T_{vo}, ΔT_{sc}, ΔT_R - ^oF

h_{fg} - BTU/lb

C_p - BTU/lb ^oF

χ, K_1, $\Delta\overset{o}{P}_\ell$ $\Delta\overset{o}{P}_v$, $\overset{o}{A}_1$, $\overset{o}{A}_2$, $\overset{o}{\beta}$, $\overset{o}{m}_R$, $\overset{o}{A}_{th}$, H_j', C_d - non-dimensional parameters

$$\Delta T_{sc} = \left(h_{fg}/C_p\right)\left[\frac{\frac{1}{K_1} - \frac{K_2}{\overset{o}{m}_R} + 1}{K_2 - \overset{o}{m}_R - \frac{1}{K_1} + \frac{K_2}{\overset{o}{m}_R} - 1}\right] \tag{39}$$

and

$$\Delta T_R = \left(h_{fg}/C_p\, \overset{o}{m}_R\right)\left[1 + \frac{\frac{1}{K_1} - \frac{K_2}{\overset{o}{m}_R} + 1}{K_2 - \overset{o}{m}_R - \frac{1}{K_1} + \frac{K_2}{\overset{o}{m}_R} - 1}\right] \tag{40}$$

Where K_1 = value of $\chi V_{\ell o}\, V_R$ at a particular $\overset{o}{\rho}$ from Fig. 45 (41)

$$K_2 = \overset{o}{\rho}\,\overset{o}{A}_2/(1 - \overset{o}{A}_2) = 0.081\,\overset{o}{\rho} \tag{42}$$

These relations are shown in Figs. 65 and 66 for vapor temperatures of 600°F and 700°F. ($\overset{o}{\rho} \approx 6500$ and $\overset{o}{\rho} \approx 2620$). Since the curves for ΔT_{sc} are mainly dependent on Fig. 45 for their derivation, a range of about ± 20 percent in the value of ΔT_{sc} may be encountered at one mass flow ratio. At any mass flow ratio the values of ΔT_R and ΔT_{sc} required for operation of the jet condenser with the interface at the throat location can be obtained from these curves. The lowest values of ΔT_{sc} obtained during testing are indicated by the dashed portion of the curves. For example, for $T_{vo} \approx 600°$ the smallest value of ΔT_{sc} obtained during testing with the interface at the throat location was about 11°F. For T_{vo} = 700°F the lowest subcooling obtained was 13°F. As larger mass flow ratios are used, the value of ΔT_{sc} will increase while the radiator temperature drop, ΔT_R, is lowered. From Fig. 65 changing the mass flow ratio from 25 to 50 changes ΔT_{sc} from 30°F to 115°F while ΔT_R drops from 160°F to 80°F. The sum of these two temperature drops is shown in both figures for reference and is the total drop in temperature from the temperature of the inlet vapor to the injected liquid temperature.

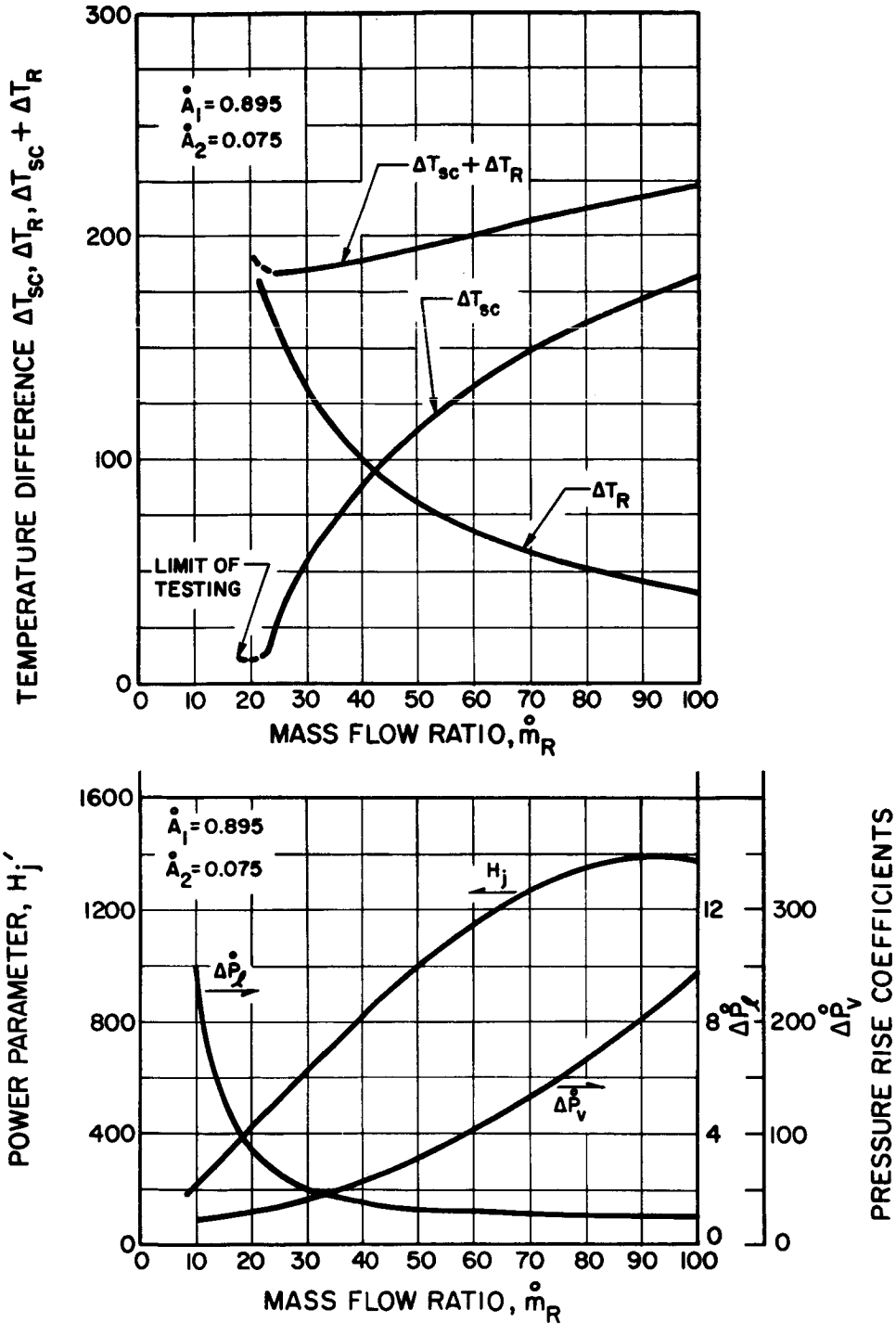

FIG. 65 PRESSURE RISE, RADIATOR TEMPERATURE DROP AND OUTLET SUBCOOLING VS MASS FLOW RATIO FOR JET CONDENSER OPERATING WITH MERCURY VAPOR AT 600°F, $\dot{A}_1$ = 0.895, $\dot{A}_2$ = 0.075

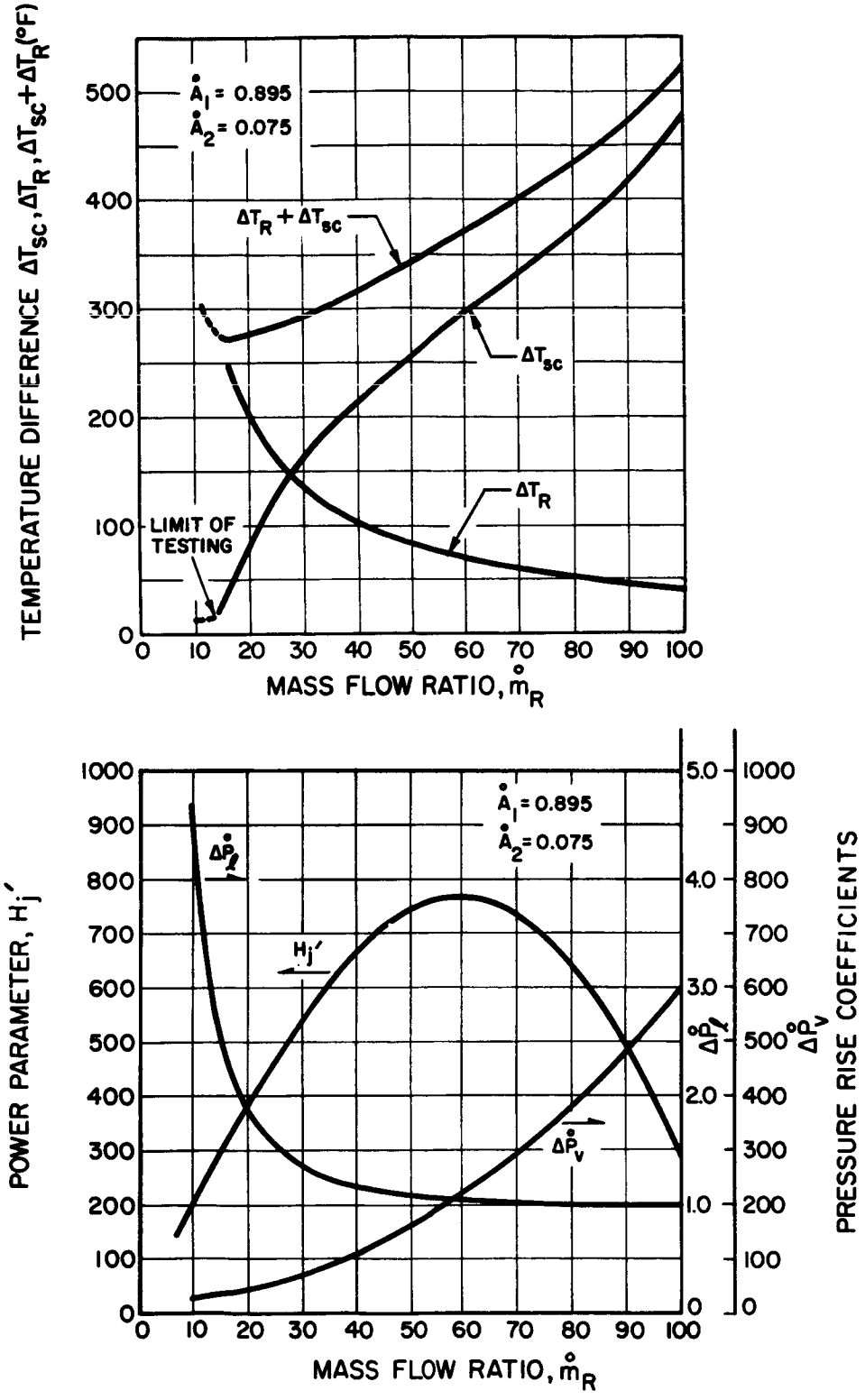

FIG. 66 PRESSURE RISE RADIATOR TEMPERATURE DROP AND OUTLET SUBCOOLING VS MASS FLOW RATIO FOR JET CONDENSER OPERATING WITH MERCURY VAPOR AT 700°F $\dot{A}_1$= 0.895 $\dot{A}_2$= 0.075

The decrease of the total temperature drop at lower mass flow ratios would indicate choice of these operating conditions to obtain the highest average radiator temperature ($T_{vo} - \Delta T_{sc} - \Delta T_R/2$). However, a tradeoff with pressure rise and jet condenser power output exists which must be considered before choice of the design mass flow ratio can be made.

In order to provide this information, the two pressure rise coefficients, $\Delta\overset{o}{P}_{\ell}$ and $\Delta\overset{o}{P}_{v}$, and the jet condenser power parameter, H_j', were calculated and are plotted versus mass flow ratio on the same figures. The useful power output exhibits maxima at $\overset{o}{m}_R = 60$ for $T_{vo} = 700^{\circ}F$ and at $\overset{o}{m}_R = 93$ for $T_{vo} = 600^{\circ}F$. However, these values of mass flow ratio result in excessively high values of outlet subcooling for the geometry considered. A decrease in power output is therefore required to be able to use lower values of total temperature drop. For example, from Fig. 65 changing mass flow ratio from 90 to 30 results in a change of the power parameter from about 1400 to 620 and the total temperature drop decreases from $217^{\circ}F$ to $185^{\circ}F$. The corresponding changes in ΔT_{sc}, ΔT_R, $\Delta\overset{o}{P}_{\ell}$ and $\Delta\overset{o}{P}_{v}$ are $172^{\circ}F$ to $55^{\circ}F$, $45^{\circ}F$ to $132^{\circ}F$, 1.0 to 2.0, and 205 to 40. These curves, therefore, relate jet condenser heat transfer and pressure rise performance characteristics to system parameters such that weight tradeoffs can be established when sufficient information on the liquid heat rejection loop and radiator characteristics are available.

6.2 Design Example

In order to illustrate the use of the above relations an example will be given in this section. Consider the following variables to be fixed for the design:

$T_{vo} = 600^{\circ}F$ ($\rho_v = 0.125$ lb/ft^3, $P_{vo} \approx 7$ psia)

$\dot{m}_{vo}/x_{vo} = 7200$ lb/hr (total vapor flow rate)

$x_{vo} = 0.95$

$V_{vo} = 200$ fps

Items 1 through 8 of Table V can be used to determine the geometry:

1. $A_{to} = \frac{(7200)\ (.95)}{(.925)(.125)(200)(3600)} = 0.0821\ ft^2$

2. $d_{to} = (.0821/.785)^{1/2} = 0.322\ ft$

3. $A_{\ell o} = (0.075)(0.0821) = 0.00615\ ft^2$

4. $d_{\ell o} = (.00615/.785)^{1/2} = .0885\ ft$

5. $L_c = (1.3)(.322) = 0.418\ ft$

6. $d_{t1} = 0.0885/.947 = 0.0935\ ft$

7. $L_{th} = (2)(.322) = 0.644\ ft$

8. $\alpha_d = 10^o$

If the design temperature were chosen to be other than 600^oF or 700^oF then Items 9 through 13 of Table V would be used to find the mass flow ratio, $\overset{o}{m}_R$, which gave the best combination of ΔT_{sc}, ΔT_R and pressure rise for the rest of the system. However, for this case, Fig. 65, which was computed for $T_{vo} = 600^oF$ can be used. Since information on the other components of this type of heat rejection system is not available for this example, a typical value of $\overset{o}{m}_R$ will be selected to indicate the values of other parameters resulting from this choice. If $\overset{o}{m}_R = 30$ is chosen, then from Fig. 65:

$\Delta T_{sc} = 55^oF$

$\Delta T_R = 132^oF$

$\Delta \overset{o}{P}_\ell = 2.0$

$\Delta \overset{o}{P}_v = 44$

$H_j' = 630$

In order to determine the absolute magnitude of pressure rise and pumping power, it is necessary to determine the dynamic pressure terms.

$$\dot{m}_{\ell o} = \overset{o}{m}_R \dot{m}_{vo} = (30)(.95)(7200) = 2.05 \times 10^5 \text{ lb/hr} \quad (43)$$

$$V_{\ell o} = \dot{m}_{\ell o}/\rho_\ell A_{\ell o} \approx (2.05 \times 10^5)/(800)(.00615)(3600) = 11.6 \text{ fps} \quad (44)$$

$$\rho_\ell V_{\ell o}^2/2g = (800)(11.6)^2/64.4 = 1670 \text{ psf} = 11.6 \text{ psi}$$

$$\rho_v V_{vo}^2/2g = (.125)(200)^2/64.4 = 77.6 \text{ psf} = .540 \text{ psi}$$

The total pressure rise is then:

$$\Delta P_a = (2.0)(11.6) = 23.2 \text{ psi}$$

The ideal pumping power available for circulation of the outlet liquid through the liquid radiator loop is

$$H_j = H_j' \frac{1}{\overset{o}{\rho}} \frac{V_{vo}^2 \dot{m}_{vo}}{1470g} = \frac{(630)}{(6500)} \frac{(200)^2 (2)(.95)}{(1470)(g)} = .156 \text{ kw} \quad (45)$$

Due to a discharge coefficient less than unity the power available for circulation of liquid external to the jet condenser would be somewhat reduced. For $C_d = 0.98$ and $\Delta\overset{o}{P}_\ell = 2$ the power output would become

$2 - (1/.98)^2 \quad .156 = .15$ kw.

The above jet condenser flow conditions are shown schematically below

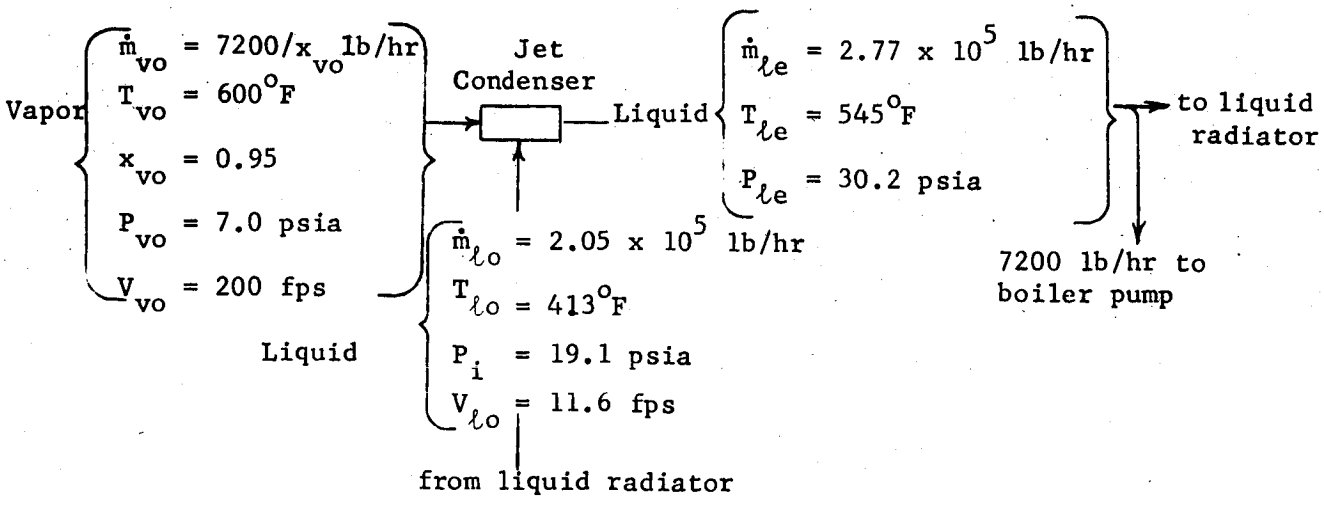

The above example demonstrates typical performance for a jet condenser system which appears attainable without changing any geometric ratios. As indicated in Sections 3 and 5, increases in pressure rise and power output may be obtained by use of a smaller ratio of injector area to tube area and/or by operating at higher mass flow ratios. The value of ΔT_{sc} can be lowered by use of a longer condensation distance ($\bar{L}_c/d_{to} > 1.3$) and/or by operating at a lower mass flow ratio. For example, as indicated in Fig. 65, values of ΔT_{sc} as low as $11^{\circ}F$ were obtained at the lower mass flow ratios. The maximum performance potential of jet condensers can be estimated using the analytical results of Section 3 but until confirmed for other geometries, they should not be used as the basis of system design.

7. CONCLUDING REMARKS

The present investigation has provided performance characteristics of jet condensers using a liquid metal working fluid (mercury). Design relations have been prepared for a specific geometry for preliminary design of jet condensers for space power systems operating on the Rankine cycle with mercury as the working fluid.

The most significant result of this program was demonstration of the high values of pressure rise possible in convergent-divergent jet condensers. Absolute values of pressure rise as high as 62 psid were obtained. Values of the ratio of pressure rise to the dynamic pressure of injected liquid ranged up to 12.2. The latter result was obtained through the conversion of vapor thermal energy to mechanical energy in the outlet liquid. Thus, the jet condensers tested performed both as condensers and as vapor driven circulation pumps. The experimental values of pressure rise for larger geometries agree to within about + 30 percent and - 25 percent with values predicted by the analysis. The recommended equation for predicted pressure rise is:

$$\Delta \overset{o}{P}_{\ell} = 2\overset{o}{A}_1 \left[1 + \left(\frac{\overset{o}{\rho}}{\overset{o}{m}_R^{\,2}} \right) \frac{\overset{o}{A}_2}{1-\overset{o}{A}_2} \right] - \left[\overset{o}{A}_1^{\,2} + \overset{o}{A}_2^{\,2} \right] \left[1 + \frac{1}{\overset{o}{m}_R} \right]^2 \qquad (46)$$

(The various non-dimensional coefficients and ratios are defined in the Nomenclature Table at the front of the report and are discussed in Section 3.)

Scaling relations were applied to test results obtained for small diameter units (0.19 inches i.d.) to design larger (0.75 inches i.d.) jet condenser geometries. These larger units performed with all-liquid flow at the outlet and fluctuations of pressures, flows and temperatures

which were less than 1 - 2 percent of the average values. Simple startup techniques were possible and no gravity effects on the final interface were observed. Values of the heat transfer parameter, Y, ranged from 0 to 40 percent (depending on vapor temperature) greater than values obtained for the smaller units. Thus, for the same values of $V_{\ell o}$ and V_R, higher values of χ were obtained for the large diameter jet condensers than for the smaller geometries.

Results of cursory tests conducted on a multi-tube jet condenser indicate performance to be degraded from single units. Both stability and pressure rise were affected by the particular manifolding used in the one unit tested in this program. Further study of multi-tube units is needed.

Performance of jet condensers with other geometric variables and other liquid metals can be estimated using the results of the pressure rise and heat transfer analyses reported in Section 3. However, experimental verification should be obtained before these estimates are used as the basis for preliminary design.

In order to provide more general results for design of mercury systems, several parameters should be varied in a manner not possible during the present program. Changes in injector-tube area ratio, convergence angle (ratio of L_c/d_{to}), and injector-throat area ratio should be studied further. Operation with near sonic inlet vapor velocities and more extensive tests with vapor qualities less than unity should be conducted. In addition to steady-state performance testing, the interactions of jet condensers with other components of a Rankine cycle system should be studied. Performance should be determined during startup at very low vapor flow rates and subsequently, during transition to design operating conditions. Internal measurements of pressure distribution in the mixing chamber should enable a more accurate pressure rise prediction method to be formulated.

Results from investigations using mercury as a working fluid may be somewhat applicable to other liquid metals such as potassium or rubidium. For example, the pressure rise characteristics predicted by Equation 46

should be valid for any fluid since the density ratio is the only fluid property appearing. A similar expression offered satisfactory agreement with constant area test results obtained both with mercury and with water (Ref. 4). Surface tension forces in jet condensers are very small (< 1 percent) compared with the large liquid and vapor inertial forces occurring. Therefore, whether the fluid is non-wetting or wetting should not have an important influence upon stability and/or pressure rise. However, in view of the potential application of jet condensers to alkali metal power systems, the performance characteristics with these fluids should be determined experimentally.

REFERENCES

1. J. Payne, "SNAP-8 Radiator Topical Report" Aerojet General Nucleonics Report No. AN-551 (June 1962)

2. "Sunflower Power Conversion System Quarterly Report", Tapco Report No. ER-4608 (June - August 1961)

3. R. Denington, et al., "Space Radiator Study", Tapco Report No. ER-4544, ASD Technical Report No. 61-697, (April 1962)

4. L. Hays, "Condenser Space Heat Rejection Systems", Electro-Optical Systems, Report No. 500-F. Prepared for Army Ballistic Missile Agency under Contract DA-04-495-506-ORD-2007, (December 1960)

5. J. Perry "Chemical Engineer's Handbook", McGraw-Hill, 1950

6. Penberthy Manufacturing Company, Prophetstown, Illinois, Commercial Literature

7. Schutte and Koerting Co., Cornwells Heights, Pa., Commercial Literature.

8. J. Kaye, et al., "Condensuctor for Deep Running Torpedoes" Joseph Kaye and Co. Report No. N-2, Contract N298-(122)11039, (October 1956)

9. J. Levy, "The Mixing of Vapor and Liquid Jets" Aerojet-General Corp. Report No. 1344(Final), Contract Nonr 869(00) Task NR 062-157, (October 1957)

10. V. Konovalov, "To the Problem on Heat Transfer from Condensing Steam to a Turbulent Water Jet", Izvestia Vyshikh Uchebnych Zavedeniy, (1958) (Electro-Optical Systems Internal Translation No. 2).

11. L. Hays, J. Collins, J. Neustein, "Investigation of Spray-Type Condensers with Mercury and Water", Proceedings of the 1961 Heat Transfer and Fluid Mechanics Institute (1961)

12. H. Brown, et al., "Temperature and Velocity Distribution and Transfer of Heat in a Liquid Metal," Trans. Amer. Society, Mechanical Engineers (1957)

13. W. Ranz, "On Sprays and Spraying", Engineering Research Bulletin B-65 of Pennsylvania State Univ. (March 1956)

14. A. Fuhs, "Spray Formation and Breakup, and Spray Combustion" Sunstrand Turbo Report-AMF/TD No. 1199, (February 1958)

(Cont'd)

15. L. Hays, "Investigation of Condensers Applicable to Space Power Systems, Part I - Direct Condensers", Electro-Optical Systems Report No. 1588-Final, prepared for the National Aeronautics and Space Administration under Contract NAS 7-11, (September 1962)

16. R. Daugherty and A. Ingersoll, "Fluid Mechanics" McGraw-Hill (1954)

APPENDIX A

CONSTANT AREA JET CONDENSER PRESSURE RISE

APPENDIX A

CONSTANT AREA JET CONDENSER PRESSURE RISE

The model used for constant area calculations is shown below.

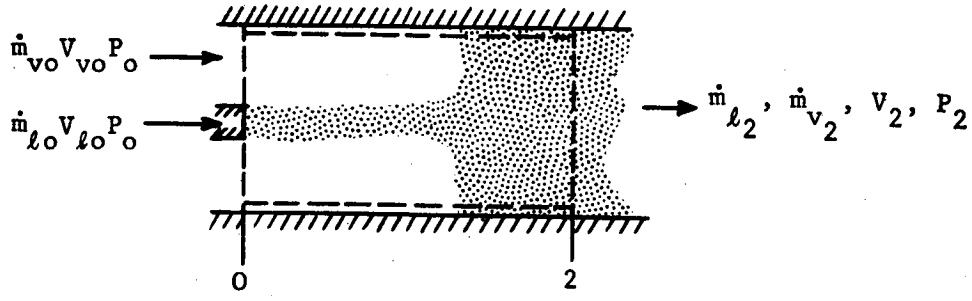

Vapor and liquid are injected at Station 0. Condensation of the vapor takes place as the flow proceeds downstream. The injected liquid serves as a heat and mass sink for the condensing vapor. At some point within the control volume (denoted by the dashed boundary), a vapor-liquid interface occurs. The exit point, designated by the subscript 2, is defined as the downstream station where the flow is homogenous (but not necessarily all liquid) and in thermal equilibrium. The radial pressure profile at the end points is taken to be constant and wall friction is neglected. Furthermore, the assumption is made that the saturated liquid (quality less than 1) associated with the entering vapor is traveling at the same velocity as the vapor (no "slip"). Using these assumptions, the equation of conservation of momentum for the control volume becomes:

$$\frac{\dot{m}_{\ell o} V_{\ell o}}{g} + \frac{\dot{m}_{vo} V_{vo}}{g} + \frac{\dot{m}_f V_{vo}}{g} + P_o A_t = \frac{\dot{m}_{\ell 2} V_2}{g} + \frac{\dot{m}_{v2} V_2}{g} + P_2 A_t \quad (1)$$

The quality at station 0 is given by:

$$X_{vo} = \frac{\dot{m}_{vo}}{\dot{m}_{vo} + \dot{m}_f} \quad (2)$$

for complete condensation $\dot{m}_{v2} = 0$. Substituting (2) in (1) gives

$$\frac{\dot{m}_{\ell o} V_{\ell o}}{g} + \frac{\dot{m}_{vo} V_{vo}}{g X_{vo}} + P_o A_t = \frac{\dot{m}_{\ell 2} V_{\ell 2}}{g} + P_2 A_t \quad (3)$$

However,

$$V_{\ell o} = \frac{\dot{m}_{\ell o}}{\rho_\ell A_{\ell o}} \quad (4)$$

$$V_{vo} \approx \frac{\dot{m}_{vo}}{\rho_v A_{vo}} \quad (5)$$

$$V_{\ell 2} = \frac{\dot{m}_{\ell 2}}{\rho_\ell A_t} \quad (6)$$

$$\dot{m}_{\ell 2} = \dot{m}_{\ell o} + \dot{m}_{vo} X_{vo} \quad (7)$$

Substituting (4), (5), (6), and (7) into (3) gives

$$\frac{\dot{m}_{\ell o}^2}{g\rho_\ell A_{\ell o}} + \frac{\dot{m}_{vo}^2}{g\rho_v A_{vo} X_{vo}} + P_o A_t = \frac{(\dot{m}_{\ell o} + \dot{m}_{vo} X_{vo})^2}{g\rho_\ell A_t} + P_2 A_t \quad (8)$$

or $$P_2 - P_o = \frac{\dot{m}_{\ell o}^2}{g\rho_\ell A_{\ell o} A_t} + \frac{\dot{m}_{vo}^2}{g\rho_v A_{vo} A_t X_{vo}} - \frac{(\dot{m}_{\ell o} + \dot{m}_{vo} X_{vo})^2}{g\rho_\ell A_t^2} \quad (9)$$

if the inlet quality is unity then eq. 9 becomes,

$$P_2 - P_o = \frac{\dot{m}_{\ell o}^2}{g\rho_\ell A_{\ell o} A_t} + \frac{\dot{m}_{vo}^2}{g\rho_v A_{vo} A_t} - \frac{(\dot{m}_{\ell o} + \dot{m}_{vo})^2}{g\rho_\ell A_t^2} \tag{10}$$

Dividing by $\rho_\ell V_{\ell o}^2/2g$ gives:

$$\frac{\Delta P_a}{\rho_\ell V_{\ell o}^2/2g} \equiv \Delta \overset{o}{P}_\ell = 2\frac{A_{\ell o}}{A_t} + \frac{\overset{o}{\rho}}{\overset{o}{m}_R^2}\frac{2A_{\ell o}^2}{A_{vo}A_t} - (1 + 1/\overset{o}{m}_R)^2 2\frac{A_{\ell o}^2}{A_t^2} \tag{11}$$

If the following definition is made

$$\frac{A_{\ell o}}{A_t} \equiv \overset{o}{A}_2 \tag{12}$$

then:

$$\Delta \overset{o}{P}_\ell = 2\left[\overset{o}{A}_2 + \frac{\overset{o}{\rho}}{\overset{o}{m}_R^2}\frac{\overset{o}{A}_2^2}{1-\overset{o}{A}_2}\right] - 2\overset{o}{A}_2^2(1 + 1/\overset{o}{m}_R)^2 \tag{13}$$

If the pressure rise referred to the inlet vapor dynamic pressure is desired then,

$$\Delta \overset{o}{P}_v = \frac{\rho_\ell V_{\ell o}^2/2g}{\rho_v V_{vo}^2/2g}\Delta \overset{o}{P}_\ell = \frac{\overset{o}{m}_R^2}{\overset{o}{\rho}}\frac{(1-\overset{o}{A}_2)^2}{\overset{o}{A}_2^2}\Delta \overset{o}{P}_\ell \tag{14}$$

or substituting (14) in (13) gives

$$\Delta \overset{o}{P}_v = 2\left[\frac{\overset{o}{m}_R^2}{\overset{o}{\rho}}\frac{(1-\overset{o}{A}_2)^2}{\overset{o}{A}_2} + (1-\overset{o}{A}_2)\right] - \frac{2(1-\overset{o}{A}_2)^2}{\overset{o}{\rho}}(\overset{o}{m}_R + 1)^2 \tag{15}$$

APPENDIX B

CONVERGING-DIVERGING JET CONDENSER THEORETICAL PRESSURE RISE

APPENDIX B

CONVERGING-DIVERGING JET CONDENSER
THEORETICAL PRESSURE RISE

The general equation for the theoretical pressure rise from vapor to outlet condensate in a converging-diverging jet condenser can be obtained by application of the conservation equations. Lack of information on the detailed nature of the internal flow, however, prevents a definite result for pressure rise in terms of inlet flow parameters and condenser geometry. Numerical results will therefore be presented for certain limiting cases which may be likely to occur in a convergent-divergent jet condenser.

General Equation

Consider the geometry of Fig. B-1. Subcooled liquid enters the condenser from the left in the form of a central jet. Vapor flows from left to right in an annulus about the liquid jet. At station (1) the vapor flow is entirely condensed and an interface is formed. The resulting flow, which is entirely liquid, is diffused from the area at (1) to the original tube area, which occurs at station (2). For deriving the general equation the following assumptions will be made:

1. Liquid pressure equals vapor pressure at station 0
2. No heat loss from the condenser wall
3. Entering vapor quality equals unity
4. Homogeneous flow within each phase exists at all stations. (No mixing losses.)
5. The radial pressure gradient at the inlet and outlet are zero.

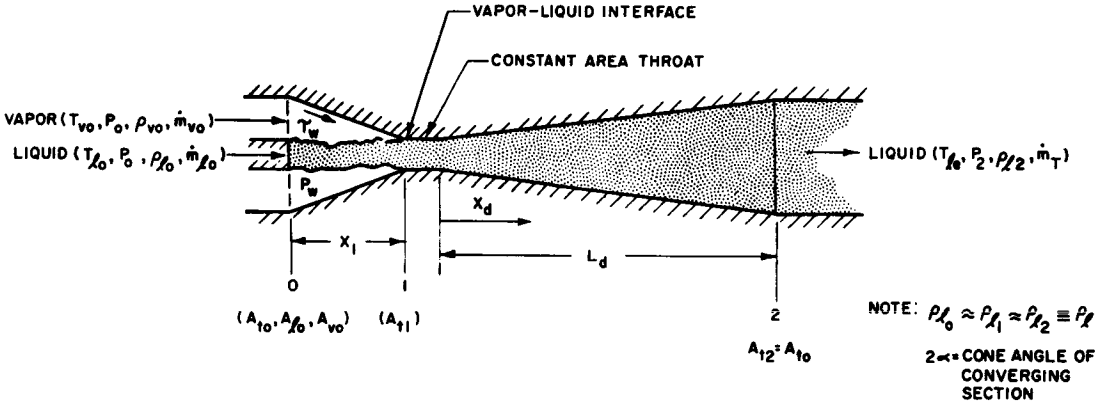

FIG. B-1 JET CONDENSER NOMENCLATURE AND MODEL OF ANALYSIS OF PRESSURE RISE

With these assumptions conservation of momentum from 0 to 1 yields the following expression:

$$\frac{\dot{m}_{vo}V_{vo}}{g} + P_o A_{vo} + \frac{\dot{m}_{\ell o}V_{\ell o}}{g} + P_o A_{\ell o} = \tau_w A_w \cos\alpha + \int_0^{X_1} P_w \pi d_t \tan\alpha \, dx$$

$$+ P_1 A_{t1} + \frac{\dot{m}_T V_{\ell 1}}{g} \qquad (1)$$

Conservation of energy from 1 to 2 gives

$$P_1 + \rho_\ell V_{\ell 1}^2/2g = P_2 + \rho_\ell V_{\ell 2}^2/2g + K_d \rho_\ell V_{\ell 1}^2/2g \qquad (2)$$

Solving for P_1 from (1) gives:

$$P_1 = P_o A_{to}/A_{t1} + \dot{m}_{vo}V_{vo}/gA_{t1} + \dot{m}_{\ell o}V_{\ell o}/gA_{t1} - \dot{m}_T V_{\ell 1}/gA_{t1}$$

$$- \tau_w A_w \cos\alpha/A_{t1} - \int_0^{X_1} P_w \pi d_t \tan\alpha \, dx/A_{t1} \qquad (3)$$

Substituting for P_1 in equation (2) and solving for P_2 gives:

$$P_2 = P_o A_{to}/A_{t1} + (1/gA_{t1})\,(\dot{m}_{vo}V_{vo} + \dot{m}_{\ell o}V_{\ell o} - \dot{m}_T V_{\ell 1})$$

$$- \rho_\ell V_{\ell 1}^2/2g + \rho_\ell V_{\ell 1}^2/2g\,(1-K_d) - \tau_w A_w \cos\alpha/A_{t1}$$

$$- \int_0^{X_1} P_w \pi d_t \tan\alpha \, dx/A_{t1} \qquad (4)$$

However, from continuity:

$$V_{vo} = \dot{m}_{vo}/\rho_v A_{vo} \qquad (5)$$

$$V_{\ell o} = \dot{m}_{\ell o}/\rho_{\ell} A_{\ell o} \tag{6}$$

$$V_{\ell 1} = \dot{m}_T/\rho_{\ell} A_{t1} \tag{7}$$

$$V_{\ell 2} = \dot{m}_T/\rho_{\ell} A_{t2} \tag{8}$$

Substitution into (4) yields the following expression:

$$P_2 - P_o \equiv \Delta P_a = P_o\,(A_{to}/A_{t1} - 1) + (1/gA_{t1})(\dot{m}_{vo}^2/\rho_v A_{vo} + \dot{m}_{\ell o}^2/\rho_{\ell} A_{\ell o} - \dot{m}_T^2/\rho_{\ell} A_{t1})$$
$$+ (1-K_d)\,\dot{m}_T^2/2g\rho_{\ell} A_{t1}^2 - \dot{m}_T^2/2g\rho_{\ell} A_{t2}^2 - \tau_w A_w \cos\alpha/A_{t1} - \int_0^{X_1} P_w \pi d_t \tan\alpha\, dx/A_{t1} \tag{9}$$

Relating tube area and injector area to vapor and liquid gives:

$$\Delta P_a = P_o(A_{to}/A_{t1} - 1) + (1/gA_{t1})\left\{\left[\dot{m}_{vo}^2/\rho_v(A_{to} - A_{\ell o})\right] + \left[\dot{m}_{\ell o}^2/\rho_{\ell} A_{\ell o}\right] - \left[\dot{m}_T^2/\rho_{\ell} A_{t1}\right]\right\}$$
$$+ (\dot{m}_T^2/2g\rho_{\ell})\left\{\left[(1-K_d)/A_{t1}^2\right] - \left[1/A_{to}^2\right]\right\} - \tau_w A_w \cos\alpha/A_{t1} - \int_0^{X_1} P_w \pi d_t \tan\alpha\, dx/A_{t1} \tag{10}$$

Equation 10 expresses the total pressure rise in terms of (1) geometry and inlet flow parameters and (2) two unknown terms which contain properties of the boundary flow; i.e., the shear stress of the vapor on the wall and the internal vapor pressure distribution at the wall. In order to obtain numerical results assumptions must be made of the value of these quantities. In all cases it is felt that the friction term is small relative to the total pressure rise. (The extremely short condensation distances, relative to direct condensers, and high values of ΔP_a measured during testing support this simplification.) Other assumptions related to the wall pressure integral will now be treated.

Constant Chamber Wall Pressure = Vapor Inlet Pressure

Perhaps the simplest model which can be formulated is constant vapor pressure in the condensing chamber. This model of flow would be approached if the rate of vapor mass condensed on the jet is such that

in the axial direction:

$$1/\dot{m}_c \; \partial\dot{m}_c/\partial x = 1/A_t \; \partial A_t/\partial x \tag{11}$$

However, even if this relation were not satisfied, the relation between the rate of condensation and chamber contour may be such that the flow process occurs with nearly constant vapor pressure.

Substitution of $P_w = P_o$ into the pressure integral term of equation (3) and neglecting vapor friction ($\tau_w = 0$) and diffuser losses ($K_d = 0$) gives

$$P_1 = P_o A_{to}/A_{t1} + \left[1/gA_{t1}\right]\left\{\left[\dot{m}_{vo}^2/\rho_v(A_{to}-A_{\ell o})\right] + \left[\dot{m}_{\ell o}^2/\rho_\ell A_{t1}\right]\right\} - P_o(A_{to}-A_{t1})/A_{t1} \tag{12}$$

$$\text{or} \quad \Delta P_{th} = P_1 - P_o = (1/gA_{t1})\left\{\left[\dot{m}_{vo}^2/\rho_v(A_{to}-A_{\ell o})\right] + \left[\dot{m}_{\ell o}^2/\rho_\ell A_{\ell o}\right] - \left[\dot{m}_t^2/\rho_\ell A_{t1}\right]\right\} \tag{13}$$

This expression relates the pressure rise from the vapor inlet to the throat in terms of inlet flow parameters and geometry. Equation (13) may be made non-dimensional by dividing either by the injected liquid dynamic pressure or the inlet vapor dynamic pressure:

$$\overset{\circ}{P}_{th_\ell} \equiv \left[P_1 - P_o\right]/\rho_\ell V_{\ell o}^2/2g = (\Delta P_{th})(2g\rho_\ell A_{\ell o}^2/\dot{m}_{\ell o}^2)$$

$$= 2\left[A_{\ell o}/A_{t1}\right]\left\{(\rho_\ell/\rho_v)(\dot{m}_{vo}^2/\dot{m}_{\ell o}^2)\left[A_{\ell o}/(A_{to}-A_{\ell o})\right] + 1 - (\dot{m}_T^2/\dot{m}_\ell^2)(A_{\ell o}/A_{t1})\right\} \tag{14}$$

for convenience let the following definitions hold

$$A_{\ell o}/A_{t1} = \overset{\circ}{A}_1$$

$$A_{\ell o}/A_{to} \equiv \overset{\circ}{A}_2$$

$$A_{t1}/A_{to} \equiv \overset{\circ}{A}_2/\overset{\circ}{A}_1 = \overset{\circ}{A}_{th}$$

$$\dot{m}_{\ell o}/\dot{m}_{vo} \equiv \overset{\circ}{m}_R$$

$$\rho_\ell/\rho_v \equiv \overset{\circ}{\rho}$$

Equation (14) then becomes

$$\Delta \overset{o}{P}_{th\ell} = 2\overset{o}{A}_1 \left[1 + \frac{\overset{o}{\rho}}{\overset{o}{m}_R{}^2} \frac{\overset{o}{A}_2}{1-\overset{o}{A}_2} - (1 + 1/\overset{o}{m}_R)^2 \overset{o}{A}_1 \right] \tag{15}$$

Similarly:

$$\Delta \overset{o}{P}_{thv} = \frac{P_1 - P_o}{\rho_v V_{vo}{}^2/2g} = 2 \frac{\overset{o}{A}_1}{\overset{o}{A}_2} (1-\overset{o}{A}_2) \left[\frac{\overset{o}{m}_R{}^2}{\overset{o}{\rho}} \frac{1-\overset{o}{A}_2}{\overset{o}{A}_2} + 1 - (\overset{o}{A}_1/\overset{o}{A}_2)(1-\overset{o}{A}_2)(1/\overset{o}{\rho})(\overset{o}{m}_R+1)^2 \right]$$

$$= 2 \frac{(1-A_2)}{\overset{o}{A}_{th}} \left[1 + \frac{\overset{o}{m}_R{}^2}{\overset{o}{\rho}} \frac{(1-\overset{o}{A}_2)}{\overset{o}{A}_2} - \frac{(\overset{o}{m}_R + 1)^2}{\overset{o}{\rho}} \frac{(1 - \overset{o}{A}_2)}{\overset{o}{A}_{th}} \right] \tag{16}$$

and the relation between $\Delta \overset{o}{P}_{th\ell}$ and $\Delta \overset{o}{P}_{thv}$ is:

$$\Delta \overset{o}{P}_{thv} = \frac{\overset{o}{m}_R{}^2}{\overset{o}{\rho}} \frac{(1 - \overset{o}{A}_2)^2}{(\overset{o}{A}_2)^2} \Delta \overset{o}{P}_{th\ell} \tag{17}$$

The additional pressure gain experienced through the diffuser is obtained from equation (10) in a similar fashion:

$$\overset{\circ}{\Delta P}_\ell \equiv \Delta P_a/\rho_\ell V_{\ell o}{}^2/2g = 2\overset{o}{A}_1 \left[1 + \frac{\overset{o}{\rho}}{\overset{o}{m}_R{}^2} \frac{\overset{o}{A}_2}{1-\overset{o}{A}_2} - (1 + 1/\overset{o}{m}_R)^2 \overset{o}{A}_1 \right]$$

$$+ A_{\ell o}{}^2 \frac{\overset{o}{m}_T{}^2}{\overset{o}{m}_{\ell o}{}^2} \left(\frac{1}{A_{t1}{}^2} - \frac{1}{A_{to}{}^2} \right)$$

or

$$\overset{\circ}{\Delta P}_\ell = 2\overset{o}{A}_1 \left[1 + \frac{\overset{o}{\rho}}{\overset{o}{m}_R{}^2} \frac{\overset{o}{A}_2}{(1-\overset{o}{A}_2)} \right] - (1 + 1/\overset{o}{m}_R)^2 \left[\overset{o}{A}_1{}^2 + \overset{o}{A}_2{}^2 \right] \tag{18}$$

and

$$\overset{\circ}{\Delta P}_v \equiv \Delta P_a/\rho_v V_{vo}{}^2/2g = 2 \frac{(1-\overset{o}{A}_2)}{\overset{o}{A}_{th}} \left[1 + \frac{\overset{o}{m}_R{}^2(1-\overset{o}{A}_2)}{\overset{o}{\rho}\overset{o}{A}_2} \right] - \frac{(\overset{o}{m}_R + 1)^2}{\overset{o}{\rho}} (1-\overset{o}{A}_2) \left[\frac{1}{\overset{o}{A}_{th}{}^2} + 1 \right] \tag{19}$$

Constant Chamber Wall Pressure = Outlet Saturation Pressure

A more sophisticated treatment of the pressure rise analysis would include the fact that a variation of wall pressure occurs in the mixing chamber; hence the integral term in equation (10) is not as simple as in the case above. In order to illustrate the importance of this effect upon pressure rise, a limiting case will be considered. In Figure B-1 consider that condensation of the inlet vapor occurs immediately after station 0. That is, the jet temperature is raised to T_f, the outlet temperature immediately after station 0. The chamber pressure would then take the value of saturation vapor pressure corresponding to the temperature T_f (P_{Tf}). If the pressure were to drop any lower, liquid would evaporate from the jet to raise the vapor pressure to P_{Tf} (since equilibrium vapor liquid flow is assumed). Similarly any increases in vapor pressure would result in equilibrium condensation on the jet to reduce the vapor pressure to P_{Tf}.

The inlet conditions (cf. Figure B-1) are the same and the only term of equation (10) affected (other than friction) is the pressure integral. With these assumptions equation (10) becomes:

$$
\begin{aligned}
P_2 - P_o &= P_o\left(\frac{A_{to}}{A_{t1}} - 1\right) + \frac{1}{gA_{t1}}\left(\frac{\dot{m}_{vo}^2}{\rho_v(A_{to}-A_{\ell o}} + \frac{\dot{m}_{\ell o}^2}{\rho_\ell A_{\ell o}} - \frac{\dot{m}_T^2}{\rho_t A_{t1}}\right) \\
&\quad + \frac{\dot{m}_T^2}{2g\rho_\ell}\left(\frac{1}{A_{t1}^2} - \frac{1}{A_{to}^2}\right) - \int_0^{X_1} \frac{P_{Tf}\,\pi\, d_t \tan\alpha\, dx}{A_{t1}} \\
&= P_o\left(\frac{A_{to}}{A_{t1}} - 1\right) + \frac{1}{gA_{t1}}\left(\frac{\dot{m}_{vo}^2}{\rho_v(A_{to}-A_{\ell o})} + \frac{\dot{m}_{\ell o}^2}{\rho_\ell A_{\ell o}} + \frac{\dot{m}_T^2}{\rho_\ell A_{t1}}\right) \\
&\quad + \frac{\dot{m}_T^2}{2g\rho_\ell}\left(\frac{1}{A_{t1}^2} + \frac{1}{A_{\ell o}^2}\right) - P_{Tf}\left(\frac{A_{to} - A_{t1}}{A_{t1}}\right)
\end{aligned}
\qquad (20)
$$

or rearranging gives

$$\Delta P_{LP} \equiv P_2 - P_o = (P_o - P_{Tf}) \left(\frac{A_{to}}{A_{t1}} - 1 \right) + \frac{1}{gA_{t1}} \left(\frac{\dot{m}_{vo}^2}{\rho_v (A_{to} - A_{\ell o})} + \frac{\dot{m}_{\ell o}^2}{\rho_\ell A_{\ell o}} - \frac{\dot{m}_T^2}{\rho_\ell A_{t1}} \right)$$

$$+ \frac{\dot{m}_T^2}{2g\rho_\ell} \left(\frac{1}{A_{t1}^2} + \frac{1}{A_{to}^2} \right) \qquad (21)$$

subtracting the expression for constant pressure from equation 21 gives

$$\Delta P_{LP} - \Delta P_a = (P_o - P_{Tf}) \left(\frac{A_{to}}{A_{t1}} - 1 \right) = (P_o - P_{Tf}) \left(\frac{\overset{o}{A}_1}{\overset{o}{A}_2} - 1 \right) \qquad (22)$$

Linear Variation in Chamber Wall Pressure

The case of a linear variation in chamber pressure will also be considered. If the pressure is assumed to vary from P_{vo}, the inlet vapor pressure, to P_{Tf}, the saturation pressure, then the wall pressure integral in equation 10 becomes

$$\int_0^{X_1} P_w \pi d_t \tan \alpha \, dx = \int_0^{X_1} \pi \left[\frac{X}{X_1} (P_{vo} - P_{Tf}) + P_{Tf} \right] \left[\frac{X}{X_1} (d_{to} - d_{t1}) + d_{t1} \right] \tan \alpha \, dx \qquad (23)$$

$$= \pi \tan \alpha \left\{ \int_0^{X_1} \left(\frac{X}{X_1} \right)^2 (P_{vo} - P_{Tf})(d_{to} - d_{t1}) \, dx \right.$$

$$+ \int_0^{X_1} \frac{X}{X_1} \left[(P_{vo} - P_{Tf})(d_{t1}) + (d_{to} - d_{t1}) P_{Tf} \right] dx$$

$$\left. + \int_0^{X_1} P_{Tf} \, d_{t1} \, dx \right\} \qquad (24)$$

$$= \pi \tan\alpha \left\{ \frac{X_1}{3}(P_{vo} - P_{Tf})(d_{to} - d_{t1}) + \frac{X_1}{2}\left[(P_{vo} - P_{Tf})d_{t1} + (d_{to} - d_{t1})P_{Tf}\right] + P_{Tf}\, d_{t1}\, X_1 \right\}$$

$$= \pi \tan\alpha\, X_1 \left[\frac{(P_{vo} - P_{Tf})(d_{to} - d_{t1})}{3} + \frac{(P_{vo} - P_{Tf})d_{t1} + (d_{to} - d_{t1})P_{Tf}}{2} + P_{Tf}\, d_{t1} \right]$$

but

$$(\tan\alpha)(X_1) = \frac{d_{to} - d_{t1}}{2} \qquad (25)$$

$$\therefore \text{ the wall integral} = \frac{1}{2}\left[\frac{(P_{vo} - P_{Tf})\pi(d_{to} - d_{t1})^2}{3} + \frac{(P_{vo} - P_{Tf})\pi d_{t1}(d_{to} - d_{t1})}{2} + \frac{P_{Tf}\,\pi(d_{to} - d_{t1})^2}{2} + P_{Tf}\,\pi d_{t1}\,(d_{to} - d_{t1}) \right] \qquad (26)$$

Substitution of equation (26) into equation (10) and rearranging gives

$$P_2 - P_o = P_o\left(\frac{A_{to}}{A_{t1}} - 1\right) - \frac{(P_o - P_{Tf})\,\pi(d_{to} - d_{t1})^2}{6\,A_{t1}} - \frac{(P_o - P_{Tf})\,\pi d_{t1}(d_{to} - d_{t1})}{4\,A_{t1}} - \frac{P_{Tf}\,\pi(d_{to} - d_{t1})^2}{4\,A_{t1}} - \frac{P_{Tf}\,\pi d_{t1}(d_{to} - d_{t1})}{2\,A_{t1}} + \frac{1}{gA_{t1}}\left[\frac{\dot{m}_{vo}^{\circ\,2}}{\rho_v(A_{to} - A_{\ell o})} + \frac{\dot{m}_{\ell o}^{\circ\,2}}{\rho_\ell A_{\ell o}} - \frac{\dot{m}_T^{\circ\,2}}{\rho_\ell A_{t1}}\right] + \frac{\dot{m}_T^{\circ\,2}}{2g\rho_\ell}\left[\frac{1}{A_{t1}^2} + \frac{1}{A_{to}^2}\right] \qquad (27)$$

Subtracting the expression derived for constant inlet pressure from equation 26 gives

$$\Delta P'' - \Delta P_a = P_o\left(\frac{\overset{\circ}{A}_1}{\overset{\circ}{A}_2} - 1\right) - \frac{(P_o - P_{Tf})\,\pi(d_{to} - d_{t1})^2}{6\,A_{t1}} - \frac{(P_o - P_{Tf})\,\pi d_{t1}(d_{to} - d_{t1})}{4\,A_{t1}} - \frac{P_{Tf}\,\pi(d_{to} - d_{t1})^2}{4\,A_{t1}} - \frac{P_{Tf}\,\pi\, d_{t1}\,(d_{to} - d_{t1})}{2\,A_{t1}} \qquad (28)$$

Interface Downstream of Throat

The effect of incomplete condensation of the inlet vapor flow rate upon condenser pressure rise can be illustrated in a simple example. Consider the constant vapor pressure model to hold through the vapor region in the condenser. Moreover, the assumption is made that the central liquid jet is coherent up to the place of formation of the interface. It is then desired to express the theoretical pressure rise for a given set of inlet conditions as a function of the location of the interface in the converging section of Figure B-1. With the assumptions above and neglecting friction, the effect of changing interface location is to change $\overset{\circ}{A}_1$ in equation (18). If X_d is the distance from the throat to the interface location in the diffuser then:

$$\overset{\circ}{\Delta P}_{\ell} = 2\overset{\circ}{A}_1 \left(\frac{r}{r + X_d \tan\alpha}\right)^2 \left[1 + \frac{\overset{\circ}{\rho}}{\overset{\circ}{m}_R^{\,2}} \frac{\overset{\circ}{A}_2}{1-\overset{\circ}{A}_2}\right] - \left(1 + \frac{1}{\overset{\circ}{m}_R}\right)^2 \left[\overset{\circ}{A}_1^{\,2} \left(\frac{r}{r + X_d \tan\alpha}\right)^4 + \overset{\circ}{A}_2^{\,2}\right] \tag{29}$$

or

$$\overset{\circ}{\Delta P}_{\ell} = 2\overset{\circ}{A}_1 \left[1 + \frac{\overset{\circ}{\rho}}{\overset{\circ}{m}_R^{\,2}} \frac{\overset{\circ}{A}_2}{1-\overset{\circ}{A}_2}\right] \left[\frac{1}{1 + \frac{X_d}{r}\tan\alpha}\right]^2 - \left[1 + \frac{1}{\overset{\circ}{m}_R}\right]^2 \left[\overset{\circ}{A}_1^{\,2} \left(\frac{1}{1 + \frac{X_d}{r}\tan\alpha}\right)^4 + \overset{\circ}{A}_2^{\,2}\right] \tag{30}$$

APPENDIX C

JET CONDENSER ENERGY CONSERVATION

APPENDIX C

JET CONDENSER ENERGY CONSERVATION

Consider the figure of Appendix B. Neglecting friction and heat losses the energy equation written between 0) and 2) is:

$$\dot{m}_{vo}\, h_{vo} + \dot{m}_{\ell o}\, h_{\ell o} + (\dot{m}_{vo}\, V_{vo}^{2}/2J) + (\dot{m}_{\ell o}\, V_{\ell o}^{2}/2J)$$

$$= \dot{m}_T\, h_2 + (\dot{m}_T\, V_2^{2}/2J) \qquad (1)$$

where

$\dot{m}$ = mass flow rate

h = enthalpy

V = velocity

Substituting for velocities in terms of the mass flow rates gives:

$$\dot{m}_{vo}\, h_{vo} + \dot{m}_{\ell o}\, h_{\ell o} + (\dot{m}_{vo}^{3}/\rho_v^{2} A_{vo}^{2}\, 2J) + (\dot{m}_{\ell o}^{3}/\rho_{\ell o}^{2}\, A_{\ell o}^{2}\, 2J)$$

$$= \dot{m}_T\, h_2 + (\dot{m}_T^{3}/\rho_{\ell 2}^{2}\, A_2^{2}\, 2J) \qquad (2)$$

Further rearrangement gives:

$$u_{vo} + (P_{vo}/\rho_v J) + (\dot{m}_{vo}^{2}/\rho_v^{2}\, A_{vo}^{2} g 2J) + \overset{o}{m}_R \left[u_{\ell o} + (P_{\ell o}/\rho_{\ell o} J) + (\dot{m}_{\ell o}^{2}/\rho_{\ell o}^{2}\, A_{\ell o}^{2} g 2J)\right]$$

$$= (\overset{o}{m}_R + 1)\left[u_2 + (P_2/\rho_{\ell 2} J) + (\dot{m}_{vo} + \dot{m}_{\ell o})^{2}/\rho_{\ell o}^{2}\, A_2^{2} g 2J\right] \qquad (3)$$

For a particular design the left side of Eq. 3 is fixed. The right side then furnishes information as to the exchange of outlet internal energy (u_2) or temperature for a high outlet pressure (P_2). Consider, for example, the following set of conditions which are representative of a test run (No. 10-28-12, cf Appendix D).

$\overset{o}{m}_R = 24.5$

$\dot{m}_{vo} = 44.8$ lb/hr $= 3.87 \times 10^{-4}$ slugs/sec

$\dot{m}_{\ell o} = 1096$ lb/hr $= 9.45 \times 10^{-3}$ slugs/sec

$T_{vo} = 684^{\circ}$F

$T_{\ell o} = 284^{\circ}$F

$A_{vo} = 1.82 \times 10^{-4}$ ft^2

$$A_{\ell o} = 1.473 \times 10^{-5} \text{ ft}^2$$
$$\rho_v = 0.29 \text{ lb/ft}^3 = 0.900 \times 10^{-2} \text{ slugs/ft}^3$$
$$\rho_{\ell o} = 825 \text{ lb/ft}^3 = 25.6 \text{ slugs/ft}^3$$
$$A_2 = 1.967 \times 10^{-4} \text{ ft}^2$$
$$\rho_{\ell 2} \approx 802 \text{ lb/ft}^3 = 24.9 \text{ slugs/ft}^3$$
$$P_{vo} \approx P_{\ell o} = 2960 \text{ lbf/ft}^2$$

Then the following equation holds:

$$\left[h_{vo} + (3.87 \times 10^{-4})^2/(0.9 \times 10^{-2})^2 (1.82 \times 10^{-4})^2 (2)(778)(32.2)\right]$$
$$+\left[24.5\, h_{\ell o} + (9.45 \times 10^{-3})^2 (24.5)/(25.6)^2 (1.473 \times 10^{-5})^2(2)(778)(32.2)\right]$$
$$= 25.5\, h_2 + (25.5)(9.84 \times 10^{-3})^2/(24.9)^2(1.967)^2 (10^{-8})(2)(778)(32.2) \quad (4)$$

or

$$h_2 \approx 0.0392\, h_{vo} + 0.962\, h_{\ell o} + 0.0561 \quad (5)$$

and

$$h_{vo} \approx 169 \text{ BTU/lbm}$$
$$h_{\ell o} \approx 30.7 \text{ BTU/lbm}$$

Therefore for the example considered

$$h_2 \approx 6.62 + 29.5 + 0.06 \approx 36.2 \text{ BTU/lbm} \quad (6)$$

or

$$u_2 + P_2/\rho_{\ell 2} J = 36.2 \quad (7)$$

In order for Eq. 7 to be satisfied, increases in outlet pressure, P_2 must be accompanied by a decrease in outlet temperature T_2. In order to illustrate the magnitude of this effect first consider the case of no pressure rise or $P_2 = 2960$ psf

then

$$u_2 + 2960/802 \times 778 = 36.2$$
$$u_2 = 36.2 - .00473 \quad (8)$$

For the actual case, which was a pressure rise of 62 psi the outlet internal energy is given by

$$u_2' = 36.2 - .0190 \quad (9)$$

The change in internal energy is then given by

$$\Delta u_2 = C_p \Delta T_2 \approx 0.0143 \text{ BTU/lbm}$$

or

$$\Delta T_2 \approx \frac{0.0143}{0.032} = 0.447^\circ F$$

This result shows then, that the trade of thermal for pressure energy at the spray condenser outlet can be accomplished for large pressure rises (62 psi) and high ratios of outlet pressure to vapor pressure (4) with very small decreases in internal energy (0.0395%) and temperature (0.447° F) of the outlet liquid.

APPENDIX D

CONSTANT AREA JET CONDENSER TEST DATA

APPENDIX D

CONSTANT AREA JET CONDENSER TEST DATA

(Test Section No. 1)

Test Run No.	$\dot{m}_{vo}$	T_{vo}	P_{vo}	$\dot{m}_{\ell o}$	$T_{\ell o}$	$T_{\ell e}$	ΔP_a	ΔP_1	X	$\dot{m}_R$	$V_{\ell o}$	V_{vo}	$\Delta \overset{\circ}{P}_\ell$	$\Delta \overset{\circ}{P}_v$	$\overset{\circ}{\rho}$	$\Delta \overset{\circ}{P}_{\ell\ calc}$	$X\left(\frac{100}{v_R}\right)^{\frac{1}{4}}$	Q_R	Re_{vo}	η_1	η_a	L_c
1	28.3	724	24	808	533	671	3.9	45.0	0.723	28.5	19.7	122	0.116	6.09	2010	0.168	0.720	3570	14,800	0.750	0.693	3/8
2	29.1	733	26	897	516	644	5.1	64.0	0.590	30.8	21.8	126	0.123	6.91	1870	0.162	0.585	3670	15,200	0.646	0.763	1/16
3	28.8	724	24	647	523	698	2.2	34.0	0.871	22.5	15.7	124	0.101	3.28	2010	0.186	0.853	3620	15,100	0.632	0.544	3-1/2±1/2
4	28.7	715	22	649	480	654	3.1	32.0	0.741	22.6	15.7	124	0.143	4.91	2190	0.189	0.727	3610	15,000	0.675	0.755	1/4
5	29.6	720	23	649	480	660	3.1	32.0	0.750	21.9	15.7	125	0.144	4.75	2080	0.190	0.733	3740	15,500	0.675	0.769	5/16
6	28.1	720	23	644	513	685	3.1	32.0	0.832	22.9	15.8	121	0.142	4.97	2060	0.185	0.819	3550	14,700	0.675	0.769	1-1/4±1/4
7	28.4	721	23	648	510	683	3.1	35.0	0.820	22.8	15.7	123	0.144	4.89	2060	0.186	0.815	3590	14,900	0.614	0.777	7/8±1/8
8	28.9	720	23	658	499	672	3.3	35.0	0.783	22.8	16.0	125	0.148	5.05	2080	0.186	0.768	3640	15,100	0.637	0.795	9/16±1/16
9	30.1	723	24	658	493	673	3.4	36.0	0.783	21.9	15.9	130	0.156	4.72	2030	0.189	0.759	3790	15,800	0.614	0.825	1/2±1/8
10	30.4	723	24	665	483	664	3.5	38.0	0.754	21.8	16.1	132	0.154	4.65	2030	0.189	0.727	3850	15,900	0.598	0.814	7/16±1/16
11	30.4	723	24	666	479	659	3.5	38.0	0.738	21.9	16.1	131	0.155	4.75	2030	0.189	0.714	3840	15,900	0.595	0.820	5/16
12	28.2	722	24	660	470	638	3.4	38.0	0.666	23.4	16.0	122	0.152	5.32	2030	0.182	0.655	3550	14,800	0.588	0.836	3/16±1/16
13	29.8	723	24	661	461	638	3.3	38.0	0.675	22.2	16.0	128	0.149	4.73	2030	0.188	0.657	3740	15,600	0.588	0.795	3/16
14	31.4	723	24	661	459	645	3.3	36.0	0.705	21.1	16.0	135	0.149	4.26	2030	0.192	0.677	3930	16,500	0.621	0.778	3/16
15	31.0	723	24	645	450	639	3.3	36.0	0.692	20.8	15.6	133	0.157	4.37	2030	0.192	0.664	3900	16,300	0.591	0.818	1/8
16	30.5	725	24	675	432	610	3.5	36.0	0.608	22.1	16.3	132	0.151	4.57	2030	0.188	0.586	3850	16,000	0.648	0.805	1/16
17	28.7	723	24	656	392	564	3.1	36.0	0.520	22.9	15.8	124	0.133	4.69	2050	0.185	--	3610	15,000	0.648	0.720	0
18	42.1	714	22	665	206	455	2.8	15.0	0.490	15.8	15.7	181	--	2.07	2240	0.246	--	5300	22,100	--	--	0
19	30.2	716	22	453	213	476	0.9	15.0	0.523	15.0	10.7	130	--	1.30	2240	0.258	--	3810	15,800	--	--	0
20	27.1	721	24	371	396	684	1.2	12.0	0.885	13.7	8.93	117	0.169	2.06	2100	0.272	0.865	3420	14,200	0.581	0.623	2 ± 1
21	27.3	723	24	371	401	690	0.6	12.0	0.898	13.6	8.93	117	0.087	1.04	2030	0.268	0.878	3430	14,300	0.585	0.325	5 ± 1
22	28.9	727	25	399	403	689	1.3	--	0.878	13.8	9.60	125	0.155	1.80	1980	0.267	0.847	3650	15,100	--	0.581	2-1/2±1
23	28.9	727	25	399	398	683	--	12.0	0.867	13.8	9.60	125	--	--	2000	0.263	0.837	3640	15,100	--	--	3/4±1
24	27.9	720	23	419	340	603	1.1	15.0	0.692	15.0	10.0	121	0.121	1.75	2100	0.249	--	3530	14,600	0.588	0.436	0
25	29.9	720	23	461	385	640	1.2	17.0	0.761	15.4	11.0	129	0.110	1.69	2100	0.243	--	3760	15,700	--	0.453	0
26	26.1	720	23	427	432	672	1.5	17.0	0.833	16.4	10.3	112	0.161	2.85	2080	0.231	0.830	3280	13,700	0.550	0.697	5/16
27	26.1	720	23	426	440	682	1.6	17.0	0.864	16.3	10.3	113	0.168	2.92	2080	0.232	0.862	3300	13,700	0.546	0.725	1/2±1/8
28	26.9	720	23	435	443	688	1.6	17.0	0.884	16.2	10.5	116	0.167	2.86	2080	0.233	0.870	3390	14,100	0.602	0.717	7/8±1/4
29	27.7	723	24	435	443	694	1.0	17.0	0.896	15.7	10.4	119	0.108	1.67	2030	0.237	0.879	3480	14,500	0.555	0.445	3±1/2
30	27.2	720	23	433	443	690	1.4	15.0	0.892	15.9	10.1	114	0.159	2.62	2080	0.236	0.885	3320	14,300	0.600	0.655	1-1/4±1/4
31	25.3	718	23	420	443	680	1.5	15.0	0.862	16.6	10.0	107	0.171	3.13	2080	0.240	0.865	3140	13,300	0.585	--	7/16±1/8
32	24.8	720	23	414	450	686	1.5	15.0	0.874	16.7	10.0	107	0.166	3.03	2080	0.228	0.879	3120	13,000	0.581	0.729	5/8±1/8

APPENDIX D

CONSTANT AREA JET CONDENSER TEST DATA

(Test Section No. 1)

Test Run No.	$\dot{m}_{vo}$	T_{vo}	P_{vo}	$\dot{m}_{\ell o}$	$T_{\ell o}$	$T_{\ell e}$	ΔP_a	ΔP_1	X	Q_R	$V_{\ell o}$	V_{vo}	ΔP^o_ℓ	ΔP^o_v	β^o	$\Delta P^o_{\ell calc}$	$X\left(\frac{100}{V_R}\right)^{\frac{1}{4}}$	Q_R	Re_{vo}	η_1	η_a	L_c
33	25.0	720	23	413	452	690	1.5	15.0	0.888	16.5	10.0	108	0.166	2.97	2080	0.229	0.894	3150	13,100	0.581	0.725	5/8±1/8
34	24.9	720	23	413	454	691	1.5	15.0	0.891	16.6	10.4	112	0.158	2.77	2080	0.228	0.889	3280	13,000	0.613	0.691	1±1/4
35	--	723	24	--	454	694	--	15.0	0.892	--	--	--	--	--	2030	--	--	--	--	--	--	2-1/2±1/2
36	--	727	25	--	454	700	--	15.0	0.901	--	--	--	--	--	1980	--	--	--	--	--	--	4-1/2±1/2
37	15.0	705	20	439	482	617	1.1	13.0	0.605	29.2	10.6	65	0.115	7.00	2300	0.195	0.705	1900	7,860	0.764	0.589	1/4
38	14.1	707	20	454	528	650	1.1	13.0	0.682	32.2	11.1	61	0.107	7.94	2300	0.164	0.815	1780	7,400	0.820	0.653	5/8±1/8
39	13.7	708	21	456	550	668	1.1	13.0	0.747	33.4	11.1	59	0.106	8.47	2300	0.162	0.897	1720	7,180	0.826	0.654	1±1/8
40	--	710	21	--	564	679	--	13.0	0.788	--	--	--	--	--	2240	--	--	--	--	--	--	3-1/2
41	12.2	733	26	875	515	570	4.8	64.0	0.252	71.6	21.2	53	0.123	36.3	1830	0.142		1540	6,400	0.614	0.864	0
42	12.9	733	26	879	580	638	5.1	68.0	0.379	67.9	21.5	56	0.127	34.2	1830	0.143	0.495	1630	6,770	0.585	0.889	1/8
43	12.4	730	26	829	610	669	4.6	61.0	0.492	66.7	20.4	54	0.127	33.8	1900	0.144	0.648	1570	6,500	0.588	0.882	3/16
44	12.7	730	26	863	625	683	4.9	69.0	0.552	67.9	21.2	55	0.127	35.1	1900	0.143	0.724	1600	6,660	0.562	0.885	1/4
45	12.5	731	26	862	631	688	5.0	69.0	0.570	69.1	21.2	54	0.129	36.3	1860	0.143	0.749	1570	6,560	0.562	0.900	3/8±1/8
46	12.1	731	26	867	631	686	5.1	72.0	0.550	71.6	21.3	52	0.132	40.2	1860	0.143	0.736	1530	6,350	0.540	0.926	3/8±1/8
47	12.1	730	26	825	626	684	4.6	72.0	0.558	67.9	20.3	52	0.128	36.4	1900	0.143	0.740	1530	6,350	0.540	0.816	3/8
48	12.9	729	25	818	630	692	4.1	59.0	0.626	63.5	20.1	56	0.119	28.6	1900	0.143	0.810	1620	6,770	0.588	0.836	3/4±1/8
49	12.9	730	26	817	634	696	4.1	59.0	0.646	63.5	20.1	56	0.119	27.6	1900	0.143	0.838	1620	6,770	0.588	0.836	1
50	12.7	730	26	817	639	700	4.1	59.0	0.670	64.5	20.1	55	0.119	28.9	1900	0.143	0.875	1600	6,660	0.588	0.833	1-1/2
51	12.4	732	26	816	646	706	4.1	59.0	0.698	65.6	20.1	54	0.119	30.1	1860	0.143	0.916	1570	6,500	0.588	0.836	2-1/2
52	12.9	732	26	816	647	709	4.1	59.0	0.729	63.5	20.1	55	0.119	28.9	1860	0.143	0.945	1620	6,770	0.588	0.835	4
53	32.7	720	23	870	354	502	4.3	51.0	0.405	26.6	20.8	141	0.112	5.15	2100	0.164	0.386	4120	17,100	0.752	0.682	0
54	32.4	721	23	895	429	580	4.7	53.0	0.515	27.6	21.6	140	0.114	5.73	2080	0.162	0.493	4080	17,000	0.775	0.706	1/16
55	29.3	720	23	875	470	602	4.8	55.0	0.529	29.8	21.2	127	0.122	7.05	2080	0.158	0.522	3700	15,400	0.661	0.773	1/8
56	31.0	722	24	886	483	621	3.3	58.0	0.577	28.6	21.4	134	0.127	4.21	2080	0.160	0.561	3910	16,200	0.710	0.795	3/16
57	28.4	720	23	860	518	648	4.7	53.0	0.644	30.3	21.1	122	0.122	7.58	2060	0.157	0.641	3580	14,900	0.735	0.776	1/4±1/16
58	30.0	722	24	904	529	650	5.1	60.0	0.679	30.1	22.0	130	0.121	7.03	2060	0.157	0.667	3790	15,700	0.704	0.771	1/4±1/16
59	28.0	723	24	895	546	669	4.7	61.0	0.696	32.0	20.8	121	0.126	7.49	2060	0.155	0.695	3520	14,700	0.612	0.813	3/8±1/16
60	28.8	726	24	906	557	682	5.0	62.0	0.740	31.5	22.1	124	0.119	7.40	1960	0.154	0.740	3620	15,100	0.680	0.772	1/2±1/8
61	28.6λ	729	25	880	570	698	4.7	59.0	0.806	30.8	21.5	123	0.118	6.88	1920	0.155	0.803	3600	15,000	0.675	0.764	3/4±1/4
62	28.1	731	26	880	579	705	4.0	58.0	0.829	31.3	21.6	122	0.098	5.61	1870	0.153	0.828	3550	14,700	0.695	0.638	1-3/4±1/4
63	28.1	738	28	880	586	712	3.4	60.0	0.829	31.3	21.7	122	0.083	4.71	1790	0.152	0.828	3550	14,700	0.680	0.544	3±1/2
64	28.5	739	28	906	590	714	3.3	61.0	0.833	31.8	22.2	123	0.077	4.45	1790	0.152	0.831	3600	15,000	0.695	0.507	3-1/2±1/2
65	35.1	740	28	985	560	700	6.4	83.0	0.778	28.1	24.0	151	0.127	5.77	1750	0.157	0.733	4420	18,400	0.610	0.815	5/8±1/8

APPENDIX E

SMALL DIAMETER VARIABLE AREA JET CONDENSER TEST DATA

APPENDIX E

SMALL DIAMETER VARIABLE AREA JET CONDENSER TEST DATA

(Test Sections No. 3,4,5,6)

Test Run No.	$\dot{m}_{vo}$	T_{vo}	P_{vo}	$\dot{m}_{\ell o}$	$T_{\ell o}$	$T_{\ell e}$	ΔP_a	ΔP_i	X	$\overset{\circ}{m}_R$	$V_{\ell o}$	V_{vo}	$\overset{\circ}{\Delta P}_\ell$	$\overset{\circ}{\Delta P}_v$	$\overset{\circ}{\rho}$	$\overset{\circ}{\Delta P}_{\ell\ calc}$	Re_{vo}	η_a	L_c
9-27-61																			
TS3 1	25.8	670	15	568	440	620	5.3	25.3	0.783	22.1	13.1	152	0.458	9.14	3380	2.19	13,900	0.209	3/4
2	24.0	660	14	608	440	597	6.4	32.9	0.714	25.4	14.1	154	0.354	11.4	3690	1.82	12,900	0.195	1/2
3	24.7	665	14	620	440	598	6.7	34.7	0.703	25.1	14.4	152	0.354	11.7	3530	1.83	13,300	0.194	1/2
4	28.8	665	14	673	430	600	7.5	34.5	0.728	23.4	15.6	143	0.352	14.6	3530	1.62	12,600	0.217	1/4
5	38.8	680	16	582	170	445	3.1	22.6	0.500	15.0	13.0	210	0.192	2.51	3210	1.31	20,900	0.147	1/4
6	35.8	660	14	644	186	410	9.2	29.7	0.473	18.0	14.6	229	0.458	7.40	3790	1.48	19,200	0.309	
7	36.2	670	15	644	215	455	8.2	29.2	0.505	17.8	14.6	212	0.409	7.04	3460	1.46	19,400	0.280	
8	34.4	668	16	644	278	495	9.2	29.7	0.558	18.8	14.7	203	0.316	8.83	3510	1.02	18,200	0.310	3/8
9	32.3	660	14	644	300	503	10.2	30.7	0.564	19.9	14.7	207	0.532	9.99	3740	1.60	17,400	0.333	
10	27.4	710	21	620	390	620	9.1	27.9	0.719	22.7	14.3	107	0.507	20.5	2270	1.55	14,700	0.327	
11	36.6	715	22	620	392	628	8.9	27.9	0.731	17.0	14.3	143	0.495	11.8	2270	1.55	19,700	0.320	
12	37.6	715	22	766	405	602	8.9	53.9	0.636	20.4	17.7	207	0.215	10.6	2260	1.30	20,200	0.165	3/8
13	34.0	720	23	660	400	608	7.1	53.1	0.650	19.4	14.3	137	0.376	10.0	2330	2.81	18,300	0.134	
14	33.6	715	22	686	398	595	9.2	45.2	0.622	20.4	15.9	139	0.397	13.0	2400	3.30	18,000	0.120	
15	32.5	712	21	574	370	590	8.2	30.2	0.643	18.3	13.7	139	0.474	11.9	2480	1.74	17,500	0.272	
10-10-61																			
TS4 1	23.4	608	7.9	766	248	375	37.5	44.0	0.356	32.7	17.3	237	1.39	44.3	5980	1.65	13,500	0.843	
2	37.2	648	12	796	292	442	26.5	45.0	0.493	20.6	17.6	263	0.956	17.7	4120	2.10	21,300	0.455	1/4
3	27.1	612	8.2	728	233	387	22.0	35.0	0.401	26.9	16.0	239	0.922	22.3	5370	1.76	15,500	0.524	1/4
4	45.5	680	16	807	318	546	53.0		0.629	17.8	18.5	226	1.73	33.5	2940	1.85	26,000	0.935	1/4
5	52.4	700	19	832	350	603	43.5	62.0	0.724	15.9	19.2	217	1.33	25.1	2410	2.00	30,000	0.665	1/4
10-20-61																			
TS4 1	41.1	685	17	792	335	546	43.5	55.0	0.603	19.3	18.2	207	1.33	33.5	2930	1.70	23,500	0.782	1/4
2	41.0	690	18	798	362	570	44.0	56.0	0.627	19.5	18.4	199	1.46	35.6	2825	1.70	23,400	0.859	1/4
3	40.9	699	19	845	395	590	47.5		0.642	20.7	19.5	175	1.41	47.9	2470	1.60	23,500	0.882	1/4
4	14.2	580	5.9	548	314	420	14.0	23.0	0.399	38.7	12.6	200	0.990	32.4	8230	1.55	8,120	0.640	1/4
5	13.2	579	5.8	548	342	440	14.6	24.0	0.414	41.5	12.6	186	1.03	39.1	8210	1.50	7,550	0.687	1/4

APPENDIX E

SMALL DIAMETER VARIABLE AREA JET CONDENSER TEST DATA

(Test Sections No. 3,4,5,6)

Test Run No.	$\dot{m}_{vo}$	T_{vo}	P_{vo}	$\dot{m}_{\ell o}$	$T_{\ell o}$	$T_{\ell c}$	ΔP_a	ΔP_f	X	$\dot{m}_R^\circ$	$V_{\ell o}$	V_{vo}	$\Delta\hat{P}_\ell$	$\Delta\hat{P}_v$	$\hat{\rho}^\circ$	$\Delta\hat{P}_{\ell\ calc}$	Re_{vo}	η_a	L_c
10-21-61 TS4 1	14.5	676	15	713	503	585	4.3	36.3	0.474	49.2	16.6	78.7	0.178	24.9	3110	1.08	8,330	0.165	1/4
2	10.7	685	17	521	493	576	0.5	14.0	0.433	48.7	12.2	52.0	0.039	5.92	2790	1.08	6,130	0.036	1/4
3	15.1	686	17	521	454	572	0.5	15.0	0.58	34.5	12.1	73.5	0.039	2.94	2800	1.19	8,670	0.033	1/4
4	17.8	684	16	521	432	570		14.0	0.548	29.2	12.0	86.7			2840		10,200		1/4
5	23.4	641	11	580	400	562	6.6	20.1	0.672	24.8	13.3	174	0.419	10.6	4340	1.70	13,400	0.246	1/4
6	23.8	635	10	580	380	545	8.2	20.6	0.648	24.4	13.2	186	0.526	12.2	4580	1.75	13,600	0.300	1/4
7	23.9	630	10	580	357	523	8.2	21.2	0.609	24.2	13.4	198	0.519	11.3	4820	2.00	13,700	0.260	1/4
8	24.7	628	9.4	733	336	473	9.8	42.3	0.469	29.7	16.8	232	0.390	11.2	5480	1.65	14,200	0.236	1/4
9	25.4	626	9.3	606	312	483	9.9	22.4	0.543	23.9	13.9	239	0.570	10.6	5490	2.06	14,600	0.276	1/4
10	21.2	624	9.1	587	300	448	10.7	22.6	0.457	27.7	13.4	199	0.669	15.3	5490	1.80	12,100	0.371	1/4
11	24.6	624	9.1	598	294	462	11.2	24.6	0.508	24.4	13.7	231	0.670	12.9	5500	2.05	14,100	0.326	1/4
12	24.2	622	9.0	598	290	455	12.5	27.8	0.512	24.7	13.7	227	0.744	15.0	5510	2.05	13,900	0.363	1/4
13	24.0	621	8.9	614	286	447	14.2	28.0	0.482	25.6	14.0	226	0.008	17.6	5500	1.90	13,800	0.425	1/4
14	24.0	621	8.9	614	290	450	14.6	28.0	0.484	25.6	14.1	226	0.817	17.7	5510	1.90	13,800	0.430	1/4
15	24.0	623	9.0	614	290	450	14.7	27.7	0.482	25.6	14.1	226	0.822	17.9	5510	1.90	13,800	0.433	1/4
16	23.1	622	9.0	627	295	446	17.3	32.8	0.463	27.1	14.3	217	0.948	22.6	5500	1.80	13,200	0.527	1/4
17	23.2	624	9.1	647	310	457	18.6	32.1	0.478	27.9	14.8	218	0.949	24.1	5490	1.80	13,100	0.528	1/4
18	23.0	624	9.1	654	330	473	19.6	34.1	0.487	28.4	15.0	216	0.979	26.9	5480	1.75	13,000	0.560	1/4
19	22.7	628	9.4	660	350	490	20.5	37.0	0.504	29.1	15.2	213	1.00	27.8	5470	1.70	12,800	0.588	1/4
20	23.0	630	9.6	673	370	509	21.5	37.5	0.535	29.3	15.5	202	1.00	30.4	5110	1.65	12,950	0.607	1/4
21	22.3	636	10	686	400	532	23.5	37.0	0.560	30.8	15.9	176	1.05	36.8	4280		13,400	>0.500	1/4
22	44.3	680	16	790	270	500	22.5	45.5	0.561	17.9	18.0	223	0.773	14.9	2950	1.25	25,000	0.619	1/4
23	43.2	680	16	806	290	510	28.0	49.5	0.564	18.7			0.920	19.4	2940	1.30	24,400	0.708	1/4
24	42.4	680	16	818	310	522	31.0	50.5	0.574	19.3	18.7	214	0.989	22.3	2940		24,000		1/4
25	43.0	684	16	832	330	540	32.0	51.0	0.594	19.3	19.1	202	1.01	24.2	2740	1.70	24,200	0.582	1/4
26	43.0	684	16	1 832	340	550	32.0	51.0	0.611	19.3	19.1	202	1.01	24.2	2730	1.70	24,200	0.582	1/4
27	45.2	693	18	832	354	570	29.2	49.0	0.638	18.4	19.2	199	0.896	21.2	2560	1.70	25,500	0.527	1/4
28	44.4	700	19	806	395	598	26.5	47.0	0.666	18.2	18.6	184	0.865	21.2	2395	1.80	25,100	0.480	1/4
29	36.8	710	21	790	416	604	21.0	42.0	0.640	21.5	18.3	144	0.711	25.8	2260	1.50	20,800	0.474	1/4
30	23.2	615	8.4	734	242	374	18.5	42.5	0.354	31.6	16.7	218	0.738	24.0	5490	1.55	31,100	0.477	1/4
31	21.7	605	7.6	753	239	360	23.5	48.5	0.330	34.7	17.1	236	0.890	30.0	6370	1.55	12,300	0.574	1/4
32	21.6	604	7.6	766	238	356	27.5	50.5	0.323	35.5	17.4	235	1.01	35.4	6370	1.55	12,200	0.649	1/4
33	20.7	604	7.6	806	258	365	35.5	55.5	0.310	38.9	18.4	224	1.17	50.0	6350	1.45	11,600	0.808	1/4

APPENDIX E

SMALL DIAMETER VARIABLE AREA JET CONDENSER TEST DATA

(Test Sections No. 3,4,5,6)

Test Run No.	$\dot{m}_{vo}$	T_{vo}	P_{vo}	$\dot{m}_{\ell o}$	$T_{\ell o}$	$T_{\ell e}$	ΔP_a	ΔP_1	X	$\overset{\circ}{m}_R$	$V_{\ell o}$	V_{vo}	$\overset{\circ}{\Delta P}_\ell$	$\overset{\circ}{\Delta P}_v$	$\overset{\circ}{\rho}$	$\overset{\circ}{\Delta P}_{\ell(calc)}$	Re_{vo}	η_a	L_c
10-23-61																			
T84 1	33.7	665	14	647	342	553	10.3	27.5	0.653	19.2	14.9	198	0.527	10.2	3420	1.95	18,200	0.270	1/4
2	10.3	697	19	587	425	565	4.5	21.0	0.519	28.9	13.6	84.2	0.278	17.3	2390	1.20	11,000	0.232	1/4
3	19.6	700	19	607	442	572	5.5	22.0	0.507	31.0	14.1	78.9	0.316	23.5	2320	1.20	10,600	0.263	1/4
4	19.5	700	19	644	442	565	8.5	24.0	0.477	32.9	15.0	78.8	0.434	36.3	2320	1.15	10,600	0.376	1/4
5	21.7	700	19	734	443	563	0.5	34.0	0.468	33.8	17.1	87.5	0.020	1.73	2320	1.15	11,800	0.017	1/4
6	10.6	697	19	713	510	570	-3.0	32.0	0.321	67.5	16.7	43.9	-0.124	-42.4	2370		5,740		1/4
7	20.8	700	19	724	461	577	-2.5	32.0	0.485	34.8	16.8	83.8	-0.101	-11.5	2320		11,350		1/4
8	32.3	685	17	750	415	589	2.5	37.5	0.645	23.2	17.3	122	0.095	5.18	2710	1.55	13,900	0.061	1/4
9	38.3	680	16	778	383	581	8.5	43.0	0.667	20.3	17.9	180	0.296	8.06	2730	1.70	20,800	0.174	1/4
10	39.3	675	15	806	353	550	14.5	46.0	0.613	20.5	18.5	205	0.479	11.8	3040	1.85	21,200	0.258	1/4
11	42.6	680	16	832	332	540	17.5	49.0	0.598	19.6	19.2	200	0.535	13.5	2740	1.70	23,000	0.314	1/4
12	50.2	697	19	755	290	560	23.5	36.0	0.663	15.0	17.3	208	0.882	14.8	2430	2.15	27,200	0.410	1/4
13	51.2	697	19	750	260	538	22.6	34.0	0.636	14.6	17.1	212	0.603	13.7	2440	2.15	27,200	0.280	1/4
14	50.6	645	11	737	249	530	25.9	34.0	0.630	19.6	16.7	210	1.03	16.1	2440	1.60	27,400	0.645	1/4
15	50.4	690	18	755	240	514	27.0	37.5	0.609	15.0	17.1	215	1.03	16.4	2520	2.15	27,300	0.480	1/4
16	51.0	690	18	761	235	510	28.5	38.5	0.604	14.9	17.3	218	1.07	16.9	2520	2.15	27,600	0.495	1/4
17	50.1	690	18	777	240	505	32.5	41.5	0.588	15.5	17.6	214	1.17	19.9	2520	2.15	27,100	0.546	1/4
18	50.7	690	18	800	260	520	35.0	43.5	0.605	15.8	18.2	216	1.19	20.8	2510	2.15	27,400	0.553	1/4
19	49.2	691	18	800	300	550	37.0	44.5	0.640	16.3	18.3	210	1.12	23.6	2500	2.00	26,700	0.562	1/4
20	48.4	700	19	800	330	575	34.5	42.0	0.662	16.5	18.4	195	1.15	24.0	2350	1.80	26,200	0.641	1/4
21	45.8	703	20	777	360	598	32.0	39.5	0.695	17.0	17.9	184	1.14	25.0	2340	2.15	24,800	0.528	1/4
22	43.7	709	21	765	372	602	28.5	37.0	0.683	17.5	17.6	161	1.04	28.1	2270	1.80	22,300	0.580	1/4

APPENDIX E

SMALL DIAMETER VARIABLE AREA JET CONDENSER TEST DATA

(Test Sections No. 3,4,5,6)

Test Run No.	$\dot{m}_{vo}$	T_{vo}	P_{vo}	$\dot{m}_{\ell o}$	$T_{\ell o}$	$T_{\ell e}$	ΔP_a	ΔP_i	x	$\frac{g}{g_R}$	$V_{\ell o}$	V_{vo}	ΔP_ℓ	ΔP_v	ρ°	ΔP_{ℓ} calc	Re_{vo}	η_a	L_c
10-28-61																			
TS5 1	45.7	689	17	700	210	480	11.5	31.5	0.564	15.5	15.8	222	0.513	7.47	2870	2.55	24,800	0.202	Metal Unit; no data
2	45.6	689	17	745	215	469	18.5	37.5	0.548	16.4	16.9	222	0.724	12.0	2860	2.40	24,800	0.302	
3	43.8	683	16	762	219	457	24.0	41.0	0.514	17.4	17.3	220	0.897	16.5	2960	2.35	23,700	0.381	
4	44.8	680	16	792	221	454	29.0	47.0	0.508	17.7	18.0	226	1.00	18.8	2960	2.30	24,300	0.437	
5	45.6	679	16	805	221	451	31.0	48.0	0.503	17.6	18.3	229	1.04	19.6	2960	2.30	24,600	0.450	
6	43.5	679	16	845	247	460	38.0	55.0	0.493	19.4	19.2	219	1.15	26.2	2960	2.02	23,600	0.570	
7	41.7	694	18	673	340	590	12.0	28.0	0.707	16.1	16.3	178	0.504	10.7	2510	2.40	27,600	0.210	
8	46.1	682	16	976	158	359	24.0	76.0	0.384	21.2	22.0	232	0.552	14.8	2990	1.80	25,000	0.306	
9	46.9	676	15	1096	191	371	39.5	106	0.373	23.4	24.0	245	0.714	22.6	3090	1.63	25,400	0.438	
10	47.1	680	16	1115	211	389	55.0	106	0.380	23.7	25.2	237	0.968	32.5	2970	1.65	25,500	0.587	
11	44.9	680	16	1090	245	418	59.0	103	0.398	24.3	24.5	226	1.10	38.3	2960	1.51	24,300	0.729	
12	44.8	684	16	1096	284	454	62.0	104	0.426	24.5	25.0	218	1.11	41.7	2840	1.50	24,300	0.735	
11-4-61																			
TS6 1	35.3	658	13	720	330	529	18.0	34.0	0.607	20.4	16.5	216	0.740	15.5	3570	2.10	19 600	0.352	Metal Unit; no data
2	35.1	661	14	739	336	529	23.0	40.0	0.594	21.0	17.0	215	0.900	18.9	3560	2.05	19,500	0.439	
3	31.5	662	14	772	341	524	26.0	42.0	0.571	24.5	17.7	193	0.934	28.2	3560	1.75	17,500	0.533	
4	28.9	648	12	700	356	523	18.5	34.5	0.573	24.2	16.1	194	0.803	21.7	3900	1.94	16,100	0.414	
5	26.6	640	11	700	360	514	18.0	35.0	0.551	26.3	16.1	147	0.782	22.8	4310	1.80	14,800	0.434	
6	28.2	652	12	1117	402	505	29.0	107	0.412	39.6	25.8	203	0.494	32.6	4070	1.36	16,000	0.363	
7	37.5	640	11	1030	110	268	44.0	82.0	0.298	27.5	23.1	278	0.912	27.7	4410	1.73	20,800	0.527	

APPENDIX F

LARGE DIAMETER VARIABLE AREA JET CONDENSER TEST DATA

APPENDIX F

LARGE DIAMETER VARIABLE AREA JET CONDENSER TEST DATA

(Test Sections no. 7 and 8)

Test Run No.	$\dot{m}_{vo}$	T_{vo}	P_{vo}	$\dot{m}_{\ell o}$	$T_{\ell o}$	$T_{\ell e}$	ΔP_a	ΔP_i	X	$\frac{g}{m}_R$	$V_{\ell o}$	V_{vo}	ΔP_ℓ	ΔP_v	β	$\Delta P_{a\,(calc)}$	ϕ	Q_R	Re_{vo}	$Re_{\ell o}$	η_i	η_a	L_c
12-27-61(TS#7)																							
1	184	690	18	2540	365	650	2.5	5.0	0.876	13.3	3.73	57.5	2.02	24.1	2810	3.9	0.0607	23,100	29,300	69,000	0.206	0.646	~1.00
2	194	690	18	2530	373	675	2.5	6.0	0.952	13.0	3.71	60.6	2.06	21.8	2810	3.9	0.0621	24,500	30,800	68,700	0.170	0.637	~1.00
3	202	691	18	2850	381	660	3.5	7.0	0.900	14.1	4.18	63.1	2.27	28.2	2810	6.0	0.0640	25,500	32,100	77,500	0.184	0.587	~1.00
4	208	707	20	3370	400	652	4.5	9.5	0.820	16.2	4.94	60.8	2.09	36.4	2630	5.25	0.0723	26,200	33,100	91,500	0.189	0.869	~1.00
5	205	708	21	3350	419	660	4.7	10.5	0.840	16.3	4.92	59.9	2.19	39.1	2630	5.1	0.0750	25,800	32,600	71,000	0.154	0.923	~1.00
6	211	706	20	3400	427	671	5.0	9.5	0.875	16.1	4.99	61.7	2.27	39.2	2630	5.3	0.0770	26,600	33,600	92,400	0.189	0.953	~1.00
7	213	720	23	3240	412	672	5.0	9.0	0.850	15.2	4.76	--	2.50	38.5	--	5.2	0.0600	26,900	33,900	88,000	0.184	0.969	~1.00
8	214	724	24	3240	433	684	5.2	8.0	0.868	15.1	4.76	49.7	2.60	50.2	2090	4.6	0.0920	26,000	33,700	88,000	0.207	1.14	~1.00
9	214	725	24	3200	441	694	5.3	9.0	0.890	14.9	4.70	48.6	2.72	52.2	2040	4.5	0.0953	26,000	34,100	87,000	0.182	1.17	~1.00
10	204	730	26	3200	449	700	5.5	9.0	0.893	15.7	4.70	44.1	2.82	62.8	1940	4.3	0.1065	25,700	32,500	87,000	0.182	1.28	~1.00
11	228	749	31	3640	454	701	7.0	13.0	0.837	16.0	5.34	43.2	2.78	72.4	1700	4.8	0.0931	28,800	36,400	99,000	0.0685	1.46	~1.00
12	201	787	42	3850	491	696	6.0	17.0	0.743	19.1	5.65	29.4	2.13	105.0	1315	4.7	0.1765	25,300	32,000	104,800	0.0595	1.30	~1.00
12-28-61(TS#7)																							
1	127	693	18	2440	403	610	<1.5>	5.0	0.714	19.2	3.59	37.1	1.33	32.6	2630	2.2	0.0765	16,200	16,700	64,800	0.224	0.685	~1.00
2	129	694	18	2440	410	620	<1.8>	5.0	0.740	18.9	3.60	37.7	1.59	38.0	2630	2.3	0.0782	16,400	17,100	64,800	0.225	0.760	~1.00
3	127	691	18	2440	423	631	<2.0>	5.0	0.776	19.2	3.60	38.4	1.77	42.0	2710	2.2	0.0815	16,200	16,700	64,800	0.225	0.908	~1.00
4	122	692	18	2440	435	635	<1.5>	5.0	0.778	20.0	3.61	36.9	1.26	34.1	2710	2.2	0.0944	15,600	14,900	64,800	0.227	0.669	~1.00
5	132	690	18	2320	426	629	2.5	6.0	0.738	20.2	3.61	33.2	2.19	63.8	2460	2.1	0.0900	15,500	15,900	64,800	0.190	1.18	~1.00
6	121	700	19	2440	430	629	2.5	6.0	0.738	20.2	3.61	33.2	2.19	63.8	2460	2.1	0.0900	15,500	15,900	64,800	0.190	1.18	~1.00
7	123	702	19	2640	454	640	2.5	8.0	0.750	21.5	3.90	32.8	1.87	65.4	2380	2.3	0.1010	15,700	16,200	70,100	0.167	1.07	~1.00
8	119	705	20	2630	459	639	2.25	7.0	0.732	22.1	3.88	31.7	1.71	61.0	2380	2.3	0.1020	15,200	15,700	69,800	0.188	1.00	~1.00
9	120	735	27	3000	490	659	2.75	10.0	0.690	25.0	4.43	24.2	1.60	97.0	1800	2.4	0.1540	15,300	15,800	79,600	0.172	1.20	~1.00
10	127	735	27	2970	490	660	3.0	10.0	0.694	23.4	4.39	25.6	1.77	94.2	1800	2.4	0.1437	16,200	16,700	78,800	0.169	1.27	~1.00
11	121	752	32	2850	525	695	3.0	11.0	0.749	23.5	4.21	21.5	1.93	118	1580	2.2	0.1820	15,500	15,900	75,700	0.141	1.37	~1.00
12	120	755	33	2850	532	700	3.2	11.0	0.753	23.8	4.21	20.9	2.06	130	1550	2.2	0.1890	15,300	15,800	75,700	0.141	1.49	~1.00
13	123	775	39	3580	462	611	3.1	16.0	0.477	29.1	5.29	18.0	1.26	143	1310	2.9	0.1984	16,100	16,200	95,000	0.153	1.07	~1.00
14	128	775	39	3560	467	622	3.6	16.0	0.504	27.8	5.26	18.7	1.49	111	1310	2.8	0.2010	16,700	16,900	94,500	0.151	1.27	~1.00
15	179	786	42	3420	480	690	5.0	16.0	0.684	19.1	5.06	25.0	2.23	114	1250	3.3	0.1730	23,000	23,600	90,800	0.140	1.52	~1.00
16	186	786	42	3440	477	694	5.1	16.0	0.703	18.5	5.08	26.0	2.26	108	1250	3.4	0.1710	23,900	24,500	91,300	0.140	1.50	~1.00
17	200	784	41	3470	450	682	5.0	16.0	0.694	17.3	5.13	27.9	2.16	91.8	1250	3.6	0.1560	25,800	26,300	92,100	0.144	1.38	~1.00
18	201	785	41	2830	453	734	5.0	--	0.848	14.1	4.18	28.1	3.26	90.5	1250	2.9	0.1485	25,500	26,500	75,100	--	1.74	~1.00

APPENDIX F

LARGE DIAMETER VARIABLE AREA JET CONDENSER TEST DATA

(Test Sections No. 7 and 8)

Test Run No.	$\dot{m}_{vo}$	T_{vo}	P_{vo}	$\dot{m}_{\ell o}$	$T_{\ell o}$	$T_{\ell e}$	ΔP_a	ΔP_i	X	$\frac{\dot{m}_{\ell}}{\dot{m}_R}$	$V_{\ell o}$	V_{vo}	$\Delta \bar{P}_{\ell}$	$\Delta \bar{P}_v$	β	$\Delta P_{a(calc)}$	ψ	Q_R	Re_{vo}	$Re_{\ell o}$	η_i	η_a	L_c
1-3-62																							
TS7 1	127	642	11	2450	418	622	2.2	3.1	0.910	19.3	3.62	59.0	1.91	30.1	4170	2.9	0.0585	16,000	19,200	62,700	0.372	0.750	~1.00"
2	166	648	12	3630	410	594	4.2	6.5	0.765	21.8	5.22	74.3	1.75	34.6	4010	5.3	0.0578	21,100	25,100	92,800	0.368	0.800	0.90
3	160	633	9.9	3260	428	622	3.8	6.3	0.948	20.4	4.82	83.0	1.86	29.2	4650	5.2	0.0586	20,200	24,200	83,500	0.324	0.730	0.90
4	194	622	9.0	3840	412	611	5.2	7.1	0.949	19.8	5.67	109	1.85	25.1	5050	7.9	0.0518	24,400	29,300	98,200	0.396	0.660	0.90
5	182	632	9.8	3800	432	620	3.7	7.3	0.941	20.9	5.61	97.0	1.34	21.5	4780	6.7	0.0577	22,900	27,400	97,100	0.378	0.550	Vapor thru throat
6	168	630	9.6	3510	418	607	4.7	2.7	0.788	20.9	5.18		1.99			5.0		21,300	25,400	89,800	0.875	0.950	1.0"
7	209	632	9.8	4020	414	619	4.5	8.3	0.941	19.3	5.93	112	1.46	19.7	4780	8.5	0.0527	26,400	31,600	103,000	0.372	0.530	Vapor thru throat
8	206	632	9.8	4020	408	611	6.2	5.1	0.872	19.5	5.93		2.01			7.9		26,100	31,100	103,000	0.605	0.790	1.0"
9	197	630	9.6	3800	404	619	4.9	6.8	0.923	19.3	5.61	108	1.77	23.4	4940	7.8	0.0505	24,900	29,800	97,100	0.407	0.630	1.0"
10	205	626	9.3	4200	418	611	6.2	9.1	0.942	20.5	6.20	115	1.84	26.9	5020	9.0	0.0537	25,900	31,100	107,600	0.370	0.690	1.0"
11	212	610	8.0	5210	422	583	8.2	16.2	0.857	24.6	7.70	143	1.58	27.7	6030	12.0	0.0490	26,800	32,100	133,500	0.322	0.650	1.0"
12	189	590	6.6	5280	413	555	8.7	16.8	0.772	27.9	7.80	143	1.63	33.0	6780	11.5	0.0445	24,000	28,600	135,100	0.318	0.760	1.0"
13	179	582	6.1	6360	423	535	10.7	28.2	0.705	35.5	9.39	159	1.46	40.9	7970	13.2	0.0442	22,800	27,100	163,000	0.260	0.810	1.0"
14	180	578	5.8	6380	413	525	11.0	30.3	0.684	35.5	9.42	170	1.43	36.7	8470	14.3	0.0400	22,900	27,500	163,300	0.254	0.770	1.0"
15	166	564	4.9	6340	411	515	13.2	29.8	0.679	38.2	9.36	184	1.72	44.2	9920	14.7	0.0364	21,100	25,100	162,400	0.258	0.900	1.0"
16	132	562	4.7	6340	386	470	14.2		0.477	48.1	9.36	152	1.85	72.6	10,300	12.2	0.0314	17,000	19,900	162,400		1.16	1.0"
17	125	562	4.7	6460	290	370	16.7	30.2	0.294	51.7	9.54	144	2.09	95.0	10,900	12.1	0.0195	16,500	18,900	165,500	0.264	1.38	1.0"
18	100	565	4.9	6610	254	317	16.7	31.0	0.203	66.1	9.79	103	2.04	166	10,000	11.5	0.0213	13,300	15,100	169,200	0.269	1.46	1.0"
1-29-62																							
TS7 1	181	564	4.9	4080	272	450	9.1		0.609	22.5	5.93	200	2.91	25.8	10,080	12.0	0.0186	23,200	28,200	102,300			~1.0"
2	178	552	4.1	5470	343	474	11.5	16.9	0.627	30.8	8.02	231	2.03	28.6	11,700	15.5	0.0226	22,900	27,800	137,000	0.335	0.760	~1.0"
3	180	552	4.1	5520	333	464	12.4	17.9	0.598	30.7	8.07	233	2.15	30.3	11,720	15.9	0.0215	23,100	28,000	138,300	0.322	0.740	~1.0"
4	182	553	4.2	5630	330	460	14.0	17.9	0.583	30.9	8.23	236	2.34	33.3	11,720	16.3	0.0210	23,400	28,400	141,000	0.334	0.780	~1.0"
5	188	553	4.2	5680	351	479	15.8	18.9	0.633	30.2	8.33	244	2.54	35.1	11,690	17.4	0.0229	24,200	29,300	142,400	0.330	0.860	~1.0"
6	169	556	4.4	6720	372	473	15.8	31.7	0.549	39.8	9.87	210	1.84	45.6	11,200	17.2	0.0270	21,700	26,400	168,500	0.271	0.910	~1.0"
7	170	550	4.0	6770	356	457	16.5	32.0	0.521	39.8	9.93	223	1.89	44.6	11,870	18.5	0.0243	21,900	26,400	170,000	0.272	0.920	~1.0"
8	172	560	4.6	6770	348	450	17.1	33.5	0.481	39.4	9.92	198	1.96	51.2	10,380	16.6	0.0254	22,100	26,800	170,000	0.258	0.890	~1.0"
9	168	565	4.9	6610	380	482	16.8	33.3	0.551	39.3	9.72	181	2.16	56.8	9.740	14.4	0.0313	21,600	26,100	166,000	0.250	1.03	~1.0"
10	167	565	4.9	6570	379	481	17.6	33.3	0.548	39.4	7.64	180	2.15	60.3	9,740	15.3	0.0311	21,400	26,000	164,200	0.246	1.17	~1.0"
11	171	570	5.3	6980	390	488	18.7	39.0	0.544	40.8	10.45	176	1.98	63.8	9,110	16.4	0.0343	21,900	26,600	175,000	0.214	1.15	~1.0"
12	163	570	5.3	6980	395	489	20.5	41.0	0.537	42.8	10.47	168	2.17	76.5	9,100	18.0	0.0356	21,000	25,400	175,000	0.230	1.14	~1.0"

APPENDIX F

LARGE DIAMETER VARIABLE AREA JET CONDENSER TEST DATA

(Test Sections No. 7 and 8)

Test Run No.	$\dot{m}_{vo}$	T_{vo}	P_{vo}	$\dot{m}_{\ell o}$	$T_{\ell o}$	$T_{\ell e}$	ΔP_a	ΔP_i	χ	$\frac{Q}{m_R}$	$V_{\ell o}$	V_{vo}	$\Delta\rho_\ell$	$\Delta\rho_v$	ρ	$\Delta P_{a(calc)}$	ψ	Q_R	Re_{vo}	$Re_{\ell o}$	η_i	η_a	L_c
1-31-62 (TS #7)																							
1	150	554	4.2	1960	140	450	8.7	-	0.748	13.1	2.82	184	12.1	32.1	10,880	7.6	0.0165	19,450	32,300	49,200	-	1.14	~1.00
* 2	48.9	538	3.4	1270	348	500	1.5	-	0.800	26.0	1.86	71	4.92	43.9	13,240	-	-	6,180	7,780	31,800	-	-	~1.00
2-7-62 (TS #8)																							
1	163	554	4.2	3860	273	443	12.8	7.8	0.605	23.7	5.62	200	4.58	40.2	11,160	10.6	0.0175	21,000	25,600	96,700	0.361	1.21	~1.00
2	162	552	4.1	3880	272	440	13.5	7.9	0.600	23.9	5.72	204	4.76	42.1	11,460	11.0	0.0173	20,900	25,500	97,200	0.368	1.23	~1.00
3	158	552	4.1	3840	275	440	12.9	7.9	0.596	24.3	5.58	199	4.65	41.9	11,460	10.6	0.0155	20,300	27,500	96,200	0.351	1.22	~1.00
4	158	554	4.2	3950	271	432	15.4	-	0.570	25.0	5.75	194	5.23	51.1	11,160	10.6	0.0174	20,400	24,900	99,000	-	1.45	~1.00
2-8-62 (TS #8)																							
** 1	152	546	3.8	3760	293	456	12.6	-	0.645	24.7	5.48	209	4.75	41.5	12,500	10.6	0.0174	19,600	24,000	94,000	-	1.19	0.9
2	156	551	4.1	3710	311	480	12.4	8.0	0.705	23.8	5.41	199	4.71	42.1	11,600	10.6	0.0205	19,900	22,900	96,200	0.353	1.09	1.0
*** 3	154.5	552	4.1	3850	319	481	11.4	7.9	0.695	24.9	5.62	196	4.05	36.8	11,400	10.5	0.0205	19,900	22,900	96,200	0.353	1.09	1.0
3-13-62 (TS #8)																							
1	173	536	3.4	4200	240	408	14.9	11.1	0.572	24.2	6.09	273	4.51	32.5	14,300	14.9	0.0131	22,600	29,300	107,500	0.298	1.00	~1.00
2	173	545	3.7	41900	262	430	13.4	10.4	0.593	24.2	6.09	248	4.06	30.7	12,500	13.2	0.0149	22,500	28,100	104,500	0.317	1.02	~1.00
3	168	541	3.5	4990	242	380	18.2	18.5	0.462	29.7	7.24	246	3.88	45.1	13,400	15.0	0.0140	22,000	26,200	124,500	0.254	1.21	~1.00
4	169	541	3.5	4970	255	394	17.6	18.1	0.486	29.4	7.21	247	3.79	43.2	13,400	15.1	0.0145	22,100	26,300	124,000	0.256	1.17	~1.00
3-15-62 (TS #8)																							
1	178	542	3.6	3370	136	354	14.0	4.5	0.537	18.9	4.84	261	6.64	30.9	13,500	13.4	0.0101	23,500	27,800	84,100	0.469	1.05	~1.00
2	175	542	3.6	3370	142	356	14.8	4.5	0.535	19.3	4.84	256	6.99	33.9	13,500	12.8	0.0103	23,100	27,300	84,100	0.470	1.16	~1.00
3	168	538	3.4	3350	141	348	13.2	4.6	0.522	19.9	4.81	258	6.34	31.5	14,200	12.9	0.0099	22,200	26,100	83,600	0.453	1.02	~1.00
**** 3a	180	662	13.5	2040	106	470	10.5	-	0.655	11.3	2.92	67.9	11.4	88.0	3,500	-	-	23,800	28,000	50,900	-	-	0-1.00
4	177	553	4.2	2680	120	390	8.2	-	0.624	15.1	3.03	227	6.18	20.8	11,810	11.2	0.0107	23,200	27,700	66,900	-	0.735	~1.50
5	172	538	3.4	2680	108	372	13.0	-	0.614	15.6	3.83	265	9.74	29.2	14,200	9.5	0.0090	22,600	26,900	66,900	-	1.37	~1.00
6	175	550	4.0	2680	116	385	13.0	-	0.620	15.3	3.84	227	9.74	33.4	12,000	10.9	0.01065	23,000	27,300	66,900	-	1.19	1.25
7	178	542	3.6	2700	113	384	13.5	-	0.633	15.2	3.87	261	9.98	29.8	13,500	11.9	0.0096	23,400	27,800	67,400	-	1.13	1.25
8	178	541	3.5	2720	111	380	14.3	-	0.627	15.3	3.90	261	10.40	31.6	13,500	11.8	0.0095	23,400	27,800	67,900	-	1.21	1.25
3-16-62 (TS #8)																							
1	176	539	3.4	5800	274	398	18.5	25.6	0.468	32.9	8.43	266	2.93	40.4	13,900	17.7	0.0153	23,000	27,400	144,700	0.247	1.05	0.9
2	178	539	3.4	5800	283	408	19.0	25.6	0.488	32.5	8.42	269	3.02	40.7	13,700	17.6	0.0157	23,200	27,900	144,700	0.245	1.08	0.9
3	180	539	3.4	5800	273	400	21.0	25.6	0.477	32.3	8.43	272	3.32	43.8	13,700	18.4	0.0152	23,600	28,000	144,700	0.247	1.14	0.9
4	177	564	4.9	6280	280	396	23.0	31.1	0.408	35.5	9.11	196	3.11	67.8	10,060	15.5	0.0199	23,300	27,600	156,800	0.238	1.48	0.9
5	179	551	4.1	7270	319	419	25.5	-	0.431	40.6	10.62	229	2.54	63.7	11,400	19.1	0.0210	23,300	27,900	181,000	-	1.34	0.9
6	169	564	4.9	8500	323	405	33.5	-	0.340	50.3	12.45	187	2.44	108.0	10,000	20.6	0.0242	22,300	26,400	212,000	-	1.63	0.9
7	169	562	4.7	8590	319	400	30.5	-	0.333	50.8	12.55	187	2.18	98.9	9,980	21.1	0.0240	22,200	26,400	214,200	-	1.45	0.9
8	171	562	4.7	8700	319	400	27.0	-	0.333	50.9	12.71	189	1.88	85.9	9,980	21.6	0.0241	22,500	26,600	217,000	-	1.25	0.9
***** 9	139	490	1.8	7170	320	398	19.0	-	0.459	51.5	10.49	395	1.94	35.3	25,700	22.6	0.0125	17,900	21,700	179,000	-	0.843	1.0

* Unstable, pressures and temperatures are transient.

** Lowest χ for tube to be operable: T_{vo} = 545, $T_{\ell o}$ = 265, $T_{\ell e}$ = 425.

*** Highest χ for tube to be operable: T_{vo} = 555, $T_{\ell o}$ = 321, $T_{\ell e}$ = 482.

**** Unstable, pressures and temperatures are transient.

***** Vapor quality ≈0.81.

APPENDIX G

MULTI TUBE JET CONDENSER

APPENDIX G

MULTI TUBE JET CONDENSER

(Test Section No. 9)

Test Run No.	$\dot{m}_{voT}$	T_{vo}	P_{vo}	$\dot{m}_{\ell oT}$	$T_{\ell o}$	$T_{\ell e1}$	$T_{\ell e2}$	$T_{\ell e3}$	$T_{\ell em}$	ΔP_a	x_1	x_2	x_3	x_m	$\dot{m}_{RT}$	$V_{\ell o}$	V_{VOT}	ΔP_ℓ°	β°	$\Delta P_{a(calc)}$	ΔP_ℓ° calc. $x_m\left(\frac{V_{\ell o}}{V_{VOT}-V_{\ell o}}\right)$		Q_{RT}	η_a	L_{c_1}	L_{c_2}	L_{c_3}
4-4-62																										
* 1	-	509	2.4	-	66	159	180	170	165	0.2	0.210	0.257	0.235	0.224	-	-	-	-	19,050	-	-	-	-	no data		
2	95.2	645	11.0	2500	189	352	372	381	350	-0.6	0.357	0.401	0.421	0.353	26.3	3.81	43.3	-0.490	3,960	2.19	1.79	-	12,900	-0.274			
3	111	660	14.0	2300	250	424	571	430	450	-1.0	0.425	0.783	0.439	0.488	20.8	3.49	43.3	-0.951	3,400	2.29	2.18	-	14,700	-0.436			
4	123	660	14.0	2200	262	532	600	444	490	-0.5,0	0.678	0.850	0.457	0.573	17.8	3.35	52.5	-0.516	3,400	2.42,0	2.50	-	16,100	-0.207			
5	117	685	17.0	2040	340	573	590	610	572	-1.1	0.676	0.725	0.783	0.673	17.5	3.11	36.5	-1.32	2,710	1.86	2.21	-	15,100	-0.593			
6	124	682	16.0	2040	348	603	600	617	590	-2.0	0.764	0.755	0.805	0.725	16.5	3.11	39.8	-2.39	2,800	2.01	2.40	-	15,800	-0.996			
7	125	680	16.0	2020	350	605	605	619	598	-2.0	0.773	0.773	0.815	0.752	16.2	3.07	41.0	-2.46	2,860	2.03	2.50	-	16,000	-0.984			
8	-	660	14.0	1980	-	669	666	-	-	-3.0	-	-	-	-	-	~3.01	-	~3.82	3,400	-	-	-	-	-			
9	125	670	15.0	1940	360	626	625	620	617	-4.0	0.858	0.855	0.839	0.830	15.5	2.95	46.0	-5.32	3,200	2.15	2.86	-	15,900	-1.86			
10	131	638	10.0	2300	330	565	552	550	559	-1.0	0.764	0.722	0.714	0.744	17.5	3.49	63.4	-0.951	4,210	3.00	2.87	-	16,800	-0.331			
11	113	602	7.4	3910	331	469	525	398	449	0.5 to 1.0	0.509	0.717	0.247	0.436	34.7	5.95	79.9	0.152 to 0.303	6,150	5.62,5.65	1.71	-	14,800	0.089,0.177			
12	131	589	6.6	5120	315	410	470	370	420	2.7	0.346	0.566	0.201	0.303	39.1	7.80	106.	0.508	7,070	8.55	1.61	-	17,200	0.316			
13	129	575	5.6	5590	305	406	430	355	400	3.5	0.374	0.463	0.185	0.352	43.2	8.51	124.	0.555	8,340	10.2	1.61	-	17,000	0.344			
14	74	555	4.3	5610	280	382	410	331	335	2.5	0.371	0.473	0.185	0.200	75.8	8.54	90.8	0.397	10,680	8.75	1.39	-	9,870	0.286			
15	128	574	5.5	5820	340	430	469	380	430	3.7	0.385	0.552	0.171	0.384	45.4	8.86	124.	0.544	8,430	10.8	1.58	-	16,800	0.344			
16	116	565	4.9	6040	332	411	442	378	411	4.2	0.339	0.472	0.198	0.339	51.9	9.18	126.	0.578	9,420	10.9	1.50	-	15,300	0.385			
17	70.7	550	4.0	4470	335	399	415	370	400	4.5	0.298	0.372	0.163	0.302	63.3	6.80	92.9	1.13	11,420	6.07	1.52	-	9,280	0.742			
5-15-62																										
** 1	198	661	14	2340	79	445	465	423	431	0	0.629	0.664	0.591	0.605	11.8	3.56	77.6	0	3,400	-	4.45	0.0291	26,400	-	1/4	1/4	1/4
2	199	650	12	2280	79	459	440	450	440	0	0.665	0.630	0.648	0.632	11.5	3.47	87.2	0	3,810	-	5.10	0.0262	26,400	-	1/4	1/4	1/4
3	194	658	13	2220	79	487	345	509	441	0	0.706	0.460	0.743	0.625	11.5	3.38	77.4	0	3,480	-	4.75	0.0286	25,700	-	1/4+	1/4+	1/4+
4	183	656	13	2070	79	559	341	495	445	0	0.831	0.454	0.720	0.634	11.3	3.18	73.0	0	3,480	-	4.80	0.0289	24,200	-	3/8	3/8	3/8
5	181	660	14	1920	79	599	345	450	469	0	0.895	0.457	0.638	0.670	10.6	2.92	70.7	0	3,400	-	5.37	0.0289	23,800	-	1/2	1/8	1/8
6	171	661	14	1650	79	609	426	622	503	0	0.910	0.595	0.935	0.726	9.64	2.52	67.0	0	3,400	-	-	0.0284	22,400	-	1/4	3/8	1
7	180	680	16	1520	79	625	600	635	560	0	0.909	0.867	0.925	0.800	8.45	2.32	59.2	0	2,860	-	-	0.0327	23,400	-	2	2	2
8	224	690	18	1770	79	610	612	573	590	-0.3	0.869	0.871	0.805	0.835	7.90	2.70	66.4	-0.470	2,580	-	-	0.0354	28,900	-	3	3	3
9	171	671	15	1870	80	640	418	330	459	-0.2	0.947	0.572	0.424	0.641	10.9	2.85	62.8	-0.280	3,200	-	4.76	0.0305	22,600	-	1½	3/8	3/8
10	165	665	14	3850	363	510	599	435	537	0.8 to 1.0	0.487	0.782	0.238	0.576	23.3	5.86	62.0	0.269 to 0.336	3,260	5.30	1.80	0.0601	21,400	0.150-0.187	5/8	5/8	0
11	168	680	16	3890	385	599	610	460	559	1.0 to 1.5	0.726	0.763	0.254	0.590	23.2	5.93	55.0	0.329 to 0.494	2,860	5.00	1.70	0.0713	21,700	0.200-0.300	5/8	5/8	0
12	199	670	15	4420	412	600	582	589	592	2.5	0.728	0.659	0.685	0.698	22.2	6.73	73.2	0.638	3,200	7.30	1.85	0.0697	25,500	0.345	3	3	3
13	176	669	15	4450	421	599	582	575	580	3.0	0.718	0.649	0.621	0.641	25.2	6.78	64.7	0.758	3,200	6.70	1.70	0.0748	22,600	0.448	3	3	3
14	162	740	28	7220	550	650	648	639	640	-6.0	0.526	0.515	0.408	0.474	44.6	11.0	31.6	-0.570	1,705	11.5	1.09	0.253	20,800	-	3	3	3
15	164	672	15	4110	420	578	559	535	580	7.0	0.626	0.551	0.456	0.635	25.0	25.0	6.25	~0 to 2.07	2,960	5.60	1.65	0.800	21,100	0-1.25	5/8	5/8	5/8
16	111	716	22	3850	480	609	606	583	597	6.0	0.546	0.535	0.437	0.495	34.6	5.87	26.9	~0 to 2.01	2,100	3.60	1.21	0.138	14,400	0-1.65	5/8	5/8	5/8
17	110	699	19	4620	474	579	580	560	570	3.0 to 8.2	0.467	0.471	0.382	0.426	42.0	7.04	30.5	0.700 to 1.92	2,420	5.10	1.19	0.128	14,200	0.590-1.61	5/8	5/8	5/8
18	106	689	16	4840	471	700	570	553	560	4.0 to 9.0	1.05	0.455	0.376	0.408	45.5	7.37	31.5	0.852 to 1.92	2,580	5.50	1.16	0.125	13,800	0.735-1.65	5/8	5/8	5/8

* Metal mixing sections.
** Quartz mixing sections.